


May 2019

Incorporation, Morphology, and Extinction of Framework-Building Metazoans in Early Cambrian Reef Ecosystems from the Western Usa and Mongolia and Their Effects on Reef Diversity

David Russell Cordie
University of Wisconsin-Milwaukee

Follow this and additional works at: <https://dc.uwm.edu/etd>

 Part of the [Ecology and Evolutionary Biology Commons](#), [Geology Commons](#), and the [Paleontology Commons](#)

Recommended Citation

Cordie, David Russell, "Incorporation, Morphology, and Extinction of Framework-Building Metazoans in Early Cambrian Reef Ecosystems from the Western Usa and Mongolia and Their Effects on Reef Diversity" (2019). *Theses and Dissertations*. 2055.
<https://dc.uwm.edu/etd/2055>

This Dissertation is brought to you for free and open access by UWM Digital Commons. It has been accepted for inclusion in Theses and Dissertations by an authorized administrator of UWM Digital Commons. For more information, please contact open-access@uwm.edu.

INCORPORATION, MORPHOLOGY, AND EXTINCTION OF FRAMEWORK-BUILDING METAZOANS
IN EARLY CAMBRIAN REEF ECOSYSTEMS FROM THE WESTERN USA AND MONGOLIA AND THEIR
EFFECTS ON REEF DIVERSITY

by

David Russell Cordie

A Dissertation Submitted in
Partial Fulfillment of the
Requirements for the Degree of

Doctor of Philosophy

in Geosciences

at

The University of Wisconsin-Milwaukee

May 2019

ABSTRACT

INCORPORATION, MORPHOLOGY, AND EXTINCTION OF FRAMEWORK-BUILDING METAZOANS IN EARLY CAMBRIAN REEF ECOSYSTEMS FROM THE WESTERN USA AND MONGOLIA AND THEIR EFFECTS ON REEF DIVERSITY

by

David Russell Cordie

The University of Wisconsin-Milwaukee, 2019
Under the Supervision of Professor Stephen Q. Dornbos

The early Cambrian represents an important transition in the evolution of life, perhaps most vividly exemplified by reef ecosystems as they changed from microbial-supported to metazoan-supported framework reefs. Microbial reefs were initially composed of *Renalcis*- and *Epiphyton*-group calcifying microbes. Subsequent reefs began to incorporate archaeocyathan sponges within this framework. This represents a shift in the source of carbonate production, which can be quantified using thin section point counts. In archaeocyathan reefs from the western USA, carbonate contribution from metazoan framework builders increased from zero to 29.7%. Similar reefs from Mongolia increased from zero to 5.0%. Increases in Laurentian archaeocyath contributions are not associated with shifts in carbon isotopic composition or changes in global redox conditions, while Gondwana examples might be associated with a negative carbon isotopic excursion and increase in redox sensitive elements. The incorporation of metazoan framework builders is not associated with an increase in reef dwellers, as one might expect based on the niche supporting roles that framework builders play in modern reefs.

To further explore the timing of reef dweller biodiversity, a literature survey was conducted that shows an increase in reef-dweller abundance (17.9% in the Cambrian to 28.8% considered “frequent” in the Ordovician), functional richness (3.8 to 5.9 functional groups), and skeletonization. Furthermore, archaeocyath gross morphologies are also highly constrained to a few (3-6 categories) simple morphologies and smaller body sizes compared to lithistid and modern demosponges. It therefore may not be unusual for early Cambrian reefs to have reduced reef-dweller diversity, potentially due to a combination of low ocean productivity and restricted morphological diversity.

Archaeocyaths went extinct at the end of Stage 4 of the Cambrian. This ushered in a period of low reef carbonate contribution from metazoans. This post-archaeocyath interval is preserved in western Nevada, but this locality does not contain substantial evidence of either metazoan or microbial framework building. As archaeocyaths were an important framework builder, their extinction may have resulted in a local reef eclipse. This work highlights the early Cambrian as a transitional period between the minimal diversity of the Proterozoic and high diversity reefs of the later Paleozoic.

© Copyright by David Russell Cordie, 2019
All Rights Reserved

To my grandparents
Robert “Gramps” Cordie (1932-2018) and
Marilyn “Nana” Cordie (1930-2018)

TABLE OF CONTENTS

	List of Figures	viii
	List of Tables	x
	Acknowledgments	xi
Chapter		
I.	Introduction	1
	Purpose of study and synopsis	1
	Background	3
	References	12
II.	Increase in carbonate contributions from framework-building metazoans in microbial-archaeocyathan reefs from the early Cambrian of the western USA and Mongolia	20
	Introduction to carbonate contributions in reefs	20
	Geologic settings	23
	Materials and methods	29
	Results	35
	Sedimentological observations	52
	Discussion	64
	Geochemical diagenetic and chemostratigraphic interpretations	72
	Conclusions	76
	References	77
III.	Depauperate skeletonized reef-dwelling fauna of the early Cambrian: a literature survey to determine the timing of reef-dweller diversity	92
	Typical reef dwellers of the early Cambrian	94
	Materials and methods	96
	Results	98
	Discussion	102
	Conclusions	106
	References	106

IV.	Restricted morphospace occupancy of early Cambrian reef-building archaeocyaths	119
	Cambrian morphospace occupancy and sponge morphology	119
	Materials and methods	122
	Results	126
	Discussion	133
	Conclusions	143
	References	144
V.	Exploring the Cambrian metazoan reef gap in the Mule Spring Limestone of Nevada	157
	The Cambrian “reef gap”	157
	Geologic setting	160
	Materials and methods	162
	Results and discussion	165
	Conclusions	187
	References	188
VI.	Conclusions	200
	Outcome of started goals	200
	Shifts towards metazoan reefs	201
	Delayed biodiversity of Cambrian reefs	204
	Cambrian reefs are different	204
	Future directions	205
	Appendix A: Point count data	211
	Appendix B: Geochemical data	216
	Appendix C: Literature survey data	221
	Appendix D: Morphological data	228
	Appendix E: Additional statistical data	263
	Curriculum Vitae	269

LIST OF FIGURES

Fig. 1.1	Outcrop, thin section, and hand sample specimens of archaeocyaths observed in this study	5
Fig. 1.2	Diversity curve of the Cambrian	7
Fig. 1.3	Paleogeography of archaeocyathan reefs	8
Fig. 1.4	Framework building processes in early Cambrian reefs	10
Fig. 2.1	Field localities in White-Inyo Mountains region	27
Fig. 2.2	Stratigraphy of White-Inyo Mountains region	27
Fig. 2.3	Field localities and stratigraphy in Mongolia	29
Fig. 2.4	Sensitivity analysis of thin section point counts	37
Fig. 2.5	Point count data for White-Inyo Mountains region	38
Fig. 2.6	Additional transects at Stewart’s Mill	39
Fig. 2.7	Point count data for Mongolia	42
Fig. 2.8	Fauna from Salaagol Formation in Mongolia	43
Fig. 2.9	Archaeocyath size distribution data	45
Fig. 2.10	Biodiversity statistics for all localities	47
Fig. 2.11	Non-metric multidimensional scaling of lithofacies composition	48
Fig. 2.12	Trace element data for White-Inyo Mountains region	50
Fig. 2.13	Trace element data for Mongolia	51
Fig. 2.14	Field and thin section photos of Montenegro Member	52
Fig. 2.15	Field, thin section, and hand samples of Poleta Formation	54
Fig. 2.16	Field, thin section, and hand samples of Harkless Formation	56
Fig. 2.17	Outcrop photos of Salaagol Formation	62
Fig. 2.18	Thin section fabric interpretations of Salaagol Formation	63
Fig. 2.19	Thin section comparison of White-Inyo Mountains and Mongolia	71
Fig. 2.20	Reconstruction of early Cambrian reef ecosystems	72
Fig. 2.21	Early Cambrian carbon isotope composition	76
Fig. 3.1	Primary reef builders during the Neoproterozoic and early Paleozoic	96
Fig. 3.2	Results of literature survey for 40 selected Neoproterozoic and early Paleozoic reef papers on reef dwellers	101

Fig. 4.1	Overview of materials and methods for morphological study	126
Fig. 4.2	Continuous variable measurements for museum specimens of archaeocyaths	128
Fig. 4.3	Size comparison of archaeocyath and modern sponge museum specimens	131
Fig. 4.4	Discrete character distribution for archaeocyath and modern sponges	133
Fig. 4.5	Archaeocyaths and modern demosponges used in study	139
Fig. 4.6	Loculus size distribution	141
Fig. 5.1	Clayton Ridge map and stratigraphic context	162
Fig. 5.2	Clayton Ridge outcrop photos	167
Fig. 5.3	Mule Spring Limestone common facies microanalysis images	171
Fig. 5.4	Peloid size distribution	172
Fig. 5.5	Mule Spring Limestone infrequent facies microanalysis images	174
Fig. 5.6	Mule Spring Limestone stratigraphy and carbonate contributions	175
Fig. 5.7	Framework builders of the Mule Spring Limestone	179
Fig. 5.8	Encrusting microbial activity and leiolite hand sample	180
Fig. 5.9	Cambrian reef occurrences from PARED	182
Fig. 5.10	Stable carbon isotopic composition of the Mule Spring Limestone	183
Fig. 5.11	Mule Spring Limestone paleoenvironmental reconstruction	187
Fig. 6.1	Ternary diagram of Phanerozoic reef ecosystems	203

LIST OF TABLES

Table 1.1	Summary of early Cambrian geochemical studies	11
Table 2.1	Average contribution percentages for thin section point count analysis	38
Table 2.2	Biodiversity statistics across lithological units	47
Table 3.1	Abundance data for functional groups by geologic interval collected from literature survey	99
Table 4.1	Size measurements (mm) for all archaeocyaths (museum and field), lithistid sponges and modern demosponges	132
Table 5.1	Point count data from Clayton Ridge	168

ACKNOWLEDGMENTS

First, I could not have done this work without the help of my adviser Dr. Stephen Q. Dornbos. Steve has always been approachable and willing to hear my opinions on any topic, from paleontology to current affairs. Our weekly meetings were always a source of confidence and approval during my PhD studies. Also, I would like to thank him for introducing me to this project which both incorporated my existing interests in reefs and taught me new concepts about early ecosystems.

Second, I would like to thank the rest of my committee members for guiding me through this dissertation and putting up with my frequent committee meeting requests. Thanks to Dr. Mark Harris for his enthusiasm in helping me identify the fuzziest of “bleebs” and squiggliest of “weird” Problematica in my thin sections. I always enjoyed and learned so much from our discussions on carbonates. Thank you, Dr. Peter Sheehan, for providing perspective and encouragement on all of my new ideas, and always being eager to help. Thank you also to Dr. Margaret Fraiser and Dr. Lindsay McHenry for pushing me to learn more about functional diversity and geochemistry.

Third, a huge portion of this dissertation would have been impossible if not for the support and knowledge of Dr. Pedro Marengo of Bryn Mawr College. Pedro was so gracious in offering me access to his geochemical equipment and helping me interpret redox proxies. Your help added new dimensions to this project that would never have been possible on my own. Furthermore, you opened your home to me and treated me as a colleague. I greatly appreciated your kindness. Thank you as well to my other co-authors, field assistants, and helpful figures throughout this project: Dr. Tatsuo Oji, Prof. Sersmaa Gonchigdorf, Caige Tubic,

Lisa Mowery, Dr. Pat Druckenmiller, Dr. Erica Clites, Julia Colby, Dr. John Isbell, and everyone at the White Mountain Research Center at Owen's Valley. I would also like to thank the many sources of funding for this project: UWM Department of Geosciences, UWM College of Letters and Sciences, Wisconsin Geological Society (WGS), Geological Society of America (GSA), Paleontological Society (PS), Society of Sedimentary Research (SEPM), American Museum of Natural History (AMNH), Sigma Xi, White Mountain Research Center (WMRC), and the Clem Nelson Award.

Lastly, I would like to thank my fellow graduate students, friends, and family. To Megan, Keenan, Nick, Liz, Kate(s), Chase, Chad, Gayantha and everyone else, I have never been in a department as friendly as ours. To all my friends throughout my schooling, you made it more than just an education in science. Thanks to my friends at Caliburn, Anahit, Mat, Rachel, Dave, John and others. And to my parents - Jeff and Ann - aunts, uncles, grandparents, and sister Elizabeth, love you guys.

Time is the best teacher, unfortunately, it kills all of its students.

- Robin Williams

Chapter I. Introduction

Purpose of Study and Synopsis

The purpose of the present study is to investigate the changes in framework building contribution from archaeocyathan sponges during the early Cambrian and their effects on the diversity of reef dweller organisms. Throughout this work any organism that stabilizes, binds, or produces a rigid framework for other organisms to attach to or inhabit is considered a framework builder. They are also *usually* attached benthic organisms with robust skeletons. Organisms that do not contribute to this construction, and instead live within this framework, are considered reef dwellers. Admittedly, this distinction can be fluid for some organisms (i.e., bryozoans), but the most common life habitat and frequency of these organisms are used when making this distinction. Additionally, the term reef is used in the broadest sense (*sensu lato*) as any repetitive association of mutually attached framework-building organisms. Qualifiers are used in front of the word reef (e.g., microbial reef, archaeocyathan reef) to denote the major framework-building organisms in that ecosystem. In general, the taxonomy of archaeocyaths, microbes, and reef dwellers beyond broad taxonomic ranks is beyond the scope of this study, though some identifications have been made when possible. Instead it will focus more on the paleoecology and abundance of framework builders and reef dwellers within reef ecosystems with data from geochemical and sedimentological sources as warranted.

The three primary goals within this project are:

1. Quantify the proportion of framework-building organisms during early Cambrian archaeocyathan reefs and assess the biodiversity and geochemical conditions associated with these changes.

2. Associate these changes in framework-building organisms with changes in the reef-dwelling organisms that inhabited these ecosystems. Furthermore, investigate the morphological diversity in archaeocyathan sponges and how it might relate to their ability to perform a niche creating role in reefs.
3. Investigate potential occurrences of microbial reefs during the post-archaeocyath interval of the Cambrian and the diversity they may harbor.

This work is divided into six chapters. **Chapter I** contains the scope of study and background information on the origination, extinction, and paleoecology of archaeocyaths during the Cambrian, as well as general redox conditions of the early Cambrian. **Chapter II** describes the work performed in the Campito, Poleta, and Harkless formations of the western USA and Salaagol Formation of Mongolia using thin section point counts to assess reef carbonate contributions. Furthermore, carbon isotopic compositions and trace element analysis using ICP-MS are used for both localities to provide stratigraphic context and paleoredox conditions. Environmental conditions and reconstruction based on sedimentological observations are also addressed. Here, I show that the proportion of framework builders in the early Cambrian did increase, however, their association with changes in geochemical proxies was inconsistent. **Chapter III** includes a literature survey of additional early Cambrian reef ecosystems to further contextualize the first-hand data collected by the author with more data from other localities. In this survey, abundances, functional richness, and skeletonization of reef dwelling organisms from the Ediacaran through Ordovician are assessed. I find that despite having an established framework in the Cambrian, reefs did not become more diverse until the Ordovician when additional skeletonized organisms evolved, and ocean productivity increased.

In **Chapter IV** one of the potential reasons for this lack of diversity, namely restricted morphological diversity of archaeocyaths, is quantified. Over 1,000 museum and field specimens were measured for continuous variable traits along with a database survey of discrete traits to show that archaeocyaths are smaller and had fewer unique morphologies than other types of sponges. Next, **Chapter V** details additional thin section analysis of the post-archaeocyathan extinction interval of the Cambrian and finds no evidence for metazoan or microbial reef building. Numerous trilobite fragments and calcareous shells are found, so the benthic ecosystem may have been in the early stages of restructuring. Cryptic metazoans and microbes may have been present during this interval, however, diversity of these ecosystems is severely limited. **Chapter VI** provides an overview of the project conclusions.

Background

Reefs play a significant role in modern and ancient marine ecosystems by serving as cradles of evolution (Kiessling *et al.*, 2010), refugia during periods of high extinction (Cowman and Bellwood, 2011), and providing ecological stability over long timescales (Kiessling, 2005). Modern reef environments occupy between 0.1% and 0.5% of the ocean floor, yet they comprise as much as one-third of ocean biodiversity (Moberg and Folke, 1999). Despite the importance of these ecosystems, modern reefs are undergoing a substantial decline in biodiversity due to ocean acidification (Hoegh-Guldberg *et al.*, 2007), coral bleaching (Hughes *et al.*, 2017), and phase shifts (Hughes *et al.*, 2007) due in large part to changing oceanic conditions as a result of anthropogenic climate change (Pandolfi *et al.*, 2011). Specifically, decreasing pH in the oceans has resulted in reduction of carbonate production (Comeau *et al.*, 2016) in reefs and therefore reduced functionality of reefs as biodiversity drivers (Wild *et al.*,

2011). Fortunately, we can use the fossil record to study changes in framework builder carbonate contributions and their effects on diversity (Pandolfi and Kiessling, 2014).

Archaeocyaths are a class of extinct carbonate-producing sponges that existed during the early Cambrian. In cross section, archaeocyaths have a double walled structure separated by an intervallum. A central cavity, opening in a distal osculum, is enclosed by the innermost of these two walls (Fig. 1.1A). No soft tissue of archaeocyaths has ever been found, therefore, the placement of soft tissue within this skeleton is speculative. One suggestion is that the soft tissue was spread across the outer wall and lined the internal central cavity (as has been suggested for stromatoporoids), while a second supposes that tissue inhabited some portion of the internal chambers of the organism such as in modern *Vaceletia* (Hill, 1964). Radial-longitudinal septa and transverse tabulae partitions connect the inner and outer walls (Fig. 1.1B), all of which are covered in small pores (Fig. 1.1C). Archaeocyaths have aspiculate, robust skeletons with a homogenous microgranular, presumably originally high Mg-calcite, microstructure (Fig.1.1D; Kruse and Debrenne, 1989). Archaeocyathan gross morphology resembles a conical tube, often with a slightly thickened holdfast (Fig. 1.1E).

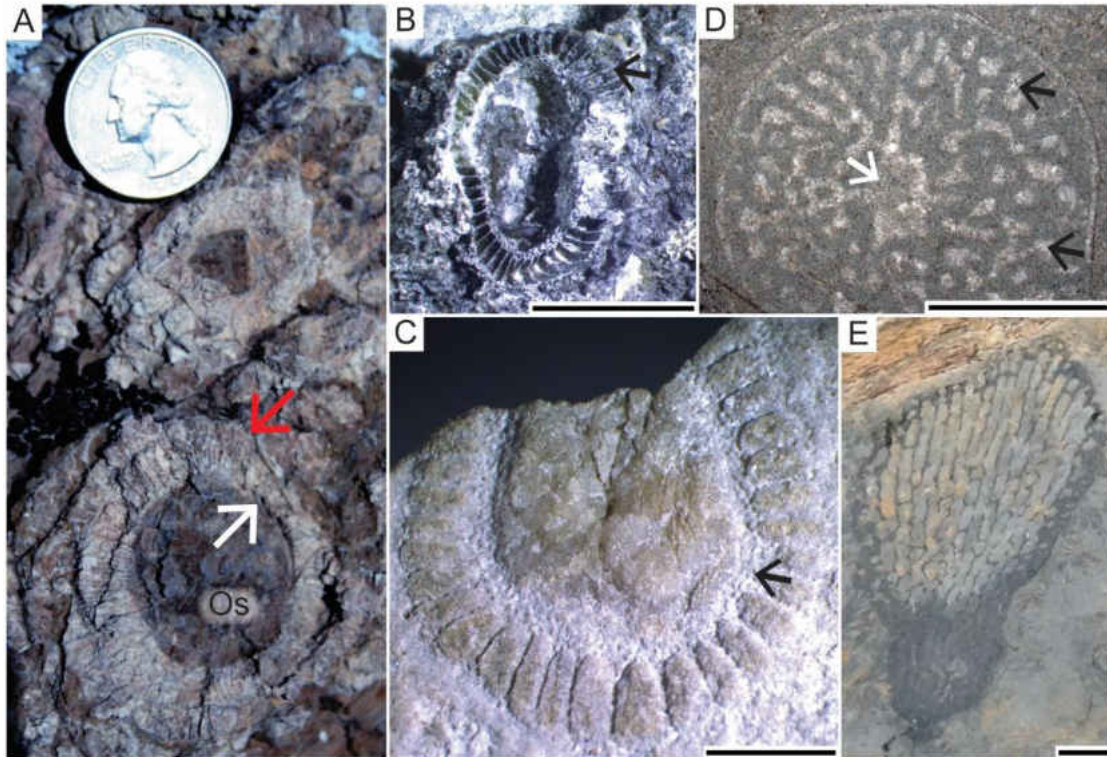


Figure 1.1: Outcrop, thin section, and hand sample specimens of archaeocyaths observed in this study. A, Archaeocyaths from Harkless Formation in Esmeralda County, Nevada, USA. Red arrow pointing to outer wall, white arrow pointing to inner wall. Os - osculum. B, Archaeocyath from Jones Ridge Formation in Alaska, USA. UAMES 7356. Arrow pointing to septum in interwall cavity. C, Internal mold of archaeocyath from Adams Argillite in Alaska, USA. UAMES 6075. Arrow pointing to flattened inner wall showing pores. D, Thin section of archaeocyath from Poleta Formation in Nevada, USA. Black arrow pointing to internal interwall space filled with cement. White arrow pointing to central cavity. E, Archaeocyath from Poleta Formation at Stewart's Mill. Photo credit Lisa Mowery. Scale bars equal 2 mm in B-D; 3 mm in E.

Because of the unusual aspiculate nature of archaeocyaths their classification had been difficult. Archaeocyaths were originally thought to be either corals or algae, while others placed them within their own phylum (Rowland, 2001). However, studies that constructed models of archaeocyaths found that water flowed in through the outer wall pores and out the central osculum, functionally identical to sponges (Balsam and Vogel, 1973). Later discoveries of

modern aspiculate sponges further confirmed these interpretations, placing Archaeocyatha within the phylum Porifera, most likely related to Demospongiae (Kruse, 1990).

Archaeocyaths originated during the Tommotian (late Stage 2) on the Siberian Platform (Kruse *et al.*, 1995). They quickly diversified during the Atdabanian and reached a maximum diversity of over 300 genera during the late Atdabanian/early Botomian (Stage 3) (Fig. 1.2; Zhuravlev and Naimark, 2005). However, archaeocyaths experienced a two-pulsed extinction event at the end of the Botomian known as the Botomian Extinction which coincides with the widespread loss of small shell fauna (SSF), specifically the Tommotian taxa, as well as redlichiid and olenellid trilobites (Bond and Grasby, 2017). An initial phase of anoxia occurred at the end of the Botomian which may have forced dysaerobic adaptation of the Cambrian fauna and decreased diversity within Archaeocyatha (Fig. 1.2; Ivantsov *et al.*, 2005). A second phase of the extinction occurred at the end of the Toyonian (Stage 4/Wuliuan boundary) when a global regression event occurred known as the Toyonian Regression or Hawke's Bay Regression (Lasemi and Amin-Rasouli, 2016). These events are also temporally linked with a large igneous province (LIP) in Australia which could have affected the chemical makeup of the oceans (Glass and Phillips, 2006). Regardless of the cause, archaeocyaths went virtually extinct by the Wuliuan - except for some rare occurrences in Antarctica lasting through the middle Cambrian - a span of only ~20 million years from origination to extinction (Zhuravlev and Wood, 1996).

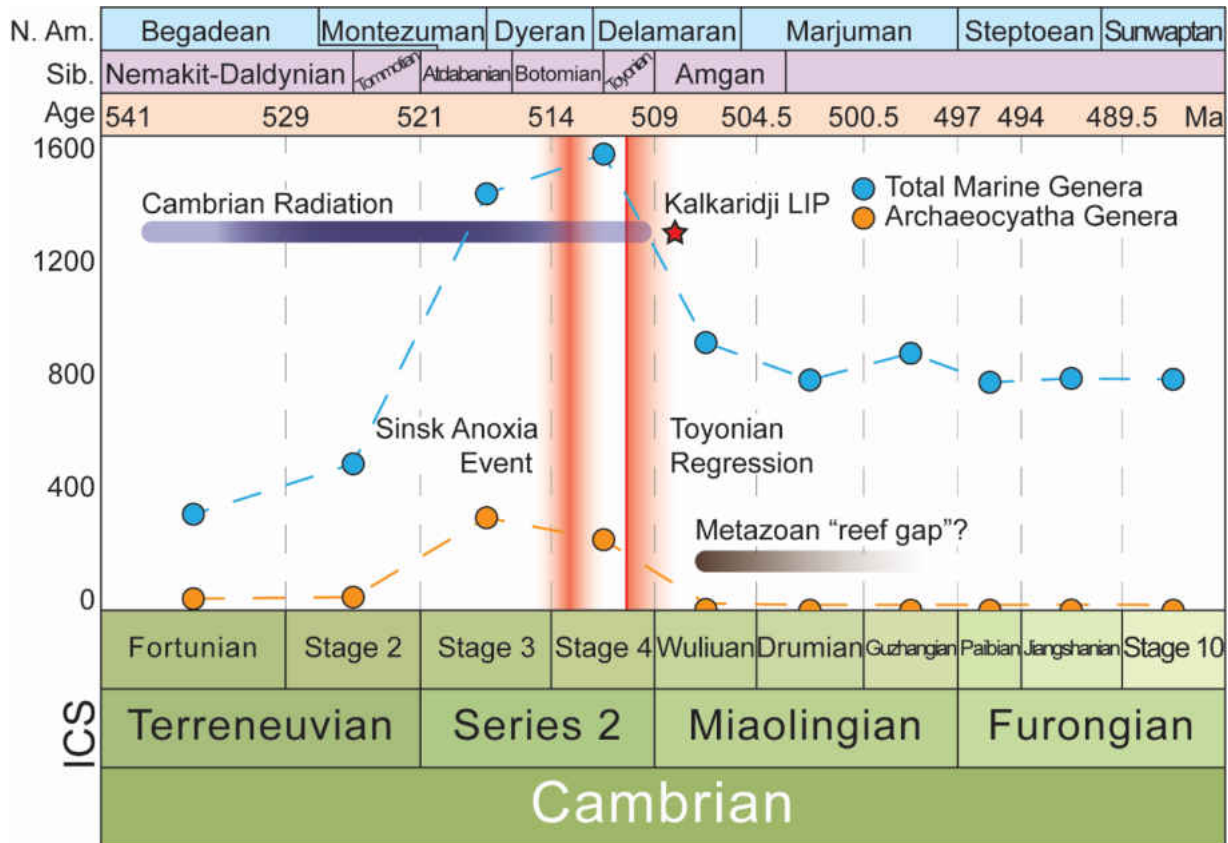


Figure 1.2: Diversity curve of the Cambrian. From top to bottom: North America regional stage names, Siberian regional stage names, age in millions of years, generic diversity curves with important evolutionary and extinction events marked, ICS nomenclature. Data generated from The Paleobiology Database in June 2018. All valid genera, grouped by stage - including singletons - used.

The paleogeography of the early Cambrian is greatly influenced by the breakup of Pannotia roughly 560 million years ago (Scotese, 2009). Archaeocyathan reefs originated on the Siberia craton, which served as the major diversity center during the Terreneuvian (Stage 2) of the Cambrian (Debrenne *et al.*, 1999). From there they spread to South China, northern Gondwana, and the Baltic before oceanic currents later brought them to Laurentia by Series 2 (Stage 3) of the Cambrian (McKerrow *et al.*, 1992). Archaeocyathan reefs from later Series 2 (Stage 4) can also be found in the Iberian Peninsula, Mexico, the western USA, Appalachia, and

Newfoundland (Debrenne *et al.*, 1989; Álvaro and Vennin, 1998; McMenemy *et al.*, 2000; Pruss *et al.*, 2012). Finally, later deposits during the Miaolingian and the Furognian can be found in Australia and Antarctica (Rees *et al.*, 1989; Kruse, 1991), however, the distribution of archaeocyaths had already begun to thin at this point prior to their global extinction (Fig. 1.3).

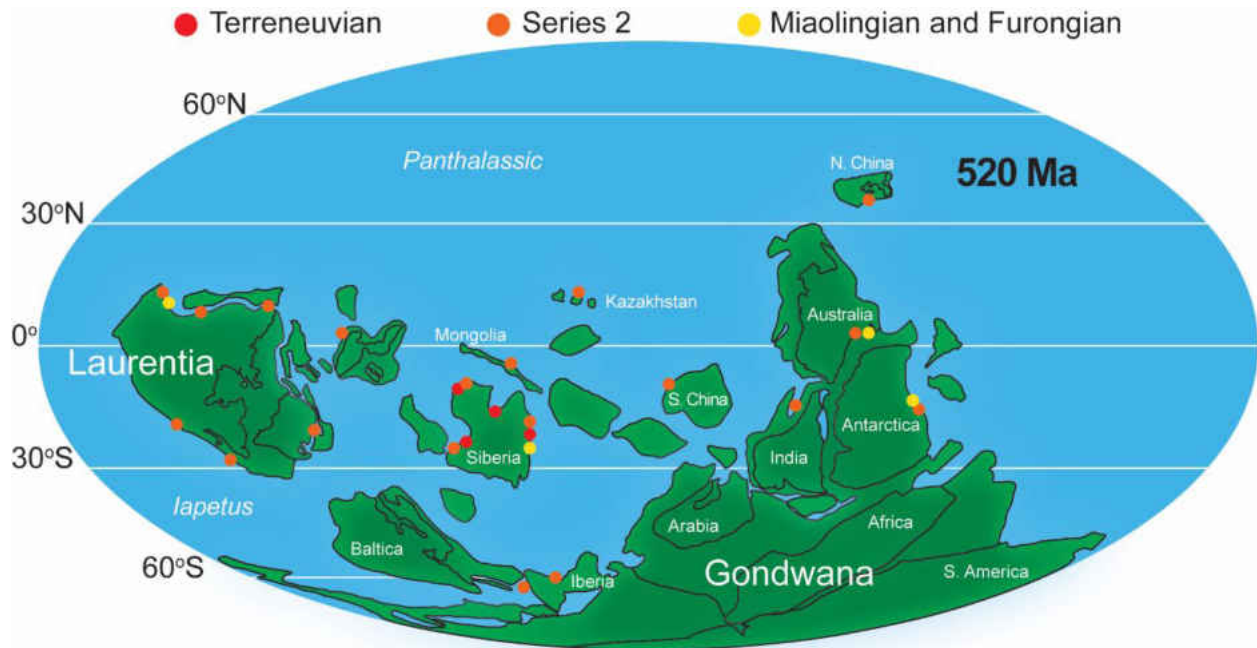


Figure 1.3: Paleogeography of archaeocyathan reefs. Colored dots represent occurrences of archaeocyathan reefs. Occurrence data generalized from The Paleobiology Database in June 2018. Base map depicts 520 Ma, though data from other time periods is all plotted on single map. See Gandin and Debrenne (2010) for details on locality distribution.

Archaeocyath ecology and role in reefs.— Archaeocyaths are filter feeding, sessile organisms that most likely used passive entrainment to filter food from seawater passed through their skeletons (Savarese, 1992). They primarily occurred in soft sediment environments (except for rare massive/encrusting forms). Archaeocyaths have a narrow latitudinal distribution between 30° N/S of the equator (Fig. 1.3). Their narrow distribution and lack of occurrences in evaporitic environments suggests that archaeocyaths were stenothermal and stenohaline organisms (Debrenne *et al.*, 2015). Furthermore, archaeocyaths are frequently

associated with ooid grainstones (e.g., in both the White-Inyos and western Mongolia) suggesting that they occurred in shallow, usually high energy, environments. This is further confirmed by their diminished occurrence in deeper water, shale possessing formations. Archaeocyathan reefs are suspected to have occurred in meso- to eutrophic environments as evidenced by higher rates sedimentation. In high nutrient environments high bioerosion is favored and greater chemical micritization of skeletal grains occurs, thereby creating more sedimentation, which is common in early Cambrian reefs (Wood, 1993). Furthermore, solitary and low integration organisms are favored in high nutrient environments (Wood, 1993) and are also common in early Cambrian reefs (see Chap. IV).

The bioconstruction ability of archaeocyaths is well documented from early Cambrian reefs (Debrenne *et al.*, 1989; Debrenne, 2007; Adachi *et al.*, 2014). Initial reefs from the lowest Cambrian (Nemakit-Daldnian) were composed largely of thrombolites and *Renalcis*- or *Epiphyton*-group calcifying microbes (Wood, 1999). Archaeocyaths were later incorporated by the Tommotian stage, though the majority of the volume these of reefs was probably already established by microbial organisms, as well as their wave resisting ability. In general, archaeocyaths appear to have acted as a baffler for sediment and served as a substrate for binding *Girvanella* (Fig. 1.4A). This stabilized surface then allowed for domal microbial organism of *Epiphyton*-group to attach (Fig. 1.4B). Bushy *Renalcis*-group microbes, sediment, and /or cement then filled in remaining cavity space (Adachi *et al.*, 2014; Fig. 1.4C and D). Additional metazoan framework builders were also present - such as radiocyaths, coralomorphs - however, they are less common globally compared to archaeocyaths. Studying the relationship

between archaeocyaths and other reef builders or reef dwellers could help us better understand the role archaeocyaths played in early reef ecosystems.

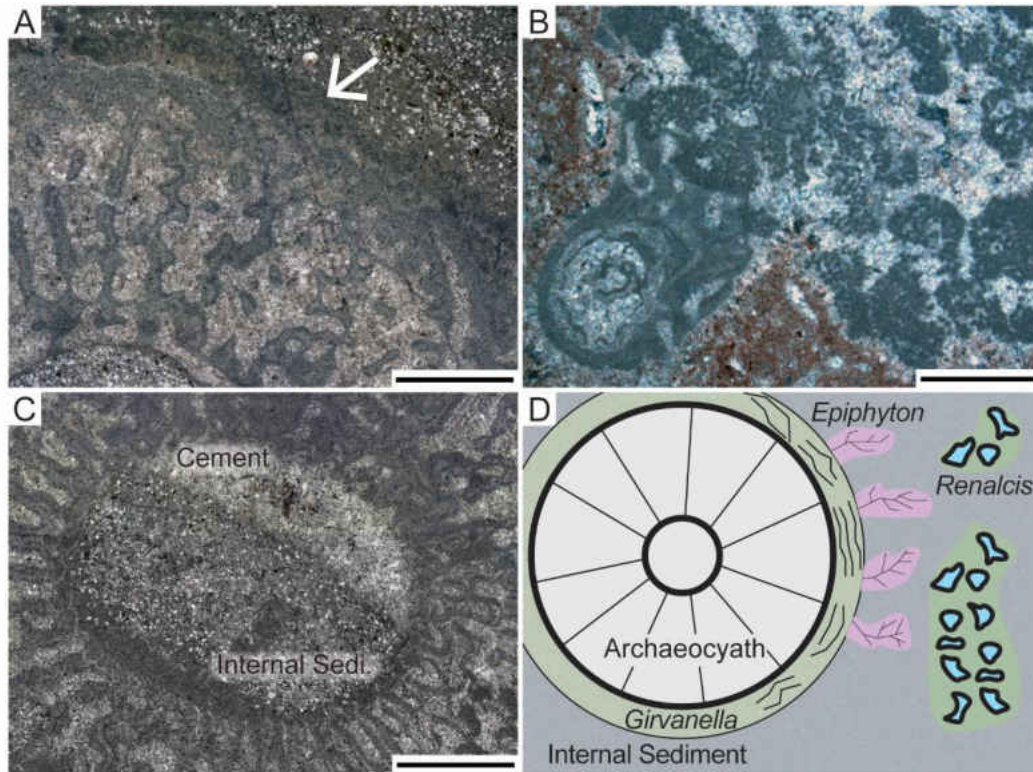


Figure 1.4: Framework building processes in early Cambrian reefs. A, Archaeocyath with unidentified microbes encrusting outer wall (arrow). B, *Epiphyton*-group attached to archaeocyath. C, Central cavity of archaeocyath with internal sediment and cement. Shows evidence of syndepositional sedimentation. D, Line drawing of framework building process. Modified from Adachi *et al.*, 2014. Scale bars all equal 1 mm.

Geochemistry of Cambrian oceans.— The Proterozoic had stratified ferruginous oceans until around 580 million years ago (Narbonne, 2010). From then on, oxygenated surface waters became more common and large multicellular lifeforms began to evolve. This stratified oxic/anoxic ocean system continued into the Cambrian, however, with periodic pulses of anoxia (Table 1.1). Starting in the Wuliuan and Drumian stages of the Cambrian, oxygen levels in surface waters appear to have decreased, creating more persistent anoxia in shallow water

environments. Anoxia is hypothesized to have played a substantial role in the extinction of archaeocyaths (Zhuravlev and Wood, 1996), and persistent oxygen deprivation after other mass extinctions has been shown to slow recovery of ecosystems (Twitchett *et al.*, 2004). Increasing oxygen levels in the early oceans could have potentially triggered the rapid radiation of metazoans in the early Cambrian (Sperling *et al.*, 2013), however, additional evidence suggests that sponges may not have required much oxygen to survive (Mills *et al.*, 2014). Therefore, understanding the oxygen conditions of the oceans during the time of archaeocyathan reefs and the conditions after their extinction could help us understand controls on the early diversity of life in reef ecosystems.

Table 1.1: Sampling of early Cambrian geochemical studies. Boxes in blue denote findings suggesting oxygenated surface waters, grey denotes findings of anoxia, yellow denotes mixed conditions. Listed in stratigraphic order from bottom to top.

Study	Finding	Interval	Method
Wallace <i>et al.</i> , 2017	Oxygenated in early Cambrian, anoxic late Cambrian	Cambrian	Ce anomalies in carbonates
Gill <i>et al.</i> , 2011	Anoxia	Paibian	S isotopes and trace elements in shales
Pagès and Schmid, 2016	Pluses of euxinic conditions	Drumian	C isotopes and trace elements in carbonates
Novek <i>et al.</i> , 2016	Persistent oxygenated conditions	Stage 3 - Stage 4	Trace elements from XRF in shales
Jin <i>et al.</i> , 2016	Oxygenated surface waters, euxinic mid-waters	Stage 3	Fe-S-C-Al-trace elements in shales and carbonates
Cai <i>et al.</i> , 2015	Oxygenated surface waters, euxinic bottom waters	Stage 2 - Stage 3	Fe speciation in shales
Wei <i>et al.</i> , 2018	Oxygenated early, anoxic pulse in Stage 2	Ediacaran - Stage 3	U isotopes in carbonates
Wen <i>et al.</i> , 2015	Oxygenated surface waters and anoxic/euxinic deep water	Terreneuvian	Mo isotopes in shale
Derry <i>et al.</i> , 1994	Periodic anoxia	“Lower” Cambrian	Sr and C isotopes in carbonates

References

- Adachi, N., Nakai, T., Ezaki, Y., and Liu, J. 2014. Late early Cambrian archaeocyath reefs in Hubei Province, South China: modes of construction during their period of demise. *Facies* **60**: 703-717.
- Álvaro, J., and Vennin, E. 1998. Stratigraphic signature of a terminal Early Cambrian regressive event in the Iberian Peninsula. *Canadian Journal of Earth Sciences* **35**: 402-411.
- Balsam, W. L., and Vogel, S. 1973. Water movement in archaeocyathids: evidence and implications of passive flow in models. *Journal of Paleontology* **47**: 979-984.
- Bond, D. P. G., and Grasby, S. E. 2017. On the causes of mass extinctions. *Palaeogeography, Palaeoclimatology, Palaeoecology* **478**: 3-29.
- Cai, C., Xiang, L., Yuan, Y., He, X., Chu, X., Chen, Y., and Xu, C. 2015. Marine C, S and N biogeochemical processes in the redox-stratified early Cambrian Yangtze ocean. *Journal of the Geological Society* **172**: 390-406.
- Comeau, S., Lantz, C., Edmunds, P., and Carpenter, R. 2016. Framework of barrier reefs threatened by ocean acidification. *Global Change Biology* **22**: 1225-1234.
- Cowman, P. F., and Bellwood, D. R. 2011. Coral reefs as drivers of cladogenesis: expanding coral reefs, cryptic extinction events and the development of biodiversity hotspots. *Journal of Evolutionary Biology* **24**: 2543-2562.
- Debrenne, F. 2007. Lower Cambrian archaeocyathan bioconstructions. *Comptes Rendus Palevol* **6**: 5-19.

- Debrenne, F., Gandin, A., and Rowland, S. 1989. Lower Cambrian bioconstructions in northwestern Mexico (Sonora) - depositional settings, paleoecology and systematics of archaeocyaths. *Geobios* **22**: 137-195.
- Debrenne, F., Maidanskaya, I., and Zhuravlev, A. 1999. Faunal migrations of archaeocyaths and early Cambrian plate dynamics. *Bulletin de la Société Géologique de France* **170**: 189-194.
- Debrenne, F., Zhuravlev, A. Y., and Kruse, P. D. 2015. General features of the Archaeocyatha. *In*: Debrenne, F. Hartman, W. D., Kershaw, S. Kruse, P. D., Nestor, H., Rigby Sr., J. K., Senowbari-Daryan, B., Stern, C. W., Stock, C. W., Vacelet, J., Webby, B. D., West, R. R., Willenz, P., Wood, R. A., and Zhuravlev, A. Y. eds. *Treatise on Invertebrate Paleontology, Part E, Porifera (Revised), Hypercalcified Porifera Volume 5*. The University of Kansas Paleontological Institute, Lawrence, Kansas. pp. 845-1084.
- Derry, L., Brasier, M., Corfield, R., Rozanov, A., and Zhuravlev, A. Y. 1994. Sr-isotope and C-isotope in Lower Cambrian carbonates from the Siberian Craton - a paleoenvironmental record during the Cambrian Explosion. *Earth and Planetary Science Letters* **128**: 671-681.
- Gandin, A., and Debrenne, F. 2010. Distribution of archaeocyath-calcimicrobial bioconstructions of the early Cambrian shelves. *Palaeoworld* **19**: 222-241.
- Gill, B. C., Lyons, T. W., Young, S. A., Kump, L. R., Knoll, A. H., and Saltzman, M. R. 2011. Geochemical evidence for widespread euxinia in the later Cambrian oceans. *Nature* **469**: 80-83.

- Glass, L. M., and Phillips, D. 2006. The Kalkarindji continental flood basalt province: a new Cambrian large igneous province in Australia with possible links to faunal extinctions. *Geology* **34**: 461-464.
- Hill, D. 1964. The phylum Archaeocyatha. *Biological Reviews* **39**: 232-258.
- Hoegh-Guldberg, O., Mumby, P. J., Hooten, A. J., Steneck, R. S., Greenfield, P. Gomez, E., Harvell, C. D., Sale, P. F., Edwards, A. J., Caldeira, K., Knowlton, N., Eakin, C. M., Iglesias-Prieto, R., Muthiga, N., Bradbury, R. H., Dubi, A., and Hatziolos, M. E. 2007. Coral reefs under rapid climate change and ocean acidification. *Science* **318**: 1737-1742.
- Hughes, T. P., Rodrigues, M. J., Bellwood, D. R., Ceccarelli, D., Hoegh-Guldberg, O., McCook, L., Moltschaniwskyj, N., Pratchett, M. S., Steneck, R. S. and Willis, B., 2007. Phase shifts, herbivory, and the resilience of coral reefs to climate change. *Current Biology* **17**: 360-365.
- Hughes, T. P., Kerry, J. T., Álvarez-Noriega, M., Álvarez-Romero, J. G., Anderson, K. D., Baird, A. H., Babcock, R. C., Beger, M., Bellwood, D. R., Berkelmans, R., Bridge, T. C., Butler, I. R., Byrne, M., Cantin, N. E., Comeau, S., Connolly, S. R., Cumming, G. S., Dalton, S. J., Diaz-Pulido, G., Eakin, C. M., Figueira, W. F., Gilmour, J. P., Harrison, H. B., Heron, S. F., Hoey, A. S., Hobbs, J-P. A., Hoogenboom, M. O., Kennedy, E. V., Kuo, C-Y., Lough, J. M., Lowe, R. J., Liu, G., McCulloch, M. T., Malcolm, H. A., McWilliam, M. J., Pandolfi, J. M., Pears, R. J., Pratchett, M. S., Schoepf, V., Simpson, T., Skirving, W. J., Sommer, B., Torda, G., Wachenfeld, D. R., Willis, B. L., and Wilson, S. K. 2017. Global warming and recurrent mass bleaching of corals. *Nature* **543**: 373-377.

- Ivantsov, A. Y., Zhuravlev, A. Y., Leguta, A. V., Krassilov, V. A., Melnikova, L. M., and Ushatinskaya, G. T. 2005. Palaeoecology of the early Cambrian Sinsk biota from the Siberian Platform. *Palaeogeography, Palaeoclimatology, Palaeoecology* **220**: 69-88.
- Jin, C., Li, C., Algeo, T., Planavsky, N., Cui, H., Yang, X., Zhao, Y., Zhang, X., and Xie, S. 2016. A highly redox-heterogeneous ocean in South China during the early Cambrian (~529-514): implications for biota-environment co-evolution. *Earth and Planetary Science Letters* **441**: 38-51.
- Kiessling, W. 2005. Long-term relationships between ecological stability and biodiversity in Phanerozoic reefs. *Nature* **433**: 410-413
- Kiessling, W., Simpson, C., and Foote, M. 2010. Reefs as cradles of evolution and sources of biodiversity in the Phanerozoic. *Science* **327**: 196-198.
- Kruse, P. 1990. Are archaeocyaths sponges, or are sponges archaeocyaths. *The Evolution of a late Precambrian-early Palaeozoic rift complex: the Adelaide Geosyncline, Geological Society of Australia Special Publication* **6**: 310-323.
- Kruse, P. 1991. Cyanobacterial-archaeocyathan-radiocyathan bioherms in the Wirrealpa Limestone of South Australia. *Canadian Journal of Earth Sciences* **28**: 601-615.
- Kruse, P., and Debrenne, F. 1989. Review of archaeocyath microstructure. *Memoirs of the Association of Australian Palaeontologists* **8**: 133-141.
- Kruse, P. D., Zhuravlev, A. Y., and James, N. P. 1995. Primordial metazoan-calcimicrobial reefs: Tommotian (early Cambrian) of the Siberian Platform. *Palaios* **10**: 291-231.

- Lasemi, Y., and Amin-Rasouli, H. 2016. The lower-middle Cambrian transition and the Sauk I-II unconformable boundary in Iran, a record of late early Cambrian global Hawke Bay regression. *In: Sorkhabi, R. ed. Tectonic Evolution, Collision, and Seismicity of Southwest Asia: In Honor of Manuel Berberian's Forty-Five Years of Research Contributions. Geological Society of America Special Paper 525: 343-366.*
- McKerrow, W., Scotese, C., and Brasier, M. 1992. Early Cambrian continental reconstructions. *Journal of the Geological Society 149: 599-606.*
- McMenamin, M., Debrenne, F., and Zhuravlev, A. 2000. Early Cambrian Appalachian archaeocyaths: further age constraints from the fauna of New Jersey and Virginia, U.S.A. *Geobios 33: 693-708.*
- Mills, D. B., Ward, L. M., Jones, C., Sweeten, B., Forth, M., Treusch, A. H., and Canfield, D. E. 2014. Oxygen requirements of the earliest animals. *Proceedings of the National Academy of Sciences 111: 4168-4172.*
- Moberg, F., and Folke, C. 1999. Ecological goods and services of coral reef ecosystems. *Ecological Economics 29: 215-233.*
- Narbonne, G. M. 2010. Ocean chemistry and early animals. *Science 328: 53-54.*
- Novek, J. M., Dornbos, S. Q., and Mchenry, L. 2016. Palaeoredox geochemistry and bioturbation levels of the exceptionally preserved early Cambrian Indian Springs biota, Nevada, USA. *Lethaia 49: 604-616.*

- Pages, A., and Schmid, S. 2016. Euxinia linked to the Cambrian Drumian carbon isotope excursion (DICE) in Australia: geochemical and chemostratigraphic evidence. *Palaeogeography, Palaeoclimatology, Palaeoecology* **461**: 65-76.
- Pandolfi, J. M., and Kiessling, W. 2014. Gaining insights from past reefs to inform understanding of coral reef response to global climate change. *Current Opinion in Environmental Sustainability* **7**: 52-58.
- Pandolfi, J., Connolly, S., Marshall, D, and Cohen, A. 2011. Projecting coral reef futures under global warming and ocean acidification. *Science* **333**: 418-422.
- Pruss, S., Clemente, H., and LaFlamme, M. 2012. Early (Series 2) Cambrian archaeocyathan reefs of southern Labrador as a locus for skeletal carbonate production. *Lethaia* **45**: 401-410.
- Rees, M. N., Pratt, B., and Rowell, A. 1989. Early Cambrian reefs, reef complexes, and associated lithofacies of the Shackleton Limestone, Transantarctic Mountains. *Sedimentology* **36**: 341-361.
- Rowland, S. M. 2001. Archaeocyaths: a history of phylogenetic interpretation. *Journal of Paleontology* **75**: 1065-1078.
- Savarese, M. 1992. Functional analysis of archaeocyathan skeletal morphology and its paleobiological implications. *Paleobiology* **18**: 464-480.
- Scotese, C. R. 2009. Late Proterozoic plate tectonics and palaeogeography: a tale of two supercontinents, Rodinia and Pannotia. *Geological Society, London, Special Publication* **326**: 67-83.

- Sperling, E. A., Frieder, C. A., Raman, A. V., Girguis, P. R., Levin, L. A., and Knoll, A. H. 2013. Oxygen, ecology, and the Cambrian radiation of animals. *Proceedings of the National Academy of Sciences* **110**: 13446-13451.
- Twitchett, R. J., Krystyn, L., Baud, A., Wheelley, J. R., and Richoz, S. 2004. Rapid marine recovery after the end-Permian mass-extinction event in the absence of marine anoxia. *Geology* **32**: 805-808.
- Wallace, M., Hood, A., Shuster, A., Greig, A., Planavsky, N., and Reed, C. 2017. Oxygenation history of the Neoproterozoic to early Phanerozoic and the rise of land plants. *Earth and Planetary Science Letters* **466**: 12-19.
- Wei, G., Planavsky, N., Tarhan, L., Chen, X., Wei, W., Li, D., and Ling, H. 2018. Marine redox fluctuation as a potential trigger for the Cambrian explosion. *Geology* **46**: 587-590.
- Wen, H., Fan, H., Zhang, Y., Cloquet, C., and Carignan, J. 2015. Reconstruction of early Cambrian ocean chemistry from Mo isotopes. *Geochimica et Cosmochimica Acta* **164**: 1-16.
- Wild, C., Hoegh-Guldberg, O., Naumann, M., Colombo-Pallotta, M., Ateweberhan, M., Fitt, W., Iglesias-Prieto, R., Palmer, C., Bythell, J., Ortiz, J., Loya, Y., and van Woesik, R. 2011. Climate change impedes scleractinian corals as primary reef ecosystem engineers. *Marine and Freshwater Research* **62**: 205-215.
- Wood, R. A. 1993. Nutrients, predation and the history of reef-building. *Palaios* **8**: 526-543.
- Wood, R. A. 1999. *Reef Evolution*. Oxford University Press, Inc., Oxford. 354 p.

Zhuravlev, A. Y., and Wood, R. A. 1996. Anoxia as the cause of the mid-early Cambrian (Botomian) extinction event. *Geology* **24**: 311-314.

Zhuravlev, A. Y., and Naimark, E. B. 2005. Alpha, beta, or gamma: numerical view on the early Cambrian world. *Palaeogeography, Palaeoclimatology, Palaeoecology* **220**: 207-225.

Chapter II. Increase in carbonate contributions from framework-building metazoans in microbial-archaeocyathan reefs from the early Cambrian of the western USA and Mongolia

Introduction to Carbonate Contribution in Reefs

Modern reef ecosystems are typically envisioned as highly diverse and integrated communities of calcareous, sessile organisms (Kiessling, 2009; Fisher *et al.*, 2015). Several geological (e.g., ocean chemistry, sea level) and biological (e.g., biodiversity, competition) controls are known to affect reef development and ecology (Kiessling, 2009). However, the structural support provided by framework-building organisms has a significant influence on the development of heterogeneous habitats by constructing a framework of rigid organisms and secondary encrusters (Buhl-Mortensen *et al.*, 2010). This framework then allows for microhabitats, such as overhangs and crevices, to house additional organisms. For example, 19% of a Holocene reef ecosystem, supported by scleractinian corals, is vacant cavity space (Hubbard *et al.*, 1990). However, scleractinian corals did not occur in the fossil record until 237 Ma in the late Ladinian of the Triassic Period and Paleozoic examples of reefs were instead supported by other metazoans (Stanley and Fautin, 2001).

Carbonate from metazoans in reef ecosystems first occurred in measurable amounts in the terminal Neoproterozoic when skeletonized *Cloudina* and *Namacalathus* began to form associations with thrombolitic microbialites (Grotzinger *et al.*, 2000). However, it is debated whether metazoans were contributing to framework in these ecosystems, as opposed to detrital inputs, and they are therefore not considered as part of this study (Mehra and Maloof, 2018). Subsequent Phanerozoic reefs were first built primarily by calcifying microbial organisms

and later by microbial-metazoan consortiums during Stage 2 of the Cambrian (Kruse *et al.*, 1995). Still, these earliest Phanerozoic reefs were distinct from modern reef environments in that a much larger proportion of carbonate contribution came from microbial organisms (Kiessling, 2002, fig. 16). These microbial reefs grow by precipitation of carbonate as well as trapping and binding sediment as opposed to metazoan reefs in which growth is controlled by the enzymatic processes of organisms (Burne and Moore, 1987; Webb, 1996). Thus, the transition from microbial to metazoan reefs represents a major transition in how reefs form and potentially in the diversity they can support.

To study this transition, I focus on how the proportion of metazoan framework-building organisms changed across a succession of early Cambrian microbial-archaeocyath reefs from the western Basin and Range and Mongolia. The bulk of early Cambrian reefs are composed of mostly granular micrite (Adachi *et al.*, 2014a), but microbial and metazoan elements are common. Microbial organisms can become primary framework builders in the absence of metazoans (Adachi *et al.*, 2014b; Thesien and Sumner, 2016). But during the early Cambrian, archaeocyathan sponges were the principle framework-building metazoans (Debrenne, 2007) - with radiocyaths and coralomorphs also contributing in some localities (Kruse *et al.*, 1996). Archaeocyaths originated on the Siberian Platform during Stage 2 of the Cambrian and quickly diversified to include over 50 species by Stage 3 (Kruse *et al.*, 1995; Zhuravlev *et al.*, 2015). In addition to the Siberian Platform, archaeocyaths also spread to Gondwana (Hicks and Rowland, 2009; Álvaro *et al.*, 2013; Kruse and Moreno-Eiris, 2013) and Laurentia (Rowland and Gangloff, 1988; Pruss *et al.*, 2012).

Archaeocyathan reefs around the world have been studied in detail to understand biogeographic conditions (Debrenne *et al.*, 1999; Gandin and Debrenne, 2010), substrate changes (Álvaro *et al.*, 2006; Zamora and Álvaro, 2010), and sea level (Álvaro and Vennin, 1998; Lasemi and Amin-Rasouli, 2016) during the early Cambrian. Furthermore, paleoecological studies of these communities reveal an ecosystem composed of deposit and generalist, opportunistic passive filter feeders (Pratt *et al.*, 2001; Debrenne, 2007). Archaeocyathan species were largely restricted to specific communities creating a large amount of endemic communities and heterogenetic reef ecosystems as a result (Zhuravlev and Naimark, 2005). However, within a local community archaeocyaths may have been taxonomically diverse (Wood *et al.*, 1993; Zhuravlev and Wood, 1995), but many of these sponges had low levels of modular integration (Wood *et al.*, 1992). This suggests that these organisms may not have been functionally distinct from an ecological standpoint. Although functional group definitions for level-bottom paleocommunities (Novack-Gottshall, 2007) and modern sponges (Bell, 2007; Maldonado *et al.*, 2016) have been performed, these same techniques have not been applied to early Cambrian reef communities. Consequently, studies quantifying the change in faunal contributions during the early phases of reef development in Laurentia have not been performed (except Pruss and Clemente 2011, 2012). In addition, more studies utilizing functional diversity can improve our understanding of the ecology of ancient reefs. Understanding these aspects can help clarify the early evolution of metazoans during the Cambrian, including the timing of metazoan reef evolution.

In addition, chemostratigraphic correlations using changes in carbon isotopic composition could provide a better constraint on the timing of dispersal of archaeocyaths to

Laurentia. While correlation of archaeocyaths and carbon isotopic changes has been performed in Siberian reefs (Kouchinsky *et al.*, 2007), Laurentian archaeocyathan reefs are believed to be younger in age (Pruss *et al.*, 2012). Thus, a more precise timing of dispersal between these localities is warranted. The $\delta^{13}\text{C}$ of seawater and the inventory of dissolved redox-sensitive elements (such as uranium, vanadium, and molybdenum) are closely tied to the burial of organic matter. Because of this relationship, the abundance of redox-sensitive elements in carbonates can help to test if trends in the $\delta^{13}\text{C}$ of carbonates were produced by global or localized processes.

The goal of this study is to investigate the faunal contributions and geochemical parameters within archaeocyathan reefs of the early Cambrian. Our results show that (1) quantifiable changes in framework-builder carbonate contributions do occur between reef-building intervals; (2) these changes in carbonate contribution are associated with higher diversity, but have an uncertain effect on reef-dwellers; and (3) these changes in fauna do not appear to be driven or impacted by global changes in redox conditions.

Geologic Settings

Western USA, general.— During the early Cambrian, the northern edge of Laurentia was located less than 20° north of the equator (McKerrow *et al.*, 1992). This passive margin gradually accumulated several kilometers of lower Cambrian strata in the form of decameter scale alternating siliciclastic and carbonate units (Mount and Rowland, 1981; Mount and Bergk, 1998). Broadly, these strata are found in the cratonward Death Valley sequence to the south and seaward White-Inyo sequence, focus of this study, to the northwest. The White-Inyo

sequence was later uplifted as two broad anticlines running parallel to the basin and range structures to the east (Moore, 1976). The western edge of the White-Inyo Mountains anticlines is disturbed with reverse faults and granitic intrusions occurring in the southern portions. The eastern side of the range is a thick deposit of lower Paleozoic material with few unconformities (Moore, 1976). I provide a brief summary of this region with references to more thorough studies for more information. Four reef localities in the western USA were investigated, two in the White-Inyo Mountains and two in Lida Valley to the east (Fig. 2.1 and 2.2). An additional two from western Mongolia (below) were also investigated.

White-Inyo Mountains, CA. — Locality 1 (Bristlecone Trail: 37° 19.162' N 118° 10.707' W) contains the upper Montenegro Member of the Campito Formation and a small portion of the Lower Poleta Formation. The Campito Formation includes the Andrews Mountain Member (quartzite and coarse sandstones) overlain by the Montenegro Member of green to brown shale with carbonate bioherms. The entire Montenegro Member is ~350 m thick and lower portions correlate to the *Fallotaspis* trilobite zone, which is lower Montezuman or Stage 3 (Hollingsworth, 2006). The term bioherm is used here for historical reasons, though these features may more appropriately be termed matrix-supported agglutinated microbial reefs or carbonate mud mounds depending on the support structure (per Riding, 2002). Previous work has found that these bioherms are *in situ* accumulations of *Renalcis*-group microbes and three genera (*Archaeocyathus*, *Syringothalamus*, and *Palmericyathellus*) of archaeocyaths (Xiaoping, 1995). The bioherms here have previously been interpreted as a brief carbonate bank within a largely siliciclastic setting (Morgan, 1976). However, micrite-dominated matrix appears to be

the primary support for these bioherms as opposed to archaeocyaths and secondarily encrusting *Renalcis*-group, which appear sporadically (Xiaoping, 1995).

Locality 2 (Westgard Pass: 37° 15.460' N 118° 09.121' W) is located in Westgard Pass, on either side of highway 168 east of the one lane portion of the road. It contains the Poleta Formation that conformably overlies the Campito Formation. The Poleta Formation has previously been informally divided into three members (Stewart, 1970). Here, ~100 m of the Lower Member of the Poleta Formation is exposed and contains abundant microbial and microbial-archaeocyath reefs with occasional beds of greenish-grey siltstone (Stewart, 1970). The succeeding Middle and Upper Members of the Poleta Formation are siliciclastic dominated and thinly bedded limestone respectively, and contain little to no archaeocyaths (Stewart, 1970; Novek *et al.*, 2016). Overall, the three members of the Poleta Formation have previously been interpreted to represent shifts from carbonate banks to a siliciclastic-dominated transgression sequence and back to carbonate shelf deposits as relative sea level fluctuated (McKee and Moiola, 1962; Mount and Signor, 1985; English and Babcock, 2010).

Lida Valley, NV.— Two additional localities were located in Lida Valley, Esmerelda County, Nevada. Locality 3 (Stewart's Mill: 37° 25.700' N 117° 27.415' W) contains a thick succession of reefs within the lower Poleta Formation (Rowland and Gangloff, 1988). Stewart's Mill is a three-dimensionally exposed reef with largely continuous carbonate strata and minor shale interbeds. Clotted microbialite is the dominant fabric in the Poleta Formation and archaeocyath-filled cavities are dispersed within this fabric. These cavities are filled with micrite and skeletal grains, suggesting previously self-supporting void space (Kobluk, 1981). Metazoan contributions at this locality primarily consist of two solitary archaeocyaths (*Protophareta* and

Paranacyathus, see Rowland and Gangloff, 1988) as well as large saucer-shaped *Diplocyathellus vulgaris*, which produce a distinct archaeocyath assemblage from the underlying Campito Formation. The Lower Poleta Formation here is capped with a thick unit of ooid grainstones (Rowland and Gangloff, 1988), which have *Skolithos* trace fossils.

Finally, locality 4 (Gold Point Hills: 37° 22.993' N 117° 17.221' W) is near the town of Gold Point and contains additional reef deposits within the overlying Harkless Formation. The lower part of the Harkless here is carbonaceous sandstones and siltstones with a thin (~1 m) reef-bearing limestone unit separated by an erosional contact (Stewart, 1970). These reefs have a large portion of subangular detrital quartz and occasional fibrous anhydrite (Hicks, 2006a). Previous studies have noted hummocky cross stratified and wavy laminations as evidence of a shallow subtidal environment, similar to other settings in the White-Inyo Mountains (Bailey *et al.*, 2006). Other carbonate units of the Harkless have reported an ecosystem dominated by *Retilamina*, *Arrhythmocricus*, *Metaldetes*, and *Diplocyathellus* archaeocyaths and encrusting *Renalcis*-group (Savarese and Signor, 1989). Additionally, the Harkless Formation is the only unit to contain coralomorphs (Hicks, 2006a). Together, these four localities represent distinct snapshots of at least three reef-building environments within the early Cambrian of western Laurentia.

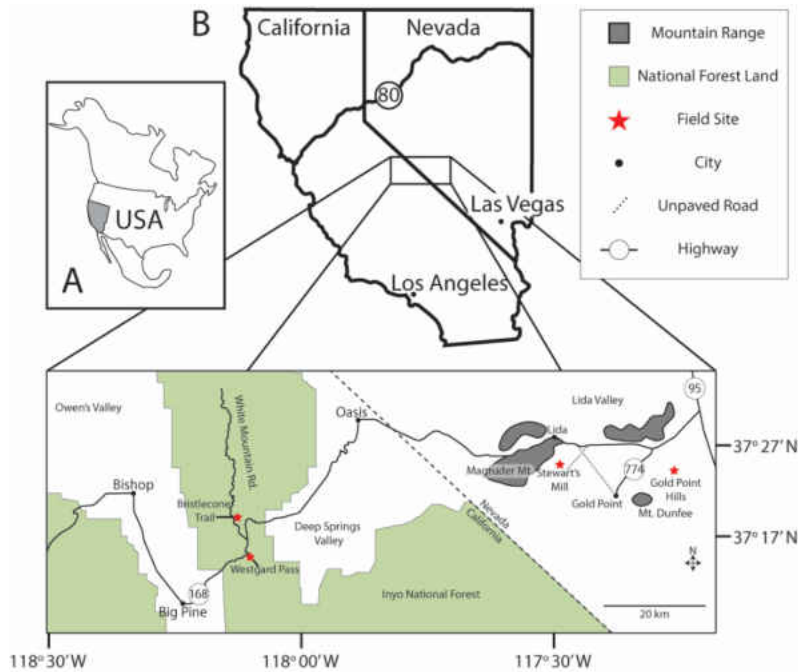


Figure 2.1: Field localities in White-Inyo Mountains region. A, Map of North America. B, Close-up of shaded area in A with first four localities denoted by red stars.

	ICS		North American Stages and Zones		Great Basin Lithology	This Study
"Mid." Cambrian	Miaolingian	Wuliuan	Delamaran	<i>Eokochaspis</i>	Emigrant Formation	4
"Early" Cambrian	Series 2	Stage 4	Dyeran	<i>Bonnia-Olenellus</i>	Mule Spring Limestone	
		Stage 3	Montezuman	<i>Nevadella</i>	Poleta Formation	
	Campito Formation				Middle	
			<i>Fallotaspis</i>		Lower	2
					Montenegro	3

Figure 2.2: Stratigraphy of White-Inyo Mountains region. From left to right, chronostratigraphy with ICS and North American stage names, trilobite biostratigraphy (Hollingsworth, 2006), and lithostratigraphy. Rightmost column shows intervals sampled in this study with numbers denoting localities. 1 = Bristlecone Trail, 2 = Westgard Pass, 3 = Stewart's Mill, 4 = Gold Point Hills.

Zavkhan Basin, western Mongolia.— The Zavkhan Terrane in modern southwestern Mongolia was first described by Bezzubetsev (1963; additionally see Zonenshain *et al.*, 1985) and Brasier *et al.* (1996) translated the geologic maps into English. This terrane contains Archean to Paleoproterozoic crystalline basement rock and during the early Cambrian was located south of the equator at low latitude between the North China and Siberia cratons (Cocks and Torsvik, 2007; Bold *et al.*, 2016). During the Ediacaran, arc accretion transformed the southern passive margin to a foreland basin, which created the Zavkhan Basin located southwest of the city of Uliastai (Fig. 2.3A). Approximately 1 km of Cambrian sedimentary material was overlain on Ediacaran deposits and weakly metamorphosed due to later Paleozoic orogenies and plutons in the region (Bold *et al.*, 2016).

The Neoproterozoic and Cambrian formations within the Zavkhan Basin include the Zuun-Arts, Bayangol, Salaagol, and Khairkhan formations (Fig. 2.3B). The Zuun-Arts and Bayangol Formations are mixed carbonate-siliciclastic successions underlying the reef-bearing Salaagol Formation central to this study. I use the term reef here in the broad sense of a mutually attached association of framework-building organisms (Riding and Zhuravlev, 1995). The Salaagol Formation (alternative spelling Salaany Gol) is ~400 m thick with several microbial-metazoan boundstone fabrics present and minor interbeds of silt and conglomerate (Smith *et al.*, 2016). Boundstones have a patchy distribution, but display a diverse array of assemblages (Wood *et al.*, 1993). The Salaagol Formation is overlain by the siliciclastic-dominated Khairkhan Formation. The Salaagol Formation was studied at two localities, locality 5 at Salaa Gorge (Fig. 2.3C; 46° 48.805' N 95° 46.306' E) and locality 6 near Zuun-Arts Ridge (47° 17.519' N 96° 30.950' E).

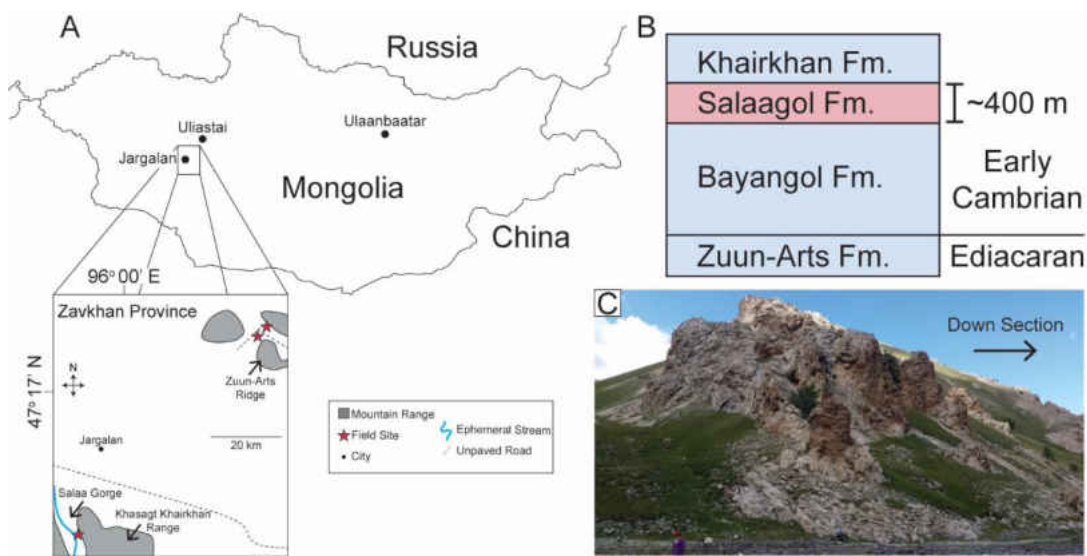


Figure 2.3: Field localities and stratigraphy in Mongolia. A, Map of Mongolia with detailed insert. Red stars denote field localities 5 and 6 (two stars). B, Schematic regional stratigraphic context column, see figure 2.7 for details. C, Outcrop at top of Salaagol Formation at Salaa Gorge.

Materials and Methods

Sampling strategy.— Fist-sized samples were collected at ~1 to 5 m intervals depending on the stratigraphic thickness and accessibility of the outcrop. A total of 201 orientated samples were collected (132 from White-Inyo region and 69 from Mongolia). One transect was performed at each locality, except for Stewart’s Mill where four transects were performed in order to capture the spatial variability of the locality. In addition, one large slab (12 x 10 x 7 cm) was collected to verify point counts on a larger sample from the White-Inyos. Total surface area of one slab surface and the proportion of surficial archaeocyaths present were calculated using ImageJ. Four slides with abundant *Epiphyton*-group were also examined to quantify growth direction from the Mongolian samples.

Archaeocyath size distribution was measured to test for changes in morphology across localities. All archaeocyaths preserved in cross section within three 1 x 1 m quadrants were measured at Stewart's Mill and Gold Point Hills. Measurements of archaeocyath size from Mongolia were performed on cut slabs in the lab. Four measurements on each specimen were taken: (1) body diameter on the longest axis, (2) osculum diameter on longest axis, (3) body diameter on axis perpendicular to first axis, and (4) osculum diameter on axis perpendicular to first axis. The two body diameters were averaged, and the two osculum diameters were averaged to decrease bias from archaeocyaths bisected at an angle. The osculum: body ratio (OBR) was also calculated, as this has been shown to be controlled by environmental factors with larger ratios being found in lower energy environments (Savarese, 1995).

Thin section point counts.— A total of 174 petrographic thin sections were analyzed using plane- and cross-polarized microscopy. On each thin section a series, 200 for White-Inyos and 300 for Mongolia, of regularly spaced points were viewed and the grain type at each point was counted to assess changes in carbonate contribution (Pruss *et al.*, 2010, 2012; Pruss and Clemente, 2011). In this study I counted clotted features that could positively be attributed to microbial form genera as calcifying microbes and any featureless, granular microcrystalline material as simply micrite or granular micrite. This method is useful for identifying both abundant and minor contributors of a reef ecosystem that may not be observable in outcrop alone. Staining with Alizarin red S and potassium ferricyanide (ARSPF) was used on selected slides to help distinguish carbonate mineralogy. Alizarin red S distinguished between calcite and dolomite whereas potassium ferricyanide distinguished between ferrous and non-ferrous carbonate (Dickson, 1965). With rare exceptions, species level identification in thin sections is

challenging due to disarticulated specimens. Therefore, broad, often phylum level, designations such as 'echinoderm' or 'trilobite' were used when point counting. Taxonomic identification of archaeocyaths and reef-dwelling organisms is beyond the scope of this study, however, a number of unique morphological forms of archaeocyaths were recognized, but not identified to genus level. The taxonomic identification of organisms will not affect the results of this study as all metazoan framework builders, calcifying microbes, and reef-dwelling organisms are either grouped together for studying trends in carbonate contribution changes or grouped into polyphyletic functional groups.

Biodiversity metrics.— While point counting may not represent the true number of individuals in an environment, because large grains can be counted multiple times, an increase in contribution to carbonate fabrics can still be used as a proxy for abundance and the distribution of abundance across taxa in an ecosystem. This allows for a reasonable calculation of biodiversity change (Wu *et al.*, 2017). Therefore, taxonomic richness (S), evenness, and Shannon's diversity were calculated from point count percentages. For this study I used Pielou's evenness index which is defined as: $E = \frac{H'}{\ln(S)}$. Shannon's diversity index is defined as: $H' = -\sum_{i=1}^S p_i \ln p_i$. Again, because these biodiversity metrics are calculated from percent contribution, as opposed to individuals and are based on high taxonomic ranks, they may not be comparable to other biodiversity studies. They still provide for a comparison within this study and to methodologically similar studies for changing biodiversity levels. Additionally, 9,999 permutations were run on all biodiversity statistics to determine 95% confidence intervals.

Functional diversity.— In addition to taxonomic diversity, functional diversity can reveal more about the types of ecological interactions occurring in an ecosystem. For this study, I define ecological function as the ecological role of a species within an ecosystem (Jax, 2005). Functional groups can be defined based on a number of different ecological characteristics and organisms that have the same states for each of these characters are considered a single functional group. From this, functional richness can be defined as the number of functional groups present. Functional evenness is a measure of the abundance of organisms spread across all of the functional groups (akin to ecological overlap) and has been shown to be useful in determining susceptibility of an ecosystem to environmental changes (Dineen *et al.*, 2014). Finally, functional diversity is similar to Shannon’s diversity, except using functional evenness and functional richness. Based on nine characters from previous studies and three new to this study a total of 12 ecological characters and 36 character states were defined (Novack-Gottshall, 2007; Dineen *et al.*, 2014). Characters used here are based on: (1) substrate composition, (2) substrate attachment, (3) substrate microhabitat, (4) sediment consolidation ability, (5) mobility, (6) condition of food, (7) feeding habit, (8) diet, (9) feeding energetics, (10) rigidity, (11) wave resistance, and (12) size. Additional descriptions of characters and states as well as all coding can be found in the Appendix C and Table C1.

Statistical analysis.— Mann-Whitney *U* tests were used to compare archaeocyath size. Spearman’s rho and Kendall’s tau were calculated to determine if the proportion of framework-building organisms is correlated with the proportion of reef-dwelling metazoans other than framework builders (hereafter termed reef dwellers) and microbes in the reef. Selected diversity t-tests were also performed to determine significantly different communities based on

Shannon's diversity. A non-metric multidimensional scaling (NMDS) with Bray-Curtis similarity was performed to determine samples that are similar to each other based on the proportions of metazoan framework builders, reef dwellers, calcifying microbes, and abiotic grains. NMDS is preferred over principal component analysis in situations where data are not linearly correlated (Clapham, 2011). A MANOVA analysis with Bonferroni-corrected pairwise comparisons was also performed on these data to determine statistically significant localities. Finally, a Kolmogorov-Smirnov test with permutation resampling was used to determine if concentrations of fauna had distinct distributions within Mongolia localities. Shapiro-Wilk's tests were used throughout to determine whether parametric or non-parametric analysis should be used. All statistical analysis was performed in *PAST 3.14* software (Hammer *et al.*, 2001).

Geochemistry.— Stable carbon isotopes from carbonate material were measured on a Picarro Cavity Ring Down Spectrometer (N = 121). Micrite samples were powdered with a diamond tipped drill while avoiding recrystallized areas. Approximately 3 mg of powder were placed in septum-capped vials, which were then evacuated. Next, approximately 3 ml of 10% phosphoric acid were injected and allowed to react for a minimum of 12 hours. NBS19 and two laboratory standards were used to calibrate measurements and control for drift. All samples were run in duplicate and averaged. The standard deviation of sample replicates averaged < 0.1‰.

An Agilent 7500 series ICP-MS was used to measure trace elemental compositions of 137 samples in order to constrain paleoenvironmental conditions and diagenetic alteration. Approximately 2 mg of powdered sample (same as for isotopes) was acidified in 1 ml of 0.32 M trace metal grade nitric acid for 3 - 4 hours. After centrifuging, 0.5 ml of sample was removed

and diluted to 10 ml. Samples were run with 10% replication and 10% blanks. All samples were analyzed for Na, Mg, Al, Ca, Mn, Fe, Sr, Mo, Th, V, and U. Elemental abundances are normalized to concentrations of calcium and magnesium to account for the amount of carbonate dissolved (e.g., Marenco *et al.*, 2016). Normalized abundances are then reported as X_{element} , where $X_{\text{Mo}} = \text{Mo}/(\text{Ca}+\text{Mg})$, and multiplied by either 10^6 or 100 to be reported as ppm or percentages.

Strontium often substitutes for calcium within carbonate rocks. Manganese on the other hand is rare in unaltered carbonates because of its low availability in seawater. As fluid flow within carbonate sediments and rocks alters the chemical composition of a carbonate rock Sr will decrease and Mn will increase. Thus, the ratio of these two elements is typically used as an indicator of alteration. Montanez *et al.* (1996) considered samples with Sr/Mn ratios greater than two reliable sources of original geochemical signatures. For this study, Sr/Mn values less than one are considered to be altered. $X_{\text{Na+Al}}$ was measured to assess terrestrial input variations with values > 1% excluded due to potential for siliciclastic leaching.

In shale deposits, the concentration of redox-sensitive elements is closely tied to local oxygen levels of the oceans (Jin *et al.*, 2016). In carbonates, the abundance of redox-sensitive elements, such as uranium, molybdenum, and vanadium, are largely controlled by their global availability in seawater (Emerson and Huested, 1991; Brennecka *et al.*, 2011; Romaniello *et al.*, 2013; Marenco *et al.*, 2016). Because redox-sensitive elements are removed from seawater in reducing shale environments, their dissolved inventories in the global ocean will decrease if anoxic deposition increases in the oceans (e.g., Marenco *et al.*, 2016). Thus, I use changes in these redox-sensitive elements in carbonates as indicators of changes in global redox.

Furthermore, many redox-sensitive element studies have been performed in shale deposits, but

fewer in carbonates (though see Pagès and Schmid, 2016). This study will provide insight into oxygenation of different paleoenvironments. Mo and V, however, will have a muted response compared to U because of low concentrations in carbonate, but serve as a useful check on changes in U concentration. Because redox-sensitive elements are removed from seawater in reducing shale environments, changes in global ocean redox affects the dissolved availability of these elements in seawater such that decreases in the U and Mo content of carbonates reflect more reducing conditions in the deep ocean (e.g., Brennecke *et al.*, 2011, Marenco *et al.*, 2016).

Results

Faunal carbonate contributions

To first assure thorough sampling, a comparison of standard error against sample size was performed. Standard error decreases with increasing sample size, but typically reaches a minimum after which addition of more samples does not reduce standard error (Pruss and Clemente, 2011). Flattening of standard error changes suggests that outcrop was sufficiently sampled at our localities (Fig. 2.4). Despite a heterogenous habitat, our dataset approached the minimum standard error for metazoan framework builder contributions, suggesting a well-sampled dataset and allows for analysis of quantitative trends.

White-Inyos.— Metazoan framework builders were observed in outcrop in the Montenegro Member at the Bristlecone Trail, however, they are too sparse to be found in thin section (Fig. 2.5A). The Montenegro Member bioherms are instead dominated by micrite. The Bristlecone Trail locality also contains a portion of the Lower Poleta Formation and this interval was treated as a distinct unit from the underlying Montenegro Member. The Poleta Formation

observed at the Bristlecone Trail (Fig. 2.5A), Stewart's Mill (Fig. 2.5B), and Westgard Pass (Fig. 2.5C) contains eight samples with at least 10% metazoan framework-builder skeletons. Furthermore, this formation has a larger component of carbonate from calcifying microbes. Concentrations of metazoan framework builders occur in clusters throughout the formation. For example, at Stewart's Mill metazoan framework builders are most prevalent between 15 - 25 meters and between 40 - 60 meters above the base of the formation (Fig. 2.5B). This pattern is consistent across different transects (Fig. 2.6). Finally, the reef-building interval of the Harkless Formation contains high amounts of framework builders, with all slides containing at least 16.5% framework (Fig. 2.5D).

Skeletal grains comprised 12.3% of point counts while the remaining 87.7% was composed of micrite (79.8%), sparry cement (4.9%), and clastic grains (3.0%). Carbonate contribution from metazoans framework-building organisms was 4.2% across all thin sections (Table A1). The Montenegro Member thin sections contained no metazoan framework builders, the Poleta Formation contained an average of 2.7% (14.5% from Bristlecone Trail, 0.5% from Westgard Pass, and 3.0% from Stewart's Mill), and the Harkless Formation contained 29.7%. Slab surface measurements indicate that metazoan framework builders make up 15.5% of carbonate contribution. However, hardened spicule material comprises only 30 - 35% of the volume of a sponge (Meroz-Fine *et al.*, 2005). Using these estimates, the slab surface was made of 3.8 - 5.3% metazoan framework builders. All other bioclast elements of thin sections contributed 7.9% (6.6% from microbes and 1.3% from reef dwellers) of carbonate material.

Of the skeletal grains, contributions from metazoans came from archaeocyaths (33.3%), echinoderms (12.3%), coralomorphs (10.7%), trilobites (1.2%), and brachiopods (0.4%). The

remaining skeletal elements were composed of calcifying microbes (42.1%) (*Renalcis?*). Two distinct genera of archaeocyaths (archaeocyath gen. 1 *cf. Protopharetra*, archaeocyath gen. 2 *cf. Paranacyathus*) were observed at Stewart’s Mill and two additional genera were observed in the Harkless Formation (archaeocyath gen. 3 *cf. Metaldetes*, archaeocyath gen. 4 *cf. Diplocyathellus*). The coralomorph *Harklessia yuenglingensis* was observed only in the Harkless Formation. Reef-dwelling organisms such as lingulids and echinoderms, most likely eocrinoids, helicoplacoids, and/or edrioasteroids, were sparsely spread though all intervals and minor compared to archaeocyaths (Dornbos, 2006).

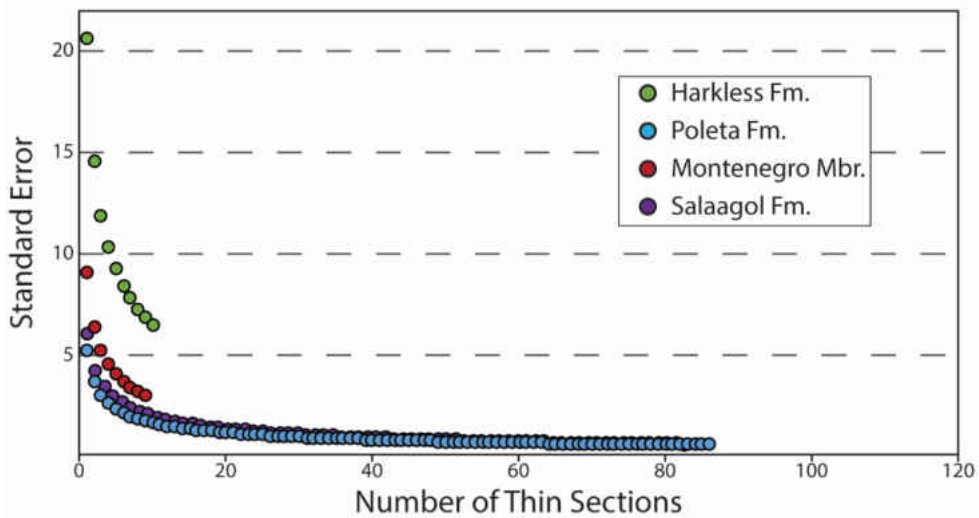


Figure 2.4 Sensitivity analysis of thin section point counts. Based on metazoan framework builder contributions.

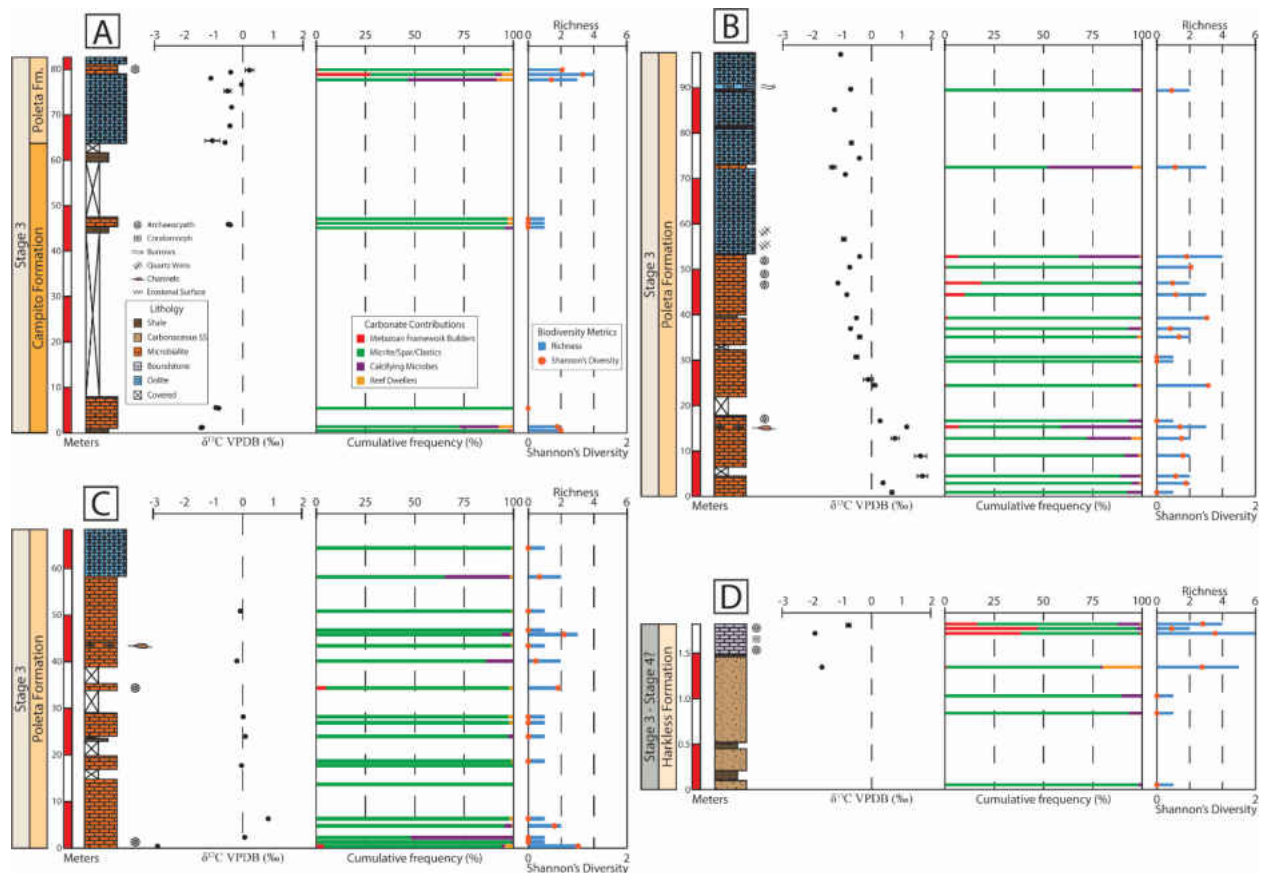


Figure 2.5: Point count data for White-Inyo Mountains region. Stratigraphic columns with data collected from point count and carbon isotope analysis. A, Bristlecone Trail. B, Westgard Pass. C, Stewart's Mill. D, Gold Point Hills. For all columns from left to right: lithology, stable carbon isotope data (VPDB) with error bars (data points without error bars have error smaller than symbol), percent contribution of carbonate material from percentage of points in thin section point counts, and biodiversity indices. Lithology symbols shown in A apply to all portions of figure.

Table 2.1: Average contribution percentages for thin section point count analysis.

Formation/Locality	Framework Builders	Microbial	Other Fossils
Montenegro Mbr.	-	4.3 ± 7.9	2.4 ± 2.8
Poleta Fm.	2.7 ± 5.8	6.9 ± 11.4	1.1 ± 1.8
Harkless Fm.	29.7 ± 13.5	7.0 ± 5.5	0.5 ± 0.5
White-Inyo Total	4.2 ± 9.7	6.6 ± 10.8	1.3 ± 2.6
Lower Salaa Gorge	-	13.6 ± 8.5	0.2 ± 0.5
Upper Salaa Gorge	4.9 ± 5.2	2.3 ± 5.9	0.0 ± 0.2
Zuun-Arts Ridge	6.1 ± 7.1	6.1 ± 9.2	0.5 ± 0.8
Mongolia Total	5.0 ± 6.3	5.4 ± 8.6	0.3 ± 0.7

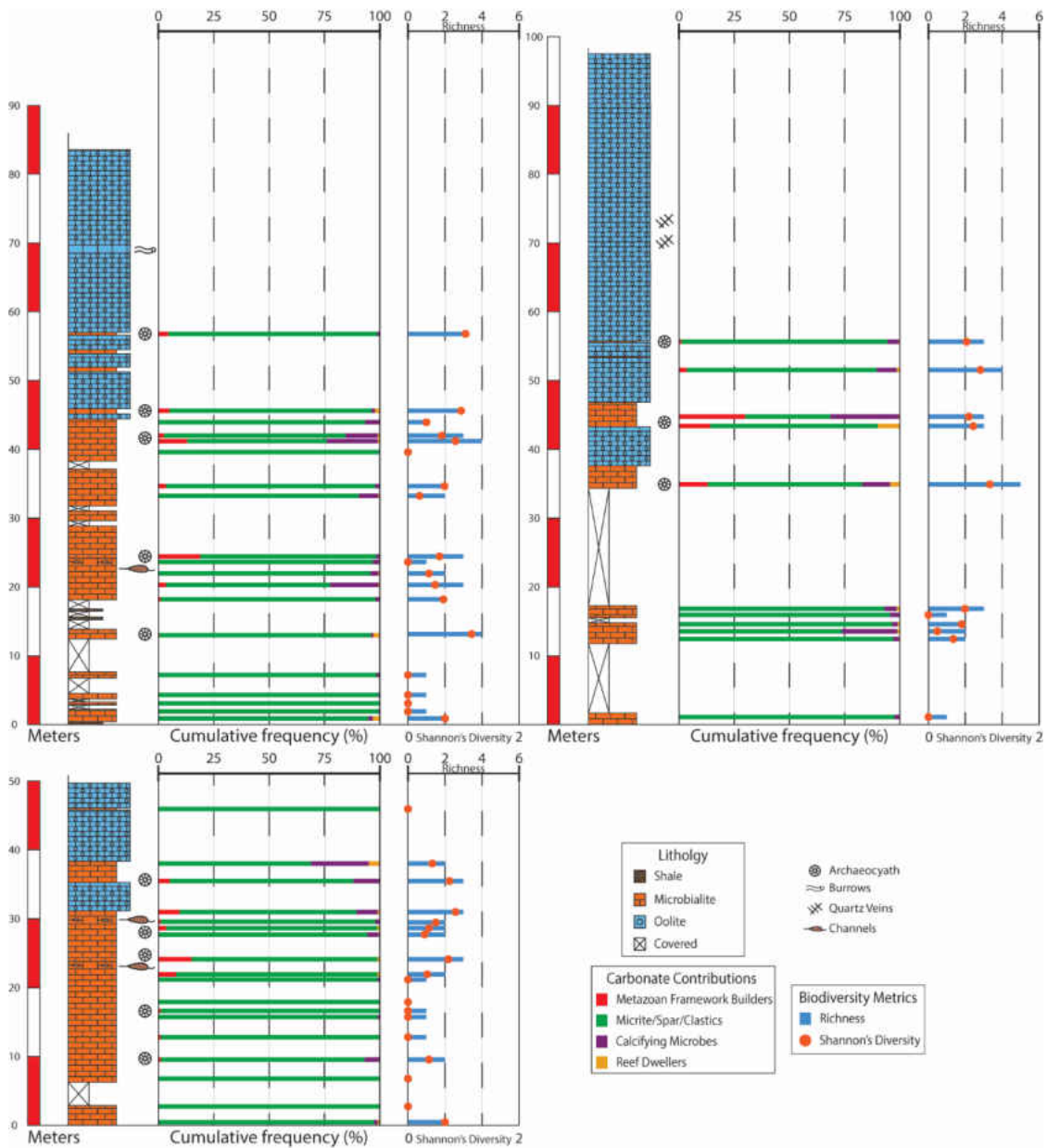


Figure 2.6: Additional transects at Stewart's Mill. Showing lithology, carbonate contribution, and biodiversity. Top left = southeast face; top right = north face; bottom left = south face.

Western Mongolia.— Micrite/microspar, clastic material, and sparry calcite were the largest contributors to material in the Salaagol Formation at 89.3%, while microbial fabrics (all forms), archaeocyaths, and other fossils were the next most common contributors at 5.4%, 5.0%, and 0.3% respectively (Table 2.1). These contributions were unevenly distributed across

the upper and lower Salaa Gorge locality (treated as two localities for statistical analysis due to the large missing section) and Zuun-Arts Ridge. All sections are largely composed of microspar. But other than microspar, the lower Salaa Gorge contained only microbial material (13.6%) while the upper Salaa Gorge contained more archaeocyaths (4.9%) than microbes (2.3%). Zuun-Arts Ridge contained more fossil material overall with the largest concentrations of microbes, archaeocyaths and other fossils all found higher in the section, though lower in the section archaeocyaths were occasionally common (Fig. 2.7; Table A2).

Previous research found upwards of two dozen archaeocyathan species in the Zuun-Arts Ridge locality (Voronin *et al.*, 1983). Additional studies of the Salaa Gorge found assemblages dominated by *Archaeopharetra* and *Cambrocyathellus* with contributions from >30 other genera (Kruse *et al.*, 1996). In this study, there are at least six archaeocyathan genera. The most common genus (~45% of archaeocyathan point counts) is *Cambrocyathellus* sp. 1 (Fig. 2.8A and C). *Cambrocyathellus* sp. 1 had large cups (3-8 mm), porous pseudosepta and one row of simple pores per inner wall intersept (Debrenne *et al.*, 2015). *Cambrocyathellus* sp. 1 was primarily found at the Zuun-Arts Ridge locality (Fig. 2.8C). Secondary but substantial contributions came from *Archaeopharetra*, *Cambrocyathellus* sp. 2, and *Okulitchicyathus* contributing approximately 24.5%, 20%, and 7.5% respectively (Fig. 2.8B). *Archaeopharetra* was found throughout both sections and had a concentrically porous outer wall and occasional segmented tabulae (Debrenne *et al.*, 2015). *Cambrocyathellus* sp. 2 had completely porous septa which thickened at the inner wall and a massively thickened anchoring process (Debrenne *et al.*, 2015). *Okulitchicyathus* had a characteristic wavy cup-shape with porous pseudosepta (Debrenne *et al.*, 2015). Minor, isolated, specimens of *Degeletticyathus?*, *Nochoroicyathus*, and

Ajacyathus were also present. The genera found in this study are similar to past studies, however, the point counts allowed for a more detailed analysis of relative contributions. Other archaeocyathan genera may have been present but were not preserved in the analyzed thin sections.

Subtifloria (24.2% of microbial point counts) was only found in the lower Salaa Gorge. *Subtifloria* resembles bundles of wavy, parallel striations directly connected to one another or, in cross-section, circular, reticulate patterns (Fig. 2.8D). Throughout the formation, at least three other microbial forms were observed *Tarthinia* (23.5%), *Renalcis*-group, and *Epiphyton*-group (52.2% collectively). *Tarthinia* has an irregular, clotted micrite texture that darkens distally (Fig. 2.8E). *Epiphyton*-group calcimicrobes have a dark (micrite) microstructure and dendritic morphology (Fig. 2.8F) and are commonly attached to archaeocyaths.

Two semi-circular, thin-walled calcitic shells are preserved (Fig. 2.8G and H). These could represent a conical tube-dwelling fauna or other small shelly fossils. Two potential brachiopod fragments were found. Several void spaces secondarily filled with sparry calcite were concentrated in the upper Zuun-Arts Ridge locality and may be from replaced skeletal material (Fig. 2.8I).

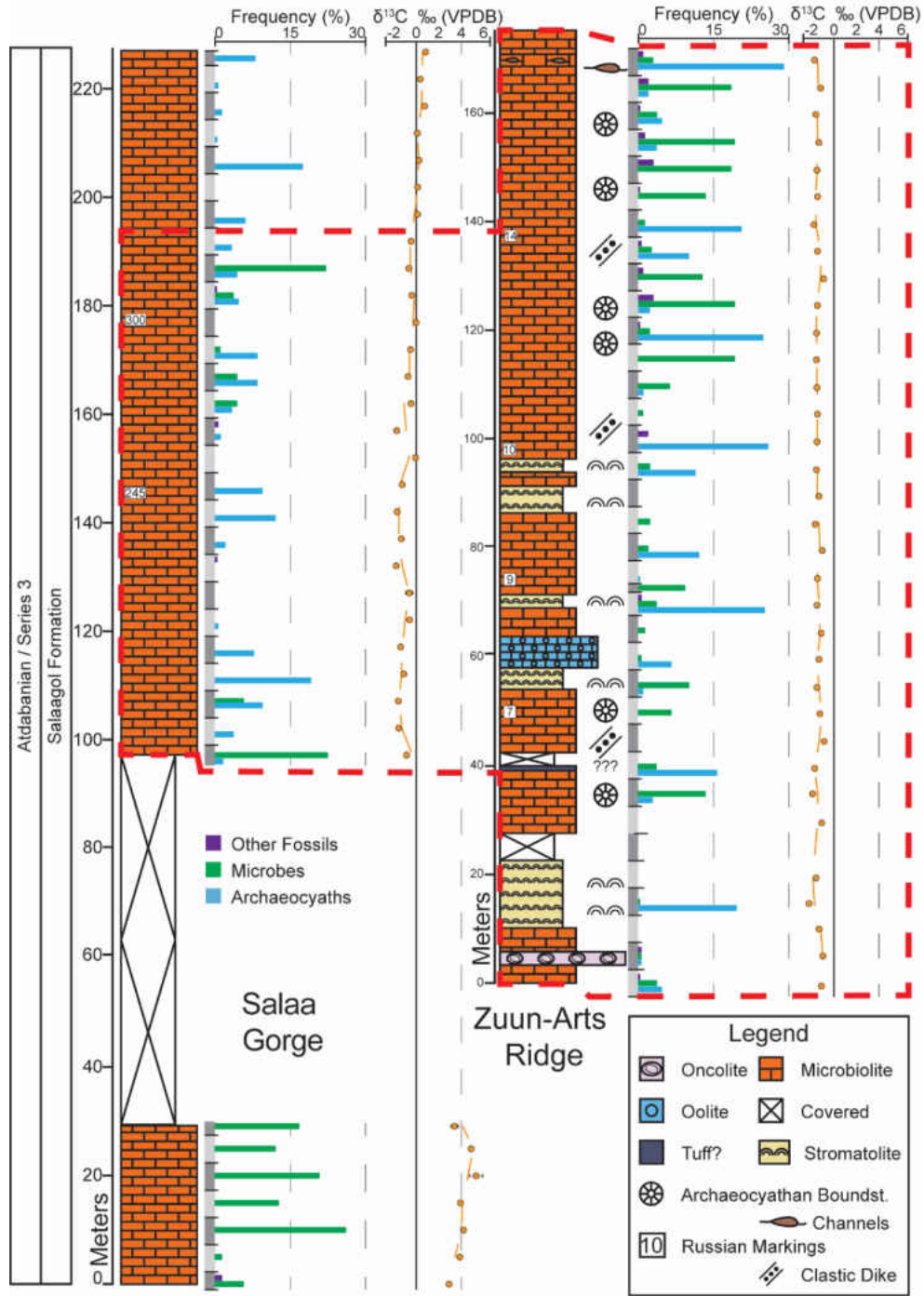


Figure 2.7: Point count data for Mongolia. Stratigraphic column for Salaagol Formation in Salaa Gorge and Zuun-Arts Ridge with lithology, point count data from thin section, and stable carbon isotopes (VPDB) with three point moving averages. Data points without error bars have error smaller than symbol. Red line denotes stratigraphic correlation between sites based on isotopes and trace elements. Zuun-Arts locality represents an expanded section of Salaa Gorge.

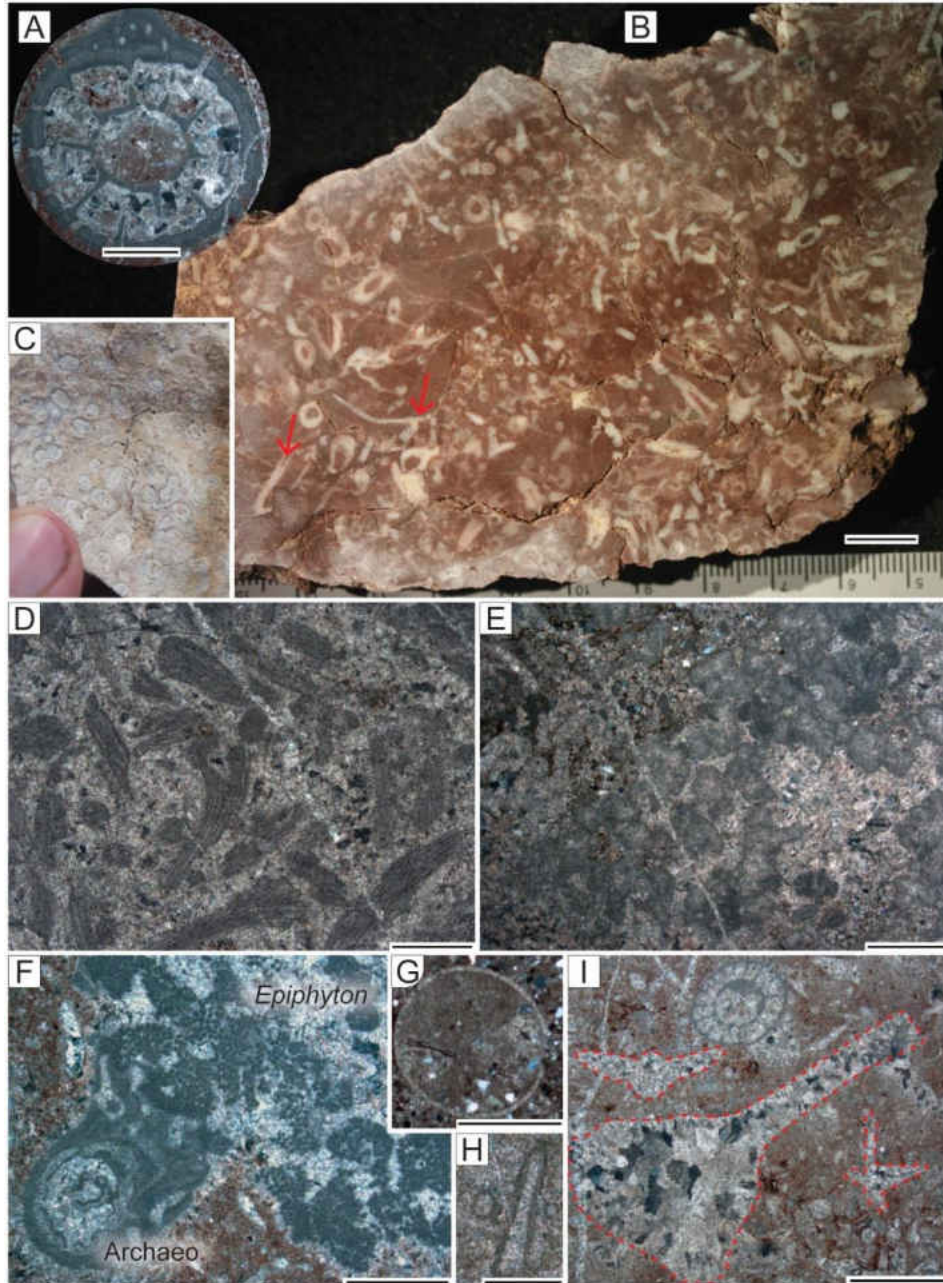


Figure 2.8: Fauna from the Salaagol Formation in Mongolia. A, *Cambrocyathellus* sp. 1 from Salaa Gorge. B, Polished slab from Zuun-Arts Ridge showing numerous fragments of archaeocyathan debris. *Okulitchicyathus* showed by red arrows. C, *Cambrocyathellus* sp. 1 from Zuun-Arts Ridge showing bifurcation of cups. D, *Subtifloria* longitudinal and transverse cross-sections from lower Salaa Gorge. E, *Tarthinia*. F, *Epiphyton*-group microbe *Gordonophyton* attached to archaeocyath. G, Unidentified circular calcitic fossil. H, Unidentified conical fossil. I, Secondarily neomorphosed grains (red outlines) with sparry calcite. Shape of void space similar to chancelloriid or SSF fragments. Scale bars equal 0.5 mm for A, D, E, G, and H; 1 mm for B, F, and I; finger for C.

Archaeocyath size distribution

White-Inyos.— A total of 478 archaeocyaths were measured, 223 at Stewart's Mill and 255 at Gold Point Hills (Fig. 2.9A and C). Median body size at Stewart's Mill and Gold Point Hills was 8.5 mm and 13.5 mm respectively and this difference was statistically significant based on a Mann-Whitney *U* test (p -value = 8.02×10^{-25}). Furthermore, the OBR increased from 0.39 to 0.48 between the two locations (p -value = 4.85×10^{-11}). Both areas displayed very strong relationships between osculum and body diameters (Fig. 2.9B and D).

Western Mongolia.— Median body size of 133 archaeocyaths from Mongolia was 3.69 mm and was significantly smaller than White-Inyo archaeocyaths (p -value = 6.14×10^{-42}) regardless of formation (Poleta Formation: p -value = 1.14×10^{-17} ; Harkless Formation: p -value = 2.44×10^{-44}). In addition, OBR for Mongolia was 0.47 and again was significantly different from the White-Inyo archaeocyaths as a whole (p -value = 0.002), but was only significantly different from the Poleta Formation and not the Harkless Formation (Poleta Formation: p -value = 2.22×10^{-09} ; Harkless Formation: p -value = 0.87). Mongolian archaeocyaths were smaller, but had larger osculum relative to body size than Laurentian archaeocyaths in this study (Fig. 2.9E and F).

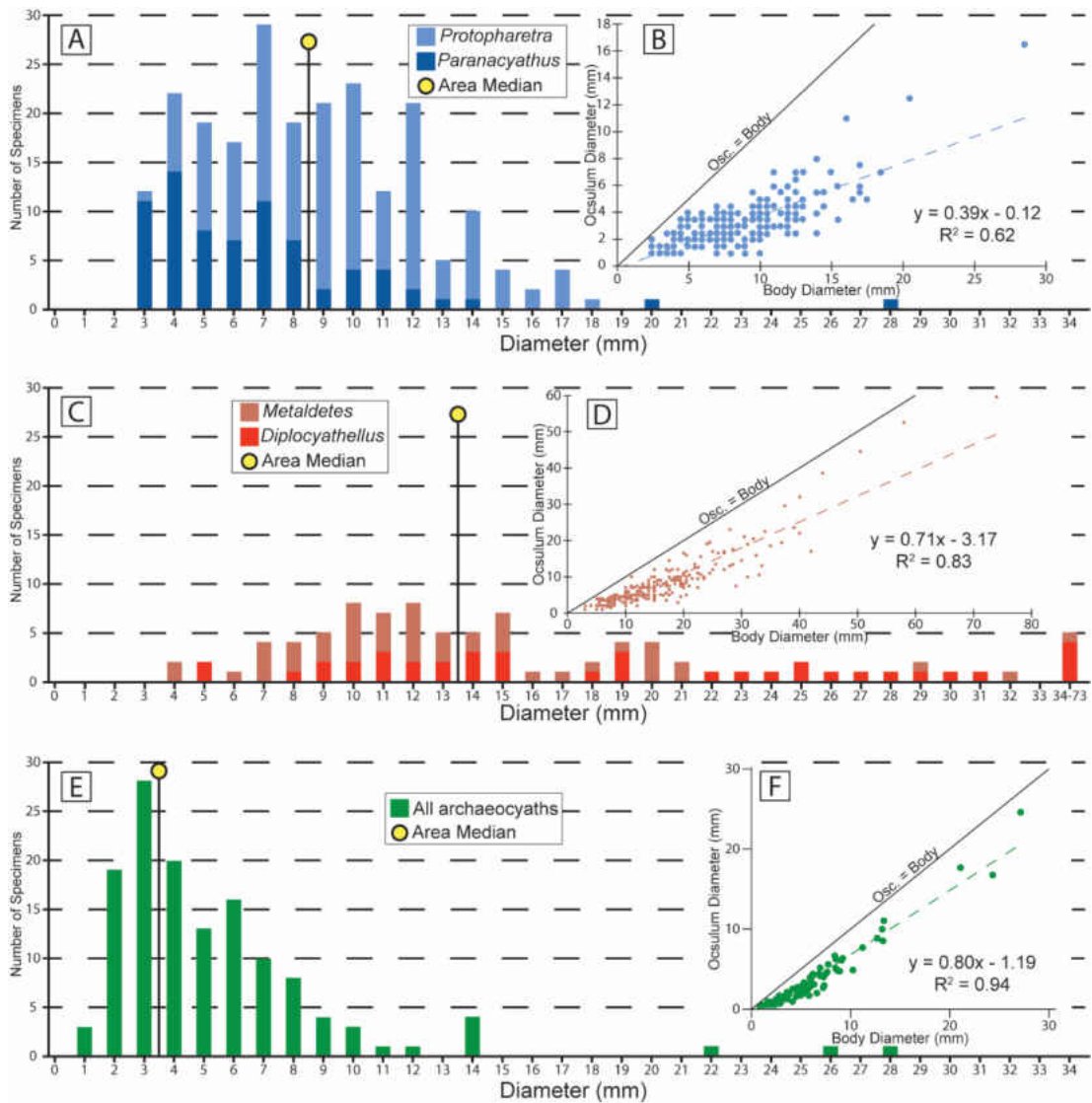


Figure 2.9: Archaeocyath size distribution data. A and B, Stewart’s Mill. C and D, Gold Point Hills. E and F, Mongolia. Histograms (A, C, and E) displaying archaeocyath body size. Note bin size change at far right of C. Ratio of osculum size to body size shown in B, D, and F for their respective areas.

Biodiversity metrics and statistics

White-Inyos.— Shapiro-Wilks tests found that the data do not have a normal distribution and therefore only non-parametric statistics could be used. The results from correlation tests failed to reject the null hypothesis that microbes or reef-dwelling organisms are randomly distributed with respect to metazoan framework-building organisms. Based on

Spearman's rho ($\rho = 0.05$, p -value = 0.58) and Kendall's tau ($\tau = 0.08$, p -value = 0.24) calcifying microbial organism distribution was not correlated with metazoan framework builders. The same tests ($\rho = 0.02$, p -value = 0.80, $\tau = 0.08$, p -value = 0.25) were not found to be significant for reef-dwelling organisms and metazoan framework builder distributions.

Western Mongolia.— While the overall proportion of microbial and archaeocyathan material was not statistically different across the whole formation (Table 2.2; Mann-Whitney p -value = 0.145), the distribution of where material was found was statistically different (Kolmogorov-Smirnov p -value = 0.044). The lower Salaa Gorge locality was statistically different from both other localities driven by higher concentrations of microbial material (Fig. 2.7; Table E2). Finally, a Spearman's rank test failed to reject the null hypothesis that reef-dwelling organisms and archaeocyaths were not correlated to each other (p -value = 0.68).

All localities.— Biodiversity varied substantially across reef building environments (Table 2.2 and Fig. 2.10). The Montenegro Member had the lowest Shannon's diversity. The Poleta Formation in general had higher Shannon's values than the Montenegro Member reefs (Fig. 2.10; Table 2.2). The Harkless Formation had the highest diversity observed in this study (Fig. 2.10). Evenness was highest in the Montenegro Member and Harkless Formation with a decrease in the Poleta Formation (Fig. 2.10). The Salaagol Formation had a higher Shannon's diversity than the Montenegro Member, but was smaller than the Harkless Formation making it more similar to the Poleta Formation (Table 2.2). Evenness was more similar to the Poleta Formation than the other two, but the Salaagol Formation had a lower richness than the Poleta Formation (Table 2.2).

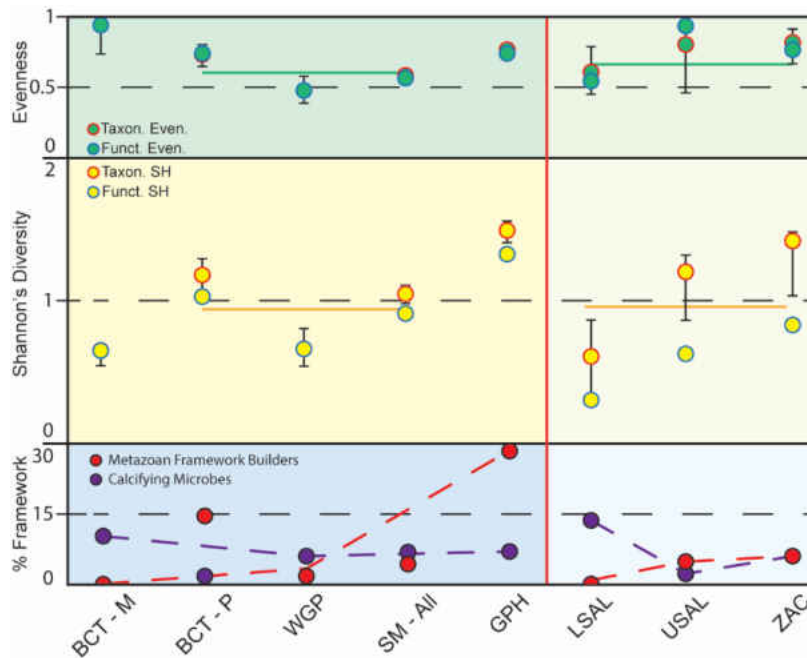


Figure 2.10: Biodiversity statistics for all localities. Evenness (upper), Shannon’s diversity (middle), and framework percentages (lower) across localities. Error bars represent 95% confidence intervals, shown for taxonomic (red outlines) biodiversity only. Functional biodiversity (blue outlines) occasionally directly overlap taxonomic biodiversity values. Horizontal bars represent entire Poleta or Salaagol Formation, dashed line shows regional trend. BCT-M = Montenegro Member at Bristlecone Trail; BCT-P = Poleta Formation at Bristlecone Trail; WGP = Poleta Formation at Westgard Pass; SM – All = Poleta Formation at Stewart’s Mill (all transects); GPH = Harkless Formation at Gold Point Hills; LSAL = Salaagol Formation at Lower Salaa Gorge; USAL = Salaagol Formation at Upper Salaa Gorge; ZAC = Salaagol Formation at Zuun-Arts Ridge.

Table 2.2: Biodiversity statistics across lithological units.

Metric	Montenegro Mbr.	Poleta Fm. at BCT	Poleta Fm. at WGP	Poleta Fm. at SM	Harkless Fm.	Salaagol Fm.
Richness	2	5	4	6	7	4
Evenness	0.941	0.733	0.478	0.583	0.767	0.691
Diversity	0.652	1.18	0.663	1.045	1.492	0.959
Function Rich	2	4	4	5	6	3
Function Evenness	0.941	0.743	0.478	0.566	0.741	0.683
Function Diversity	0.652	1.029	0.663	0.910	1.327	0.751

First three rows are taxonomic richness, evenness and Shannon’s diversity. Bottom three rows are richness, evenness and Shannon’s diversity based on functional groups. BCT = Bristlecone trail; WGP = Westgard Pass; SM = Stewart’s Mill.

NMDS was conducted with proportions of metazoan framework builders, calcifying microbes, reef-dwelling organisms, and abiotic material (2D stress = 0.1068, see Figure E1 for Shepard's plot). While there is a significant amount of overlap, the four formations show a general shift towards the upper left corner of the graph, and samples generally cluster by formation (Fig. 2.11). A MANOVA test (p -value = 4.615×10^{-20}) and pairwise comparisons show the Harkless Formation reefs are significantly different in carbonate fabrics compared to any other formation (Table E1). Again the Salaagol Formation is most similar to the Poleta Formation.

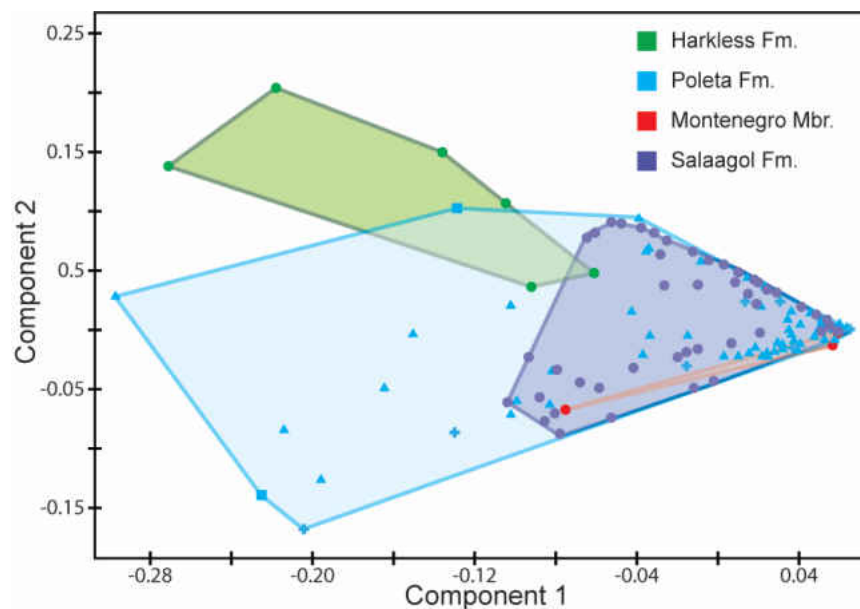


Figure 2.11: Non-metric multidimensional scaling of lithofacies composition. Lithological units enclosed in convex hulls. triangle = Stewart's Mill; plus sign = Westgard Pass; square = Bristlecone Trail.

Functional groups

The taxa found in this study were divided into six functional groups based on the 12 character criteria devised for this study (see Appendix C). All organisms were found to have a unique functional role in their environments, apart from the archaeocyaths, which were

grouped as one. Functional diversity and evenness were similar to taxonomic diversity and evenness statistics (Fig. 2.10).

Geochemistry

White-Inyos.— Stable carbon isotope data averaged -0.37 ± 0.07 VPDB (Table B1). A positive excursion of $\sim 2 - 3$ ‰ occurs in the lower Poleta Formation in both Stewart's Mill (Fig. 2.12B) and Westgard Pass (Fig. 2.12C). Sr/Mn ratios averaged 1.18 with lower values mostly isolated to the Harkless Formation and sporadically in the Poleta Formation. Relatively high Sr/Mn values are present during the positive carbon isotope excursion. $X_{\text{Na+Al}}$ concentrations averaged 0.31% and slightly elevated periods co-occur with higher concentrations of archaeocyaths (Fig. 2.12). The lower Harkless Formation had high abundances of $X_{\text{Na+Al}}$ and was excluded from further elemental analysis as they possibly represent carbonate-cemented siliciclastics. Th/U ratios averaged 6.9 and correlate poorly overall with changes in $X_{\text{Na+Al}}$ concentrations (Pearson's $r = 0.34$). X_{U} and X_{Mo} concentrations (Fig. 2.12) did not appear to vary based on the presence or absence of any particular sedimentary facies or fauna. However, Th/U exhibited the highest sustained average values and X_{U} and X_{Mo} exhibited the lowest sustained average values coincident with the positive carbon isotopic anomaly (Fig. 2.12). Finally, X_{Mg} averaged 3.11 and only exceeded 10 in three samples (Table B1).

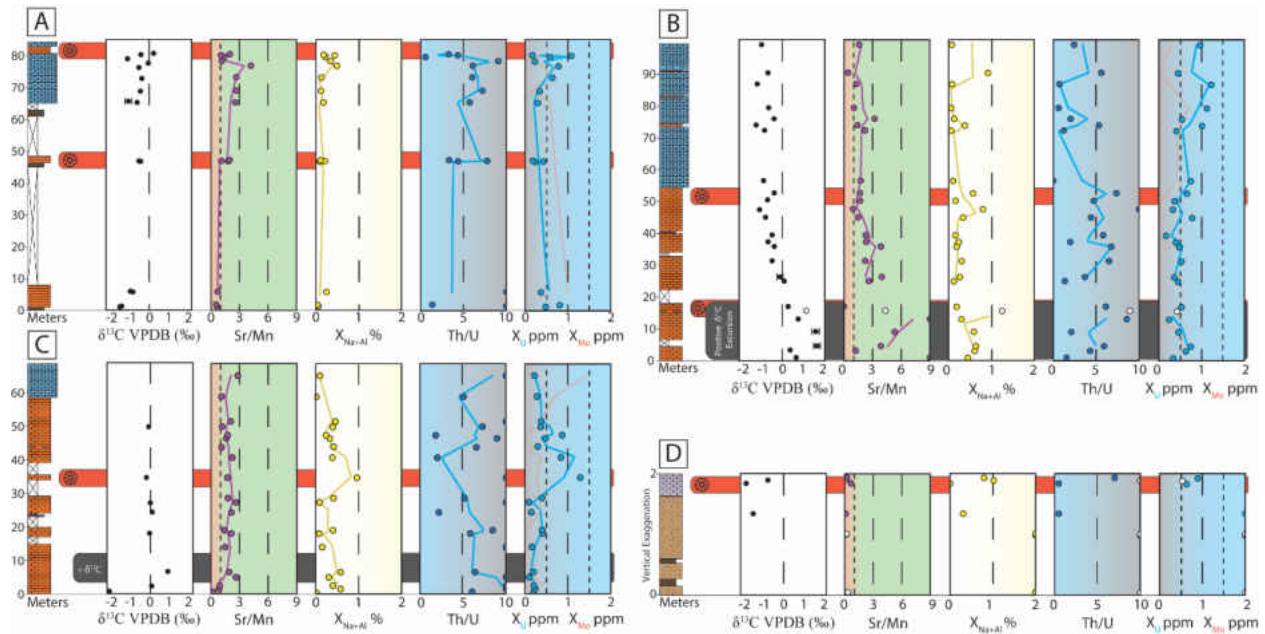


Figure 2.12: Trace element data for White-Inyo Mountain region. A, Bristlecone Trail. B, Westgard Pass. C, Stewart's Mill. D, Gold Point Hills. Lithology and archaeocyath occurrences shown as orange bars. Samples with $> 1\%$ X_{Na+Al} shown with hollow circles and excluded from trendlines. Trendlines show three-point moving averages. Right most columns show X_U (blue line and data points) and X_{Mo} (orange line). Data points at rightmost edge are greater than scale of plot. See Table B1 for complete dataset.

Western Mongolia. — The lower Salaa Gorge has a positive carbon isotopic composition around 4-5‰ VPDB (Fig. 2.13). Above the missing section of the Salaa Gorge, isotopic composition was around -1‰ VPDB before rising slightly to 0.8‰ VPDB. Carbon isotopic composition at Zuun-Arts Ridge was static and more similar in value to the middle upper Salaa Gorge (Fig. 2.13).

The rise in carbon isotopic composition, starting around 160 m at Salaa Gorge, occurs within a period of low Sr/Mn, though most values are above 1 (Fig. 2.13A). The upper Zuun-Arts Ridge locality also exhibited similar values of Sr/Mn (Fig. 2.13B). X_V and X_U concentrations started close to 0 ppm at the base of Salaa Gorge, but increase to higher values in the upper part of the section (Fig. 2.13). X_V and X_U abundances at Zuun-Arts Ridge are comparable to

those in the upper part of Salaa Gorge but with higher values for X_V . (Fig. 2.13). Increases in elemental enrichment may coincide with the first appearance of archaeocyaths (red symbol), but not other fauna (purple symbol; Fig. 2.13). Th/U values were lower in Salaa Gorge compared to Zuun-Arts Ridge, and in particular Th/U values were well below 1 for almost all of the Salaa Gorge section (Fig. 2.13A). Ten samples in Zuun-Arts Ridge had $> 1\%$ X_{Na+Al} values as well as higher X_{Th} values (see Figure B1 and Table B2 for complete dataset and Figure B2 for oxygen isotope correlations from Smith *et al.*, 2016).

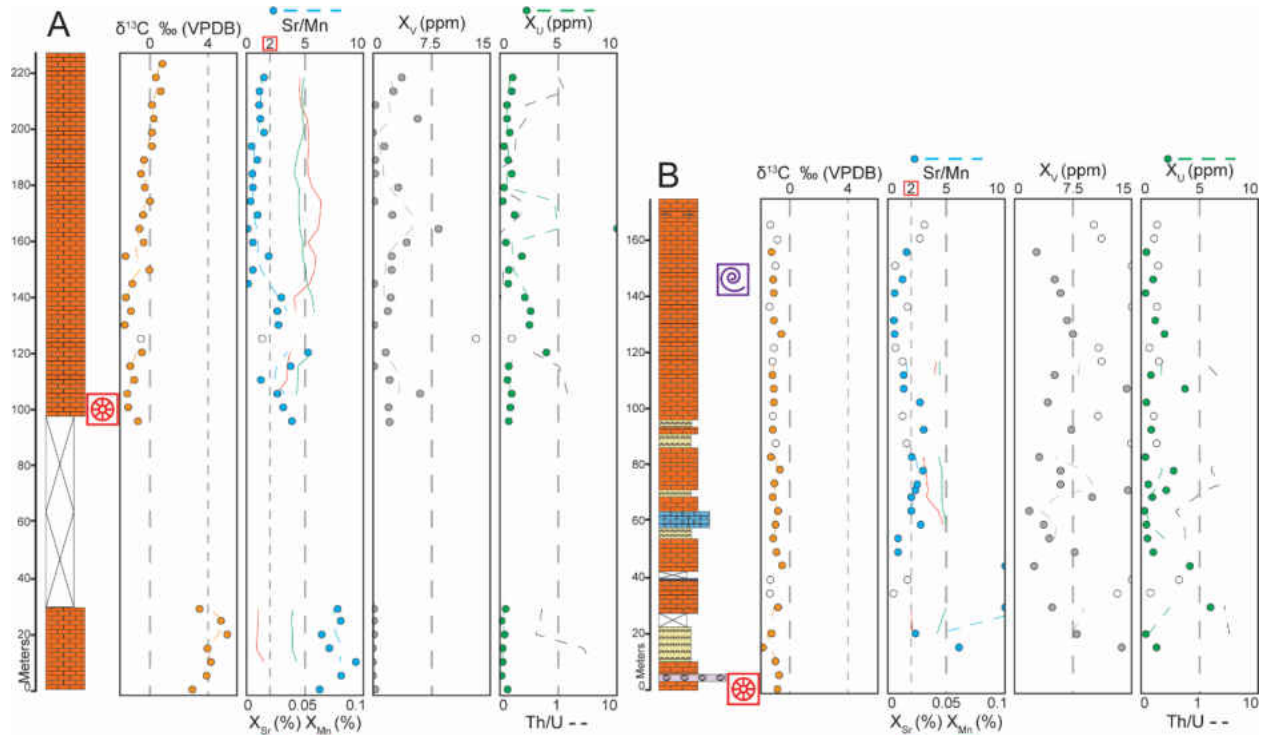


Figure 2.13: Trace element data for Mongolia. Salaagol Formation at, A, Salaa Gorge and, B, Zuun-Arts Ridge. From left to right lithology, stable carbon isotopes from carbonate (VPDB), Sr/Mn with X_{Sr} and X_{Mn} , X_V , and X_U with Th/U. Hollow circles denote samples with $> 1\%$ X_{Na+Al} . A three-point moving average trendline is shown for samples within 15 m of each other after exclusion of high X_{Na+Al} samples and sampling gaps. Lithological symbols same as previous figure. Red- and purple-boxed symbols denote first occurrence of archaeocyaths and high concentrations of other fossils.

Sedimentological Observations

White-Inyo units

Montenegro Member.— Two mudstone bioherms are contained within highly fissile, dark green shale. The lowest is roughly 4 m wide and 6.9 m thick and the highest is 3.5 m wide and 2.1 m thick (Fig. 2.14A). Evidence of binding sediments is sparsely present (Fig. 2.14B). Rather, they are composed almost entirely of micrite and sparse microbial fabrics (Fig. 2.14C and D). In outcrop a few archaeocyaths were observed, however, they were too sparse to be seen in thin sections. Very few faunal elements or clastic material was observed in the bioherms. Void space was also minimal.

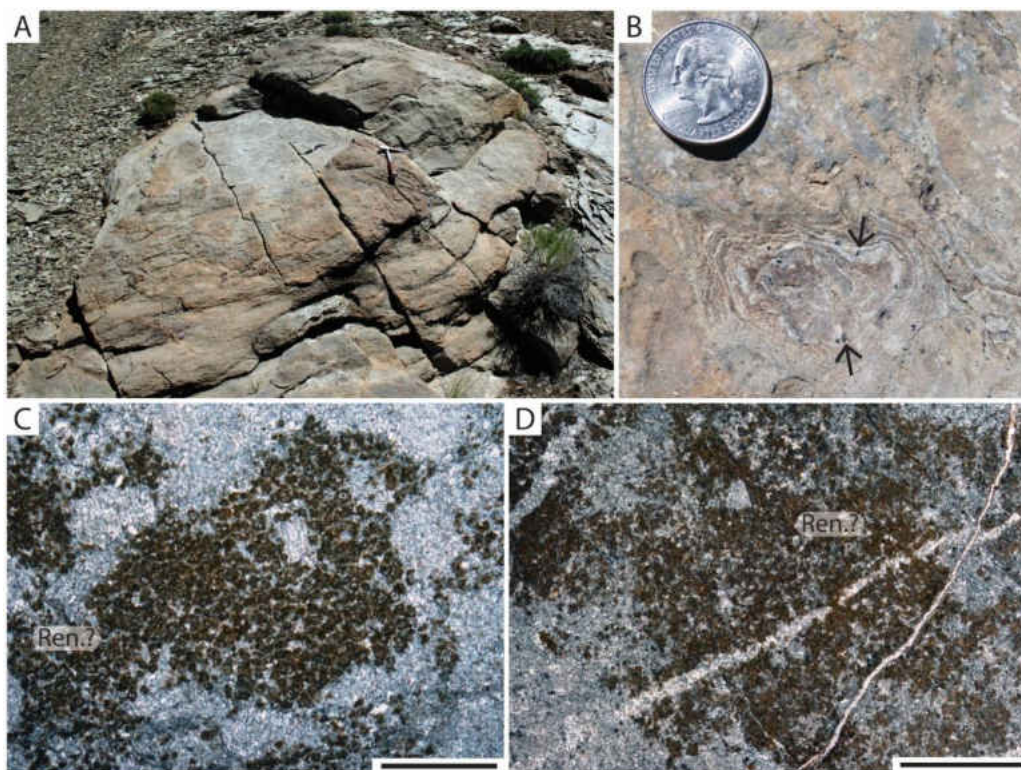


Figure 2.14: Field view and thin section photos of bioherms in Campito Formation (Montenegro Member) at Bristlecone Trail. A) Carbonate bioherm surrounded by green shale. Hammer for scale. B) Poorly-preserved archaeocyath? or coated grain from bioherm with trapped sediment particles (arrow). C and D) Thin section photos of calcifying microbes from bioherms tentatively identified as *Renalcis*-group (Ren.?), but could also be transverse sections of *Epiphyton*-group. Scale bars equal 1 mm.

Poleta Formation.— Microbial reefs within the Poleta Formation contain peloids and a larger concentration of faunal elements such as trilobites and echinoderms in mudstone to wackestone textures (Fig. 2.15A - C). Occasional, thin beds of highly fissile, brown shale are present within the microbialite. Numerous cavities, which may have been present *in vivo* (Rowland and Gangloff, 1988), are cross cut by more recent quartz veins (Fig. 2.15B). Channel fill is light brown to orange in color with a fine-grained mudstone texture (Fig. 2.15C). Potential microbial fabrics have rhombohedral floating grains that weakly stained red by ARSPF, which is consistent with dolomite. However, the faint outlines of *Renalcis*-group clotted textures suggest neomorphism. Cement-filled pores are much more common than in underlying facies, however, still fairly sparse.

Archaeocyathan reefs are defined by wackestone/packstone with large archaeocyath grains, often with cement-filled interstitial pores, within clotted (*Renalcis*?) microbialite (Fig. 2.15D - F). These facies are primarily found in the Poleta Formation and are commonly topped by ooid grainstones. Minimal clastic material is present. Again, numerous cavities are present in outcrops with archaeocyaths tending to increase in density around these cavities along ceilings and floors. No direct attachment to cavity walls is visible.

Concentric growth ooid grainstones are present at the top of the Poleta Formation in both Stewart's Mill and Westgard Pass (Fig. 2.15G). Microbialite material interfingers with oolite facies. One particular interfingering bed is 7.74 m long and 9 cm thick with squared edges. Additional interfingering beds are fairly continuous and spanned several meters. Interbeds all contain material similar to archaeocyathan reef facies. The ooid facies themselves

are devoid of any faunal elements. Ooid facies contain *Skolithos* trace fossils and slight distortion from compaction strain. Oolite facies have sharp boundaries with surrounding facies.

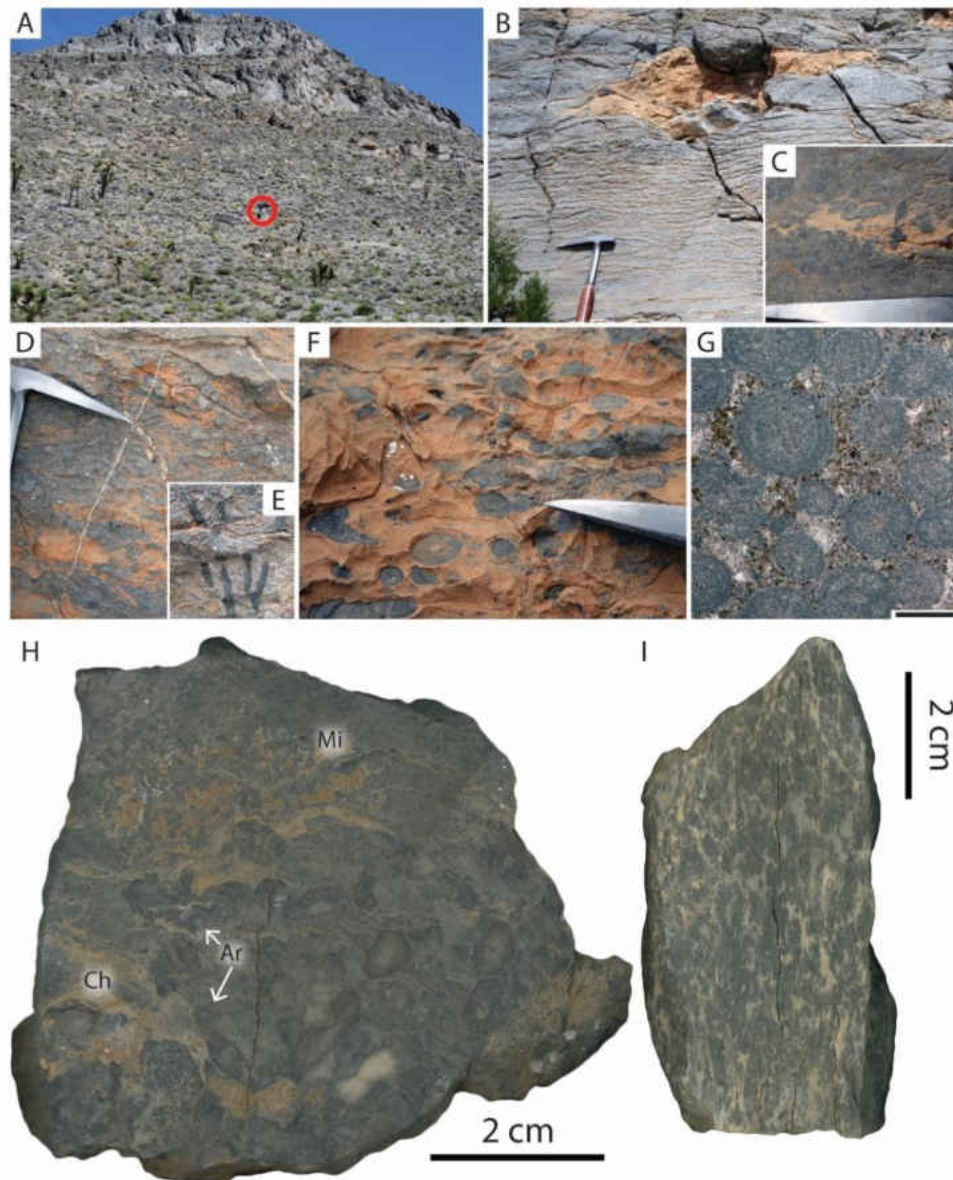


Figure 2.15: Field view, hand samples, and thin section from Poleta Formation at Stewart's Mill. A) Stewart's Mill outcrop with archaeocyath-bearing microbialite enclosed within dashed lines. Shale and ooid units present below and above microbialite respectively. Note field assistant highlighted in circle for scale. B) Cavity with orange-colored micrite fill. C) Close-up of cavity filled with small solitary archaeocyaths indicated by arrows. D) Archaeocyath packstone. E) Close-up of branching archaeocyath indicated by arrow. F) Close-up of cavity filled with orange micrite and small archaeocyath cups. G) Concentric ooids from ooid grainstones at top of Stewart's Mill. Scale bar equals 1 mm. H) Slab of archaeocyath-dominated packstone. Ch = channels; Ar = archaeocyath; Mi = microbial fabric. I) Hand sample of clotted microbialite. Hammer for scale in B – D, F. Archaeocyath in E is ~5 cm wide.

Harkless Formation.— The base of the Harkless Formation contains fine- to medium-grained quartz sandstone with carbonaceous cement (Fig. 2.16A). This facies is occasionally interrupted by fine-grained shale. The carbonaceous sandstone facies is topped by an erosional contact (Fig. 2.16B). Thin sections show dense quartz-rich grainstone with fibrous anhydrite gypsum crystals (Fig. 2.16C). Quartz grains are subangular and well sorted. This facies contains *Salterella* molds visible in outcrop and sparse echinoderm fragments visible in thin section.

Archaeocyath-coralomorph facies is only present in the Harkless Formation overlying carbonaceous sandstone facies with an erosional contact (Fig. 2.16D - E). Packstones here are composed of coralomorphs (Fig. 2.16F - H) and archaeocyaths as framework builders. In addition, there is a much higher proportion of clastic material. Archaeocyath osculum are filled with both internal sediment and cement suggesting early syndepositional cementation. Minimal microbial elements are present in these facies.

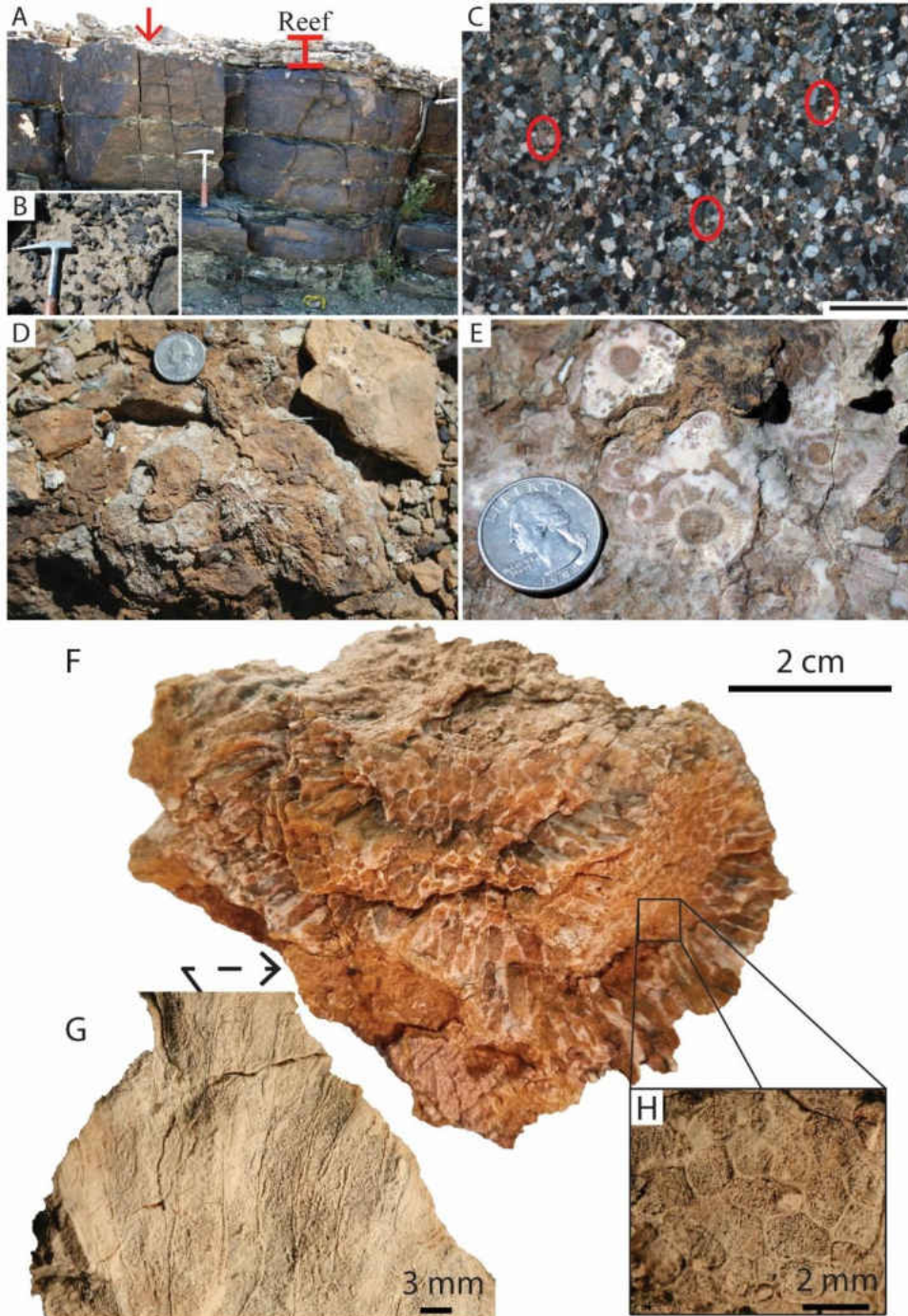


Figure 2.16: Field view, hand samples, and thin section from Harkless Formation at Gold Point Hills. A) Harkless Formation with carbonaceous sandstone and overlying reef, separated by erosional surface. Hammer for scale. B) Erosional surface found at red arrow in A. C) Cross-polarized light thin section of carbonaceous sandstone with high birefringence anhydrite gypsum circled. Scale bar equals 1 mm. D and E) Outcrop of Harkless Formation archaeocyaths with large osculum. F) Hand sample of coralomorph *Harklessia*. Photographed wet with reflected light. G) Sagittal view of coralomorph showing corallite columns. H) Top view of corallites. G and H coated in ammonium chloride.

General sedimentological observations.— Micrite was the most common non-faunal element (79.8%). Approximately 4.9% of point counts were cement and this was correlated with the presence of framework builders (Pearson's $r = 0.27$, p -value = 0.006). Cement was most commonly observed in the interstitial spaces within archaeocyath osculum and intervallum. Open pore space was minimal throughout the study area. Clastic material composed 3.0% of point counts and was mostly concentrated in the Harkless Formation. The Poleta Formation contained peloids, intraclasts of carbonate origin and overturned geopetal structures.

Outcrop observations found both colonial and solitary archaeocyaths. Archaeocyaths frequently maintained a primary branching angle of $\sim 45^\circ$ (Fig. 2.15E) suggesting directional, most likely upward, growth. However, branching forms were far less common than solitary forms and did not appear to have any specific spatial or environmental distribution. Archaeocyath skeletons were made of fine-grained carbonate, which stained pink with ARSPF. There are also several areas of turquoise staining which indicate higher concentrations of iron-rich dolomite in the carbonate matrix. Archaeocyath septa can still be identified, albeit in distorted outlines, suggesting minimal dissolution and reprecipitation of archaeocyath skeletons, which would have overprinted the internal structure of these skeletons.

Interpretation.— The beginning of the Cambrian is during the Sauk I transgression sequence (Rowland and Shapiro, 2002). These global trends are evident in this study as fine-grained shales in the Montenegro Member from an outer shelf depositional setting. Occurrences of bioherms suggests brief arrests in this transgression to allow microbial material to construct a short-lived carbonate environment. Above these shales were peloid-dominated

microbial reefs. During which the occurrence of peloids and echinoderms fragments suggests larger amounts of diversity in these microbial reefs compared to the lower bioherms. Sustained carbonate production also suggests that these facies were higher on the shelf compared to the Montenegro Member, but still deep enough to deposit occasional fine-grained shales. These peloid-dominated microbial reefs grade into archaeocyath-dominated reefs, often topped with ooids. Given the proximity of these facies to oolitic facies, the archaeocyathan reefs were most likely higher on the shelf when deposited as compared to the purely microbial reefs. In addition, higher grain proportions of packstone textures suggest a more well-washed environment as compared to microbial reefs underlying them. Ooid grainstone facies then represent the highest energy, and shallower, environments. The overtopping carbonaceous sandstones are interpreted as a minor transgression allowing finer-grained material to be deposited. Archaeocyath-coralomorph facies on top of this facies have a high terrestrial input of quartz and evaporitic minerals, which indicates a shallower environment, relative to Poleta archaeocyathan reefs. Furthermore, the larger OBR suggests a lower energy environment such as a lagoon or sheltered, cryptic reef within a crevasse.

Overall, there is a shallowing trend seen in the environmental conditions across these three formations. There are two to three complete, and one partial, shallowing upward parasequences with oolitic shoal caps. Within the second complete parasequence archaeocyaths are associated with the shallower (oolitic) facies and the microbial reefs are associated with the deeper (shale) facies. The distribution of these assemblages appears to be controlled by water depth, with archaeocyaths requiring a shallower environment and thus

appearing higher on the shelf. When sea level is low enough archaeocyathan reefs are dominant, but microbial reefs are dominant in slightly deeper settings.

Western Mongolia

Salaagol Formation.— At Salaa Gorge ~230 m of outcrop is exposed, though with a large missing portion, with poorly defined bedding and ~45° dip. Outcrop observations show that this section is composed of variable reef building units including, massive microbial-archaeocyath, radiocyath-archaeocyath-coralomorph (not discussed here, but see Kruse *et al.* 1996), and microbial boundstone. Overall, the matrix is chalky-white or rust-colored and reef building units are separated by microbial mudstone (Fig. 2.17A). In thin section, the lower Salaa Gorge contains predominately microspar and some angular, compacted quartz grain layers. Middle portions of Salaa Gorge are highly fractured with detrital quartz veins and cement. No other sedimentary structures or trace fossils were observed.

The Zuun-Arts Ridge outcrop has ~130 m of outcrop exposed, primarily of clotted microbial mudstone/wackestone with silty deposits (Fig. 2.17B) and microbial-archaeocyath boundstone with diffuse, undulating contacts and red coloration. Microbial mudstone/wackestone lacks distinct metazoan framework building, but contain small (~3 mm) fragmented archaeocyaths in a micrite or microspar matrix with sparse, angular, well-sorted detrital quartz grains seen in thin section (Fig. 2.17C). Boundstone occurs frequently throughout the section, but is more common at the top of the formation with branching and solitary archaeocyaths as well as radiocyaths (Fig. 2.17D). Again, thin sections show that microspar is

dominant, but there is a higher amount of sparry cement, mostly surrounding bioclasts, and sparse microburrows (< 1 cm) in thin section.

Several stromatolite beds occur in the lower two-thirds of the section with ~1 m in diameter stromatolites and silty deposits (Fig. 2.17E). These stromatolite beds contain entrapped bioclastic debris and very fine sand-sized, subangular detrital quartz grains and sparfilled void space in a micrite/microspar matrix (Wood *et al.*, 1993). Ooid and oncoid grainstones overlie shallowing upward cycles (Fig. 2.17F; Wood *et al.*, 1993). One such coarsening upward sequence can be seen from 40 - 60 m in Zuun-Arts Ridge with a covered, presumable shale bed, followed by microbialite, stromatolite, and topped with ooid grainstone beds. Several other partial sequences can be seen above and below this interval (Fig. 2.7). Several clastic dikes with coarse-grained, green sandstone occur in the section, but are very thin and not continuous. Across all lithofacies, sparry calcite cement coated some skeletal grains and open cavities are filled with internal micrite (Fig. 2.18A - C). Wood *et al.* (1993) also described free growing aragonitic botryoids up to 15 cm thick and aragonitic fans up to 5 cm in diameter, which presume submarine precipitation in open cavity space. *Epiphyton*-group was also present in several thin sections and did not have a consistent orientation (Fig. 2.18D and E), suggesting attachment and growth from internal cavities (Wood *et al.*, 1993; fig. 7).

Interpretations.— The lithofacies present are similar to those described by Wood *et al.* (1993) in that four are identified (1) microbial mudstone/wackestone with silt, (2) microbial-archaeocyath boundstone, (3) stromatolites, and (4) ooid and oncoid beds. Microbial mudstone/wackestone is interpreted as a mixed siliciclastic and carbonate shelf under a low energy regime. Archaeocyath boundstones are interpreted as low relief, open shelf reefs,

slightly raised compared to their surrounding area. While stromatolite and ooid/oncoid beds are interpreted as shallower intertidal or high-energy shoals respectively. Overall, this environment represents a shallow open shelf-reef-intertidal zone with several small shallowing sequences (Wood *et al.*, 1993).

The distribution of microbial-archaeocyath boundstone and microbial mudstone/wackestone could be the result of shifting environmental parameters. At Zuun-Arts Ridge, boundstones were more frequently found in the upper parts of the section, more distantly separated from the ooid and stromatolite lithofacies. As discussed above, the ooid and stromatolite lithofacies have previously been interpreted to represent shallow intertidal environments that may not have been suitable for metazoan reef construction. Thus, reefs only formed away from these types of environments. Capturing of archaeocyath fragments and silt grains in microbial mudstone/wackestone could have been the result of a sticky mat-like bed of microbial communities, which could have produced the fabric of the carbonate material (Tsein, 1985).

Comparing the White-Inyo to the Mongolia units it appears that the Salaagol Formation is most like the Poleta Formation. Sedimentologically, both contain ooids and shallowing upward sequences suggesting a shallow, higher energy system with sporadic reef building intervals. The Salaagol Formation also plotted entirely within the Poleta Formation for the fabric analysis and in terms of biodiversity and archaeocyath size distribution these two formations are also analogous. Therefore, I interpret these two formations to be equivalent environmental settings at similar stages of reef growth.

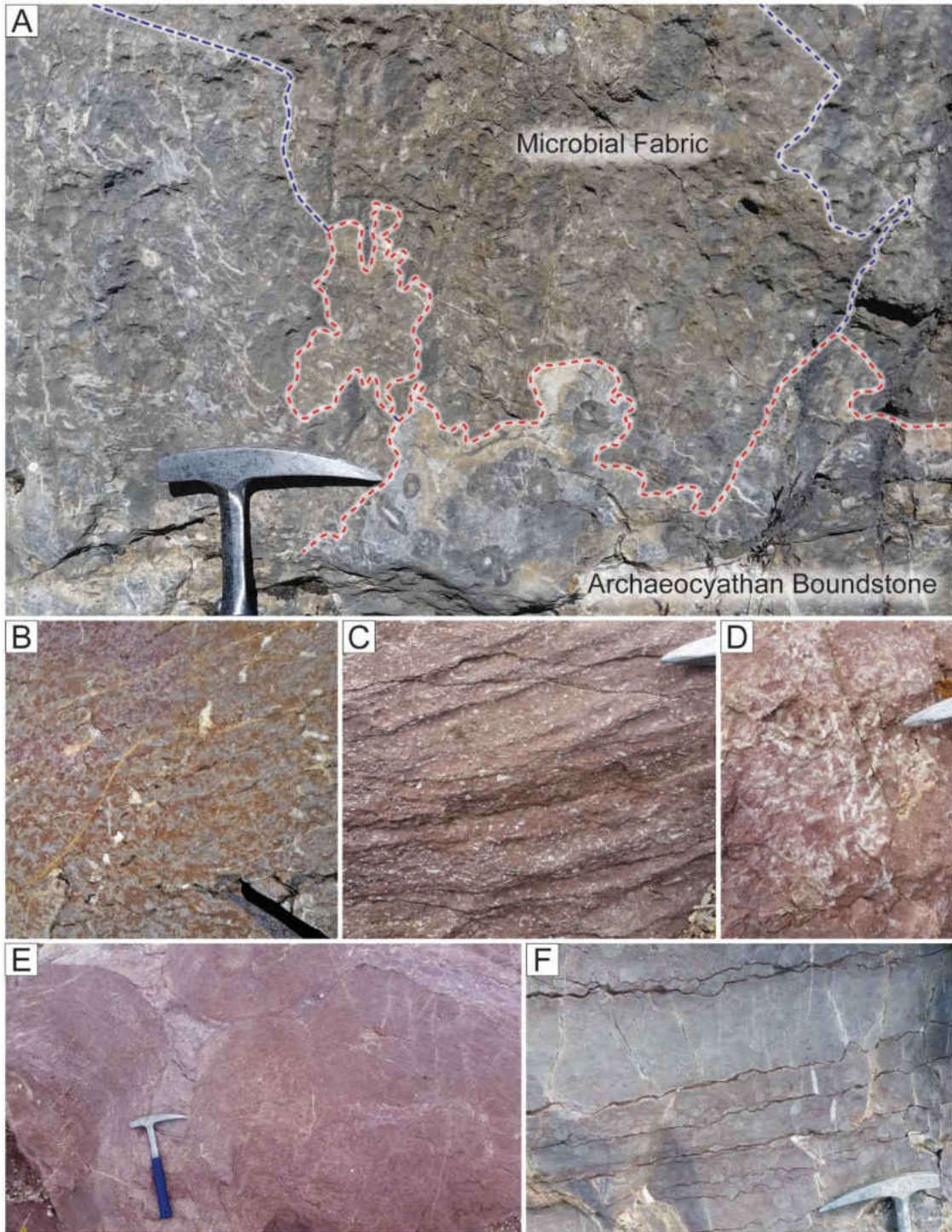


Figure 2.17: Outcrop photos of Salaagol Formation. A, Archaeocyathan reef core from Salaag Gorge with archaeocyathan reef outlined in red dashes and microbial fabric outlined in purple dashes. B, Red carbonate in clotted microbial facies of Zuun-Arts Ridge. C, Skeletal fragments in Zuun-Arts Ridge mudstone/wackestone. D, Branching archaeocyath in boundstone in Zuun-Arts Ridge. E, Stromatolite lithofacies. F, Oncoids. Hammer for scale in all photos.

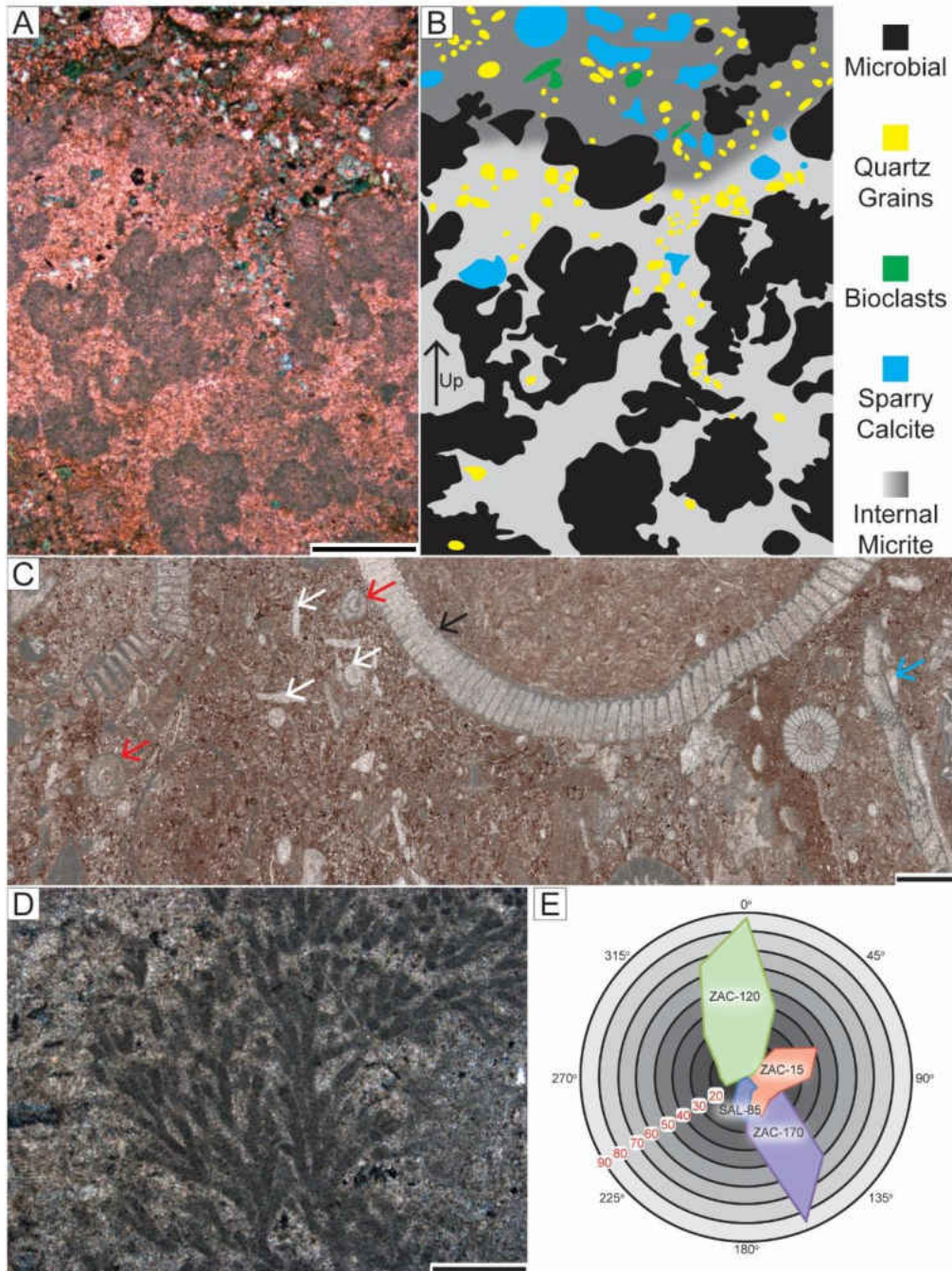


Figure 2.18: Thin section fabric interpretations of Salaagol Formation. A, ARSPF stained microbial fabric with *Tarthinia* bounding cavities filled with quartz grains (unstained) and internal micrite/microspar (pink stained). B, Illustration of A. “Up” arrow indicates orientation when sampled. C, Thin section from Zuun-Arts Ridge . White arrows – neomorphosed bioclast, black arrow - *Okulitchicyathus*, red arrow – *Cambrocyathellus* sp. 1, blue arrow – coating cement. D, *Epiphyton*-group from ZAC-120. E, Rose diagram from *Epiphyton*-group orientation analysis relative to up direction of slide. Orientations were consistent within a slide, but not across formation. ZAC – Zuun-Arts Ridge; SAL – Lower Salaa Gorge. Scale bars equal 1 mm for A and B; 2 mm for C; 0.5 for D.

Discussion

Comparison to other archaeocyathan reefs

Point count data corroborate findings of other similar studies on archaeocyathan reefs. Metazoan framework-building organisms accounted for 4.2% of carbonate contribution across the entire White-Inyo Mountains study area and 5.0% in Mongolia. These are close to previous studies, with 5.0% in southern Labrador (Pruss *et al.*, 2012), ~4.9% in Spain (Creveling *et al.*, 2013), and 9.5% from China (Hicks and Rowland, 2009). The percentage of non-archaeocyath/coralomorph fossil material was also comparable in this study (7.9% and 1.3% respectively) to other studies, which were ~5%. The single bulk sample calculated for this study agrees with these values and a volumetric percentage calculated by Rowland and Gangloff (1988) found archaeocyaths comprise approximately 2 - 20% of carbonate material. In these other studies, micrite and calcifying microbes were also very common. Based on our data and comparisons to previous studies, archaeocyath contribution is relatively minor in terms of bulk contribution to reef fabric and is similar across global localities.

Regional comparisons of carbonate facies

Montenegro Member.—The Montenegro Member of the Campito Formation contains several micrite-supported carbonate mounds, though it does appear that at least some sediment trapping and binding occurred within these structures. Metazoan framework builders are rarely present and their lack of contribution to point count analysis suggests that they are a minor component of these bioherms. Clotted calcifying microbial structures are only faintly present in outcrop and only one slide contained greater than 5% contribution from calcifying

microbes, suggesting that calcifying microbes too were a minor component. Reef dwellers, mostly echinoderms represented by sparse fragments, were evenly spread across this environment, which produced the higher evenness values despite low biodiversity overall. Thus, it appears that these bioherms were small, isolated pockets of a few organisms in shallow mud mound settings. Geochemical data suggests that these settings had low terrestrial input, which is consistent with prior interpretations of being the first carbonate deposits after the deepening interval represented by the preceding lithological member (Mount and Rowland, 1981). Redox proxies do show a slight change up section, but are not clearly associated with the occurrence of archaeocyaths. There may be too few data points within this formation to observe definite trends.

Poleta Formation.—Three sections of the Poleta Formation are present in this study. Westgard Pass and Stewart’s Mill appear to be most similar to each other, but the Bristlecone Trail section is still more similar to the other Poleta Formation outcrops, in terms of metazoan framework builder contribution and biodiversity, than it is to the other formations. Metazoan framework builders make up a larger portion of the Poleta Formation than in the underlying units. However, their distribution is still patchy and mostly confined to cavities. Though branching colonies, specifically directional growth based on consistent 45° branching angles, do suggest more established benthic communities were present. Still, large portions of the Poleta Formation contain more microbial material than they do metazoan framework builders. Reef-dwelling organisms are minimal with sparse trilobites, brachiopods, and echinoderms. The increase in richness does indicate a slightly more diverse habitat than in the underlying Montenegro Member, but organisms are sparse based on lower evenness values. Therefore,

this formation is interpreted as representing a more heterogeneous environment with mostly microbial-based framework support and occasional cavity spaces harboring smaller archaeocyaths and reef dwellers. In these cavities, archaeocyaths were locally important framework-building organisms, however, a larger portion of the formation is microbial. Archaeocyath oscula are also relatively small, suggesting a higher energy environment, which concurs with the presence of stratigraphically nearby ooid grainstones. Geochemical analyses show that terrestrial input is higher in association with archaeocyaths, which could be due to their occurrences in open cavity space into which clastic material was deposited. There is no evidence for global changes in redox that impacted the development or occurrence of archaeocyathan reefs. However, lower average X_U and X_{Mo} values did occur and are coincident with the positive carbon isotopic excursion. The decreased availability of these redox-sensitive elements is likely linked to a global increase in carbon burial that resulted in the positive isotopic excursion (*cf.*, Marenco *et al.*, 2016). However, it is unclear how these global fluctuations in redox would have affected the local development of archaeocyathan reefs. A change in the global carbon cycle was not associated with the origination archaeocyaths in the region, contrary to previous studies (Ishikawa *et al.*, 2014).

Harkless Formation.—Most conspicuous in this formation is the presence of larger archaeocyaths and hypercalcifying coralomorphs. This leads to a much higher contribution of metazoan framework builders than either preceding formation and is consistent across all samples taken within the reefs of this formation. The overall contribution of calcifying microbial material is unchanged from the Poleta Formation, but becomes relatively less common in the Harkless Formation as a result of increasing metazoan contribution. With regards to

biodiversity, despite the increase in both diversity and evenness, the fact that reef dwellers and metazoan framework builders are not correlated suggests that the addition of metazoan framework builders is what drives this increase in diversity, rather than new niche creation for reef dwellers. This suggests that archaeocyaths were not performing the same ecological engineering roles in their environments as modern reef builders. This does not necessarily mean these organisms were unable to perform these roles. Based on data from this study, the lack of an association between metazoan framework builders and dwellers could reflect the lack of new organisms being present to take advantage of potential niches opened by archaeocyath framework.

The increase in archaeocyath size suggests that selective pressures changed leading into the Harkless Formation reef environments. Terrestrial input was higher in these reefs and could have made this environment more turbid. These conditions could have led to changes in size due to larger body volumes needed to filter out larger grains of sand in the environment, larger surface area required to increase photosynthetic potential (though endosymbionts in archaeocyaths is still intensely debated, see Surge *et al.*, 1997), or predatory defenses. Because of the high amount of terrestrial input and larger oscula sizes, suggesting lower energy, these reefs are interpreted as having grown in a more nearshore, shielded setting such as a lagoon. Again, terrestrial input is high in these reef units, but there is no substantial change in geochemical redox proxies. Therefore, factors other than geochemical changes may have had a larger impact on archaeocyaths eventual disappearance from this region.

Salaagol Formation.— Microbial forms (5.4%) and archaeocyaths (5.0%) contributed statistically indistinguishable amounts of carbonate material, however, the distribution of this

material is different based on both Kolmogorov-Smirnov and pairwise tests. The lower Salaa Gorge locality has a higher proportion of microbial-derived fabrics, while the upper Salaa Gorge and Zuun-Arts localities contained more archaeocyaths. The lower Salaa Gorge may have been deeper than the upper Salaa Gorge and Zuun-Arts Ridge, thus favoring microbial over archaeocyathan growth. Overall, this formation is comparable to the Poleta Formation, but perhaps calmer energy levels given the larger OBR.

The lower, microbial-dominated part of the section also has the highest $\delta^{13}\text{C}$ values. After the gap, not only are archaeocyaths more common, but $\delta^{13}\text{C}$ is considerably lower as well and within an interval of high Sr/Mn, suggesting minimal diagenetic alteration. X_V and X_U concentrations are low in the lower Salaa Gorge and both increase at the first occurrence of archaeocyaths. A similar pattern occurs at Zuun-Arts Ridge in both cleaner carbonates and those with higher siliciclastic contents. These data cautiously suggest a change in global redox conditions concurrent with the appearance of archaeocyaths in Mongolian reefs, though a cause and effect relationship cannot be established here. Furthermore, negative carbon isotopic composition concurrent with the occurrence of archaeocyaths in this section is similar to the relationships observed in Siberian archaeocyathan reefs (Kouchinsky *et al.*, 2007), suggesting a possible response of these ecosystems to changing geochemical conditions. Gondwanan archaeocyathan reefs occur during carbon isotopic highs, but origination appears to be associated with carbon isotopic lows, both globally and in our data (Brasier *et al.*, 1994; Kouchinsky *et al.*, 2007; Ishikawa *et al.*, 2014). Both an increase in the dissolved inventory of redox-sensitive elements and lower $\delta^{13}\text{C}$ values can be explained by a decrease in the global burial of organic carbon due to more oxidizing conditions in the oceans (e.g., Marenco *et al.*,

2016). However, it is not known if this pattern is also displayed in more distant settings such as Laurentia.

Thin sections show that reef-dwelling fauna are mostly absent from archaeocyathan boundstones in the Salaagol Formation. Organisms frequently associated with Cambrian strata such as brachiopods were only observed in 2 out of 69 thin sections and constituted <1% of carbonate contributions. Specifically, in the upper 50 m of the Zuun-Arts locality, reef-dwelling organisms constitute only 1.2% of carbonate contribution. Geochemical proxies do not appear to affect reef-dweller concentration either. Furthermore, the amount of reef dwellers and archaeocyaths was not correlated, suggesting that framework builders were not increasing available niche space for other organisms at this locality. Ordinarily, reef ecosystems are pictured as harbors of diversity, however, these reefs appear to have low reef-dwelling diversity, perhaps even lower than those present in Laurentia due to their older age.

Overall trends.— First, the reefs in this study appear to show a pattern of increasing metazoan framework contribution over time through the three reef bearing formations. Changes in sea level as well as evolutionary trends likely play roles in these observations. However, the addition of new organisms and changes in morphology of existing organisms leads us to interpret these patterns as largely due to changes in biogenic carbonate contribution. Metazoan framework builders are not common in the Montenegro Member and potentially contributed little to these early bioherms. Within the Poleta Formation, metazoans are present in variable concentrations, but still calcifying microbes appear to be more common. Finally, within the Harkless Formation a substantial portion of carbonate material is derived from metazoans and a new framework-building organism, coralomorphs, was incorporated into

the reef building process. In the Salaagol Formation the lower portions of the formation are devoid of framework builders (akin to the Montenegro Member) and the upper portions contain the majority of archaeocyaths (akin to the Poleta Formation). These changes in ecology can also be seen in the shift in carbonate fabrics across these formations (Fig. 2.11 and Fig. 2.19).

Second, functional diversity closely follows trends in taxonomic diversity. This pattern is common in early Cambrian environments as ecosystems were first starting to be established. The environments observed in this study have low functional redundancy as few organisms overlap in their ecological roles, which has been observed in other Cambrian ecosystems (Villéger *et al.*, 2011). This pattern may have briefly begun to change by the late Atdabanian in reefs (Zhuravlev *et al.*, 2015) and more persistent changes in other environments started in the later Cambrian and Ordovician as novel organisms began to fill new niches (Bambach *et al.*, 2007). This is evident in this study as nearly all functional groups contained only one taxon. These findings are consistent with the taxonomic studies of previous authors suggesting high levels of globally diversity, but uniform ecological adaptations within individual communities (Wood *et al.*, 1992; Wood, 1995; Zhuravlev *et al.*, 2015). Because of the low diversity of the early Cambrian, it is not surprising that functional diversity would closely follow any trends in taxonomic diversity.

Third, early Cambrian reefs do exhibit features common to other reef settings (Rowland, 1984). First, they are biologically-produced carbonate environments with at least one common skeletal producing organism, including a hypercalcifying organism (*Harklessia*) in the same functional group as other massive corals. Second, early Cambrian reefs exhibit sedimentological

processes seen in other reef environments such as growth (i.e., reef expansion). Cavity spaces in the reef matrix suggest growth that created overhangs and crevices (Kobluk, 1981; Vennin *et al.*, 2003). This could only occur in expanding and well-lithified environments. In addition, interstitial spaces with geopetal structures provide evidence of cementation and sedimentation. Solely microbial reef environments also contain signs of sediment agglutination as shown by peloid bodies. In effect, archaeocyaths were not necessary to create reef-like environments, though they did affect its ecological diversity (Fig. 2.20; Adachi *et al.*, 2014a).

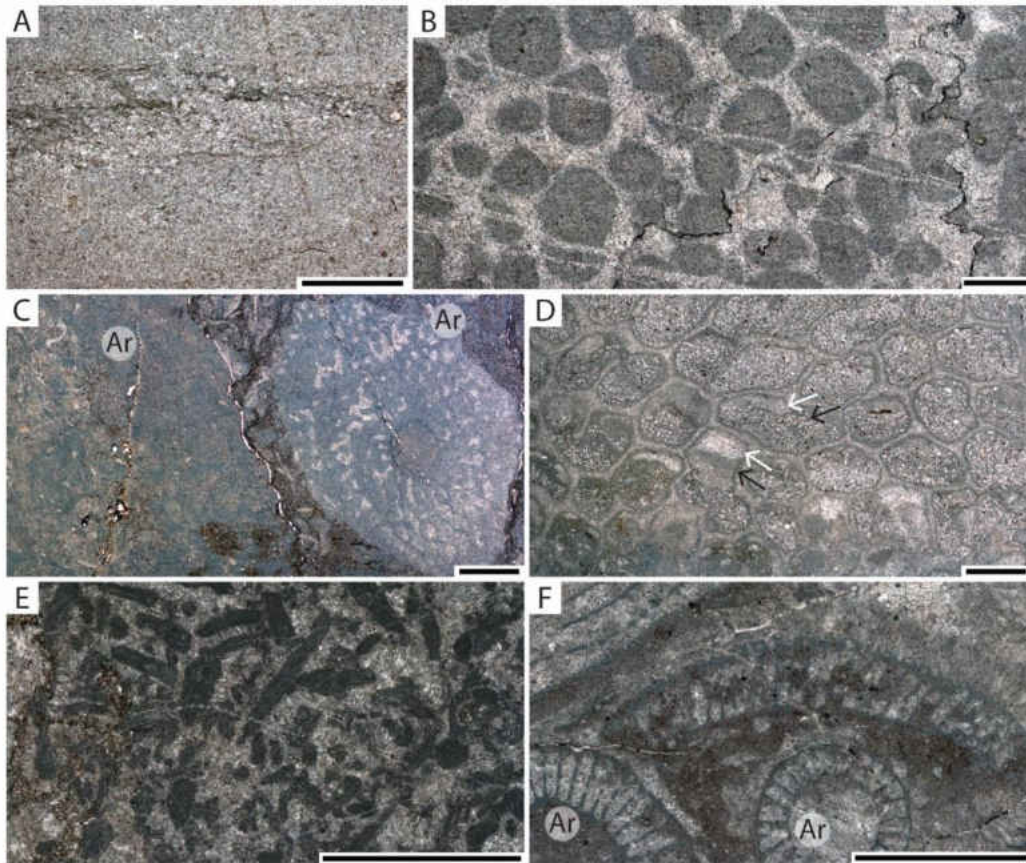


Figure 2.19: Thin section comparison of White-Inyo Mountains and Mongolia. Six localities in study show increases in framework building contribution. A, Micrite-rich bioherm from Montenegro Member. B, Peloids from Poleta Formation in Westgard Pass. C, Archaeocyaths from Poleta Formation in Stewart’s Mill. D, Coralomorph from Harkless Formation in Gold Point Hills. E, Microbial wackestone from Lower Salaagol Formation. F, Archaeocyath boundstone from Salaagol Formation at Zuun-Arts Ridge. White arrows = cement, black arrows = internal sediment fill. A, B, E, and F scale bars equal 1 mm, C and D scale bars equal 2 mm. Ar = archaeocyath.

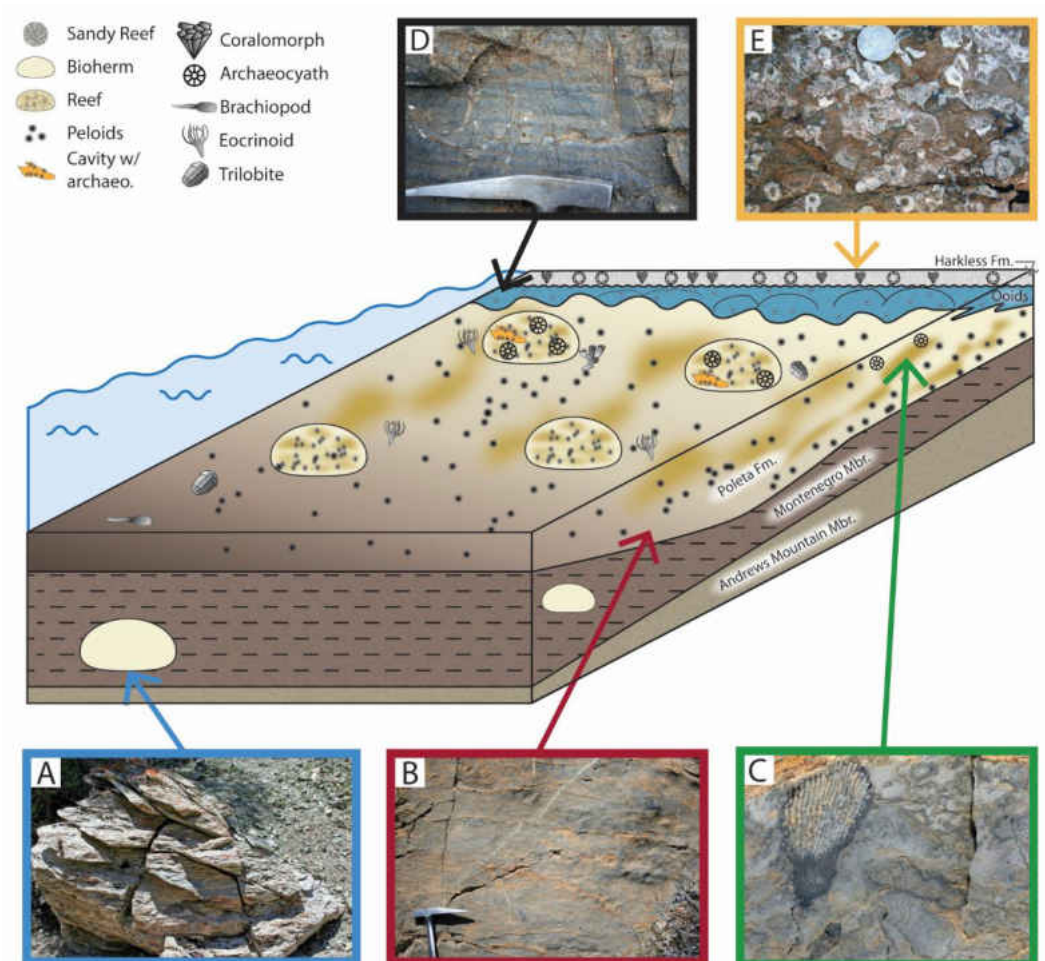


Figure 2.20: Reconstruction of early Cambrian reef ecosystems. Boxed pictures show field photos of modern outcrop preserved from those habitats. Harkless Formation does not stratigraphically overlie Lower Poleta Formation (wavy line denotes missing section). Only White-Inyo Mountains region shown in reconstruction, but Salaagol Formation is interpreted to be similar to the Poleta Formation shown here. A, Bioherm from upper Montenegro Member. B, Clotted microbialite from Lower Poleta Formation. C, Archaeocyath from Lower Poleta Formation. D, Ooid grainstone from Lower Poleta Formation. E, Archaeocyaths and coralomorphs from lower Harkless Formation.

Geochemical Diagenetic and Chemostratigraphic Interpretations

White-Inyo. — A ~2‰ positive excursion was observed in the Lower Poleta Formation.

Previous studies from this region determined that only a minor drift in isotopic composition occurred (Hicks, 2006b, fig. 3.4; Rowland *et al.*, 2008, fig. 17). However, finer sampling during

this study shows that this drifting may actually be a more pronounced excursion. I interpret this excursion as representing a global change in carbon isotope composition as opposed to overprinting of local carbon cycle changes because of the concurrent fall in uranium content. The decrease in uranium content and the shift towards higher carbon isotopic values would be expected to result from increased organic carbon burial in reducing shale environments (e.g., Marenco *et al.*, 2016). Furthermore, this signal is unlikely to be due to diagenesis. First, this signal occurs at two localities where the Poleta Formation was sampled. Second, shifts in carbon isotopes and additional trace elements do not appear to occur at a facies change, suggesting that these changes are not due to unconformities or increased fluid flow at breaks in sedimentary units. Third, low Mg concentrations suggest minimal dolomitization has occurred, which is supported by ARSPF petrographic observations. Rather, 95% of samples were found to be low-Mg calcite and none were found to be dolomite. Fourth, concentrations of Fe remain relatively low and stable throughout the interval. Fe is comparatively higher in meteoric water compared to carbonates and Fe concentration tends to increase during diagenesis (Veizer, 1983). Thus, low Fe concentrations also suggest minimal diagenesis. Finally, the positive carbon isotopic excursion occurs in an interval of high Sr/Mn ratios, driven primarily by high concentrations of Sr. For these reasons, I infer that diagenetic effects are minimal and that the Stewart's Mill locality in particular is an accurate representation of original geochemical conditions in early Cambrian reefs.

The positive carbon isotopic excursion occurs within the lower *Nevadella* trilobite zone, which also contains *Judomia* and correlates to the *Judomia* zone in Siberia (Nelson, 1976; Geyer and Shergold, 2000). The magnitude and relative age of the excursion most readily corresponds

to “Cycle VI” of the carbon isotope curve of Brasier *et al.* (1994) in the late Atdabanian or mid-Stage 3. This curve was later calibrated using $^{206}\text{Pb}/^{238}\text{U}$ geochronology in Morocco which found that tuff from the upper Atdabanian was deposited at 517.0 ± 1.5 Ma (Maloof *et al.*, 2010). This provides a rough proposed age constraint on the Stewart’s Mill and Westgard Pass localities of approximately 517 Ma. Furthermore, the global FAD of archaeocyaths is correlated to a negative excursion at the base of the Tommotian, prior to “Cycle II” of the Brasier *et al.* (1994) curve (Kouchinsky *et al.*, 2007) which was dated to 524.837 ± 0.092 Ma (Maloof *et al.*, 2010). This allows us to estimate a rough dispersion rate of at least 7.8 ± 1.6 million years for archaeocyaths to spread from Siberia to Laurentia. Sessile filter feeding organisms typically have a very short dispersal distance (Kinlan and Gaines, 2003) and modern sponges in particular are known to have short-lived (and hence short-dispersed) larva (Mariani *et al.*, 2005). Though little is known about archaeocyath reproduction, based on this long dispersal time (even for slow dispersal organisms) it is possible that archaeocyath dispersal was slowed by biological or oceanic conditions for some time during the early Cambrian (see Jablonski and Lutz, 1983; Scheltema, 1986).

Western Mongolia.— Work by Voronin *et al.* (1982) and later Kruse *et al.* (1996) designated the Salaagol Formation as late Atdabanian-early Botomian based on archaeocyathan biostratigraphy. However, later work incorporating carbon isotopic changes used a positive excursion in the Salaagol Formation and relative lack of trilobite fauna as evidence of a correlation with the early Tommotian (Smith *et al.*, 2016). This interpretation was later challenged by biostratigraphers suggesting that archaeocyath-bearing early Atdabanian deposits in the Siberian borderland and Mongolia predate the regional first appearance of

trilobites and therefore, lack of trilobites may not be useful for assertion of an earlier age (Landing and Kruse, 2017). Additionally, 21 of the 36 archaeocyathan genera in the Salaagol Formation found by Kruse *et al.* (1996) are here recognized to be Atdabanian in age and the remaining 15 are known from both the Tommotian and the Atdabanian. The isotopic composition of carbonate carbon from our study did reveal a large positive excursion in the Salaagol Formation, which may correspond to “Cycle IV” of the chemostratigraphic curve of Maloof *et al.* (2010) due to their similar magnitudes. Furthermore, carbon isotopic composition from previous studies could also be reinterpreted to fit this same cycle rather than “6p” (Fig. 2.21; Smith *et al.*, 2016). In addition, the most common archaeocyath from the Salaagol Formation, *Cambrocyathellus* originated in the late Tommotian (Debrenne *et al.*, 2015) and other genera from this section, *Archaeophareta*, *Degeletticyathus*, *Ajacyathus*, did not originate until the Atdabanian (Debrenne *et al.*, 2002; Debrenne *et al.*, 2015). If the positive excursion were actually demarcating the base of the Tommotian and the archaeocyaths in the overlying units demarcated the Atdabanian, this would suggest a 5 Myr interval within this section. Based on average carbonate accumulation rates of 200 m/Myr (Bosscher and Schlager, 1993), one would expect at minimum 1000 m of accumulated carbonate between these events, compared to the ~200 m present, or a major depositional hiatus of which there is no evidence. Given our new findings, I feel that the most parsimonious interpretation is a younger (Atdabanian) age for the Salaagol Formation nearer in agreement with Landing and Kruse (Fig. 2.20; 2017) and between 3 – 4 million years prior to the reefs in western Laurentia.

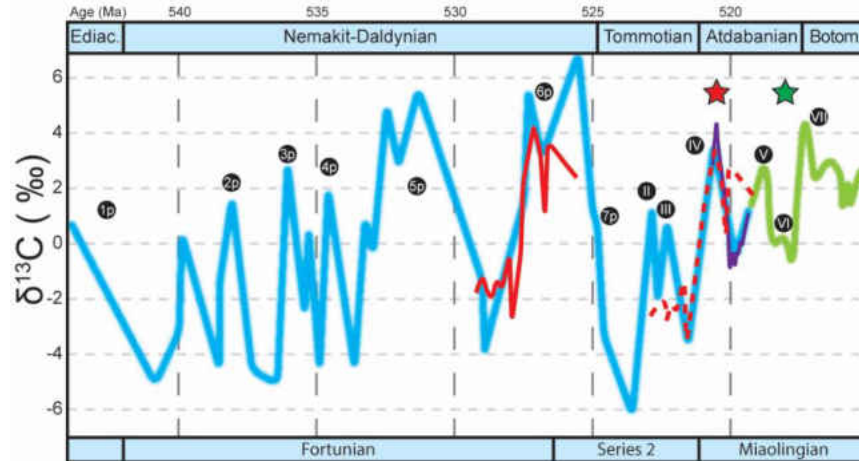


Figure 2.21: Early Cambrian carbon isotopic composition. Curve from Maloof *et al.* (2010) in blue and Kouchinsky *et al.* (2007) in green. Carbon isotope data from Smith *et al.* (2016) in red, with original placement (solid line) and reinterpreted placement (dashed). Data from Mongolian study shown in purple at Cycle IV. Red star indicates timing of Mongolian reefs and green star indicates White-Inyo reefs.

Conclusions

Archaeocyathan reefs from the White-Inyo Mountains region of western Mongolia are some of the earliest examples of metazoan-based reefs. These shallow marine ecosystems were made of distinct assemblages of reef builders that underwent a substantial transition during this time. I conclude that, (1) there is an increase in the amount of metazoan carbonate contribution over time through reef building environments at these localities, a trend that has previously been noted as occurring globally into the Ordovician as metazoans became more ecologically diverse in shallow marine environments, but is here shown to have occurred even earlier (Pruss *et al.*, 2010). In particular, the incorporation of hypercalcifying organisms into reef environments had a dramatic effect on biodiversity. This further clarifies the timing of reef ecosystem development from microbial- to metazoan-dominated. (2) I observe that changes in metazoan framework building contribution are associated with increases in diversity, however,

these changes appear to be the result of adding metazoan framework builders rather than providing new niche space for reef-dwellers. Although the diversity of reef-dwelling organisms does not appear to be affected by the presence or absence of metazoan framework builders in this study, low overall diversity in the Cambrian makes interpretation of niche creation by archaeocyaths difficult. Finally, (3) global changes in carbon burial did occur, but there is no clear effect on local conditions within these reefs. Furthermore, isotopic composition during the earliest occurrence of archaeocyaths is inconsistent between Laurentia and Mongolia. However, this study also provides a constraint on the timing of dispersal of benthic organisms. Furthermore, early Cambrian reefs from these regions do not appear to have been undergoing a prolonged period of decline prior to their regional extinction, as the youngest reefs are the most diverse.

References

- Adachi, N., Ezaki, Y., and Liu, J. 2014a. The late early Cambrian microbial reefs immediately after the demise of archaeocyathan reefs, Hunan Province, South China. *Palaeogeography, Palaeoclimatology, Palaeoecology* **407**: 45-55.
- Adachi, N., Nakai, T., Ezaki, Y., and Liu, J. 2014b. Late early Cambrian archaeocyath reefs in Hubei Province South China: modes of construction during the period of demise. *Facies* **60**: 703-717.
- Álvaro, J.J., and Vennin, E. 1998. Stratigraphic signature of a terminal early Cambrian regressive event in the Iberian Peninsula. *Canadian Journal of Earth Sciences* **35**: 402-411.

- Álvaro, J. J., Clausen, S., El Albani, A., and Chellai, E. H. 2006. Facies distribution of the lower Cambrian cryptic microbial and epibenthic archaeocyathan-microbial communities, western Anti-Atlas, Morocco. *Sedimentology* **53**: 35-53.
- Álvaro, J. J., Zamora, S., Clausen, S., Vizcaíno, D., and Smith, A. B. 2013. The role of abiotic factors in the Cambrian Substrate Revolution: a review from the benthic community replacements of west Gondwana. *Earth-Science Reviews* **118**: 69-82.
- Bailey, J.V., Corsetti, F.A., Bottjer, D.J., and Marenco, K.N. 2006. Microbially-mediated environmental influences on metazoan colonization of matground ecosystems: evidence from the lower Cambrian Harkless Formation. *Palaios* **21**: 215-226.
- Bambach, R. K., Bush, A. M., and Erwin, D. H. 2007. Autecology and the filling of ecospace: key metazoan radiations. *Palaeontology* **50**: 1-22.
- Bell, J. J. 2007. Contrasting patterns of species and functional composition of coral reef sponge assemblages. *Marine Ecology Progress Series* **339**: 73-81.
- Bezzubetsev, V. V. 1963. On the Precambrian-Cambrian stratigraphy of the Dzavkhan River Basin. *Gostoptekhizdat, Materials on the Geology of MPR* **1963**: 29-42.
- Bold, U., Smith, E., Rooney, A. D., Bowring, S. A., Buckwaldt, R., Dudás, F. Ó., Ramezani, J., Crowley, J. L., Schrag, D. P., and Macdonald, F. A. 2016. Neoproterozoic stratigraphy of the Zavkhan terrane of Mongolia: the backbone for Cryogenian and early Ediacaran chemostratigraphic records. *American Journal of Science* **316**: 1-63.
- Bosscher, H., and Schlager, W. 1993. Accumulation rates of carbonate platforms. *The Journal of Geology* **101**: 345-355.

- Brasier, M., Corfield, R., Derry, L., Rozanov, A., and Zhuravlev., A. Y. 1994. Multiple $\delta^{13}\text{C}$ excursions spanning the Cambrian explosion to the Botomian crisis in Siberia. *Geology* **22**: 455-458.
- Brasier, M. D., Dorjnamjaa, D., and Lindsay, J. F. 1996. The Neoproterozoic to early Cambrian in southwest Mongolia: an introduction. *Geological Magazine* **133**: 365-369.
- Brennecke, G. A., Hermann, A. D., Algeo, T. J., and Anbar, A. D. 2011. Rapid expansion of oceanic anoxia immediately before the end-Permian mass extinction. *Proceedings of the National Academy of Sciences* **108**: 17631-17634.
- Buhl-Mortensen, L., Vanreusel, A., Gooday, A. J., Levin, L. A., Priede, I. G., Buhl-Mortensen, P., Gheerardyn, H., King, N. J., and Raes, M. 2010. Biological structures as a source of habitat heterogeneity and biodiversity on the deep ocean margins. *Marine Ecology* **31**: 21-50.
- Burne, R. V., and Moore, L. S. 1987. Microbialites: organosedimentary deposits of benthic microbial communities. *Palaios* **2**: 241-254.
- Clapham, M. E. 2011. Ordination methods and the evaluation of Ediacaran communities. In: Laflamme, M., Schiffbauer, J. D., and Dornbos, S. Q., eds., *Quantifying the Evolution of Early Life*, Topics in Geobiology 36. Springer Science+Business Media B.V., Berlin/Heidelberg: 3-21.
- Cocks, L. R. M., and Torsvik, T. H. 2007. Siberia, the wandering northern terrane, and its changing geography through the Palaeozoic. *Earth-Science Reviews* **82**: 29-74.
- Creveling, J. R., Fernandez-Remolar, D., Rodriguez-Martinez, M., Menendez, S., Bergmann, K. D., Gill, B. C., Abelson, J., Amils, R., Ehlmann, B. L., Garcia-Bellido, D. C., Grotzinger, J. P.,

- Hallmann, C., Stack, K. M., and Knoll, A. H. 2013. Geobiology of a lower Cambrian carbonate platform, Pedroche Formation, Ossa Morena Zone, Spain. *Palaeogeography, Palaeoclimatology, Palaeoecology* **386**: 459-478.
- Debrenne, F. 2007. Lower Cambrian archaeocyathan bioconstructions. *Comptes Rendus Palevol* **6**: 5-19.
- Debrenne, F., Maidanskaya, I. D., and Zhuravlev, A. Y. 1999. Faunal migrations of archaeocyaths and early Cambrian plate dynamics. *Bulletin de la Société Géologique de France* **170**: 189-194.
- Debrenne, F., Zhuravlev, A. Y., and Kruse, P. D. 2002. Class Archaeocyatha Bornemann, 1884. In: J. N. A. Hooper, and R. W. M. Van Soest eds. *Systema Porifera: a guide to the classification of sponges*. Kluwer Academic/Plenum Publishers, New York: 1539-1692.
- Debrenne, F., Zhuravlev, A. Y., and Kruse, P. D. 2015. General Features of the Archaeocyatha. Pp. 845-1084. In: F. Debrenne, W. D. Hartman, S. Kershaw, P. D. Kruse, H. Nestor, J. K. Rigby Sr., B. Senowbari-Daryan, C. W. Stern, C. W. Stock, J. Vacelet, B. D. Webby, R. R. West, P. Willenz, R. A. Wood, and A. Y. Zhuravlev. *Porifera Revised Hypercalcified Porifera Volume 5*. Part E of P. A. Selden, ed. *Treatise on invertebrate paleontology*. Geological Society of America, New York, and University of Kansas, Lawrence.
- Dickson, J. A. D. 1965. A modified staining technique for carbonates in thin section. *Nature* **205**: 587.
- Dineen, A. A., Fraiser, M. F., and Sheehan, P. M. 2014. Quantifying functional diversity in pre- and post-extinction paleocommunities: a test of ecological restructuring after the end-Permian mass extinction. *Earth-Science Reviews* **136**: 339-349.

- Dornbos, S. Q. 2006. Evolutionary paleoecology of early epifaunal echinoderms: response to increasing bioturbation levels during the Cambrian radiation. *Palaeogeography, Palaeoclimatology, Palaeoecology* **237**: 225-239.
- Emerson, S. R., and Husteded, S.S. 1991. Ocean anoxia and the concentrations of molybdenum and vanadium in seawater. *Marine Chemistry* **34**: 177-196.
- English, A. M., and Babcock, L. E. 2010. Census of the Indian Spring Lagerstätte, Poleta Formation (Cambrian), western Nevada, USA. *Palaeogeography, Palaeoclimatology, Palaeoecology* **295**: 236-244.
- Fisher, R., O'Leary, R. A., Low-Choy, S., Mengersen, K., Knowlton, N., Brainard, R. E. and Caley, M. J. 2015. Species richness on coral reefs and the pursuit of convergent global estimates. *Current Biology* **25**: 500-505.
- Gandin, A., and Debrenne, F. 2010. Distribution of the archaeocyath-calcimicrobial bioconstructions on the early Cambrian shelves. *Palaeoworld* **19**: 222-241.
- Geyer, G., and Shergold, J. 2000. The quest for internationally recognized divisions of Cambrian time. *Episodes* **23**: 188-195.
- Grotzinger, J., Watters, W., and Knoll, A. 2000. Calcified metazoans in thrombolite-stromatolite reefs of the terminal Proterozoic Nama Group, Namibia. *Paleobiology* **26**: 334-359.
- Hammer, Ø., Harper, D. A. T., and Ryan, P. D. 2001. PAST: paleontological statistics software packages for education and data analysis. *Palaeontologica Electronica* **4**: 1-9.
- Hicks, M. 2006a. A new genus of early Cambrian coral in Esmeralda County, southwestern Nevada. *Journal of Paleontology* **80**: 609-615.

- Hicks, M. 2006b. Characterizing global archaeocyathan reef decline in the early Cambrian: evidence from Nevada and China. *Unpublished Ph.D. dissertation*, University of Nevada, Las Vegas, Las Vegas, 149 p.
- Hicks, M., and Rowland, S. M. 2009. Early Cambrian microbial reefs, archaeocyathan inter-reef communities, and associated facies of the Yangtze Platform. *Palaeogeography, Palaeoclimatology, Palaeoecology* **28**: 137-153.
- Hollingsworth, J. S. 2006. Holmiidae (Trilobita: Olenellina) of the Montezuman Stage (early Cambrian) in western Nevada. *Journal of Paleontology* **80**: 309-332.
- Hubbard, D. K., Miller, A. I., and Scaturro, D. 1990. Production and cycling of calcium carbonate in a shelf-edge reef system (St. Croix, U.S. Virgin Islands): applications to the nature of reef systems in the fossil record. *Journal of Sedimentary Petrology* **60**: 335-360.
- Ishikawa, T., Ueno, Y., Shu, D., Li, Y., Han, J., Guo, J., Yoshida, N., Maruyama, S., and Komiya, T. 2014. The $\delta^{13}\text{C}$ excursions spanning the Cambrian explosion to the Canglangpuian mass extinction in the Three Gorges area, South China. *Gondwana Research* **25**: 1045-1056.
- Jablonski, D., and Lutz, R. A. 1983. Larval ecology of marine benthic invertebrates: paleobiological implications. *Biological Reviews* **58**: 21-89.
- Jax, K. 2005. Function and “functioning” in ecology: what does it mean? *Oikos* **111**: 641-648.
- Jin, C., Li, C., Algeo, T. J., Planavsky, N. J., Cui, H., Yang, X., Zhao, Y., Zhang, X., and Xie, S. 2016. A highly redox-heterogeneous ocean in South China during the early Cambrian (~529-514 Ma): implications for biota-environment co-evolution. *Earth and Planetary Science Letters* **441**: 38-51.

- Kiessling, W. 2002. Secular variations in the Phanerozoic reef ecosystem. *In: Kiessling, W., Flügel, E., and Golonka, J. eds., Phanerozoic Reef Patterns. SEPM Special Publication No. 72*, Tulsa, p. 625-690.
- Kiessling, W. 2009. Geologic and biologic controls on the evolution of reefs. *Annual Review of Ecology, Evolution, and Systematics* **40**: 173-192.
- Kinlan, B. P., and Gaines, S. D. 2003. Propagule dispersal in marine and terrestrial environments: a community perspective. *Ecology* **84**: 2007-2020.
- Kobluk, D. 1981. Earliest cavity-dwelling organisms (coelobionts), lower Cambrian Poleta Formation, Nevada. *Canadian Journal of Earth Science* **18**: 669-679.
- Kouchinsky, A., Bengtson, S., Pavlov, V., Runnegar, B., Torssander, P., Young, E., and Ziegler, E. 2007. Carbon isotope stratigraphy of the Precambrian-Cambrian Sukharikha River section, northwestern Siberian platform. *Geological Magazine* **144**: 609-618.
- Kruse, P. D. and Moreno-Eiris, E. 2013. Archaeocyaths of the White Point Conglomerate, Kangaroo Island, South Australia. *Alcheringa: An Australasian Journal of Palaeontology* **38**: 1-64.
- Kruse, P. D., Zhuravlev, A. Y., and James, N. P. 1995. Primordial metazoan-calcimicrobial reefs - Tommotian (early Cambrian) of the Siberian Platform. *Palaios* **10**: 291-321.
- Kruse, P. D., Gandin, A., Debrenne, F., and Wood, R. A. 1996. Early Cambrian bioconstructions in the Zavkhan Basin of western Mongolia. *Geological Magazine* **133**: 429-444.
- Landing, E., and Kruse, P. D. 2017. Integrated stratigraphic, geochemical, and paleontological late Ediacaran to early Cambrian records from southwestern Mongolia: comment. *Geological Society of America Bulletin* **B31640-1**.

- Lasemi, Y., and Amin-Rasouli, H. 2016. The lower-middle Cambrian transition and the Sauk I-II unconformable boundary in Iran, a record of late early Cambrian global Hawke Bay regression. *In: Sorkhabi, R. (ed.), Tectonic Evolution, Collision, and Seismicity of Southwest Asia: In Honor of Manuel Berberian's Forty-Five Years of Research Contributions: Geological Society of America Special Paper 525*, p. 1–24
- Maldonado, M., Aguilar, R., Bannister, R., Bell, J., Conway, K., Dayton, P., Diaz, C., Gutt, J., Kelly, M., Kenchington, E., Leys, S., Pomponi, S., Rapp, H., Rutzler, K., Tendal, O., Vacelet, J., and Young, C. 2016. Sponge grounds as key marine habitats: a synthetic review of types, structure, functional roles, and conservation concerns. *In: Rossi, S., Bramanti, L., Gori, A., and Saco del Valle, C.O. eds., Marine Animal Forests: Springer International Publishing, Basel*, p. 1-39.
- Maloof, A. C., Ramezani, J., Bowring, S. A., Fike, D. A., Porter, S. M., and Mazouad, M. 2010. Constraints on early Cambrian carbon cycling from the duration of the Nemakit-Daldynian-Tommotian boundary $\delta^{13}\text{C}$ shift, Morocco. *Geology* **38**: 623-626.
- Marenco, P., Martin, K., Marenco, K. N., and Barber, D. 2016. Increasing global ocean oxygenation and the Ordovician radiation: insights from Th/U of carbonates from the Ordovician of western Utah. *Palaeogeography, Palaeoclimatology, Palaeoecology* **458**: 77-84.
- Mariani, S., Uriz, M-J., Turon, X., and Alcoverro, T. 2005. Dispersal strategies in sponge larva: integrating the life history of larvae and the hydrologic component. *Oecologia* **149**: 174-184.

- McKee, E.H., and Moiola, R.J. 1962. Precambrian and Cambrian rocks of South-central Esmeralda County, Nevada. *American Journal of Science* **260**: 530-538.
- McKerrow, W.S., Scotese, C.R., and Brasier, M.D. 1992. Early Cambrian continental reconstructions. *Journal of the Geological Society* **149**: 599–606.
- Mehra, A., and Maloof, A. 2018. Multiscale approach reveals that *Cloudina* aggregates are detritus and not in situ reef constructors. *Proceedings of the National Academy of Sciences* **115**: E2519–E2527.
- Meroz-Fine, E., Shefer, S., and Ilan, M. 2005. Changes in morphology and physiology of an east Mediterranean sponge in different habitats. *Marine Biology* **147**: 243-250.
- Montanez, I. P., Banner, J. L., Osleger, D. A., Borg, L. E., and Bosserman, P. J. 1996. Integrated Sr isotope variations and sea-level history of middle to upper Cambrian platform carbonates; implications for the evolution of Cambrian seawater $^{87}\text{Sr}/^{86}\text{Sr}$. *Geology* **24**: 917-920.
- Moore, J. N. 1976. Depositional environments of lower Paleozoic rocks in the White-Inyo range, Inyo County, California: a field trip road log. In: Moore, J. N., and Fitsche, A. E., eds., *Depositional Environments of Lower Paleozoic Rocks in the White-Inyo Mountains, Inyo County, California, Pacific Coast Paleogeography Field Guide 1*, The Pacific Section Society of Economic Paleontologists and Mineralogists, Los Angeles p. 1-11.
- Morgan, N., 1976. The Montenegro bioherms: their paleoecology, relation to other archaeocyathid bioherms and to early Cambrian sedimentation in the White and Inyo Mountains, California. In: Moore, J.N., and Fitsche, A.E., eds., *Depositional Environments of Lower Paleozoic Rocks in the White-Inyo Mountains, Inyo County, California, Pacific*

- Coast Paleogeography Field Guide 1**, The Pacific Section Society of Economic Paleontologists and Mineralogists, Los Angeles p. 13–17.
- Mount, J. F., and Rowland, S. M. 1981. Grand Cycle A (lower Cambrian) of the southern Great Basin: a product of differential rates of relative sea-level rise. *In*: Taylor, M. E. ed., *Short Papers for the Second International Symposium on the Cambrian System Open-File Report 81-743*, US Government Printing Office, Washington D.C., p. 143-146.
- Mount, J.F., and Signor, P.W. 1985. Early Cambrian innovation in shallow subtidal environments: paleoenvironments of early Cambrian shelly fossils. *Geology* **13**: 730-733.
- Mount, J. F., and Bergk, K. J. 1998. Depositional sequence stratigraphy of lower Cambrian grand cycles, southern Great Basin, U.S.A. *International Geology Review* **40**: 55-77.
- Nelson, C. A. 1976. Late Precambrian-early Cambrian stratigraphic and faunal succession of eastern California and the Precambrian-Cambrian boundary. *In*: Moore, J. N., and Fritsche, A. E., eds., *Depositional Environments of Lower Paleozoic Rocks in the White-Inyo Mountains, Inyo County, California*, **Pacific Coast Paleogeography Field Guide 1**, The Pacific Section Society of Economic Paleontologists and Mineralogists, Los Angeles, p. 31-42.
- Novack-Gottshall, P. M. 2007. Using a theoretical ecospace to quantify the ecological diversity of Paleozoic and modern marine biotas. *Paleobiology* **33**: 273-294.
- Novek, J. M., Dornbos, S. Q., and Mchenry, L. J. 2016. Palaeoredox geochemistry and bioturbation levels of the exceptionally preserved early Cambrian Indian Springs biota, Nevada, USA. *Lethaia* **49**: 604-616.

- Pagès, A., and Schmid, S. 2016. Euxinia linked to the Cambrian Drumian carbon isotope excursion (DICE) in Australia: geochemical and chemostratigraphic evidence. *Palaeogeography, Palaeoclimatology, Palaeoecology* **461**: 65-76.
- Pratt, B. R., Spincer, B. R., Wood, R. A., and Zhuravlev, A. Y. 2001. Ecology and evolution of Cambrian reefs. *In: Zhuravlev, A. Y., and Riding, R. eds., The Ecology of the Cambrian Radiation*. Columbia University Press, New York, p. 254-274.
- Pruss, S., and Clemente, H. 2011. Assessing the role of skeletons in early Paleozoic carbonate production: insights from the Cambro-Ordovician strata, western Newfoundland. *In: Laflamme, M., Schiffbauer, J. D., and Dornbos, S.Q. eds., Quantifying the Evolution of Early Life*, Topics in Geobiology 36: Springer Science+Business Media B.V., Berlin/Heidelberg, p. 161-183.
- Pruss, S., Finnegan, S., Fischer, W., and Knoll, A. 2010. Carbonates in skeleton-poor seas: new insights from Cambrian and Ordovician strata of Laurentia. *Palaios* **25**: 73-84.
- Pruss, S., Clemente, H., and LaFlamme, M. 2012. Early (Series 2) Cambrian archaeocyathan reefs of southern Labrador as a locus for skeletal carbonate production. *Lethaia* **45**: 401-410.
- Riding, R. 2002. Structure and composition of organic reefs and carbonate mud mounds: concepts and categories. *Earth-Science Reviews* **58**: 163-231.
- Riding, R., and Zhuravlev, A. Y. 1995. Structure and diversity of oldest sponge-microbe reefs: lower Cambrian, Aldan River, Siberia. *Geology* **23**: 649-652.
- Romaniello, S. J., Hermann, A. D., and Anbar, A. D. 2013. Uranium concentrations and $^{238}\text{U}/^{235}\text{U}$ isotope ratios in modern carbonates from the Bahamas; assessing a novel paleoredox proxy. *Chemical Geology* **362**: 305-316.

- Rowland, S. M. 1984. Were there framework reefs in the Cambrian? *Geology* **12**: 181-183.
- Rowland, S. M., and Gangloff, R. A. 1988. Structure and paleoecology of lower Cambrian reefs. *Palaios* **3**: 111-135.
- Rowland, S. M., Oliver, L. K., and Hicks, M. 2008. Ediacaran and early Cambrian reefs of Esmeralda county, Nevada: non-congruent communities within congruent ecosystems across the Neoproterozoic-Paleozoic boundary. *In*: Duebendorfer, E. M., and Smith, E. I., eds., The Geological Society of America Field Guide 11. *Field Guide to Plutons, Volcanoes, Faults, Reefs, Dinosaurs, and Possible Glaciation in Selected Areas of Arizona, California, and Nevada*: GSA, Boulder, CO, p. 83-100.
- Savarese, M. 1995. Functional significance of regular archaeocyathan central cavity diameter - a biomechanical and paleoecological test. *Paleobiology* **21**: 356-378.
- Savarese, M., and Signor, P. W. 1989. New archaeocyathan occurrences in the upper Harkless Formation (lower Cambrian of western Nevada). *Journal of Paleontology* **63**: 539-549.
- Scheltema, R. S. 1986. On dispersal and planktonic larvae of benthic invertebrates: an eclectic overview and summary of problems. *Bulletin of Marine Science* **39**: 290-322.
- Smith, E. F., Macdonald, F. A., Petach, T. A., Bold, U., and Schrag, D. P. 2016. Integrated stratigraphic, geochemical, and paleontological late Ediacaran to early Cambrian records from southwestern Mongolia. *Geological Society of America Bulletin* **128**: 442-468.
- Stanley, G. D., and Fautin, D. G. 2001. The origins of modern corals. *Science* **291**: 1913-1914.
- Stewart, J. H. 1970. Upper Precambrian and lower Cambrian strata in the southern Great Basin, California and Nevada. *US Geological Survey Professional Paper* **620**: 1-206.

- Surge, D., Savarese, M., Dodd, J., and Lohmann, K. 1997. Carbon isotopic evidence for photosynthesis in early Cambrian oceans. *Geology* **25**: 503-506.
- Theisen, C. H., and Sumner, D. Y. 2016. Thrombolite fabrics and origins: influences of diverse microbial and metazoan processes on Cambrian thrombolite variability in the Great Basin, California and Nevada. *Sedimentology* **63**: 2217-2252.
- Tsein, H. H. 1985. Algal-bacterial origin of micrites in mud mounds. *In*: D. Toomey, and M. H. Nitecki eds. *Paleoalgology: Contemporary Research and Applications*. Springer, Berlin: 290-296.
- Veizer, J. 1983. Chemical diagenesis of carbonates: theory and application of trace element techniques. *In*: Arthur, M. A. and Anderson, T. F. eds., *Stable Isotopes in Sedimentary Geology. Society of Economic Paleontologists and Mineralogists Short Course No. 10*, Tulsa, p. 3-1-3-100.
- Vennin, E., Álvaro, J. J., Moreno-Eiris, E., and Perejon, A. 2003. Early Cambrian coelobiontic communities in tectonically unstable crevices developed in Neoproterozoic andesites, Ossa-Morena, southern Spain. *Lethaia* **36**: 53-65.
- Villéger, S., Novack-Gottshall, P. M., and Mouillot, D. 2011. The multidimensionality of the niche reveals functional diversity changes in benthic marine biotas across geological time. *Ecology Letters* **14**: 561-568.
- Voronin, Y. I., Voronova, L. G., Grigorieva, N. V., Drosodova, N. A., Zhegallo, E. A., Zhuravlev, A. Y., Ragozina A. L., Rozanov, A. Y., Sayutina, T. A., Sysoiev, V. A., and Fonin, V. D. 1982. The Precambrian/Cambrian boundary in the geosynclinal areas (Reference section of

- Salany-Gol, Mongolian People's Republic). *Transactions of the Joint Soviet-Mongolia Paleontological Expedition* **18**. Nauka, Moscow (in Russian).
- Voronin, Y. I., Voronin, L. G., Drozdova, N. A., Zhuravlev, A. Y., Rozanov, A. Y., Satutina, T. A., and Fonin, V. D. 1983. Precambrian-Cambrian deposits of Dzun-Artsa section in western Mongolia. *Byulleten Moskovskogo Obshchestva Ispytatelei Prirody Otdel Geologicheskiiy* **58**: 53-66. (In Russian)
- Webb, G. E. 1996. Was Phanerozoic reef history controlled by the distribution of non-enzymatically secreted reef carbonates (microbial carbonate and biologically induced cement)? *Sedimentology* **43**: 947-971.
- Wood, R. A. 1993. Nutrients, predation and the history of reef-building. *Palaios* **8**: 526-543.
- Wood, R.A. 1995. The changing biology of reef-building. *Palaios* **10**: 517-529.
- Wood, R.A., Zhuravlev, A.Y., and Debrenne, F. 1992. Functional biology and ecology of archaeocyatha. *Palaios* **7**: 131-156.
- Wood, R. A., Zhuravlev, A. Y., and Chimed Tseren, A. 1993. The ecology of Lower Cambrian buildups from Zuune Arts, Mongolia: implications for early metazoan reef evolution. *Sedimentology* **40**: 829-858.
- Wu, S., Chen, Z-Q., Fang, Y., Pei, Y., Yang, H., and Ogg, J. 2017. A Permian-Triassic boundary microbialite deposit from the eastern Yangtze Platform (Jiangxi Province, South China): geobiologic features, ecosystems composition and redox conditions. *Palaeogeography, Palaeoclimatology, Palaeoecology* **486**: 58-73.
- Xiaoping, Z. 1995. Lower Cambrian bioherms in central Nevada and eastern California. *Unpublished M.S. thesis*, University of Nevada, Las Vegas, Las Vegas, 119 p.

- Zamora, S., and Álvaro, J. J. 2010. Testing for a decline in diversity prior to extinction. Languedocian (latest mid-Cambrian) distribution of cinctans (Echinodermata) in the Iberian Chains, Ne Spain. *Palaeontology* **53**: 1349-1368.
- Zhuravlev, A.Y., and Wood, R.A. 1995. Lower Cambrian reefal cryptic communities. *Palaeontology* **38**: 443-470.
- Zhuravlev, A.Y., and Naimark, E.B. 2005. Alpha, beta, or gamma: numerical view on the early Cambrian world. *Palaeogeography, Palaeoclimatology, Palaeoecology* **220**: 207-225.
- Zhuravlev, A. Y., Naimark, E., and Wood, R. 2015. Controls on the diversity and structure of earliest metazoan communities: early Cambrian reefs from Siberia. *Earth-Science Reviews* **147**: 18-29.
- Zonenshain, L. P., Kusmin, M. I., and Kononov, M. V. 1985. Absolute reconstructions of the Paleozoic oceans. *Earth and Planetary Science Letters* **74**: 103-116.

Chapter III. Depauperate skeletonized reef-dwelling fauna of the early Cambrian: a literature survey to determine the timing of reef-dweller diversity

Skeletal metazoans appeared in the latest Ediacaran (e.g., the Nama Group) and rapidly diversified into a large array of body plans during the Cambrian (Thomas *et al.*, 2000; Porter, 2007). With the rise of predation, ecological pressures promoted the development of physiologically costly and complex biomineralized skeletons which in turn allowed metazoans to create their own reefal ecosystems (Wood, 2011). By this model, ecology played a role in the origination of skeletons, emphasized further by sessile, attached organisms tending to build skeletons with weaker high-Mg calcite, as they were unable to sustain production of higher cost minerals (e.g., hydroxylapatite) compared to active organisms (Wood and Zhuravlev, 2012; Bush and Pruss, 2013). Furthermore, having a biomineralized skeleton can aid an organism in encrusting and maintaining space in a competitive reef environment as well as protect it from drilling or boring predators (Becker-Kerber *et al.*, 2017; though see Bicknell and Paterson, 2017, for alternative explanation).

Numerous studies on early Cambrian reefs have been performed to date (for review see Gandin and Debrenne, 2010). These reefs were composed of archaeocyaths as the primary metazoan constructors, but were volumetrically minor compared to calcifying microbial organisms. Archaeocyathan reefs declined during Stage 4 of the Cambrian and this resulted in increased abundance of thrombolite-stromatolite communities (Zhuravlev, 1996), though lithistid sponges and coralomorphs were minor contributors (Ezaki *et al.*, 2017). Less work has been done on the reef-dwelling fauna of these early reefs. For the purposes of this study, reef-

dwelling fauna are defined as any organism living in the reef that does not substantially contribute to the construction, binding, or encrustation of the reef. There are several groups of reef-dwelling organisms known from early Cambrian reefs, most commonly trilobites (Repina, 1983), bivalved arthropods (Kobluk and James, 1979), and cancelloriids (James and Klappa, 1983) while additionally phosphatic brachiopods (Jin *et al.*, 1993), calcitic brachiopods (James and Klappa, 1983), and molluscs (Moreno-Eiris, 1987) are relatively rare in reefs. Furthermore, stenotheccoids (Spencer, 1981), hyolithomorph hyoliths (Rozanov and Zhuravlev, 1992), salterellids (James and Klappa, 1983), and echinoderms (Kobluk and James, 1979) are absent in early Atdabanian reefs, but occur later (Pratt *et al.*, 2001). After Series 2, echinoderms are the most prevalent reef-dwelling organisms in microbial reefs (Sumall *et al.*, 1997; Rowland and Shapiro, 2002). In the following interval (Furongian to early Lower Ordovician) many reef-dwelling phyla are depressed in diversity and abundance (Rowland and Shapiro, 2002). However, assessments of reef-dwelling organisms are spread across numerous studies and have not been examined within a single analysis.

Modern reef ecosystems are well known for driving ecological diversity and ancient reef ecosystems show similar patterns (Kiessling *et al.*, 2010). Questions remain as to *when* reefs began to function in these roles as ecological drivers. Furthermore, it is not known if changes in reef-dwellers were a response to changes in framework builders or other ecological parameters. In order to answer questions about early reef diversity I performed a survey of the primary literature to address the timing and nature of reefs as ecological drivers in the early Paleozoic. I find that Ordovician reefs were greater in several biodiversity metrics compared to

the Cambrian and these changes occurred in the early to middle Ordovician. This could be due to the addition of novel heavily skeletonized reef-dwelling organisms.

Typical Reef Dwellers of the Early Cambrian

Here I briefly review the reefs considered in this study (Fig. 3.1). During the Ediacaran, stromatolite and thrombolite reefs were most prevalent (with some dendrolite reefs, see Riding, 1991 for distinctions) and contained very few reef-dwelling organisms before the incorporation of *Cloudina* and *Namacalathus* as reef dwellers (Grotzinger *et al.*, 2000). The skeletal properties (thickness, rigidity) of these organisms are a matter of debate. Some authors suggest that *Namacalathus* was thin, walls < 100 μm (Warren *et al.*, 2017), and flexible (Grotzinger *et al.*, 2000; Wood, 2011), however this could be due to constraints of skeletal growth in a tightly packed environment (Penny *et al.*, 2017). An analysis of *Namacalathus* ultrastructure did show foliated distorted walls, but much remains to be understood about them (Zhuravlev *et al.*, 2015). *Cloudina* had previously been considered a framework-building organism (Vinn and Zaton, 2012; Penny *et al.*, 2014), however, this view has recently come into question as serial sectioning of these organisms suggests that they were weakly skeletonized and did not attach to their substrates (Landing *et al.*, 2018; Mehra and Maloof, 2018, see Penny *et al.*, 2014 for contrasting interpretation). Though their skeletal properties are under debate, it is presumed that these reefs had limited biodiversity with simple ecologies. Much is still unknown about the affinities and life habits of Ediacaran reef dwellers.

Early Cambrian reefs were principally composed of *Renalcis*- and *Epiphyton*-group microbes prior to the incorporation of metazoan framework building archaeocyathan sponges

in the Tommotian (Stage 2) stage of the Cambrian (Kruse *et al.*, 1995; Riding and Zhuravlev, 1995). Early Cambrian reef communities from the Zavkhan Basin, for example, contain several seafloor tiers with radiocyaths and chancelloriids in upper tiers followed by archaeocyaths and minor elements of coralomorphs in lower tiers (Zhuravlev, 2001). Helcionelloid mollusks, tube-dwelling worms, cribricyaths, orthothecimorph hyoliths suspension feeders are found along the seafloor though they are minor compared to redlichoid trilobites (Zhuravlev, 2001). After the near extinction of archaeocyaths during late Stage 4 of the Cambrian, new organisms filled the role of metazoan framework builders, such as lithistid sponges and later, receptaculitaleans (Fig. 3.1 and citations therein). Thrombolite reefs also became more common during this interval (Chen *et al.*, 2014). These sponge and thrombolite reefs were later replaced as hypercalcifying organisms such as stromatoporoids and tabulate corals diversified during the onset of the Ordovician Radiation. Pelagic plankton diversified during the late Cambrian and Ordovician allowing for the proliferation of suspension feeding organisms such as rhynchonellate brachiopods, crinoids, rugose corals, bryozoans (Servais *et al.*, 2008) and predatory cephalopods (Kröger *et al.*, 2009). While the transition between the Cambrian and Ordovician radiations may not be a distinct event, it nonetheless represents a major change in the dominant organisms observed in the marine fossil record (Droser and Finnegan, 2003, Landing *et al.*, 2018).

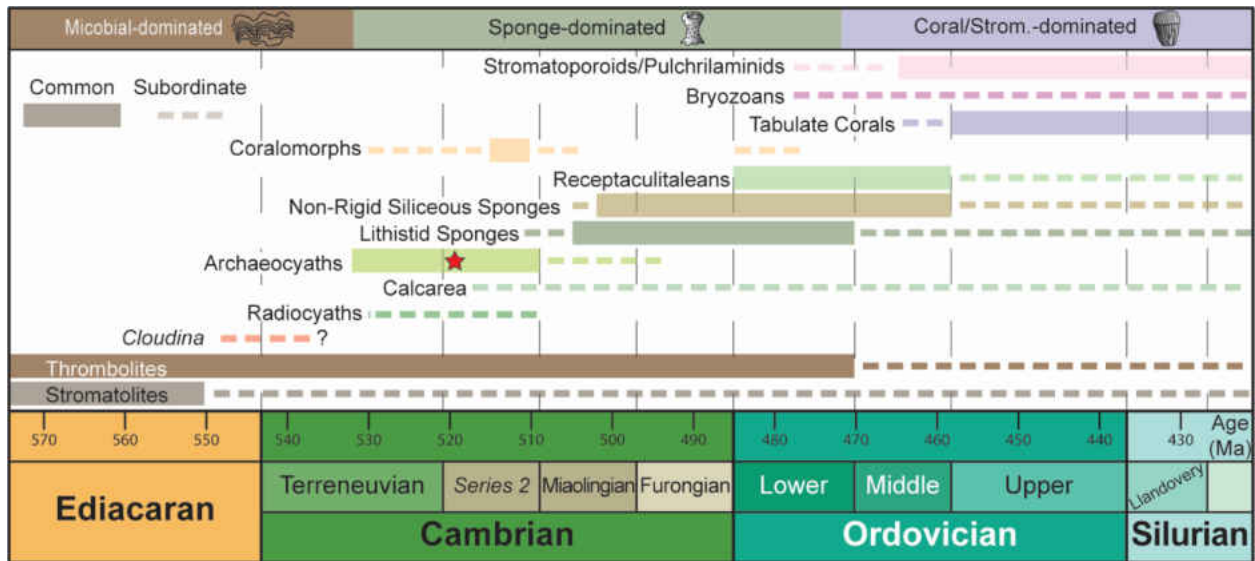


Figure 3.1: Primary reef builders during the Neoproterozoic and early Paleozoic. Neoproterozoic is primarily dominated by microbial organisms. The Cambrian is dominated by a variety of sponge organisms prior to the coral and stromatoporoid dominated Ordovician and Silurian. Red star denotes approximate interval of Mongolian reefs (see above). Ranges of reef builders defined from following studies: *Cloudina* – Penny *et al.*, 2014, “?” denotes uncertain framework building ability (Mehra and Maloof, 2018); Thrombolite – Shapiro and Awramik, 2006; Radiocyaths – Kruse, 1991; Calcarea (termed “pharetronids” in study) – Reitner *et al.*, 2017; Lithistid sponges – Lee *et al.*, 2016c; Non-rigid siliceous sponges – Lee *et al.*, 2016b; Bryozoan and stromatoporoids – Hong *et al.*, 2017.

Materials and Methods

A semiquantitative analysis of reef-dwelling organisms was conducted from 40 papers. Papers were selected to encompass a broad geographic distribution and assess skeletal macrofossils only. Localities were divided into four time intervals covering the Ediacaran, “early” Cambrian (Terreneuvian and Series 2), “late” Cambrian (Series 3 [Miaolingian] and Furongian), and Ordovician. Macroscopic reef-dwelling organisms mentioned in these papers were placed into one of three relative abundance categories based on their percent contribution (if provided), qualitative description or figures (e.g., if a fauna was described as “abundant”), and taphonomic status (only identified descriptions were used). Fauna were

classified as either “rare” (if constituting < 5% of total material or described as rare, sparse, fragmented, etc.), “frequent” (6 - 50% of total material or described as occasional, common, frequent, etc.), or “abundant” (> 50% of total material or described as abundant, dominant, dense, etc.). Literature was also surveyed for presence of trace fossils, type of framework builder, and method of observation. Presence of small shelly fossils (SSF; e.g., sachtids, halkieriids, tomotiids, coleolids, anabaritids, etc.) and macroalgae (e.g., “*Nuia*”) were also noted. However, these organisms were not used in analyses as they were not consistently identified and many do not have well-defined ecological descriptions (see Steiner *et al.*, 2007 for SSF definition used here).

Resulting macroscopic reef-dwelling fauna were then divided into functional groups based on functional group descriptions modified from Dineen *et al.* (2014). A functional group is a group of taxonomically distinct organisms that perform similar functional roles in their environment based on shared ecological characteristics. Resulting functional group richness was analyzed with Kruskal-Wallis and ordinary least squares linear regression analysis.

The skeletal characteristics of each organism were assigned to one of three categories, either (1) flexible and/or lightly skeletonized, (2) skeletonized with easily disarticulated elements (i.e., trilobites), and (3) single-large-element skeletons (i.e., cephalopods) and/or hypercalcifying (i.e., *Namapoikia*). Collecting data in this manner allows for three different comparisons of fauna, namely, (1) abundance, (2) functional richness, and (3) skeletal characteristics.

Results

General results.— The papers selected for this study have a diverse geographic (20 countries, seven continents) and temporal (13 geologic stages and the Ediacaran) distribution. Comparative graphs of functional richness grouped by geographic locality, publication author, primary framework builder, and sampling methodology showed no significant trends. Regression analysis of functional richness and year of publication also showed no trends (Figure E2). For complete dataset, including justifications for categorization, see Table C2 and C3.

Numerous lightly skeletonized enigmatic tube fossils are known from the late Ediacaran. These organisms mostly do not contribute to framework building and arguably did not even occupy reefs *in situ* (Mehra and Maloof, 2018). The following analysis was run with these organisms included. However, removal of these organisms would only strengthen the trends discussed below by reducing the diversity of the Ediacaran (Table E3).

Organismal abundance.— The proportion of frequent and abundant functional groups was higher during the Ordovician than in either the Ediacaran or Cambrian (Table 3.1; Fig. 3.2). By our criteria, no macroscopic reef-dwelling organisms were considered abundant in the Ediacaran or Cambrian, while five were considered abundant in the Ordovician (Table 3.1). The proportion of frequent organisms also increases to a maximum of 28.8% in the Ordovician. This represents a 60.9% increase between the early Cambrian and Ordovician.

Table 3.1: Abundance data for functional groups by geologic interval collected from literature survey.

Geologic Interval	Rare		Frequent		Abundant		No Indication		Total N	Fun. Av.	Skeletal
	N	%	N	%	N	%	N	%			
Ordovician	41	63.1	19	29.2	5	7.7	0	0	65	5.9	0/38/27
L. Cambrian	12	66.7	2	11.1	0	0	4	22.2	18	2.8	0/16/2
E. Cambrian	56	77.8	11	15.3	0	0	5	6.9	72	3.8	0/72/0
Ediacaran	11	91.7	1	8.3	0	0	0	0	12	2.0	11/0/1

Skeletal column shows number of functional groups in thin-wall/weak/heavy skeleton categories. Fun. Av. – functional richness average

Functional richness.— Macroscopic reef-dweller functional richness averaged 2.0, 3.7, 2.8, and 6.0 for the Ediacaran, early Cambrian, late Cambrian, and Ordovician respectively (Table 3.1). This represents a threefold increase in functional richness from the beginning to the end of the study interval. Furthermore, a Kruskal-Wallis test suggests that these averages are statistically different across time intervals (p -value $\ll 0.001$; see Table E3 for pairwise comparisons). Specifically, the Ordovician had significantly more functional richness than any other time period in this study. It is also interesting to note that the late Cambrian and the Ediacaran are statistically similar. Functional groups F6, F7, and F8 (in general trilobites, pelmetazoans, and brachiopods) are the most common and persistent functional groups and appear in 91%, 74%, and 77% respectively of Cambrian/Ordovician localities. To clarify, there is undoubtedly turnover in fauna, e.g., the extinction of Cambrian trilobites replaced by Ordovician trilobites (Foote, 1988), however, this analysis was performed with ecological descriptions and thus misses these turnover events. Nonetheless, the fact that changes are

evident even at coarse levels of group categorization supports the robustness of this increase in functional richness.

Skeletonization. — The Ediacaran reef-dwelling fauna is composed mainly (90.0%) of lightly-skeletonized organisms, such as *Cloudina* (Wood, 2011). The exceptions to this are *Namapoikia*, which had a hypercalcifying skeleton and *Namacalathus* possessing a tripartite foliated shell. The early and late Cambrian are dominated entirely (100% and 88.2%) by reef-dwelling organisms with moderately skeletonized, easily disarticulated carbonate skeletons (trilobites, echinoderms, chancelloriids), or small phosphatic and carbonate shells (brachiopods, hyoliths) which easily disarticulate after death of the organism. Finally, the Ordovician retains many of the Cambrian Fauna, but adds several single-large-element skeletonized organisms such as gastropods and cephalopods or robust modular organisms like bryozoans and rugose corals (Fig. 3.2). 40.9% of Ordovician fauna were considered heavily-skeletonized (Table 3.1).

	Locality	Fossil Groups														Num. Functional Trace Fossils	Frame Builders
		F1 (Namacalathus)	F2 (Clouatina)	F3 (Hyolithelminthida)	F4 (Chancelitoria)	F5 (Hyolitha)	F6 (Triobolus)	F7 (Pelmatozoa)	F8 (Brachiopoda)	F9 (Ostracoda, others)	F10 (Gastropoda)	F11 (Bryozoa)	F12 (Cephalopoda)	F13 (Namacopikia)	F14 (Rugosa)		
Ordovician	Russia ⁽⁴⁰⁾						○			○	○			○		4	Tabulates
	Norway ⁽³⁹⁾					○	●	○	○	○	○	○		○		8	Tabulates, Stromatoporoids
	Estonia ⁽³⁸⁾					○	●	○	○	○	○			○		6	Tabulates, Bryozoa, Receptaculitales
	North China ⁽³⁷⁾				○	○	○	○	○	○	○					7	Stromatolites, Receptaculitales
	Tennessee ⁽³⁶⁾					○	○	○	○	○	○					7	Tabulates, Stromatoporoids
	Canada ⁽³⁵⁾				○	○	○	○	○	○	○					7	Bryozoa, Tabulates, Lithistids
	Korea ⁽³⁴⁾					○	○	○	○	○	○					6	Stromatolites, Lithistids
	Utah ⁽³³⁾				○	○	○	○	○	○	○			●		6	Lithistids (?)
	South China ⁽³²⁾					○	○	○		○	○					6	Receptaculitales, Stromatoporoids, Lithistids
	South China ⁽³¹⁾					○	○	○		○	○			○	○	6	Tabulates, Bryozoa, Lithistids
	Argentina ⁽³⁰⁾					○				○	○			○	○	3	Thrombolite, Coralomorph
L. Cambrian	North China ⁽²⁹⁾					○			○	○					4	Thrombolite	
	California/Neavda ⁽²⁸⁾					○	○	○							3	Stromatolites, Lithistids	
	Iran ⁽²⁷⁾				○	○	○	○							4	Thrombolite, Lithistids	
	Korea ⁽²⁶⁾					○	○								2	Non-Rigid Siliceous Sponges	
	Inner Mongolia ⁽²⁵⁾					○									1	Thrombolite	
	Australia ⁽²⁴⁾				○	○	○	○							3	Thrombolite, Spiculate Sponges	
Early Cambrian	South China ⁽²³⁾			○	○	○	○	○							5	Thrombolite, Archaeocyaths	
	Australia ⁽²²⁾			○	○	○	○	○							5	Thrombolite, Archaeocyaths, Radiocyaths	
	N. Spain ⁽²¹⁾				○	○	○	○							4	Thrombolite, Archaeocyaths	
	Newfoundland ⁽²⁰⁾				○	○	○	○					○		4	Thrombolite, Archaeocyaths	
	France ⁽¹⁹⁾			○	○	○	○	○							5	Thrombolite, Archaeocyaths	
	Sardinia ⁽¹⁸⁾				○	○	○	○							4	Thrombolite, Archaeocyaths	
	Virginia, USA ⁽¹⁷⁾					○	○						○		2	Thrombolite, Archaeocyaths	
	Antarctica ⁽¹⁶⁾					○	○								2	Thrombolite, Archaeocyaths	
	Canada ⁽¹⁵⁾				○	○	○	○							4	Thrombolite, Archaeocyaths	
	California/Nevada ⁽¹⁴⁾					○	○	○							3	Thrombolite, Archaeocyaths	
	Mexico ⁽¹³⁾				○	○	○	○							5	Thrombolite, Archaeocyaths	
	South China ⁽¹²⁾			○	○	○	○	○							5	Thrombolite, Archaeocyaths	
	Australia ⁽¹¹⁾				○	○	○	○					○		4	Thrombolite, Archaeocyaths, Spongiomorphs	
	Morocco ⁽¹⁰⁾			○	○	○	○						○		4	Thrombolite, Archaeocyaths	
	Mongolia ⁽⁹⁾					○		○					○		2	Thrombolite, Archaeocyaths, Coralomorphs, Radiocyaths	
	Mongolia ⁽⁸⁾				○	○		○					○		3	Thrombolite, Archaeocyaths, Coralomorphs, Radiocyaths	
	Spain ⁽⁷⁾				○	○		○					○		3	Thrombolite, Archaeocyaths	
Russia ⁽⁶⁾			○	○	○							○		3	Thrombolite, Archaeocyaths, Coralomorphs		
Ediacaran	Canada ⁽⁵⁾	○	○												2	Stromatolite	
	Paraguay ⁽⁴⁾	○	○												2	Thrombolite	
	Oman ⁽³⁾	○	○												2	Stromatolite, Thrombolite	
	Namibia ⁽²⁾	○	○									○			3	Stromatolite, Thrombolite	
	South China ⁽¹⁾	○													1	Thrombolite?	

Figure 3.2: Results of literature survey. Collected from 40 selected Neoproterozoic and early Paleozoic reef papers on macroscopic reef dwellers. Papers are organized according to stages within geologic time periods with more recent stages on top (see Table C2 and C3). Taxa are organized roughly in order of skeletonization with flexible and/or lightly skeletonized organisms (white columns) on left, disarticulated skeletonized organisms (light blue columns), and single-large-element skeletonized organisms (dark blue columns) on right. Black and white circles denote organism abundances. Occurrences of SSF (which include any mineralized remains of disarticulated unknown metazoans or shells) and macroalgae denotes by purple and green circles respectively. Observation of trace fossils in reef is denoted by yellow circle. Number of functional groups and type of framework builder also displayed for each locality. Functional groups labelled as F1-F14 on top with example taxa listed in parentheses (see Appendix C for full list of included taxa in each functional group). (1) Hau *et al.*, 2007 and Cai *et al.*, 2014; (2) Penny *et al.*, 2014; (3) Amthor *et al.*, 2003; (4) Warren *et al.*, 2017; (5) Hofmann and Mountjoy, 2001; (6) Kruse *et al.*, 1995; (7) Creveling *et al.*, 2013; (8) Kruse *et al.*, 1996; (9) Cordie, see above; (10) Álvaro *et al.*, 2006; (11) James and Gravestock, 1990; (12) Hicks and Rowland, 2009; (13) Debrenne *et al.*, 1989; (14) Cordie, see above; (15) Read, 1980; (16) Rees *et al.*, 1989; (17) McMenamin *et al.*, 2000; (18) Pillola *et al.*, 1998; (19) Debrenne *et al.*, 2002; (20) Pruss *et al.*, 2012; (21) Perejón *et al.*, 2012; (22) Kruse *et al.*, 1991; (23) Adachi *et al.*, 2013; (24) Kruse and Reitner, 2014; (25) Lee *et al.*, 2016a; (26) Hong *et al.*, 2012; (27) Kruse and Zhuravlev, 2008; (28) Shapiro and Rigby, 2004; (29) Chen *et al.*, 2014; (30) Carrera *et al.*, 2017; (31) Li *et al.*, 2004; (32) Adachi *et al.*, 2013; (33) Pruss *et al.*, 2010; (34) Choh *et al.*, 2013; (35) Pratt, 1989; (36) Alberstadt *et al.*, 1974; (37) Zhang *et al.*, 2014; (38) Kröger *et al.*, 2017; (39) Harland, 1981; (40) Antoshkina, 1999.

Discussion

Depauperate reef-dwelling macrobiota.— Even though the Salaagol and Poleta Formation microbial-archaeocyathan reefs include framework builders, binding microbial organisms, and cavity space (see above), the corresponding niche filling by macroscopic, skeletal reef dwellers that one might anticipate for reef ecosystems is not observed. The literature survey suggests that this is not unusual for reefs of this age (Fig. 3.2). Rather the early Cambrian represents a transitional stage of biological development during the Cambrian Radiation but prior to the full-scale skeletonization associated with the Ordovician Radiation (Servais *et al.*, 2016). This may have resulted in reef communities with the expected

skeletonized framework-building organisms, but lacking in skeletonized metazoans adapted to living in the niches they provided. Furthermore, I infer that these reefs were able to support organisms, as thin sections do show sparse occurrences of several organisms, trace fossils are common throughout these reefs (Fig. 3.2), suggesting unaccounted for soft-bodied diversity, and previous studies have shown a variety of SSF organisms including cancelloriids, tomotiids, hyolithelminths, halkieriids, anabaritids, and helcioneloid molluscs (Esakova and Zhegallo, 1996). Yet, reefs remained reduced in diversity in terms of macrofauna. For example, acid extraction studies from the Salaagol Formation found fauna remains to, in general, be small (< 840 μm) and only 37.5% of samples had more than minor contributions from reef dwellers (Pruss *et al.*, 2017).

I conclude from these two independent datasets - point count (chapter II) and literature survey - that prior to the Ordovician, reefs had (1) low abundance, (2) low functional richness, and (3) fewer skeletonized reef-dwelling macrofossils. The fact that these patterns are expressed in three different biological diversity metrics supports a more robust claim that Cambrian reefs had fewer macroscopic reef-dwellers compared to later Paleozoic reefs. I argue that abundance and diversity should be treated as independent lines of evidence as trends in abundance and diversity are not always synchronized (Finnegan and Droser, 2005; Liu *et al.*, 2016). Furthermore, increases in skeletal contributions are observed in other studies across the Cambrian and Ordovician (Pruss *et al.*, 2010). Cambrian reefs were depauperate in skeletonized macroscopic reef dwellers, but that changed with the onset of the Ordovician Radiation and the incorporation of new hypercalcifying organisms into reef ecosystems.

Macroscopic reef-dweller biodiversity.— There are several factors that could explain the shift in reef dwellers during this interval, which may not be mutually exclusive. First, a taphonomic bias may be hiding large amounts of diversity in the Ediacaran and early Cambrian. As demonstrated by Burgess Shale-type deposits around the world, soft-bodied organisms are present in the Cambrian, but were not preserved in most depositional settings (Slater *et al.*, 2016). Furthermore, this study shows that trace fossils were observed at 11 out of 18 early Cambrian localities, suggesting additional soft-bodied diversity was present (Fig. 3.2). It is important to note that the observations made here are more representative of trends in *skeletonized* reef-dwelling fauna as opposed to all fauna. Skeletonized fauna are less susceptible to taphonomic biases, though not immune, compared to total diversity which would include soft-bodied organisms.

Second, changes in the geochemical properties of the ocean could have induced a shift in reef-building diversity in the Ordovician. Reef-builder size appears to have increased in the early Paleozoic and some have tied these changes to an increase in oxygen in these environments (Lee and Riding, 2018). This could enhance reef longevity and allow for additional reef-dwellers to inhabit these environments. However, more work needs to be performed on the morphological diversity of early Cambrian reefs to determine if changes occurred. In addition, modern reefs are typically in oligotrophic environments (Kleypas *et al.*, 1999; Wood, 1999) while Cambrian reefs were most likely in meso- to eutrophic settings (Wood *et al.*, 1992; Wood, 1993). A shift in nutrient availability could have affected reef builders and organisms within these reefs. However, this study does not provide data on nutrient levels and remains speculative at this time (though see Martin, 1996).

Third, the increase in abundance and functional richness could represent a true increase in reef-dweller diversity. During the early Ordovician, the number of microplankton species increased substantially (Servais *et al.*, 2009). This could in turn stimulate the base of the food web and result in larger resource pools for higher trophic levels (Bambach, 1993). An increase in planktonic food sources would have also provided additional resources for suspension feeding organisms and for production of biomineralized skeletons (Bush and Pruss, 2013). Therefore, the increase in abundance of reef-dwelling organisms from the Ediacaran to the Ordovician may be a result of growth in the lower trophic levels that sustain these organisms, while the increase in functional richness represents the diversification of organisms to utilize these resources. Furthermore, the increase in diversity between the Ediacaran-Cambrian-Ordovician periods shown here also concurs with the increasing trend of clonal modular organisms over this period (Landing *et al.*, 2018).

Finally, increases in skeletonized organisms could represent an ecological expansion or evolution of skeletonized reef-dwelling organisms into new niches. Reef ecosystems are highly diverse and therefore competitive environments and predator density potentially increased during this period (Bambach, 2002). For organisms to live in these environments, they would have required effective anti-predatory adaptations such as shells, spines, or modular body plans. Because reefs are also shallow, high-energy environments, protection from wave breaking and UV is also required (Jokiel, 1980). This can best be accomplished by way of hard, skeletonized body parts. Organisms that evolved these features may now have been able to expand into these environments and benefit from the nutrients and resources that reefs

provide. Thus, reefs became more diverse as skeletons evolved to allow organisms to live in these competitive environments.

Conclusions

Macroscopic reef-dwelling fauna are scarce in early Cambrian reefs due to the transitional nature of the early Cambrian. Not until the Ordovician were global productivity levels and biomass high enough to support a diverse skeletonized reef community with abundant and functionally diverse organisms. Furthermore, the development of skeletons may be a principle driver in sustaining diversity in reef environments during the Ordovician. When reef dwellers adapted to the competitive environment of reefs, these ecosystems increased in biodiversity. Therefore, during the earliest Paleozoic, having a reef framework in place does not necessarily correlate with higher diversity of skeletonized reef dwellers.

References

- Adachi, N., Liu, J., and Ezaki, Y. 2013. Early Ordovician reefs in South China (Chenjiahe section, Hubei Province): deciphering the early evolution of skeletal-dominated reefs. *Facies* **59**: 451-466.
- Alberstadt, L. P., Walker, K. R., and Zurawski, R. P. 1974. Patch reefs in the Carters Limestone (Middle Ordovician) in Tennessee and vertical zonation in Ordovician reefs. *Geological Society of America Bulletin* **85**: 1171-1182.
- Álvaro, J. J., Clausen, S., El Albani, A., and Chellai, E. 2006. Facies distribution of the Lower Cambrian cryptic microbial and epibenthic archaeocyathan-microbial communities, western Anti-Atlas, Morocco. *Sedimentology* **53**: 35-53.

- Amthor, J. E., Grotzinger, J. P., Schröder, S., Bowring, S. A., Ramezani, J., Martin, M. W., and Matter, A. 2003. Extinction of *Cloudina* and *Namacalathus* at the Precambrian-Cambrian boundary in Oman. *Geology* **31**: 431-434.
- Antoshkina, A. I. 1999. Origin and evolution of lower Paleozoic reefs in the Pechora Urals, Russia. *Bulletin of Canadian Petroleum Geology* **47**: 86-103.
- Bambach, R. K. 1993. Seafood through time: changes in biomass, energetics, and productivity in marine ecosystems. *Paleobiology* **19**: 372-397.
- Bambach, R. K. 2002. Supporting predators: changes in the global ecosystem inferred from changes in predator diversity. *Paleontological Society Papers* **8**: 319-351.
- Becker-Kerber, B., Pacheco, L. A. F., Rudnitzki, I. D., Galante, D., Rodrigues, F., and Leme, J. de M. 2017. Ecological interactions in *Cloudina* from the Ediacaran of Brazil: implications for the rise of animal biomineralization. *Scientific Reports* **7**: 5482.
- Bicknell, R. D., and Paterson, J. R. 2018. Reappraising the early evidence of durophagy and drilling predation in the fossil record: implications for escalation and the Cambrian Explosion. *Biological Reviews* **93**: 754-784.
- Bush, A. M., and Pruss, S. B. 2013. Theoretical ecospace for ecosystem paleobiology: energy, nutrients, biominerals, and macroevolution. *The Paleontological Society Papers* **19**: 1-20.
- Cai, Y., Hua, H., Schiffbauer, J. D., Sun, B., and Yuan, X. 2014. Tube growth and microbial mat-related lifestyles in the Ediacaran fossil *Cloudina*, Gaojiashan Lagerstätte, South China. *Gondwana Research* **25**: 1008-1018.

- Carrera, M. G., Astini, R. A., and Gomez, F. J. 2017. A lowermost Ordovician tabulate-like coralomorph from the Precordillera of western Argentina: a main component of a reef-framework consortium. *Journal of Paleontology* **81**: 73-85.
- Chen, J., Lee, J-H., and Woo, J. 2014. Formative mechanisms, depositional processes, and geological implications of Furongian (late Cambrian) reefs in the North China Platform. *Palaeogeography, Palaeoclimatology, Palaeoecology* **414**: 246-259.
- Choh, S-J., Hong, J., Sun, N., Kwon, S-W., Park, T-Y., Woo, J., Kwon, Y. K., Lee, D-C., and Lee, D-J. 2013. Early Ordovician reefs from the Taebaek Group, Korea: constituents, types, and geological implications. *Geosciences Journal* **17**: 139-149.
- Creveling, J. R., Fernández-Remolar, D., Rodríguez-Martínez, M., Menéndez, S., Bergmann, K. D., Gill, B. C., Abelson, J., Amils, R., Ehlmann, B. L., García-Bellido, D. C., Grotzinger, J. P., Hallmann, C., Stack, K. M., and Knoll, A. H. 2013. Geobiology of a lower Cambrian carbonate platform, Pedroche Formation, Ossa Morena Zone, Spain. *Palaeogeography, Palaeoclimatology, Palaeoecology* **386**: 459-478.
- Debrenne, F., Gandin, A., and Rowland, S. M. 1989. Lower Cambrian bioconstructions in Northwestern Mexico (Sonora). Depositional setting, paleoecology and systematics of archaeocyaths. *Geobios* **22**: 137-195.
- Debrenne, F., Gandin, A., and Courjault-Radé, P. 2002. Facies and depositional setting of the lower Cambrian archaeocyath-bearing limestones of southern Montagne Noire (Massif Central, France). *Bulletin de la Société Géologique de France* **6**: 533-546.

- Dineen, A. A., Fraiser, M. L., and Sheehan, P. M. 2014. Quantifying functional diversity in pre- and post-extinction paleocommunities: a test of ecological restructuring after the end-Permian mass extinction. *Earth-Science Reviews* **136**: 339-349.
- Droser, M. L., and Finnegan, S. 2003. The Ordovician Radiation: a follow-up to the Cambrian explosion? *Integrative and Comparative Biology* **43**: 178-184.
- Esakova, N. V., and Zhegallo, E. A. 1996. Biostratigraphy and fauna of the lower Cambrian of Mongolia. *Trudy, Sovmestnaya Rossiysko-Mongol'skaya Paleontologicheskaya Ekspeditsiya* **46**: 1-214.
- Ezaki, Y., Liu, J., Adachi, N., and Yan, Z. 2017. Microbialite development during the protracted inhibition of skeletal-dominated reefs in the Zhangxia Formation (Cambrian Series 3) in Shandong Province, North China. *Palaios* **32**: 559-571.
- Finnegan, S., and Droser, M. L. 2005. Relative and absolute abundance of trilobites and rhynchonelliform brachiopods across the lower/middle Ordovician boundary, eastern Basin and Range. *Paleobiology* **31**: 480-502.
- Foot, M. 1988. Survivorship analysis of Cambrian and Ordovician trilobites. *Paleobiology* **14**: 258-271.
- Gandin, A., and Debrenne, F. 2010. Distribution of the archaeocyath-calcimicrobial bioconstructions on the early Cambrian shelves. *Palaeoworld* **19**: 222-241.
- Grotzinger, J. P., Watters, W. A., and Knoll, A. 2000. Calcified metazoans in thrombolite-stromatolite reefs of the terminal Proterozoic Nama Group, Namibia. *Paleobiology* **26**: 334-359.
- Harland, T. L. 1981. Middle Ordovician reefs of Norway. *Lethaia* **14**: 169-188.

- Hau, H., Chen, Z., and Yuan, X. 2007. The advent of mineralized skeletons in Neoproterozoic metazoa-new fossil evidence from the Gaojiashan Fauna. *Geological Journal* **42**: 263-279.
- Hicks, M., and Rowland, S. M. 2009. Early Cambrian microbial reefs, archaeocyathan inter-reef communities, and associated facies of the Yangtze Platform. *Palaeogeography, Palaeoclimatology, Palaeoecology* **281**: 137-153.
- Hofmann, H. J., and Mountjoy, E. W. 2001. *Namacalathus-Cloudina* assemblage in Neoproterozoic Miette Group (Byng Formation), British Columbia: Canada's oldest shelly fossils. *Geology* **29**: 1091-1094.
- Hong, J., Cho, S-H., Choh, S-J., Woo, J., and Lee, D-J. 2012. Middle Cambrian siliceous sponge-calcimicrobe buildups (Daegi formation, Korea): metazoan buildup constituents in the aftermath of the early Cambrian extinction event. *Sedimentary Geology* **253-254**: 47-57.
- Hong, J., Oh, J-R., Lee, J-H., Choh, S-J., and Lee, D-J. 2017. The earliest evolutionary link of metazoan bioconstruction: laminar stromatoporoids-bryozoan reefs from the Middle Ordovician of Korea. *Palaeogeography, Palaeoclimatology, Palaeoecology* **492**: 126-133.
- James, N. P., and Klappa, C. F. 1983. Petrogenesis of early Cambrian reef limestones, Labrador, Canada. *Journal of Sedimentary Petrology* **53**: 1051-1096.
- James, N. P., and Gravestock, D. I. 1990. Lower Cambrian shelf and shelf margin buildups, Flinders Range, South Australia. *Sedimentology* **37**: 455-480.
- Jin, Y., Hou, X., and Wang, H. 1993. Lower Cambrian pediculate lingulids from Yunnan, China. *Journal of Paleontology* **67**: 788-798.
- Jokiel, P. L. 1980. Solar ultraviolet radiation and coral reef epifauna. *Science* **207**: 1069-1071.

- Kiessling, W., Simpson, C., and Foote, M. 2010. Reefs as cradles of evolution and sources of biodiversity in the Phanerozoic. *Science* **327**: 196-198.
- Kleypas, J. A., McManus, J. W., and Meñes, L. A. B. 1999. Environmental limits to coral reef development: where do we draw the line? *American Zoologist* **39**: 146-159.
- Kobluk, D. R., and James, N. P. 1979. Cavity-dwelling organisms in lower Cambrian patch reefs from southern Labrador. *Lethaia* **12**: 193-218.
- Kröger, B., Servais, T., and Zhang, Y. 2009. The origin and initial rise of pelagic cephalopods in the Ordovician. *PLoS ONE* **4**: e7262.
- Kröger, B., Hints, L., and Lehnert, O. 2017 Ordovician reef and mound evolution: the Baltoscandian picture. *Geological Magazine* **154**: 683-706.
- Kruse, P. D. 1991. Cyanobacterial-archaeocyathan-radiocyathan bioherms in the Wirrealpa Limestone of South Australia. *Canadian Journal of Earth Sciences* **28**: 601-615.
- Kruse, P. D., and Zhuravlev, A. Y. 2008. Middle-Late Cambrian *Rankenella-Girvanella* reefs of the Mila Formation, northern Iran. *Canadian Journal of Earth Science* **45**: 619-639.
- Kruse, P. D., and Reitner, J. R. 2014. Northern Australian microbial-metazoan reefs after the mid-Cambrian mass extinction. *Memoirs of the Association of Australian Palaeontologists* **45**: 31-53.
- Kruse, P. D., Zhuravlev, A. Y., and James, N. P. 1995. Primordial metazoan-calcimicrobial reefs: Tommotian (early Cambrian) of the Siberian Platform. *Palaios* **10**: 291-321.
- Kruse, P. D., Gandin, A., Debrenne, F., and Wood, R. 1996. Early Cambrian bioconstructions in the Zavkhan Basin of western Mongolia. *Geological Magazine* **133**: 429-444.

- Landing, E., Antcliffe, J. B., Geyer, G., Kouchinsky, A., Bowser, S. S., and Andreas, A. 2018. Early evolution of colonial animals (Ediacaran Evolutionary Radiation-Cambrian Evolutionary Radiation-Great Ordovician Biodiversification Interval). *Earth-Science Reviews* **178**: 105-135.
- Lee, J-H., and Riding, R. 2018. Marine oxygenation, lithistid sponges, and the early history of Paleozoic skeletal reefs. *Earth-Science Reviews* **181**: 98-121.
- Lee, J-H., Kim, D-J., Liang, K., Park, T-Y. S., Choh, S-J., Lee, D-J., and Woo, J. 2016a. Cambrian reefs in the western north China Platform, Wuhai, Inner Mongolia. *Acta Geologica Sinica (English Edition)* **90**: 1946-1954.
- Lee, J-H., Hong, J., Lee, D-J., Choh, S-J. 2016b. A new Middle Ordovician bivalve-siliceous sponges-microbe reef-building consortium from North China. *Palaeogeography, Palaeoclimatology, Palaeoecology* **457**: 23-30.
- Lee, J-H., Woo, J., and Lee, D-J. 2016c. The earliest reef-building anathaspidellid sponge *Rankenella zhangxianensis* n. sp. from the Zhangxia Formation (Cambrian Series 3), Shandong Province, China. *Journal of Paleontology* **90**: 1-9.
- Li, Y., Kershaw, S., and Mu, X. 2004. Ordovician reef systems and settings in South China before the Late Ordovician mass extinction. *Palaeogeography, Palaeoclimatology, Palaeoecology* **205**: 235-254.
- Liu, J., Ezaki, Y., Adachi, N., and Zhan, R. 2016. Evidence for decoupling of relative abundance and biodiversity of marine organisms in initial stage of GOBE: a preliminary study on lower Ordovician shellbeds of South China. *Journal of Earth Science* **21**: 44-48.

- Martin, R. E. 1996. Secular increase in nutrient levels through the Phanerozoic: implications for productivity, biomass, and diversity of marine biospheres. *Palaios* **11**: 209-219.
- McMenamin, M. A. S., Debrenne, F., and Zhuravlev, A. Y. 2000. Early Cambrian Appalachian archaeocyaths: further age constraints from the fauna of New Jersey and Virginia, U.S.A. *Geobios* **33**: 693-708.
- Mehra, A., and Maloof, A. 2018. Multiscale approach reveals that *Cloudina* aggregates are detritus and not in situ reef constructions. *Proceedings of the National Academy of Science*: <https://doi.org/10.1073/pnas.1719911115>.
- Moreno-Eiris, E. 1987. Los montículos arrecifales de algas y arqueociatos del Cámbrico Inferior de Serra Morena. *Boletín Geológico y Minero* **98**: 1-127.
- Penny, A. M., Wood, R., Curtis, A., Bowyer, F., Tostevin, R., and Hoffman, K-H. 2014. Ediacaran metazoan reefs from the Nama Group Namibia. *Science* **344**: 1504-1506.
- Penny, A. M., Wood, R. A., Zhuravlev, A. Y., Curtis, A., Bowyer, F., and Tostevin, R. 2017. Intraspecific variation in an Ediacaran skeletal metazoan: *Namacalathus* from the Nama Group, Namibia. *Geobiology* **15**: 81-93.
- Perejón, A, Moreno-Eiris, E., Bechstädt, T., Menéndez, S., and Rodríguez-Martínez, M. 2012. New Bilbilian (early Cambrian) archaeocyath-rich thrombolytic microbialite from the Láncara Formation (Cantabrian Mts., northern Spain). *Journal of Iberian Geology* **38**: 313-330.
- Pillola, G. L., Leone, F., and Loi, A. 1998. The Cambrian and early Ordovician of SW Sardinia. *Giornale di Geologia, Special Issue ECOS VII-Sardinia Guidebook* **60**: 25-38.

- Porter, S. M. 2007. Seawater chemistry and early carbonate biomineralization. *Science* **316**: 1302.
- Pratt, B. R. 1989. Small early Middle Ordovician patch reefs, Laval Formation (Chazy Group), Caughnawaga, Montreal area, Quebec. *In*: H. H. J. Geldsetzer, N. P. James, and G. E. Tebbutt eds. Reefs, Canada and Adjacent Area. *Canadian Society of Petroleum Geologists Memoir* **13**, Calgary, Canada: 218-223.
- Pratt, B. R., Spincer, B. R., Wood, R. A., and Zhuravlev, A. Y. 2001. Ecology and Evolution of Cambrian Reefs. *In*: Zhuravlev, A. Y., and Riding, R. eds. *The Ecology of the Cambrian Radiation*. New York: Columbia University Press: 254-274.
- Pruss, S. B., Finnegan, S., Fischer, W., and Knoll, A. 2010. Carbonates in skeleton-poor seas: new insights from Cambrian and Ordovician strata of Laurentia. *Palaios* **25**: 73-84.
- Pruss, S. B., Clemente, H., and Laflamme, M. 2012. Early (Series 2) Cambrian archaeocyathan reefs of southern Labrador as a locus for skeletal carbonate production. *Lethaia* **45**: 401-410.
- Pruss, S. B., Dwyer, C. H., Smith, E. F., Macdonald, F. A., and Tosca, N. J. 2017. Phosphatized early Cambrian archaeocyaths and small shelly fossils (SSFs) of southwestern Mongolia. *Palaeogeography, Palaeoclimatology, Palaeoecology*: <https://doi.org/10.1016/j.palaeo.2017.07.002>.
- Read, B. C. 1980. Lower Cambrian archaeocyathid buildups, Pelly Mountains Yukon. *Geological Survey of Canada Paper* **78-18**: 1-54.

- Rees, M. N., Pratt, B. R., and Rowell, A. J. 1989. Early Cambrian reefs, reefs complexes, and associated lithofacies of the Shackleton Limestone, Transantarctic Mountains. *Sedimentology* **36**: 341-361.
- Reitner, J., Langsford, N., and Kruse, P. 2017. An unusual ferruginous-calcite *Frutexit*es microbialite community from the lower Cambrian of the Flinders Ranges, South Australia. *PalZ* **91**: 1-3.
- Repina, L. N. 1983. Biofatsii trilobitov rannego kembriya Sibirskoy platformy [Early Cambrian trilobite biofacies on the Siberian Platform]. *Trudy, Institut geologii i geofiziki, Sibirskoe otделение, Akademiya nauk SSSR* **569**: 54-76.
- Riding, R. 1991. Classification of microbial carbonates. In: Riding, R. ed. *Calcareous Algae and Stromatolites*. Berlin: Springer: 21-51.
- Riding, R., and Zhuravlev, A. Y. 1995. Structure and diversity of oldest sponge-microbe reefs: lower Cambrian, Aldan River, Siberia. *Geology* **23**: 649-652.
- Rowland, S. M., and Shapiro, R. S. 2002. Reef patterns and environmental influences in the Cambrian and earliest Ordovician. In: Kiessling, W., Flugel, E., and Golonka, J. eds. *Phanerozoic Reef Patterns*. **SEPM Special Publication 72**: 95-128.
- RozaNov, A. Y., and Zhuravlev, A. Y. 1992. The lower Cambrian fossil record of the Soviet Union. In: Lipps, J. H., and Signor, P. W. eds. *Origin and Early Evolution of the Metazoa*. New York: Plenum Press: 205-282.
- Shapiro, R. S., and Rigby, J. K. 2004. First occurrences of and in situ anthaspidellid sponge in a dendrolite mound (upper Cambrian; Great Basin, USA). *Journal of Paleontology* **78**: 645-650.

- Shapiro, R. S., and Awramik, S. M. 2006. *Favosamaceria cooperi* new group and form: a widely dispersed, time-restricted thrombolite. *Journal of Paleontology* **80**: 411-422.
- Servais, T., Lehnert, O., Li, J., Mullins, G. L., Munnecke, A., Nützel, A., and Vecoli, M. 2008. The Ordovician Biodiversification: revolution in the oceanic trophic chain. *Lethaia* **41**: 99-109.
- Servais, T., Harper, D. A. T., Li, J., Munnecke, A., Owen, A. W., and Sheehan, P. M. 2009. Understanding the Great Ordovician Biodiversification Event (GOBE): influences of paleogeography, paleoclimate, or paleoecology? *GSA Today* **19**: 4-10.
- Servais, T., Perrier, V., Danelian, T., Klug, C., Martin, R., Munnecke, A., Nowak, H., Nützel, A., Vandenbroucke, T. R. A., Williams, M., and Rasmussen, C. M. Ø. 2016. Onset of the 'Ordovician Plankton Revolution' in the late Cambrian. *Palaeogeography, Palaeoclimatology, Palaeoecology* **458**: 12-28.
- Slater, B. J., Harvey, T. H., Guilbaud, R., and Butterfield, N. J. 2016. A cryptic record of Burgess Shale-type diversity from the early Cambrian of Baltica. *Palaeontology* **60**: 117-140.
- Spencer, L. M. 1981. Palaeoecology of a lower Cambrian archaeocyathid inter-reef fauna from southern Labrador. In Taylor, M. E. ed. *Short Papers for the Second International Symposium on the Cambrian System*. **USGS Open-File Report 81-743**: 215-218.
- Steiner, M., G. Li, Y. Qian, M. Zhu, and B-D. Erdtmann. 2007. Neoproterozoic to early Cambrian small shelly fossil assemblages and a revised biostratigraphy correlation of the Yangtze Platform (China). *Palaeogeography, Palaeoclimatology, Palaeoecology* **254**: 67-99.

- Sumall, C. D., Sprinkle, J., and Guensburg, T. E. 1997. Systematics and paleoecology of late Cambrian echinoderms from the western United States. *Journal of Paleontology* **71**: 1091-1109.
- Thomas, R. D. K., Shearman, R. M., and Stewart, G. W. 2000. Evolutionary exploitation of design options by the first animals with hard skeletons. *Science* **288**: 1239-1242.
- Vinn, O., and Zaton, M. 2012. Inconsistencies in proposed annelid affinities of early biomineralized organism *Cloudina* (Ediacaran): structural and ontogenetic evidences. *Carnets de Géologie* **3**: 39-47.
- Warren, L. V., Quaglio, F., Simões, M. G., Gaucher, C., Riccomini, C., Poiré, D. G., Freitas, B. T., Boggiani, B. C., and Sial, A. N. 2017. *Cloudina-Corumbella-Namacalathus* association from the Itapucumi Group, Paraguay: increasing ecosystem complexity and tiering at the end of the Ediacaran. *Precambrian Research* **298**: 79-87.
- Wood, R. A. 1993. Nutrients, predation and the history of reef-building. *Palaios* **8**: 526-543.
- Wood, R. A. 1999. Reef Evolution. Oxford University Press: New York. 354 p.
- Wood, R. A. 2011. Paleoecology of the earliest skeletal metazoan communities: implications for early biomineralization. *Earth-Science Reviews* **106**: 184-190.
- Wood, R., and Zhuravlev, A. Y. 2012. Escalation and ecological selectivity of mineralogy in the Cambrian Radiation of skeletons. *Earth-Science Reviews* **115**: 249-261.
- Wood, R., Zhuravlev, A. Y., and Debrenne, F. 1992. Functional biology and ecology of Archaeocyatha. *Palaios* **7**: 131-156.
- Zhang, Y., Li, Y., and Munnecke, A. 2014. Late Ordovician microbial reefs in the Lianglitag Formation (Bachu, Tarim, NW China). *Facies* **60**: 663-684.

Zhuravlev, A. Y. 1996. Reef ecosystem recovery after the early Cambrian extinction. *Geological Society, London, Special Publications* **102**: 79-96

Zhuravlev, A. Y. 2001. Paleoeecology of Cambrian Reef Ecosystems. *In*: Stanley, G. D. ed. *The History and Sedimentology of Ancient Reef Systems*. New York: Academic/Plenum Publishers: 121-157.

Zhuravlev, A. Y., Wood, R. A., and Penny, A. M. 2015. Ediacaran skeletal metazoan interpreted as a lophophorate. *Proceedings of the Royal Society B: Biological Sciences* **282**: 20151860

Chapter IV. Restricted morphospace occupancy of early Cambrian reef-building archaeocyaths

Cambrian Morphospace Occupancy and Sponge Morphology

The survival of any clade is dependent on the ability of taxa included within it to gather resources necessary for survival. Previous studies on crinoids (Kammer *et al.*, 1997, 1998), gastropods (Gili and Marinell, 1994), bivalves (Stanley, 1986; Jablonski and Hunt, 2006), as well as modern fish (Wilson *et al.*, 2007) and carnivores (Gray *et al.*, 2016) have shown that a more generalist lifestyle can promote greater taxon longevity (Raia *et al.*, 2016). Therefore, it is prudent for taxa to expand into new niches to take advantage of multiple resources, and often this requires the adaptation of novel or expanded morphological features (Hellberg *et al.*, 2001; McCormack and Smith, 2008; Bellwood *et al.*, 2014). This can be observed in the fossil record as taxa expanding their distribution within morphospace due to an adaptive radiation, often when presented with sufficient ecological opportunity (Losos, 2010). Morphospace is the mathematical and/or graphical depiction of the morphology of an organism and can be used as a proxy for exploring the occupancy of niches by extinct organisms (Mitteroecker and Huttegger, 2009).

Organisms tend to occupy far less morphospace than what is theoretically available (Raup, 1966). However, the distribution and location of taxa within morphospace can be informative of the evolutionary history and paleoecology of an organism (Ritterbush and Bottjer, 2012; Huang *et al.*, 2014). For example, morphospace studies of Cambrian organisms have suggested that disparity was similar to modern organisms (Briggs *et al.*, 1992), but may have shifted through time (Willis, 1998; Löfgren *et al.*, 2003). Furthermore, this pattern of early

maximum disparity may have also occurred prior to the Cambrian Radiation during the Ediacaran (Shen *et al.*, 2008). However, these trends are not consistent across all groups of organisms, with blastoids (Foote, 1992), stylophorans (Lefebvre *et al.*, 2006), and onychophorans (Yang *et al.*, 2015) as notable exceptions. This body of research is often framed as determining whether organisms reached an early maximum of morphological disparity, and subsequent decimation, or if disparity was proportional to taxonomic diversity (Gould, 1991; Erwin, 2007). Here, I investigate the morphological disparity within a different group of taxa, archaeocyathan sponges, to quantify the morphospace occupancy of early Cambrian reef builders.

Previous work.— Research on the morphology of sponges can be challenging due to the lack of easily definable characters (i.e., landmarks) and the plastic nature of their modular morphology. For instance, sponges are known to increase spicule density and constrict their central cavity in high-energy environments (Palumbi, 1984, 1986). Gross morphology of sponges is also influenced by environment, with more fragile branching forms common in lower-energy environments (Bell and Barnes, 2000; Bell *et al.*, 2002). Therefore, looking at the fossil record of ancient sponges and their morphological disparity can inform us of the variety of environments in which those organisms existed. Archaeocyathan morphological disparity is particularly important, because archaeocyaths were framework builders, which could have disproportionately affected their surroundings and local biodiversity (Erwin, 2008, also see Watkins, 2000; Hageman and McKinney, 2010 for morphological studies on other reef-builders). A more restricted or expanded morphological disparity can give us more information about the filling of ecospace during the early (Terreneuvian-Series 2) Cambrian.

Archaeocyaths are preserved as three-dimensional calcitic cups within a rock matrix. Cut or naturally weathered faces expose a two-dimensional cross section of the cup within the matrix. Archaeocyaths within the order Monocyathida have a single wall; however, the vast majority of archaeocyaths have a unique double-walled structure separated by an open cavity, the intervallum. During life, the intervallum was potentially the location of the bulk of soft tissue, but post-mortem this cavity appears open. The two walls may be connected by up to several hundred radial-longitudinal septa and transverse tabulae though either feature may be absent. When present, these skeletal elements together form chambers known as loculi. The inner wall encloses a central cavity with a distal osculum. Prior research on archaeocyaths has used a functional morphology approach to show that pore (ostia) density is important in creating strong water channelization and flow direction, much like other poriferans (Balsam and Vogel, 1973; Savarese, 1992). Additional morphological studies of archaeocyaths related the central cavity size to their paleoenvironments (Savarese, 1995) and categorized their cup integration (Wood *et al.*, 1992). However, little work on archaeocyathan morphology has been performed since and no extensive studies of archaeocyathan morphology from museum collections have been performed to date. Therefore, I collected measurements from several museum collections as well as discrete gross morphological characters from databases to amass a large (> 1000 specimens) dataset of archaeocyathan morphology. I find that archaeocyaths, and thus the primary reef builders of the early Cambrian, were restricted in their morphological disparity and, therefore, in the paleoenvironments they inhabited.

Materials and Methods

Archaeocyaths are, often, the most common metazoan framework builder in early Cambrian reefs. Additional enigmatic metazoans also occur in some localities. For example, coralomorphs (Hicks, 2006), radiocyaths (Kruse *et al.*, 1996), or sparse calcareous sponges do occur (Reitner *et al.*, 2017). However, I focus here on archaeocyaths as few specimens of these other reef builders were available and were comparatively minor in diversity.

Two comparative datasets were assembled to assess the differences between archaeocyathan morphology and other reef-building organisms, modern demosponges and lithistid sponges. First, modern demosponges contain several examples of calcareous organisms, e.g., *Vaceletia* and *Calcifibrospongia*, as well as several orders with aspiculate micromorphology, e.g., Dictyoceratida, Verongiida, and Dendroceratida, which instead are composed of spongin fibers. Taxonomically, archaeocyaths are suggested to either be closely related to or members of Demospongiae (Debrenne and Zhuravlev, 1994; Rowland, 2001). However, demosponges occur in more environments than archaeocyaths, for example deep marine, which allows for greater innovation of novel morphologies. Thus, a second dataset of the polyphyletic lithistid demosponges sponges was also assembled. Samples used in this study ranged in age from the Paleozoic (N = 42), Mesozoic (N = 8), Paleogene (N = 5), to modern (N = 38). Lithistid sponges form robust calcifying reefs in both ancient and modern ecosystems. They possess spicules called desmas and typically inhabit tropical to temperate environments alongside demosponges (Schuster *et al.*, 2015). Therefore, I include data on modern demosponges (here referring to extant non-lithistid varieties) as they are a single taxonomic group that may include Archaeocyatha, and a second dataset of lithistid sponges (here referring

to fossil and modern heavily calcified demosponges within the polyphyletic group “Lithistida”), as they are the closest ecologically analogous organism to archaeocyaths. Two separate methods of analysis were used as part of this study, one using continuous variables and a second with discrete variables.

Continuous variables for archaeocyaths were measured on cross sections preserved in rock slabs (N = 1108) from museum collections at the University of California Museum of Paleontology (UCMP), University of Alaska Museum of the North (UAMES), and University of Wisconsin-Milwaukee (IESAG) as well as field samples from the Poleta and Harkless Formations near Lida, Nevada, USA. Museum-based specimens (N = 630) are the primary focus of all analysis except when indicated otherwise and contain samples from three paleocontinents: Laurentia, Gondwana (Australia), and Mongolia (Zhavkhan Terrane) (Fig. 4.1A). Our dataset is heavily biased toward samples from Laurentia (> 82%), thus the trends discussed below may be more indicative of archaeocyaths from Laurentia, rather than a global phenomenon. Regardless, our data still represent a major paleocontinent with substantial biodiversity.

Measurements of cup/individual diameter (hereafter referred to as body size), osculum diameter (hereafter referred to as osculum size), loculus width, and septal thickness were collected for all museum specimens (Fig. 4.1B). Only body- and osculum-size measurements were collected for field samples. For all body- and osculum-size measurements two diameters were measured, one at the point of maximum width and a second perpendicular to the first measurement (Fig. 4.1B). These two values were averaged to reduce bias due to oblique cross sections. Samples that appeared to be extremely obliquely cross cut or fragmented were excluded. Personal observations of three-dimensionally preserved archaeocyaths suggest that

they are not always perfectly circular in cross section, but rather more elliptical. Therefore, we prefer this two-diameter method to simply using either minimum or maximum diameters to characterize body size. Multiple loculus width measurements (average 1.9 per specimen) were collected from the inner wall side when available and averaged. Loculus measurements were taken at various positions around the cup to capture variability of their width. Septal thickness was measured at the midpoint between the inner and outer wall. Intervallum area percentage was determined by using equation 1.

$$I \% = [(area\ of\ body - area\ of\ osculum) / area\ of\ body] \times 100 \quad (1)$$

Data from modern demosponges (N = 71) were collected on museum specimens housed at the Milwaukee Public Museum (MPM) for body size, osculum size, and maximum height in similar manner to the archaeocyath dataset. All measurements were made using a digital caliper accurate to within 0.01 mm. Lithistid sponge data were collected from the primary literature either from dimensions specified in the text or directly from figures (N = 93; see appendix D). Both modern and fossil examples of lithistid sponges were included.

Discrete morphological variables were compiled from database entries. Archaeocyathan gross morphology, cup shape, and elaboration for all valid genera of archaeocyaths (N = 309) were gathered from the online database *Archaeocyatha - A knowledge base* (Kerner *et al.*, 2011). For comparison all extant, marine taxa of 'Demospongiae Sollas, 1885', using the 'only accepted names' and 'all records' filters, were compiled from the World Porifera Database (N = 6274). From this list a random subset, using a random number generator, of 300 were selected and assessed for gross morphology based on their descriptions in *Systema Porifera* (Hooper and Van Soest, 2002). Lithistid sponge gross morphology was assessed from the same literature

survey as continuous variables. For both the ancient and modern discrete datasets, binary presence or absence coding was performed to determine the percentage of organisms that can display each morphological category as seen in Bell and Barnes (Fig. 4.1C, 2001).

Within the continuous dataset a PERMANOVA (10,000 replicates, Mahalanobis distance) analysis of archaeocyath measurements was performed across locality, taxonomic, and geologic formation groups. Mann-Whitney U and Levene's tests were performed on logarithmically transformed body size and osculum size for archaeocyath versus modern demosponges and lithistid sponges to determine differences in size and variance. Cohen's d was used to calculate effect sizes. To quantify the magnitude of difference between our test groups, we used Cohen's d to calculate effect size of two independent means based on equation 2 below.

$$d = (\text{mean of group A} - \text{mean of group B}) / SD_{\text{pooled}} \quad (2)$$

In our analysis, an effect size larger than 0.80 is considered large (Cohen 1992). Coupled with hypothesis testing, Cohen's d provides information not just about the occurrence of a statistical difference, but also about the size of the difference in means. For the discrete dataset, a χ^2 test was performed on archaeocyath versus modern demosponge and lithistid sponge gross morphologies. All statistical tests were performed in *Past 3.14*.

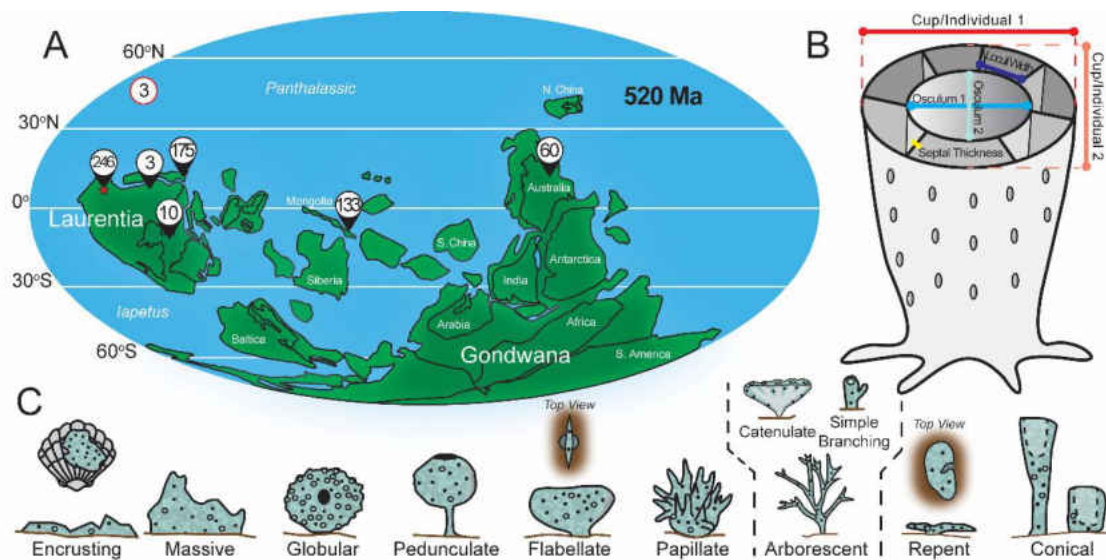


Figure 4.1: Overview of materials and methods. A, Paleogeography of early Cambrian with locality information of museum samples measured for continuous variables (N = 630). Red-circled value has unknown locality. Field sample locality denoted by red star. B, Diagram of archaeocyathan annotated with measurements taken for continuous variables. C, Nine morphological categories used in discrete character analysis (based on Bell and Barnes, 2001). Arborescent category includes catenulate and simple branching morphologies. See Boury-Esnault and Rützler (1997) for definitions of categories and appendix D for synonymized categories.

Results

Archaeocyathan morphology

Archaeocyathan body size averaged 10.6 mm and had a right skew with a maximum diameter of 74.0 mm. Osculum size averaged 5.0 mm and also had a right skew with a maximum size of 59.5 mm. Loculus width averaged 0.60 mm and septal thickness averaged 0.24 mm. Archaeocyathan cross sections were on average 21.8% intervalum compared to osculum area (Table 4.1). Nearly all samples were 2-dimensional cross sections that did not allow for height measurements, but one 3-dimensionally preserved specimen had a height of 22.9 mm and a second fragmented sample measured more than 110 mm.

In both 2-dimensional and 3-dimensional morphospace archaeocyaths tend to cluster near smaller body, osculum, and loculi sizes (Fig. 4.2A and B). When separated by locality, archaeocyaths from Mongolia appear to have smaller loculus compared to all other localities (Fig. 4.2A). However, principal component analysis (PCA) shows there is a substantial amount of overlap (Fig. 4.2C). Different taxonomic orders do have significantly different body sizes with the largest being Capsulocyathida (28.8 mm, N = 7), followed by Ajacicyathida (12.8 mm, N = 240), and Archaeocyathida (11.5 mm, N = 383). However, taxonomic groups also appear to have large amounts of morphospace overlap (Table E5). Osculum size is highly correlated with body size ($r = 0.91$). Osculum sizes from localities within Laurentia appear to be more similar to one another than to those of specimens from more distant localities (Fig. 4.2D). Continuous variables measurements failed multivariable tests of normality, therefore, non-parametric permutation tests were required. Archaeocyaths did display differences in centroid means based on locality (PERMANOVA p -value < 0.001), taxonomic order (PERMANOVA p -value < 0.001) and geologic formation (PERMANOVA p -value < 0.001). See Appendix Figures E3 - E4 and Tables E4 - E6 for pairwise comparisons.

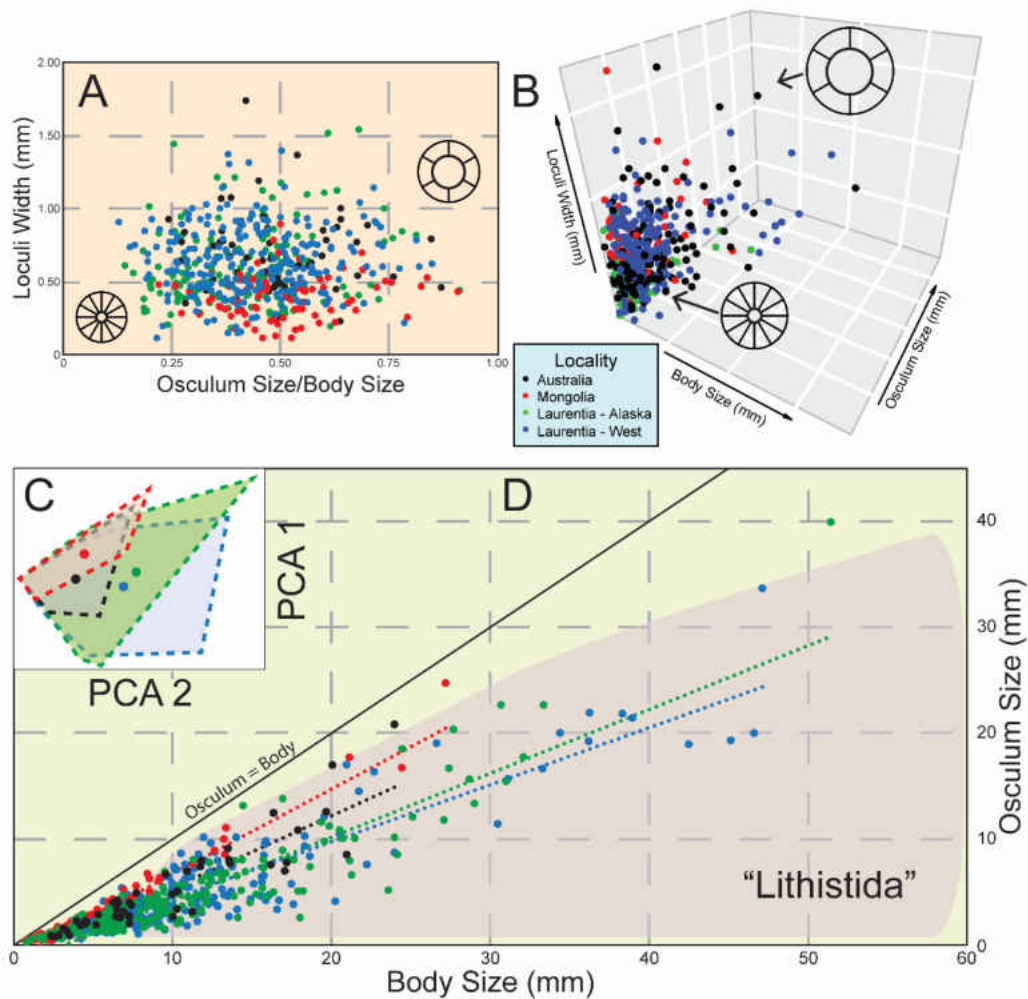


Figure 4.2: Continuous variable measurements for museum specimens of archaeocyaths. A, 2-dimensional morphospace with colors showing general locality. Color scheme same throughout figure. B, 3-dimensional morphospace with colors showing general locality. C, Principal component analysis of five continuous variables. Convex hulls with centroid centers shown. First axis accounts for 96.3% of variance. D, Body and osculum size relationship with linear trendlines for locality. Approximate morphospace distribution of lithistid sponges shown in shaded region. N = 544 for A and B, N = 630 for C and D. Raw data available in appendix D.

Contrasting archaeocyath and to other sponges

Continuous variables.— Modern demosponge body sizes measured in this study average

94.1 mm and have a substantially higher maximum value of 490.0 mm, while osculum size

averaged 17.8 mm and a maximum value of 53.5 mm. Average height of these organisms is 188.4 mm (Table 4.1). Some modern demosponges are entirely within the range of archaeocyathan body size (e.g., *Dactylia*, *Spongia*, and *Fasciospongia*) and minimal sizes for many others are also within this range (Fig. 4.3A). However, the average sizes for most demosponges and nearly all maximum values are above the maximum size for archaeocyaths. Approximately 45% of modern demosponges are larger than the largest archaeocyath (Fig. 4.3B). On the other hand, osculum sizes are more similar (Fig. 4.3A). Modern demosponge body size is significantly different (Cohen's $d = 2.4$, Mann-Whitney p -value < 0.001) from archaeocyathan body size. Osculum size is also significantly different (Cohen's $d = 1.4$, Mann-Whitney p -value < 0.001). Variance between body size (Levene's p -value < 0.001), but not osculum size (Levene's p -value = 0.53), is also significantly different.

Lithistid sponge body size averaged 66.8 mm with a maximum value of 400.0 mm. Average height of these organisms was 75.7 mm. Similar to modern demosponges, minimum body size was within the range of variability of archaeocyaths, but 94.6% of lithistid sponges were larger than the average archaeocyath and 26.8% were larger than the largest archaeocyath. Both body size (Cohen's $d = 2.3$, Mann-Whitney p -value $\ll 0.001$) and body variance (Levene's p -value = 0.022) were significantly different between archaeocyaths and lithistid sponges.

As a check on our methodology all comparisons were repeated using only minimum diameter measurements for body size and osculum sizes. All comparisons of mean body and osculum sizes using Mann-Whitney U -tests show significantly smaller sizes of archaeocyathan minimum diameters in comparison to either modern demosponges or lithistid sponges.

Variations in minimum body and osculum sizes were also significantly smaller in archaeocyaths compared to either group based on Levene's test. In summation, all results from above were reproduced using only minimum diameters with the exception of osculum variance was found to be significantly smaller in archaeocyaths compared to modern demosponges at $\alpha = 0.05$, but not at $\alpha = 0.01$ (Table E7).

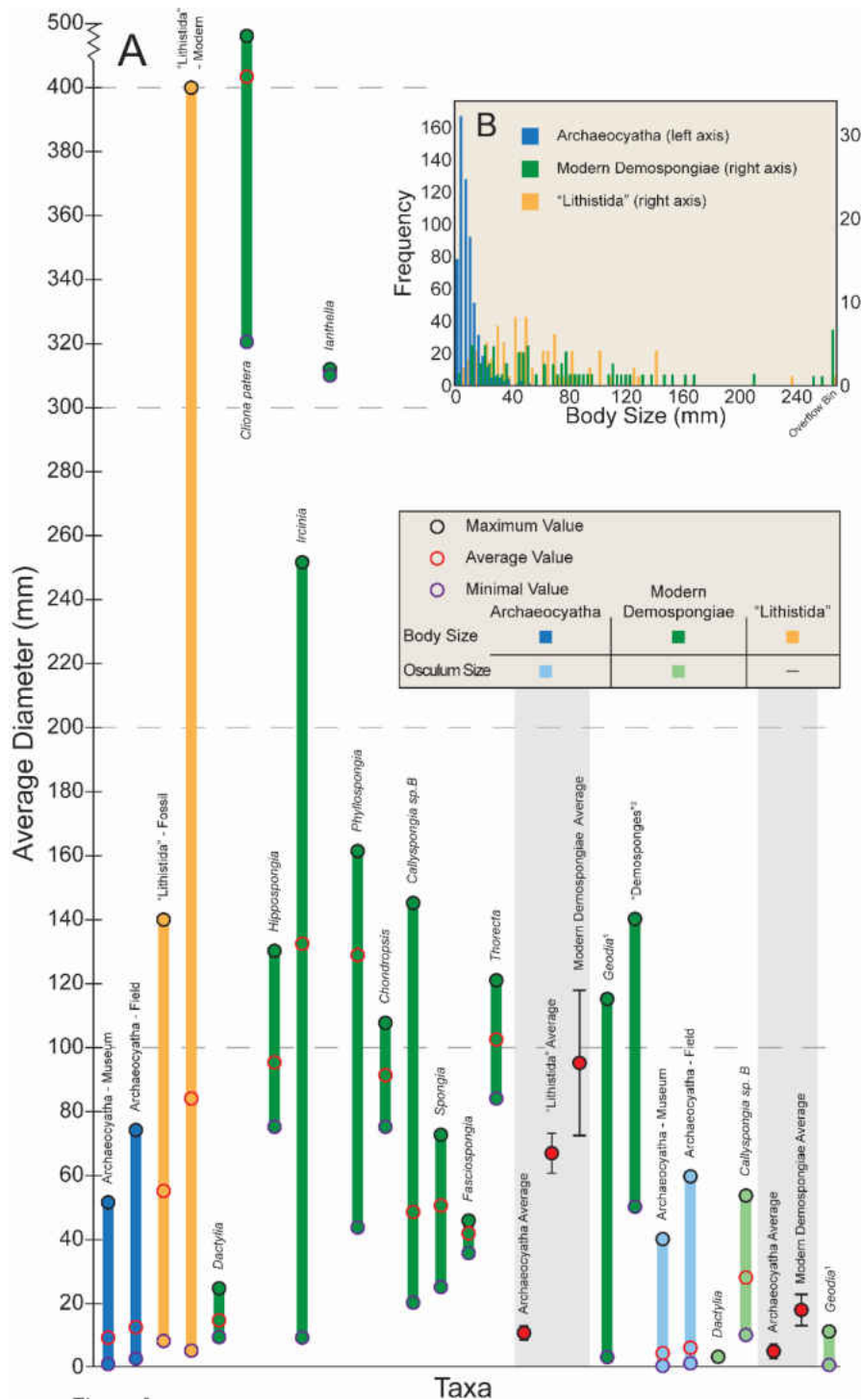


Figure 4.3: Size comparison of archaeocyaths, lithistid sponges and modern demosponges. A, Range and average diameter sizes for archaeocyaths, lithistid sponges and modern demosponges. Note break in y-axis. N = 1108 for Archaeocyatha Average, N = 93 "Lithistida" Average and N = 71 for Modern Demospongiae Average. Error bars on averages represent 95% confidence intervals. See appendix D for specimens and measurements. 1 – Barthel and Brandt, 1995. 2 – Ghiold *et al.*, 1994. B, Histogram of sponge body sizes. Right side truncated. Raw data available in appendix D.

Table 4.1: Size measurements (mm) for all archaeocyaths (museum and field), lithistid sponges and modern demosponges. 95% confidence intervals given in parentheses.

Taxa	Body Av. (Median)	Body Min./Max.	Osculum Av. (Median)	Osculum Min./Max.
Archaeocyatha	10.6 (10.1 – 11.0)	0.8 – 74.0	5.0 (4.7 – 5.3)	0.3 – 59.5
“Lithistida”	66.8 (53.8 – 79.8)	5.0 – 400.0	-	-
Modern Demospongiae	94.1 (72.9 – 119.7)	9.1 – 490.0	17.8 (12.4 – 23.3)	1.2 – 53.5
Taxa	Loculus Width Av.	Septal Thickness Av.	Intervallum Area %	Max. Height Av.
Archaeocyatha	0.60 (0.58 – 0.62)	0.24 (0.22 – 0.24)	21.8 (20.7 – 22.9)	22.9*
“Lithistida”	-	-	-	75.7 (59.7 – 93.7)
Modern Demospongiae	-	-	-	188.4 (138.0 – 193.8)

* = Based on one specimen (UCMP 220889)

Discrete variables.— Our random sampling of demosponge gross morphologies has a similar distribution to those observed directly in field studies, with the most common morphology being encrusting (Fig. 4.4A). By comparison most archaeocyaths display simple branching morphology. Lithistid sponges, on the other hand most commonly display a conical or globular gross morphology, but still occupy many of the other categories in comparison to archaeocyaths. The distribution of morphologies between archaeocyaths and either modern demosponges or lithistids is significantly different (effect size = 0.7 and 1.4 respectively, χ^2 p -value < 0.001 for both comparisons). Furthermore, archaeocyaths are extremely uniform beyond gross morphology, as 95% have simple cylindrical-conical cup shapes (Fig. 4.4B) and 92% have no external elaborations (Fig. 4.4C).

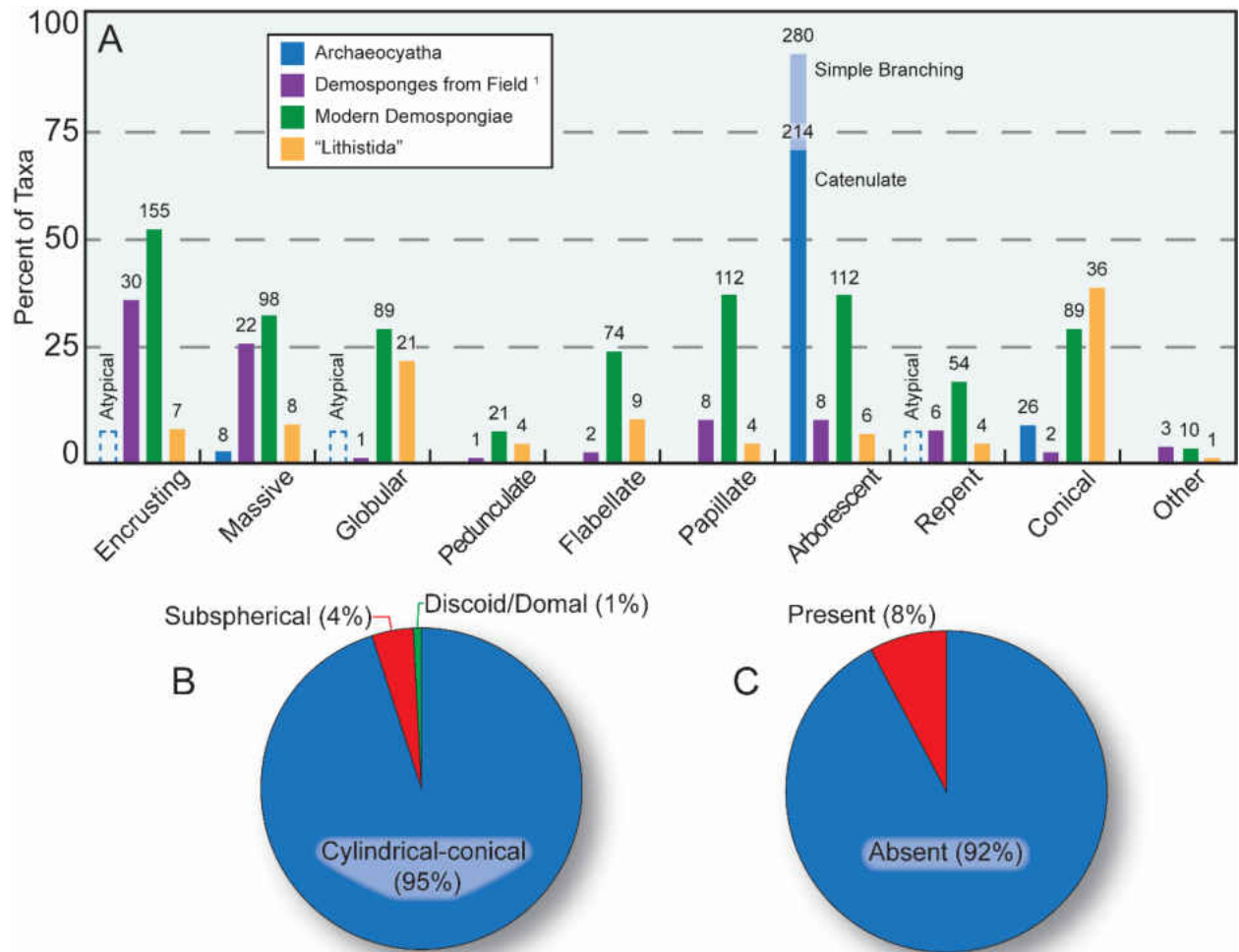


Figure 4.4: Discrete character distribution for archaeocyath, lithistid sponges and modern demosponges. A, Percent of taxa that display each morphological category. Some species display more than one morphology, hence values will not add to 100%. Numbers above bars indicate absolute number of taxa in each category, while height of bars indicates percentage. Atypical archaeocyath gross morphology shown in dashed boxes. 1 - Demosponges from field measured in Bell and Barnes, 2001. B, Pie chart of archaeocyath cup shape. C, Pie chart of archaeocyath elaboration. Raw data available in Appendix D.

Discussion

Morphological Disparity within archaeocyatha.— Archaeocyaths displayed a narrow range of continuous character variation, but there were differences between localities (Fig. 4.2). For example, archaeocyaths from Laurentia tend to have larger loculi and smaller oscula compared to archaeocyaths from Mongolia (Fig. 4.5 A - E). Archaeocyaths from different parts

of Laurentia were more similar to one another than to archaeocyaths from more distant locations, especially in terms of osculum size (Fig. 4.2C and D). PCA plots also show similar results with the center of convex hulls shifted right for Laurentian archaeocyaths compared with archaeocyaths from Mongolia and Australia (Fig. 4.2C). PERMANOVA results support these visual assessments by finding significant differences in centroid means across the different localities. However, it would be difficult to assign a specific morphotype to any particular locality. There is a large amount of overlap in occupied morphospace in both 2-dimensional and ordination-based morphospaces (Fig. 4.2A and C). Archaeocyaths with small body sizes appear to be restricted in the amount of variability they possess. Small organisms can only have small oscula and loculi as a result. Therefore, smaller archaeocyaths converge on one section of morphospace. It is possible that only larger, and most likely older, organisms had adapted to local environmental conditions. Although even with larger specimens there is no definitive separation between morphospace occupancy of different localities.

Statistical testing of archaeocyath continuous variables also found differences in centroid means based on taxonomic order and geologic formation groups (Tables E5 - E6). However, similar to differences based on locality, three-dimensional morphospace plots show no definitive pattern or separation of morphospace occupation based on taxonomic order or geological formation (Figures E3 - E4). This reaffirms our interpretation that archaeocyaths display a narrow range of morphospace occupancy based on continuous characters.

Discrete character analysis also showed very little diversity across archaeocyaths. Of 309 archaeocyath genera, 257 (83.2%) display the most common type of overall morphology (cylindrical-conical cup shape, no elaboration, arborescent gross morphology). This pattern was

consistent through time and across different paleocontinents (Figures E5 - E6). Based on descriptions used in the 'Archaeocyatha' database, archaeocyaths only occupy three of our gross morphological categories. However, this might be an underestimate of their morphological disparity. Atypical archaeocyaths, such as *Retilamina*, *Fransuasaecyathus*, *Erismacoscinus*, and *Zunyicyathus*, can have an encrusting, globular, repent or stromatoporoid-grade gross morphology (Savarese and Signor, 1989; Debrenne *et al.*, 1990; Debrenne *et al.*, 1991; Debrenne and Zhuravlev, 1992). These additional forms bring the total to six gross morphological categories. However, these forms are limited in both generic richness and abundance. Nonetheless, I reanalyzed our data with atypical morphologies included, by assuming an arbitrarily high proportion of genera belonged to these atypical categories (20%), and still found the proportion of differences between morphological categories to be statistically different (χ^2 p -value < 0.001).

The lack of morphological disparity within archaeocyaths, for both discrete and continuous variables, suggests minimal morphological distinctiveness within early Cambrian reef-building sponges. In fact, their limited morphology limits their realized niche space to patchy hard substrates or cryptic environments, reducing their utility as reef-builders and ecosystem engineers (see Wood, 1995). I do not suggest that archaeocyaths were completely excluded from other environments, only that they had very limited ability to thrive in numerous environmental settings.

It should be noted that the gross morphological characters are only a small portion of those used for taxonomic classification within Archaeocyatha. Cup diameter, osculum diameter, septal thickness, and loculus width are not taxonomically significant above the species level.

Characters such as wall type, pore shape and distribution, as well as other microscopic features (bracts, canals, microporous sheaths, etc.) would also need to be considered for classification purposes. Therefore, I do not intend here to comment on the taxonomic diversity within archaeocyaths based on these traits at this time.

Comparisons between archaeocyaths and other sponges.— Archaeocyaths occupy fewer regions of morphospace (Fig. 4.2D), have a lower range of morphological variation (Table 4.1), and were found to be smaller on average compared to modern demosponges or lithistid sponges (Fig. 4.3A and B). Furthermore, the maximum size of archaeocyaths in this study was often smaller than the minimum size of modern demosponges. The largest documented archaeocyaths belong to the plate-like genus *Okulitchicyathus*, which has possible examples of 1.5 m diameter cups (Hill, 1964). However, this perceived diameter could be due to multiple layered specimens and more conservative estimates suggest a maximum diameter of 500 mm (Debrenne *et al.*, 2015). Even these conservative estimates most likely represent outliers for archaeocyathan body size (Fig. 4.5E). Regardless, this is considerably smaller than the largest species of modern demosponges such as *Xestospongia muta* (barrel sponges) which can measure 0.98 m in diameter (McMurray *et al.*, 2008), not to mention even larger hexactinellids (> 3.5 m) in deep-water reefs (Wagner and Kelley, 2016). Interestingly, these same patterns are not observed in osculum size. While osculum size was smaller for archaeocyaths, the difference between these and modern organisms was not nearly as large and there was no difference in variance. While an exhaustive search was not performed, selected modern demosponges had an average of 9.9 ± 15.1 (N = 24) oscula per sponge, with several more containing over a hundred. By comparison, nearly all archaeocyaths contained a single osculum. Increasing

osculum size can reduce pumping efficiency, therefore, it may be more energetically favorable to produce numerous smaller oscula compared to expanding a single large one when expanding body size (Palumbi, 1986).

Comparing archaeocyaths to lithistid sponges, a greater proportion of lithistid sponges surveyed as part of this study were within the body-size range of archaeocyaths, though they were on average larger (Figs. 4.3; Table 4.1). This pattern remained even after separating fossil and modern lithistid sponges, which themselves showed a change in size through time, with the average fossil lithistid sponge within the range of archaeocyathan body size, but significantly larger overall.

Discrete characteristics also show that archaeocyaths had a limited number of morphologies. Modern demosponges are most commonly encrusting or massive and lithistid sponges are most often conical (Fig. 4.4A). While some archaeocyaths - e.g., *Retilamina*, domal shape and possible encrusting habit; order Kazakhstanicyathida and suborder Dictyofavina, stromatoporoid-grade shape and massive habit (Debrenne *et al.*, 1991) - possess unique gross morphologies, these genera make up < 3% of archaeocyaths. Otherwise, archaeocyaths usually have a simple erect habit. Furthermore, archaeocyaths rarely possess specialized elaborations that in other sponges can increase surface exposure and hydrodynamic properties (Church, 2017). Branching morphologies are most common in modular archaeocyaths and even these are often weakly integrated. A previous study by Wood *et al.* (1992) found that 94.7% of archaeocyath species were either solitary or weakly integrated (N = 508). This could lead to greater susceptibility to changes in environmental conditions or storms that could fragment poorly supported branching organisms (Wood *et al.*, 1992). I find that archaeocyaths have

smaller average body sizes, lower size variability, and lower diversity of gross morphology compared to other types of sponges, resulting in overall restricted morphospace occupancy.

This study only focused on two end points of the Phanerozoic to assess changes in reef-building sponge morphology (Fig. 4.5F). A more thorough study of the Phanerozoic would be required to assess when this change occurred, but it may most likely be tied to when archaeocyaths ceased being the primary reef-building organisms (see Lee and Riding, 2018 for a study on size changes in reef builders). Spiculate sponges within the order Protomonaxonida were already equal to or larger than archaeocyaths, with diameters between 5 - 40 mm (Xiao *et al.*, 2005; Botting and Peel, 2016), but were confined to low-energy environments until the Ordovician (Carrera and Botting, 2008). During the Miaolingian, explanate lithistid sponges formed in reefs measured between 7 - 23 mm (Kruse and Reitner, 2014, fig. 6A and 14 within). But larger lithistid sponges grew to ~2 cm wide during the Miaolingian of China (Lee *et al.*, 2016) and even larger in Iran and the western USA by the late Cambrian (Shapiro and Rigby, 2004; Kruse and Zhuravlev, 2008; Lee and Riding, 2018). Pulchrilaminids and stromatoporoids (Early and Middle Ordovician respectively) later occurred in reefs and they too were larger than early Cambrian archaeocyaths (Li *et al.*, 2016; Hong *et al.*, 2017). Thus, it seems that archaeocyaths had a limited size range and morphological disparity, which was unique for reef-building sponges in the early Paleozoic.

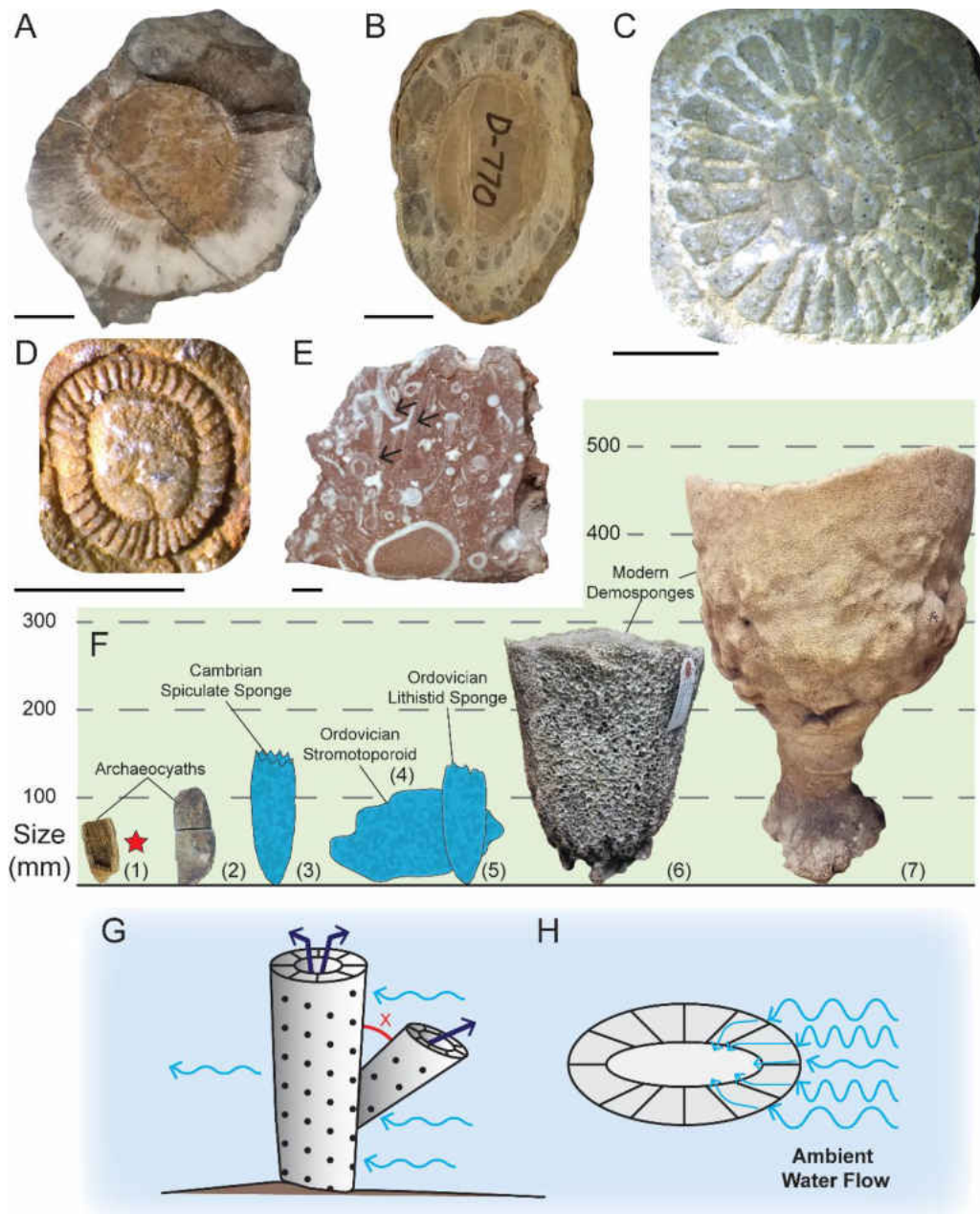


Figure 4.5: Archaeocyaths and modern demosponges used in study. A, Archaeocyath from western USA, UCMP 220846. B, Archaeocyath from western USA, UCMP 220710. C, Archaeocyath from Alaska, UAMES 6099. D, Archaeocyath from Australia, UAMES 42655. E, Archaeocyath from Mongolia, IESAG000R. *Okulitchicyathus* fragments labelled with arrows. F, Size comparison of various sponges. 1 – Archaeocyatha, UCMP 220822. 2 – Archaeocyatha, UCMP 220858. 3 – *Lantianspongia* (Xiao *et al.*, 2005). 4 – *Stratodictyon* (Webby, 1979). 5 – *Zittella* (Liu *et al.*, 2003). 6 – *Ircinia*, MPM 44. 7 – *Cliona patera*, MPM 53. Red-starred specimen is vertically exaggerated. G, Archaeocyath capturing ambient current. Angle (x) must be large enough to allow flow to reach main cup. H, Cross section of archaeocyath cup with septa redirecting and channelizing current into central cavity. Scale bars equal 10 mm for A and B, 5 mm for C, D, and E.

Why were archaeocyaths so small?.— The size of loculi within the intervallum does not appear to scale linearly with body size (Fig. 4.6A). Rather, loculus width is maintained by the insertion of new septa once the loculus width attains a certain size (McKee, 1963), with a maximum loculus width at approximately 1.25 mm (Fig. 4.6B). At small body sizes (< 10 mm) there is a stronger correlation ($r = 0.35$) compared to larger (> 10 mm) body sizes ($r = 0.27$). Flume-tank experiments with archaeocyathan models have shown that septa increase water entrainment and support unidirectional flow through the central cavity (Savarese, 1992). Therefore, it is possible that larger loculus widths would reduce the efficiency of flow patterns and hinder filter feeding (Fig. 4.5G and H).

Archaeocyaths could not grow to larger sizes as it would have been too energetically expensive to produce additional biomineralized septa to help direct fluid flow. This challenge would have been further exacerbated by the low calcite saturation state of the late-early Cambrian oceans (Pruss *et al.*, 2010; Knoll and Fischer, 2011; Riding *et al.*, 2019) which negatively impacts calcification of reef builders (Cohen and Holcomb, 2009), as well as changing seawater chemistry from aragonite to calcite seas (Lowenstein *et al.*, 2001; Porter, 2010) that has been correlated with reef-builder extinctions (Zhuravlev and Wood, 2009; Kiessling and Simpson, 2010). Furthermore, planktonic food sources may have been lower until the late Cambrian, limiting suspension-feeder food supply (Servais *et al.*, 2016).

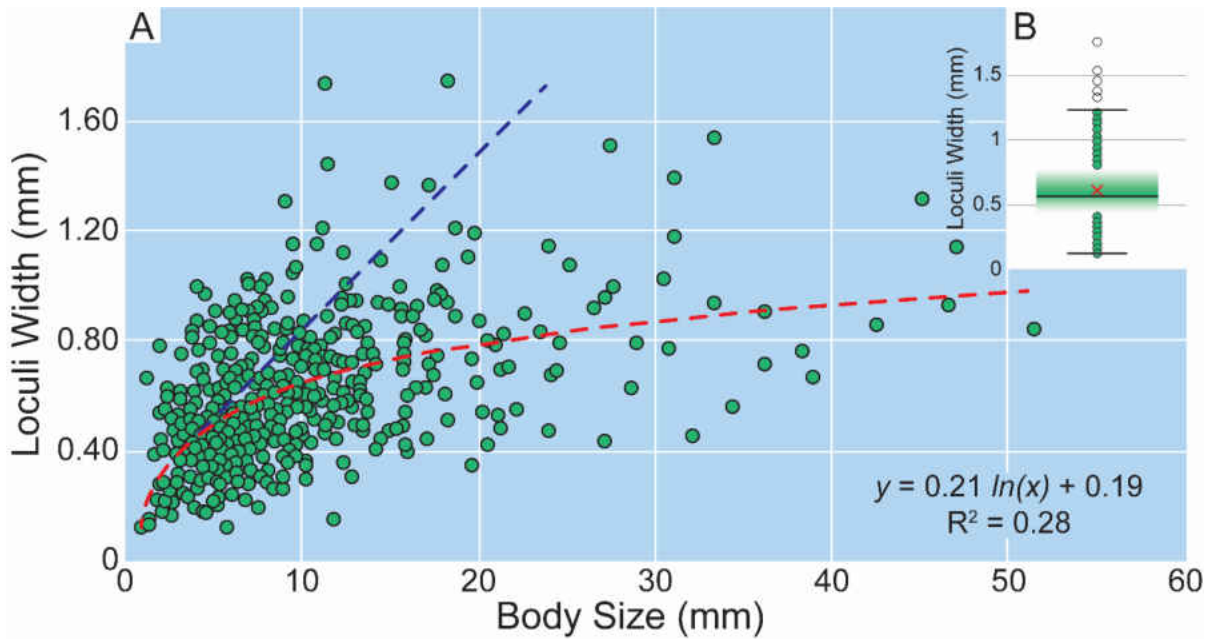


Figure 4.6: Loculus size distribution of archaeocyaths. A, Body size to loculi width relationship with logarithmic trendline shown in red. Purple line shows hypothetical continuation of loculus sizes if a linear trend of increasing width with increasing body size were occurring. B, Box and whisker plot of loculus widths, red 'X' denotes arithmetic mean. Raw data available in appendix D.

The hypothesized reliance on passive entrainment and the unique double-walled calcareous structure, which occupies over 20% of the archaeocyathan body, may represent a form of self-limiting modularity within the archaeocyathan body plan (Table 4.1). Modern experiments on glass sponges show that passive entrainment is critical for sponges, but is probably only plausible for sponges with thin walls and large oscula (Leys *et al.*, 2011).

This same evolutionary tradeoff can be seen in modern examples of calcareous demosponges, though suspension feeding is aided by active pumping with choanocytes as well as passive entrainment. The modern sponge *Vaceletia crypta* has reliably been placed within the order Demospongiae based on molecular systematics (Wörheide, 2008), despite possessing an aspiculate, aragonite skeleton with stacked chambers. Superficial similarities to

Archaeocyatha have led some to suggest an ancestral relationship between the two (Pickett, 1985), however, the earliest fossil record of *Vaceletia* is from the Triassic and would imply a long fossil record gap. Even if *Vaceletia* is not a direct descendant, a comparison of its morphology can still be useful to understanding the archaeocyathan body plan. *Vaceletia* displays a similar gross morphology with a single osculum and size (mm to cm) as many archaeocyaths (Wörheide and Reitner, 1996; Germer *et al.*, 2015).

Extinct sponge taxa also show these patterns. For instance, Triassic examples of chambered “sphinctozoan” sponges too show a convergent robust calcareous skeleton and rarely measure above 130 mm, with most being far smaller (see Senowbari-Daryan and Stanley, 1992; Senowbari-Daryan and Zamparelli, 2003). In contrast, hypercalcifying labechiid stromatoporoid sponges also lacked spicules, but could achieve large body sizes up to 15 cm across (Stern *et al.*, 1999; Hong *et al.*, 2017). Stromatoporoid sponges do not contain the same double-walled structure and instead have more densely packed, but thin, laminae and pillars (Wolniewicz, 2009) and astrorhizal canals that provide a more distributed and energetically efficient fluid-entrainment system (Boyajian and LaBarbera, 1987; LaBarbera and Boyajian, 1991; LaBarbera, 1993). Additionally, the Ordovician hypercalcifying sponge *Calathium*, which may have close affinities to archaeocyaths, has been measured at sizes of 300 mm in length and 90 mm in diameter (Li *et al.* 2015). *Calathium* is superficially similar to archaeocyaths as both have calcified inner and outer walls. However, *Calathium* walls are connected by rods as opposed to septa, which may alter the physiological demands of building such structures.

Modern spiculate sponges do not produce thick skeletons and can therefore devote more energy to body expansion and more diverse gross morphologies. It may be that spicules

present a less-energy intensive method of extending the sponge body off the seafloor while still maintaining a flexible body plan to adapt to local conditions (Uriz *et al.*, 2003; Nickel *et al.*, 2006) which is not afforded by rigid calcareous skeletons. In short, sponges with both a chambered modular structure and calcareous skeletons tend to be smaller than organisms that lack one or the other. The small body size and simple morphology of both archaeocyaths and *Vaceletia* are consistent with our interpretation that the tradeoff of building a calcareous skeleton with a unique double-walled (and/or chambered) structure is limited body size and morphological disparity.

Conclusions

I provide evidence that archaeocyaths from the early Cambrian of Laurentia were relatively restricted in both body size and gross morphological disparity. In comparison to archaeocyaths, modern demosponges and lithistid sponges are as much as an order of magnitude greater body size and body-size variability. Furthermore, both groups are well distributed across several gross morphological categories compared to a sparser distribution for archaeocyaths. In a larger context, morphospace occupancy of early Cambrian reef-building sponges was reduced compared to other sponge taxa. This suggests that morphospace occupancy for reef builders expanded, potentially sometime during the early Paleozoic and may have contributed to increases in biodiversity in macroscopic reef-builders during the Ordovician (see above). Their limited morphospace occupancy suggests that archaeocyaths of Laurentia did not adapt to a variety of environmental conditions. The restricted morphological disparity of archaeocyaths may have played a role in their ability to create additional niche space and resistance to habitat change (Wulff, 2006; Kerry and Bellwood, 2012). By investigating the

morphospace of early Cambrian reef builders we can further support the transitional nature of the Cambrian as a period of establishment of the basic ecological properties common in ecosystems today, but with more restricted diversity.

References

- Balsam, W. L., and Vogel, S. 1973. Water movement in archaeocyathids: evidence and implications of passive flow models. *Journal of Paleontology* **47**: 979-984.
- Barthel, D., and Brandt, A. 1995. *Caecognathia robusta* (G.O. Sars, 1879) (Crustacea, Isopoda) in *Geodia mesotriaena* (Hentschel, 1929) (Demospongiae, Choristidae) at 75° N off NE Greenland. *Sarsia* **80**: 223-228.
- Bell, J. J., and Barnes, D. K. A. 2000. The influences of bathymetry and flow regime upon the morphology of sublittoral sponge communities. *Journal of Marine Biological Association of the United Kingdom* **80**: 707-718.
- Bell, J. J., and Barnes, D. K. A. 2001. Sponge morphological diversity: a qualitative predictor of species diversity? *Aquatic Conservation: Marine and Freshwater Ecosystems* **11**: 109-121.
- Bell, J. J., Barnes, D. K. A., and Turner, J. R. 2002. The importance of micro and macro morphological variation in the adaptation of a sublittoral demosponge to current extremes. *Marine Biology* **140**: 75-81.

- Bellwood, D. R., Goatley, C. H. R., Brandl, S. J., and Bellwood, O. 2014. Fifty million years of herbivory on coral reefs: fossils, fish and functional innovations. *Proceedings of the Royal Society B: Biological Sciences* **281**: 20133046.
- Botting, J. P., and Peel, J. S. 2016. Early Cambrian sponges of the Sirius Passet Biota, North Greenland. *Papers in Palaeontology* **2**: 463-487.
- Boury-Esnault, N., and Rützler, K. 1997. Thesaurus of sponge morphology. *Smithsonian contributions to zoology* **596**. Smithsonian Institution, Washington DC. 55 p.
- Boyajian, G. E., and LaBarbera, M. 1987. Biomechanical analysis of passive flow stromatoporoids - morphologic, paleoecologic, and systematic implications. *Lethaia* **20**: 223-229.
- Briggs, D. E. G., Fortey, R. A., and Willis, M. A. 1992. Morphological disparity in the Cambrian. *Science* **256**: 1670-1673.
- Carrera, M. G., and Botting, J. P. 2008. Evolutionary history of Cambrian spiculate sponges: implications for the Cambrian Evolutionary Fauna. *Palaios* **23**: 124-138.
- Church, S. B. 2017. Efficient ornamentation in Ordovician anthaspidellid sponges. *Paleontological Contributions* **18**: 1-8.
- Cohen, J. 1992. A power primer. *Psychological Bulletin* **112**: 155-159.
- Cohen, A. L., and Holcomb, M. 2009. Why corals care about ocean acidification: uncovering the mechanism. *Oceanography* **22**: 118-127.
- Debrenne, F., and Zhuravlev, A. 1992. *Irregular Archaeocyaths*. CNRS Editions, Paris.

- Debrenne, F., and Zhuravlev, A. 1994. Archaeocyathan affinities: how deep can we go into the systematic affiliation of an extinct group? *In*: R. W. M. van Soest, T. M. G. van Kempen, and J. C. Braekman. eds. *Sponges in Space and Time*. Balkema, Rotterdam: 3-12.
- Debrenne, F., Rozanov, A., and Zhuravlev, A. 1990. *Regular Archaeocyaths*. CNRS Editions, Paris.
- Debrenne, F., Kruse, P. D., and Sengui, Z. 1991. An Asian compound archaeocyath. *Alcheringa* **15**: 285-291.
- Debrenne, F., Zhuravlev, A. Y., and Kruse, P. D. 2015. General Features of the Archaeocyatha. Pp. 845-1084. *In*: F. Debrenne, W. D. Hartman, S. Kershaw, P. D. Kruse, H. Nestor, J. K. Rigby Sr., B. Senowbari-Daryan, C. W. Stern, C. W. Stock, J. Vacelet, B. D. Webby, R. R. West, P. Willenz, R. A. Wood, and A. Y. Zhuravlev. Porifera Revised Hypercalcified Porifera Volume 5. Part E of P. A. Selden, ed. *Treatise on invertebrate paleontology*. Geological Society of America, New York, and University of Kansas, Lawrence.
- Erwin, D. H. 2007. Disparity: morphological pattern and development context. *Palaeontology* **50**: 57-73.
- Erwin, D. H. 2008. Macroevolution of ecosystem engineering, niche construction and diversity. *Trends in Ecology and Evolution* **23**: 304-310.
- Foote, M. 1992. Paleozoic record of morphological diversity in blastozoan echinoderms. *Proceedings of the National Academy of Sciences* **89**: 7325-7329.

- Germer, J., Mann, K., Wörheide, G., and Jackson, D. J. 2015. The skeleton forming proteome of an early branching metazoan: a molecular survey of the biomineralization components employed by the coralline sponge *Vacellatia* sp. *PLoS ONE* **10**: e0140100.
- Ghiold, J., Rountree, G. A., and Smith, S. H. 1994. Common sponges of the Cayman Islands. The Cayman Islands. In: M. A. Brunt and J. E. Davies, eds. *The Cayman Islands: Natural History and Biogeography*: 131-138.
- Gili, C., and Marinell, J. 1994. Relationship between species longevity and larval ecology in nassariid gastropods. *Lethaia* **27**: 291-299.
- Gould, S. J. 1991. The disparity of the Burgess Shale arthropod fauna and the limits of cladistic analysis: why we must strive to quantify morphospace. *Paleobiology* **17**: 411-423.
- Gray, E. L., Burwell, C. J., and Baker, A. M. 2016. Benefits of being a generalist carnivore when threatened by climate change: the comparative dietary ecology of two sympatric semelparous marsupials, including a new endangered species (*Antechinus arktos*). *Australian Journal of Zoology* **64**: 249-261.
- Hagman, S. J., and McKinney, F. K. 2010. Discrimination of fenestrate bryozoan genera in morphospace. *Palaeontologia Electronica* **13**: 1-43.
- Hellberg, M. E., Balch, D. P., and Roy, K. 2001. Climate-driven range expansion and morphological evolution in a marine gastropod. *Science* **292**: 1707-1710.
- Hill, D. 1964. The phylum Archaeocyatha. *Biological Reviews* **39**: 232-258.

- Hong, J., Choh, S-J., Park, J., and Lee, D-J. 2017. Construction of the earliest stromatoporoids framework: labechiid reefs from the Middle Ordovician of Korea. *Palaeogeography, Palaeoclimatology, Palaeoecology* **470**: 54-62.
- Hooper, J. N. A., and Van Soest, R. W. M. eds. 2002. *Systema Porifera: a guide to the classification of sponges*, **volume 1**. Kluwer Academic/Plenum Publishers, New York.
- Huang, S., Roy, K., and Jablonski, D. 2014. Origins, bottlenecks, and present-day diversity: patterns of morphospace occupation in marine bivalves. *Evolution* **69**: 735-746.
- Jablonski, D., and Hunt, G. 2006. Larval ecology, geographic range, and species survivorship in Cretaceous mollusks: organismic versus species-level explanations. *The American Naturalist* **168**: 556-564.
- Kammer, T. W., Baumiller, T. K., and Ausich, W. I. 1997. Species longevity as a function of niche breadth: evidence from fossil crinoids. *Geology* **25**: 219-222.
- Kammer, T. W., Baumiller, T. K., and Ausich, W. I. 1998. Evolutionary significance of differential species longevity in Osagean-Meramecian (Mississippian) crinoid clades. *Paleobiology* **24**: 155-176.
- Kerner, A., Debrenne, F., and Vignes-Lebbe, R. 2011. Cambrian archaeocyath metazoans: revisions of morphological characters and standardization of genus descriptions to establish an online identification tool. *In*: V. Smith and I. Penev. eds. e-Infrastructure for data publishing in biodiversity science. *ZooKeys* **150**: 381-395.

- Kerry, J. T., and Bellwood, D. R. 2012. The effect of coral morphology on shelter selection by coral reef fishes. *Coral Reefs* **31**: 415-424.
- Kiessling, W., and Simpson, C. 2010. On the potential for ocean acidification to be a general cause of ancient reef crisis. *Global Change Biology* **17**: 56-67.
- Knoll, A. H., and Fischer, W. W. 2011. Skeletons and ocean chemistry: the long view. In J-P. Gattuso and L. Hansson. eds. *Ocean Acidification*. Oxford University Press, Oxford: 67-82.
- Kruse, P. D., and Zhuravlev, A. Y. 2008. Middle-late Cambrian *Rankenella-Girvanella* reefs of the Mila Formation, northern Iran. *Canadian Journal of Earth Science* **45**: 619-639.
- Kruse, P. D., and Reitner, J. R. 2014. Northern Australian microbial-metazoan reefs after the mid-Cambrian mass extinction. *Memoirs of the Association of Australian Palaeontologists* **45**: 31-53.
- Kruse, P. D., Gandin, A., Debrenne, F., and Wood, R. 1996. Early Cambrian bioconstructions in the Zavkhan Basin of western Mongolia. *Geological Magazine* **133**: 429-444.
- LaBarbera, M. 1993. The astrorhizae of fossil stromatoporoids closely approximate an energetically optimal fluid transport system. *Experientia* **49**: 539-541.
- LaBarbera, M., and Boyajian, G. E. 1991. The function of astrorhizae in stromatoporoids: quantitative tests. *Paleobiology* **17**: 121-132.
- Lee, J-H., Hong, J., Choh, S-J., Lee, D-J., Woo, J., and Riding, R. 2016. Early recovery of sponge framework reefs after Cambrian archaeocyath extinction: Zhangxia Formation (early

- Cambrian Series 3), Shandong, North China. *Palaeogeography, Palaeoclimatology, Palaeoecology* **457**: 269-276.
- Lee, J-H., and Riding, R. 2018. Marine oxygenation, lithistid sponges, and the early history of Paleozoic skeletal reefs. *Earth-Science Reviews* **181**: 98-121.
- Lefebvre, B., Eble, G. J., Navarro, N., and David, B. 2006. Diversification of atypical Paleozoic echinoderms: a quantitative survey of patterns of stylophoran disparity, diversity, and geography. *Paleobiology* **32**: 483-510.
- Leys, S. P., Yahel, G., Reibenbach, M. A., Tunnicliffe, V., Shavit, U., and Reiswig, H. M. 2011. The sponge pump: the role of current induced flow in the design of the sponge body plan. *PLoS ONE* **6**: e27787.
- Li, Q., Li, Y., Wang, J., and Kiessling, W. 2015. Early Ordovician lithistid sponge-*Calathium* reefs on the Yangtze Platform and their paleoceanographic implications. *Palaeogeography, Palaeoclimatology, Palaeoecology* **425**: 84-96.
- Li, Q., Li, Y., and Kiessling, W. 2016. The oldest labechiid stromatoporoids from intraskeletal crypts in lithistid sponge-*Calathium* reefs. *Lethaia* **50**: 140-148.
- Liu, B., Rigby, J. K., and Zhu, Z. 2003. Middle Ordovician lithistid sponges from the Bachu-Kalpin Area, Xinjiang, Northwestern China. *Journal of Paleontology* **77**: 430-441.
- Löfgren, A. S., Plotnick, R. E., and Wagner, P. J. 2003. Morphological diversity of Carboniferous arthropods and insights on disparity patterns through the Phanerozoic. *Paleobiology* **29**: 349-368.

- Losos, J. B. 2010. Adaptive radiation, ecological opportunity, and evolutionary determinism. *The American Naturalist* **175**: 623-639.
- Lowenstein, T. K., Timofeeff, M. N., Brennan, S. T., Hardie, L. A., and Demicco, R. V. 2001. Oscillations in Phanerozoic seawater chemistry: evidence from fluid inclusions. *Science* **294**: 1086-1088.
- McCormack, J. E., and Smith, T. B. 2008. Niche expansion leads to small-scale adaptive divergence along an elevation gradient in a medium-sized passerine bird. *Proceedings of the Royal Society B: Biological Sciences* **275**: 2155-2164.
- McKee, E. H. 1963. Ontogenetic stages of the archaeocyathid *Ethmophyllum whitneyi* Meek. *Journal of Paleontology* **37**: 287-293.
- McMurray, S. E., Blum, J. E., and Pawlik, J. R. 2008. Redwood of the reef: growth and age of the giant barrel sponge *Xestospongia muta* in the Florida Keys. *Marine Biology* **155**: 159-171.
- Mitteroecker, P., and Huttegger, S. M. 2009. The concept of morphospaces in evolutionary and developmental biology: mathematics and metaphors. *Biological Theory* **4**: 54-67.
- Nickel, M., Bullinger, E., and Beckmann, F. 2006. Functional morphology of *Tethya* species (Porifera): 2. Three-dimensional morphometrics on spicules and skeletal superstructures of *T. minuta*. *Zoomorphology* **125**: 225.
- Palumbi, S. R. 1984. Tactics of acclimation: morphological changes of sponges in an unpredictable environment. *Science* **225**: 1478-1480.

- Palumbi, S. R. 1986. How body plans limit acclimation: responses of a demosponge to wave force. *Ecology* **67**: 208-214.
- Pickett, J. 1985. *Vaceletia*, the living archaeocyathid. *New Zealand Geological Survey Record* **9**: 77.
- Porter, S. M. 2010. Calcite and aragonite seas and the *de novo* acquisition of carbonate skeletons. *Geobiology* **8**: 256-277.
- Pruss, S. B., Finnegan, S., Fischer, W. W., and Knoll, A. H. 2010. Carbonates in skeleton-poor seas: new insights from Cambrian and Ordovician strata of Laurentia. *Palaios* **25**: 73-84.
- Raia, P., Carotenuto, F., Mondanaro, A., Castiglione, S., Passaro, F., Saggese, F., Melchionna, M., Serio, C., Alessio, L., Silvestro, D., and Fortelius, M. 2016. Progress to extinction: increased specialization causes the demise of animal clades. *Scientific Reports* **6**: 30965.
- Raup, D. M. 1966. Geometric analysis of shell coiling: general problems. *Journal of Paleontology* **40**: 1178-1190.
- Riding, R., Liang, L., Lee, J-H., and Virgone, A. 2019. Influence of dissolved oxygen on secular patterns of marine microbial carbonate abundance during the past 490 Myr. *Palaeogeography, Palaeoclimatology, Palaeoecology* **514**: 135-143.
- Ritterbush, K. A., and Bottjer, D. J. 2012. Westermann morphospace displays ammonoid shell shape and hypothetical paleoecology. *Paleobiology* **38**: 424-446.
- Rowland, S. M. 2001. Archaeocyaths – a history of phylogenetic interpretation. *Journal of Paleontology* **75**: 1065-1078.

- Savarese, M. 1992. Functional analysis of archaeocyath skeletal morphology and its paleobiological implications. *Paleobiology* **18**: 464-480.
- Savarese, M. 1995. Functional significance of regular archaeocyath central cavity diameter: a biomechanical and paleoecological test. *Paleobiology* **21**: 356-378.
- Savarese, M., and Signor, P. W. 1989. New archaeocyathan occurrences in the upper Harkless Formation (Lower Cambrian of western Nevada). *Journal of Paleontology* **63**: 539-549.
- Schuster, A., Erpenbeck, D., Pisera, A., Hooper, J., Bryce, M., Fromont, J., and Wörteide, G. 2015. Deceptive desmas: molecular phylogenetics suggests a new classification and uncovers convergent evolution of lithistid demosponges. *PLoS ONE* **10**: e116038.
- Senowbari-Dayan, B., and Stanley, G. D. 1992. Late Triassic thalamid sponges from Nevada. *Journal of Paleontology* **66**: 183-193.
- Senowbari-Daryan, B. and Zamparelli, V. 2003. Upper Triassic (Norian-Rhaetian) new thalamid sponges from northern Calabria (Southern Italy). *Studia Universitatis Babeş-Bolyai, Geologia* **48**: 113-124.
- Servais, T., Perrier, V., Danelian, T., Klug, C., Martin, R., Munnecke, A., Nowak, H., Nützel, A., Vandenbroucke, T. R. A., Williams, M., and Rasmussen, C. M. Ø. 2016. The onset of the 'Ordovician Plankton Revolution' in the late Cambrian. *Palaeogeography, Palaeoclimatology, Palaeoecology* **458**: 12-28.

- Shapiro, R. S., and Rigby, J. K. 2004. First occurrence of an in situ anthaspidellid sponge in a dendrolite mound (upper Cambrian; Great Basin, USA). *Journal of Paleontology* **78**: 645-650.
- Shen, B., Dong, L., Xiao, S., and Kowalewski, M. 2008. The Avalon Explosion: evolution of Ediacara morphospace. *Science* **319**: 81-84.
- Stanley, S. M. 1986. Population size, extinction, and speciation: the fission effect in Neogene Bivalvia. *Paleobiology* **12**: 89-110.
- Stern, C. W., Webby, B. D., Nestor, H., and Stock, C. W. 1999. Revised classification and terminology of Palaeozoic stromatoporoids. *Acta Palaeontologica Polonica* **44**: 1-70.
- Uriz, M-J., Turon, X., Becerro, M. A., and Agell, G. 2003. Siliceous spicules and skeletal frameworks in sponges: origin, diversity, ultrastructure patterns, and biological functions. *Microscopy Research and Technique* **62**: 279-299.
- Wagner, D., and Kelley C. D. 2016. The largest sponge in the world? *Marine Biodiversity* **47**: 367-368.
- Watkins, R. 2000. Corallite size and spacing as an aspect of niche-partitioning in tabulate corals of Silurian reefs, Racine Formation, North America. *Lethaia* **33**: 55-63.
- Webby, B. D. 1979. The oldest Ordovician stromatoporoids from Australia. *Alcheringa* **3**: 237 - 251.
- Willis, M. A. 1998. Cambrian and recent disparity: the picture from priapulids. *Paleobiology* **24**: 177-199.

- Wilson, S. K., Burgess, S. C., Cheal, A. J., Emslie, M., Fisher, R., Miller, I., Polunin, N. V. C., and Sweatman, H. P. A. 2007. Habitat utilization by coral reef fish: implications for specialists vs. generalists in a changing environment. *Journal of Animal Ecology* **77**: 220-228.
- Wolniewicz, P. 2009. Late Framennian stromatoporoids from Dębnik Anticline, Southern Poland. *Acta Palaeontologica Polonica* **54**: 337-350.
- Wood, R., Zhuravlev, A. Y., and Debrenne, F. 1992. Functional biology and ecology of archaeocyatha. *Palaios* **7**: 131-156.
- Wood, R. 1995. The changing biology of reef-building. *Palaios* **10**: 517-529.
- Wörheide, G. 2008. A hypercalcified sponge with soft relatives: *Vaceletia* is a keratose demosponge. *Molecular Phylogenetics and Evolution* **47**: 433-438.
- Wörheide, G., and Reitner, J. 1996. "Living fossil" sphinctozoan coralline sponge colonies in shallow water caves of the Osprey Reef (Coral Sea) and the Astrolabe Reefs (Fiji Islands). In: J. Reitner, F. Neuweiler, and F. Gunkel. eds. *Göttinger Arbeiten zur Geologie und Paläontologie*, Goettingen: 145-148
- Wulff, J. L. 2006. Resistance vs recovery: morphological strategies of coral reef sponges. *Functional Ecology* **20**: 699-708.
- Xiao, S., Hu, J., Yuan, X., Parsley, R. L., and Cao, R. 2005. Articulated sponges from the lower Cambrian Hetang Formation in southern Anhui, South China: their age and implications for the early evolution of sponges. *Palaeogeography, Palaeoclimatology, Palaeoecology* **220**: 89-117.

Yang, J., Ortega-Hernández, J., Gerber, S., Butterfield, N. J., Hou, J-B., Lan, T., and Zhang, X-G.

2015. A superarmored lobopodian from the Cambrian of China and early disparity in the evolution of Onychophora. *Proceedings of the National Academy of Sciences* **114**: 8678-8683.

Zhuravlev, A. Y., and Wood, R. A. 2009. Controls on carbonate skeletal mineralogy: global CO₂ evolution and mass extinctions. *Geology* **37**: 1123-1126.

Chapter V. Exploring the Cambrian metazoan reef gap in the Mule Spring Limestone of Nevada

The Cambrian “Reef Gap”

Prior to the evolution of metazoan skeletons, reef ecosystems were constructed of stromatolite framework builders during the Archean and Proterozoic (Allwood *et al.*, 2006; Kah, *et al.*, 2009). However, even when lightly skeletonized metazoans were incorporated into reef ecosystems during the Neoproterozoic, these ecosystems remained low diversity environments (Grotzinger *et al.*, 2005). Rather, it is not until the Cambrian that dramatic increases in skeletonized fauna occurred (Vermeij, 1989; Kouchinsky *et al.*, 2012), which may be crucial in promoting reef complexity and diversity (Wood, 1998; Weiss and Martindale, 2017). Specifically, robust skeletons from benthic organisms create topographic relief and additional microhabitats for reef-dwelling organisms to inhabit (Graham and Nash, 2013). Furthermore, additional surface area provided by rigid organisms creates hardground surfaces for binding and encrusting organisms, furthering reef development (Buhl-Mortensen *et al.*, 2010). The importance of robust benthic organisms is supported in the fossil record as it was not until the Tommotian stage (Cambrian: Stage 2), with the origination of heavily skeletonized archaeocyaths, that reefs supported alpha diversity on par with more diverse later Phanerozoic reef ecosystems (Zhuravlev *et al.*, 2015). Archaeocyaths had modular carbonate skeletons, some with dense packing, that were ideal for iterative growth and formation of positive relief (Fagerstrom and West, 2011).

The initial buildup of benthic metazoans in reef ecosystems is positively correlated with reef biodiversity, but this diversity is not necessarily maintained after removal of these

organisms (Cocito, 2004; Munday, 2004). Case in point, archaeocyaths became functionally extinct as framework builders prior to the Wuliuan (formally Stage 5) of the Cambrian, and reef biodiversity decreased correspondingly (Kiessling, 2005). The cause of their extinction may include global ocean anoxia (Zhuravlev and Wood, 1996) driven by volcanic activity in what is modern Australia (Glass and Phillips, 2006; Jourdan *et al.*, 2014), end of the Atdabanian-early Botomian transgression and transition into sea level regression (Álvaro and Debrenne, 2010), competition for niche space with lithistid sponges (Zhang *et al.*, 2017), or lack of morphological diversification (see above). Regardless of the cause, the first and longest “reef gap” (a period in which reef formation was severely limited during the recovery phase of a mass extinction) of the Phanerozoic occurred during the middle and late Cambrian (Miaolingian and Furongian) after the extinction of the archaeocyaths (Erwin, 2001). However, several studies have pointed out that the term reef gap is inappropriate. First, periods of hypercalcifying metazoans in reefs are relatively rare, and thus not a signal of normal conditions (Kiessling, 2009). Second, microbial reefs are found in many of these post-extinction intervals - e.g., the Late Ordovician (Kuznetsov, 2018) and Early Triassic (Pruss and Bottjer, 2005) - or were populated by distinct assemblages from prior to the extinction - e.g., the Late Devonian (Wood, 2000). True *global* reef gaps are probably rare or short lived during the Phanerozoic (Erwin, 2001). Rather, they represent a resurgence of microbialites into new environments (Mata and Bottjer, 2012) or local phenomena. Therefore, terms such as reef crisis or reef eclipse are preferred when describing local loss of reef-building activity and the term metazoan reef gap is used to describe loss of metazoans in a reef-building community.

By examining the fossil record, this study aims to understand timing and changes in framework building after the extinction of metazoan framework builders (archaeocyaths) in the late-early Cambrian of western Laurentia. In other regions of the world, the timing of metazoan reincorporation is not uniform. For example, predominantly *Epiphyton*-group microbial bioherms from China contain sparse anthaspidellid sponges as early as the latest Wuliuan (Woo *et al.*, 2008; Lee *et al.*, 2016). Siliceous sponge-*Epiphyton*-group reefs from the Drumian occur in Korea (Hong *et al.*, 2012; Hong *et al.*, 2016). Similar deposits are found in Australia by the latest Drumian-early Guzhangian (Kruse and Reitner, 2014), in Iran by the Guzhangian (Kruse and Zhuravlev, 2008), and finally in Laurentia by the Furongian (Shapiro and Rigby, 2004). This suggests that lithistid-microbial consortiums potentially radiated from a center of origin in the peri-Gondwana region as lithistid sponges began occupying ecological niches comparable to archaeocyaths (Zhang *et al.*, 2017). In China archaeocyaths may have existed slightly longer than those in Laurentia and were replaced by other metazoans, resulting in a near continuous occurrence of metazoans in reef ecosystems through the Cambrian and into the Ordovician (Zhang *et al.*, 2017). But this transitional period is less well studied on other paleocontinents, including western Laurentia.

Laurentia appears to have been unique in that lithistid sponges took much longer (12 - 17 million years) to be incorporated into reefs (Rowland and Shapiro, 2002; Shapiro and Rigby, 2004; Shapiro and Awramik, 2006). This did not transpire until the establishment of anthaspidellid sponges across western Laurentia (Johns *et al.*, 2007), which roughly corresponded to a resurgence in microbial reefs (Lee *et al.*, 2015), in the Furongian. In the present study, I investigate a formation that directly overlies the regional extinction of

archaeocyaths in Nevada that occurs prior to the earliest known lithistid sponges in the region. This period has not been extensively assessed for changes in fauna after the extinction event. I present data that suggests this locality experienced a metazoan reef gap, and potentially a total reef eclipse, with a reduction in metazoan-produced carbonate following the regional extinction of archaeocyaths.

Geochemical conditions of the Cambrian.— Anoxia has been linked to delayed recovery of reef ecosystems after several of the “Big Five” mass extinctions of the Phanerozoic (Hallam, 1996; Copper and Jin, 2012; Martindale *et al.*, 2017). However, similar connections between anoxia and delayed reef recovery have not been investigated in the late early Cambrian. Paleoredox conditions of early Cambrian oceans are thought to be complex, but they are generally considered to have been oxygenated at the surface with occasional brief spikes of anoxia (Qi *et al.*, 2017; Guilbaud *et al.*, 2018; Wang *et al.*, 2018, Wei *et al.*, 2018). The latest early Cambrian, however, is less well-studied, though later deposits in the middle/late Cambrian have suggested persistent euxinic or anoxic conditions (Saltzman *et al.*, 2011; Gill *et al.*, 2011; Dahl *et al.*, 2014). Therefore, the late early Cambrian may be a transitional period between these two paleoredox regimes. Using carbon isotopic composition and redox-sensitive elements (RSEs), this study will help illuminate shallow marine redox conditions after this extinction event.

Geologic Setting

The Mule Spring Limestone is exposed near Split Mountain in Clayton Ridge (Esmeralda County, Nevada; Fig. 5.1A and B). Paleogeographic reconstructions show that it was deposited on the northern side of Laurentia, slightly north of the palaeoequator (Scotese, 2001). The Mule

Spring Limestone is ~225 m thick in some sections and has been correlated to the lower Carrara Formation of the Death Valley succession (Palmer and Halley, 1979). Trilobite biostratigraphy places the Mule Spring Limestone within the *Olenellus* biozone of the Dyeran (Stage 4) stage (Fig. 5.1C). Overall, Clayton Ridge contains lower Cambrian to basal Ordovician carbonate deposits (Webster, 2011). The lower Cambrian portions studied here are highly faulted and discontinuous with no complete stratigraphic record. Outcrop surfaces are heavily weathered, but are predominately mottled, vuggy carbonate with only a few minor interruptions by shale units. Previous interpretations suggest this formation represents an outer to inner shelf environment (Wotte and Sundberg, 2017). Archaeocyathan reefs are found in the underlying upper Harkless Formation (Savarese and Signor, 1989). One section in Clayton Ridge contains the uppermost Harkless Formation, but no archaeocyaths are found within it (Webster, 2011). The Mule Spring Limestone here conformably overlies the Harkless Formation, while in other regions the Saline Valley Formation separates the two (Nelson, 1962). However, the Saline Valley Formation is missing at this locality but is equivalent to the upper Harkless Formation. Regardless, the Mule Spring Limestone at this locality is believed to represent the interval immediately after the regional extinction of archaeocyaths.

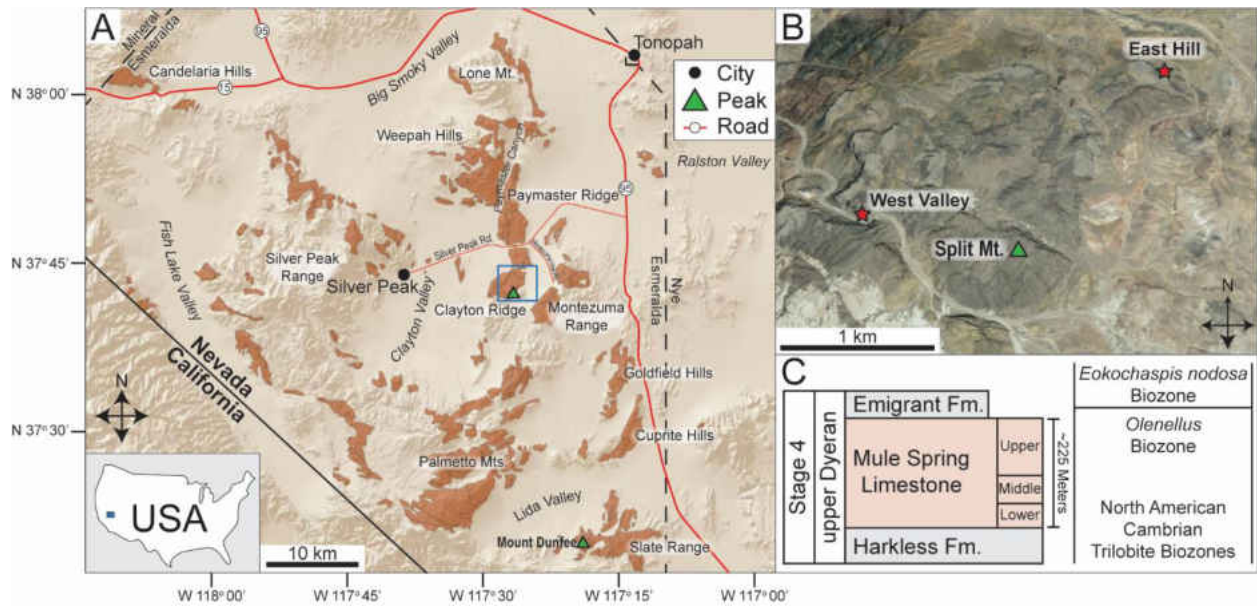


Figure 5.1: Clayton Ridge map and stratigraphic context. A, Regional map of area highlighted on inset map. Shaded areas denote early Cambrian deposits. B, Detailed satellite image of blue-boxed area in A. C, Stratigraphic context for Mule Spring Limestone.

Previous paleontological studies of early to middle Cambrian deposits in the Split Mountain region (including the Mule Spring Limestone and overlying formations) found as many as sixteen trilobite genera, including the genus *Olenellus* (Sundberg and McCollum, 2003). This genus is a known reef dweller within archaeocyathan reefs in Labrador (Pruss *et al.*, 2012). Overlying units of the Emigrant Formation contain numerous small shelly fossils and non-trilobite arthropods (Waggoner, 2003; Skovsted, 2006). Large occurrences of body fossils have not been recorded from these localities, however, data from trace fossils suggests a continued existence of soft-bodied organisms (Droser and Bottjer, 1988). There was therefore a persistent, yet poorly known, fauna present during deposition of this formation.

Materials and Methods

Sampling, point counts, and data collection.— Field observations were made within Clayton Ridge at East Hill (37° 43.560' N 117° 26.537' W; stop 7A in Webster, 2011) and West

Valley (37° 42.728' N 117° 28.279' W; stop 7B in Webster, 2011). Two sections, East Hill and East Hill 2, are within close proximity to one another, but the East Hill 2 section was detached from East Hill and contains a distinct lithology, so it is treated as a separate section. West Valley is located southwest of East Hill within an ephemeral stream bed that exposes the Mule Spring Limestone on either side of the valley wall. Samples were collected from three transects, one at each section, every two meters unless exposure was covered. A total of 49 orientated samples were collected and made into standard-sized (2" x 3") petrographic thin sections. Point count data was collected from 300 points on each slide to quantify carbonate contributions and assess Dunham texture using a Zeiss optical microscope. In addition, four slides were selected to quantify peloid size distribution by measuring maximum diameter on 250 peloids per slide. Size class distribution was determined by graphical display with log-transformed data and supported by K-means cluster analysis (2 clusters). One carbon-coated sample was analyzed under a Hitachi S-4800 SEM with an EDS system to determine elemental distributions.

Data from the PaleoReefs Database (PARED) were compiled to further contextualize changes in primary framework-building organisms during the Cambrian (Kiessling and Flügel, 2002). The database does not record International Commission on Stratigraphy (ICS) stages for reef occurrences but does record regional stage names. For this study, each reef occurrence was assigned to a single ICS stage in the Cambrian based on correlation charts from Peng *et al.* (2012). Occurrences that spanned more than one stage were assigned to the lowest stage by default. Statistical tests were performed in *Past 3.14*.

Carbon isotopes and elemental analysis. — Stable carbon isotopic compositions were collected to perform chemostratigraphic correlations. Carbonate samples (N = 49) were

powdered while avoiding veins and heavily altered segments. Approximately 3 mg were dissolved in 3 ml of 10% phosphoric acid and allowed to react for ~ 12 hrs. Gases released from this reaction were analyzed on a Picarro Cavity Ring Down Spectrometer at Bryn Mawr College and calibrated against a standard. All samples were run in duplicate and averaged with less than 0.1 permil standard deviation.

Major and minor elemental abundances were collected to assess redox conditions and post-depositional diagenesis. Redox-sensitive elements (such as uranium, vanadium, and molybdenum) tend to have muted concentrations during periods of anoxic deposition in the global seawater. During oxic conditions, soluble forms of these elements will increase in concentration in seawater and accumulate in shallow water carbonates. Hence, lower concentrations in carbonates suggests a more reducing global oceanic environment, while higher concentrations correspond to oxic conditions (Trilbovillard *et al.*, 2006; Miller *et al.*, 2017). In addition, changes in thorium concentration can be used to control for changes in sedimentation rate (Marenco *et al.*, 2016).

Strontium is typically higher in unaltered carbonates in comparison to manganese. Manganese will increase in samples that interact with meteoric waters. Sr/Mn ratios are therefore used to detect for diagenetic alteration of samples, with ratios less than one considered poorly preserved and values greater than two considered well preserved (Montañez *et al.*, 1996). Furthermore, samples with $> 1\% X_{\text{Na+Al}}$ were excluded due to the potential of leaching from siliciclastics.

Approximately 2 mg of powdered carbonate were dissolved in 1 ml of 0.32 M trace metal grade nitric acid for 3-4 hrs. After centrifuging samples, ~0.5 ml of solution was removed

and diluted to 10 ml. Abundances of Na, Al, Mn, Fe, Sr, Th, V, U, and Mo were measured on an Agilent 7500 series ICP-MS at Bryn Mawr College. Concentrations of Ca and Mg were used to normalize elemental abundances and denoted as X_{element} to compare it to other studies.

Results and Discussion

Field observations

East Hill.— A faint contact between the upper Harkless Formation and the Mule Spring Limestone is exposed at the East Hill section, however, there was very little exposure and only slight lithological differences. The Harkless Formation has thinly bedded, silty brown mudstones. Minor shale beds (< 10 cm) are present but are primarily mudstone. The lower Mule Spring Limestone at this section is grey-beige, massive to mottled mudstone and wackestones. Vertical (*Arenicolites*) and horizontal trace fossils occur in mudstone beds (Fig. 5.2A). At 12 m above the base of our measurements (6 m above tentative contact) platy, weathered peloid wackestones and packstones are most common. At 22 m above base of section, platy orange peloidal and bioclastic wackestones and packstones are more common in addition to oncoid wackestones (Fig. 5.2B). Minor lenses of microbialite are infrequently preserved as flat lying beds, often near oncoid wackestones. Oncoid wackestones do not occur over 34 m above base of measuring. Overall, in outcrop this section contains uniform lithology with only well-spaced oncoids easily recognizable.

East Hill 2.— A small 6 m hill detached from East Hill contains a distinct lithology from East Hill. At the base are silty mudstones and minor grainstone beds. At the top is thinly bedded wavy/crinkly couplets of alternating beige and grey carbonate (Fig. 5.2C). Minor raised features

(~2 cm) and vertical mudcracks are occasionally visible. Highly contorted beds show intraformational over-turned and fractured deposits (Fig. 5.2D).

West Valley.— Only the south wall of the valley was included in field observations. This whole section is dipped ~ 30° and exposes all three members of the Mule Spring Limestone. Strata below the base of the measured section contain large conglomerates followed by folded beds overtopped by flat lying beds, as in slope slumps. The Lower Mule Spring Limestone at this section is similar to that observed at East Hill, except a larger microbial component is present. It is largely platy brown mudstone and peloidal wackestone. Small beds (2 m) contain poorly preserved potential cryptic microbialite (difficult to see in outcrop, see microanalysis below) in a wackestone matrix. Covered sections sporadically expose shale beds. The Middle Mule Spring Limestone here is light-grey, blocky, mottled (bioturbation index = 3) peloidal wackestones and packstones (Fig. 5.2E and F). Two small (0.1 m) cavities filled with lithified sediment occur in this member. Cryptic microbialite beds (48 m above base) are again present but are thin. Heavily weathered surfaces vaguely resemble mounds, but internal structure and clotting is not visible in outcrop. The Upper Mule Spring Limestone is thinly-bedded brown peloidal packstones. Densely packed oncoid grainstone is also found up the cliffside. A wavy (erosional?) contact is present directly on top of this grainstone bed. The Upper Mule Spring Limestone continues a considerable distance up the cliff, but quickly becomes inaccessible because of steep slopes. Faults with some displacement are present in both the Middle and Upper Mule Spring Limestone members.

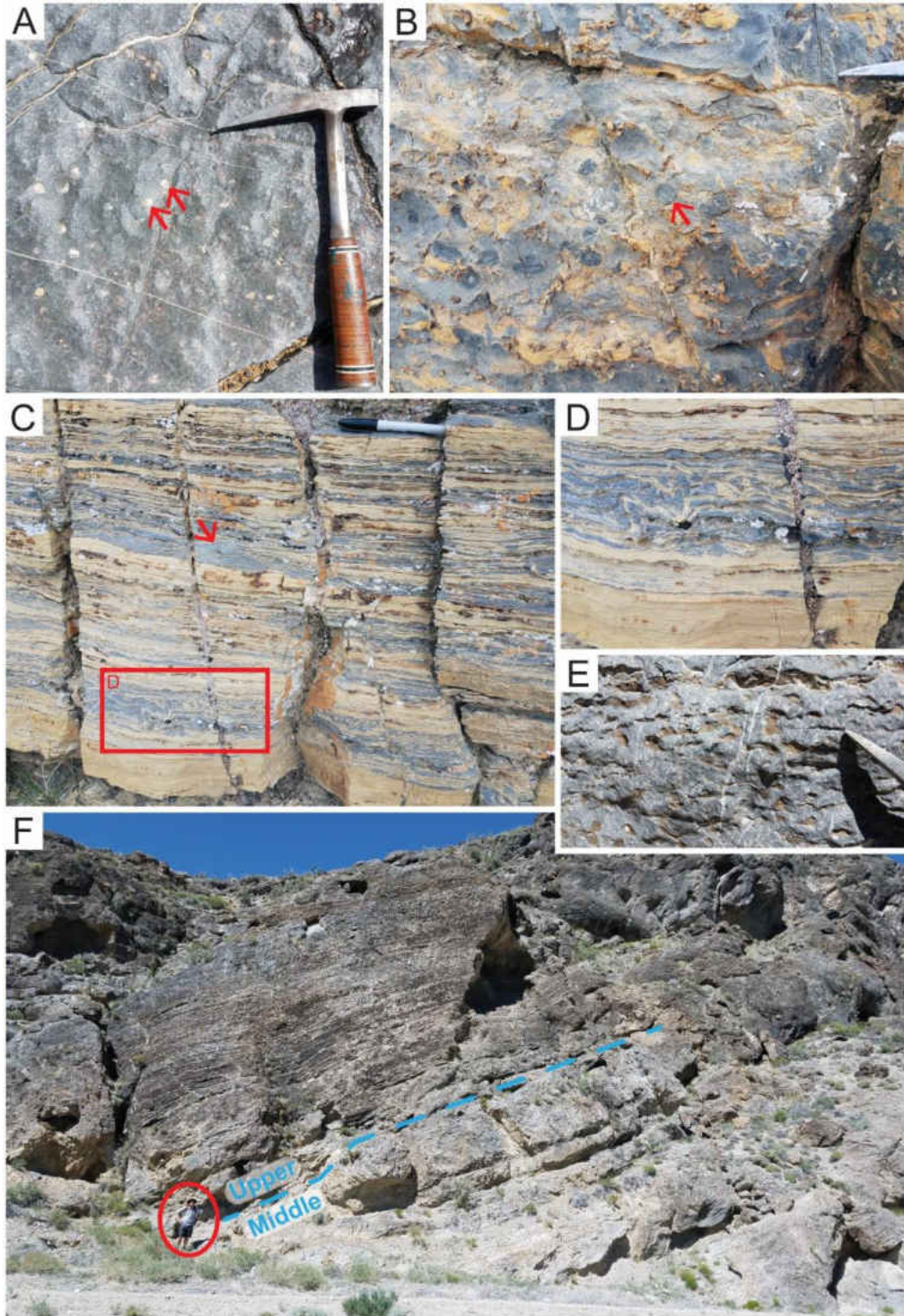


Figure 5.2: Clayton Ridge outcrop photos. A, *Arenicolites* at base of East Hill. Arrows showing paired penetrative holes. B, Well-spaced oncoids (arrow) in East Hill. C, Crinkly laminations at East Hill 2. Arrow shows minor raised surfaces. D, Close-up of over-turned bed in East Hill 2. E, Bioturbated mudstone. F, Outcrop of West Valley showing contact between middle and upper Mule Spring Limestone. Hammer for scale in A, B, and E. Pen for scale in C. Field assistant for scale in F.

Thin section microanalysis

The Mule Spring Limestone in Clayton Ridge is difficult to interpret in outcrop because of largely invariant outcrop features. Therefore, the majority of interpretations here are determined from thin section analysis of facies changes. Six microfacies are identified within this formation, described below, based on Flügel (2004). Overall, the Mule Spring Limestone is composed of 64.9% micrite, 15.0% peloids, 5.8% microbial material, and minor portions of fossils, oncoids and intraclasts (Table 5.1, Appendix Table A3).

Table 5.1 – Point count data from Clayton Ridge analysis. See figure 5.6 for pie charts of data.

Section	Micrite	Peloids	Fossils	Oncoids	Intraclast	Microbial	Pie Chart
EH2	78.3	14.5	0.2	4.3	2.8	0.0	9
EH	71.9	22.0	1.4	4.7	0.0	0.0	8
EH	73.3	23.3	3.4	0.0	0.0	0.0	7
EH	94.7	5.0	0.2	0.0	0.0	0.0	6
UWV	66.8	29.1	1.3	1.9	0.0	0.8	5
M/UWV	60.2	6.8	0.1	0.0	0.0	32.8	4
MWV	76.7	20.5	1.1	0.0	0.0	1.7	3
LWV	50.9	0.0	0.0	0.0	0.0	49.1	2
LWV	72.5	13.7	0.7	0.3	0.0	12.8	1
Average	64.9	15.0	0.8	1.2	0.2	5.8	-

Sparry calcite, dolomite, and quartz excluded from data.

Peloids include both macro- and micropeloids.

Fossils are total percent contribution from arthropods, replaced grains, and shelly material.

Average reflects all samples in study, not just those in pie charts.

Non-laminated peloidal packstone/wackestone.— Contains grain-supported subrounded to irregular-shaped peloids, some with sparry crusts (Fig. 5.3A and B). Micrite is also found in cavities and between grains, but peloid grains are generally in contact with one another. The background matrix of this facies is often a chaotic combination of jagged sparry cement and micrite, sometimes in the faint shape of replaced bioclastic grains. The most commonly

identifiable grains were peloids, which occur in two distinct size classes (Fig. 5.4, Appendix Table E7). The smaller of the two (termed 'micropeloids' here to differentiate between larger 'macropeloids' described below) is far more common (98%) and averages 0.037 mm in diameter (Fig. 5.3A). Micropeloids are oval to circular in shape, often with darkened outer edges and grey internal coloration. Internal structure is rarely preserved. The larger macropeloids average 0.630 mm (Fig. 5.3B). This distinction between size classes was supported by K-means cluster analysis (2 clusters) and were significantly different in diameter (Mann-Whitney p -value $\ll 0.001$). Macropeloids observed here come in three forms: (1) aggregated bioclastic and peloidal grains with internal micrite bound within an outer crust, (2) partially micritized oncoids with faint internal layers, (3) irregularly-shaped and structureless, bounded micrite. The multiple types of macropeloids suggests numerous origins for them. Occasional bioclastic material found in this facies includes trilobite segments and/or arthropod shells, small calcitic shells, and one echinoderm ossicle (Fig. 5.3C - E). In addition, this facies contains elongated oval-shaped fenestral cavities, though this was isolated to ~4 meters in East Hill (Fig. 5.3D). These cavities typically occurred in a vertically stacked arrangement. Peloidal packstones represents ~18% of facies measured, however, this increases to ~53% when peloidal wackestones are included. Non-laminated peloidal wackestone facies are similar in appearance to packstones, but with a larger percentage of micrite present. Peloidal wackestones often contain very faint micropeloids, difficult to differentiate from background micrite, suggesting that peloid concentration may be undercounted in these samples. Therefore, I describe the wackestone facies in conjunction with packstone facies.

Non-laminated mudstone.— This facies contains fine-grained grey to beige microcrystalline mud, as well as some dolomicrite (Fig. 5.3F). Intermixed with micrite are sparse, well-sorted, sand-sized subangular quartz grains. Occasional penetrative trace fossils are present, but at a low density (ichnofabric index = 2). Overall, non-laminated micrite facies are homogenous and represent ~ 16% of section measured. This facies is most common at the base of East Hill and East Hill 2.

Microbial wackestone.— Mud-supported grains of *Renalcis*-group and *Epiphyton*-group microbes appear as bushy, semi-lunate darkened clusters (Fig. 5.3G). *Renalcis*-group microbes have no internal structure and cluster into semi-circles with sparry cement filling gaps between clusters. These larger clots are in turn surrounded by micrite and micropeloids. Rare *Subtifloria* grains are also present and consist of parallel laminations of wavy filaments. This facies is relatively rare at ~10% of measured strata and is only found in the West Valley section.

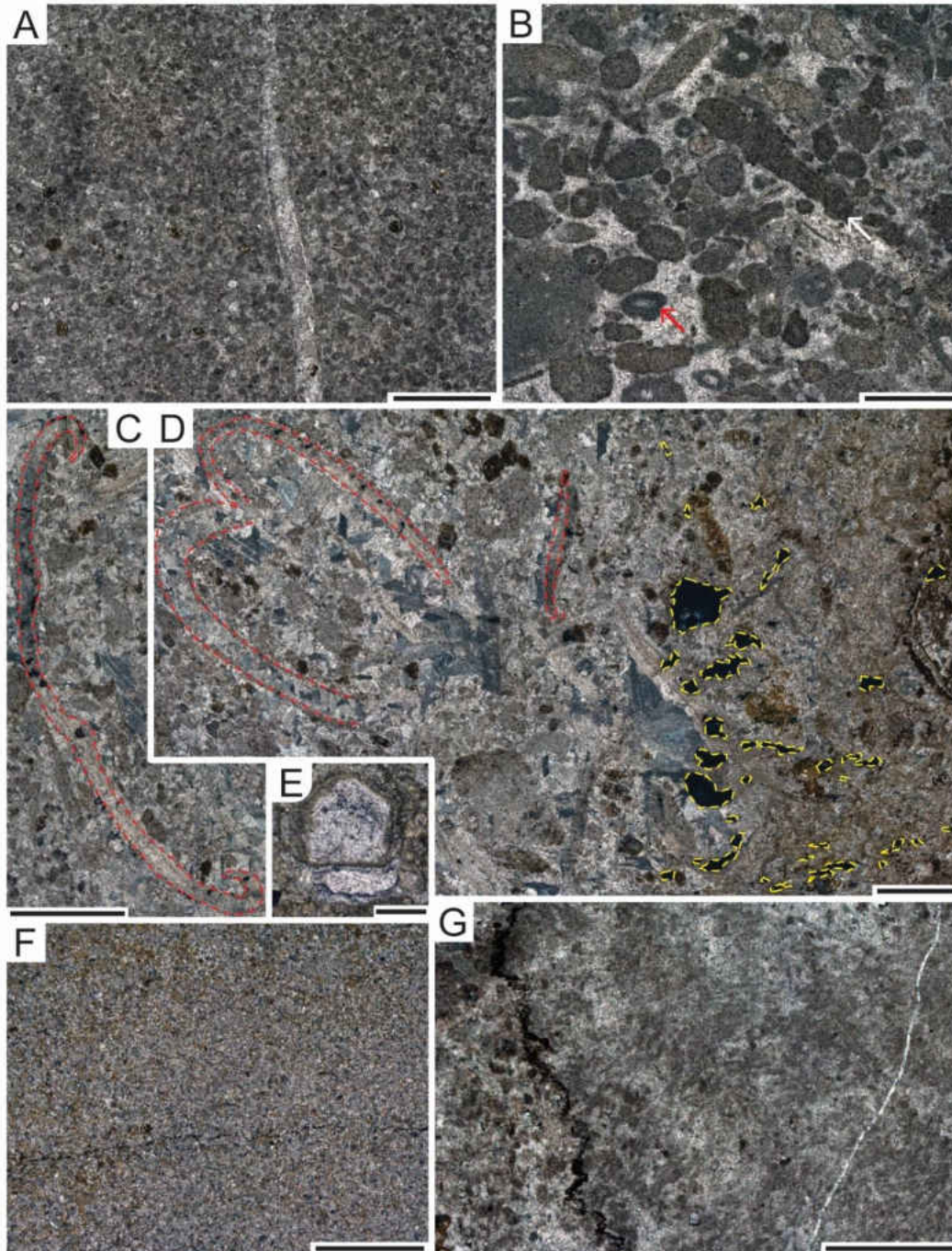


Figure 5.3: Mule Spring Limestone common facies microanalysis images. Non-laminated peloidal packstone/wackestone (A - E), non-laminated mudstone (F), microbial wackestone (G). A, Micropeloidal packstone. B, Mixture of macro- and micropeloidal packstone. Some partially micritized oncoïds with dropped nuclei (red arrow) and irregularly-shaped bounded grains (white arrow). C, Trilobite segment highlighted in red. D, Large bioclasts highlighted in red, fenestra highlighted in yellow. E, Pentamerel echinoderm ossicle. F, Micrite in mudstone. G, Faint branching to clustered microbial material in wackestone. All images in cross-polarized light. Scale bars equal 1 mm in all but E, which equals 0.2 mm.

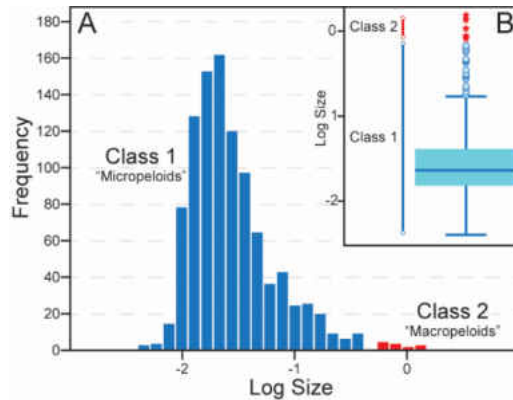


Figure 5.4: Peloid size distribution. A, Histogram of log-transformed peloid sizes (N = 1,000). 250 peloids were measured from samples taken at section denoted by stars on Fig. 5.6. B, Box and whisker plot of data from A.

Leiolite. — In outcrop these facies appear aphanitic and uniform in texture. They lack the characteristic clotted or laminated texture of thrombolites or stromatolites, but do have a cryptic microbial texture when seen in thin section (Dupraz *et al.*, 2011). In thin section, this facies appears as agglutinated micropeloidal material within a dense micrite background matrix. The dense background material occasionally encloses small cavities that were later filled with sparry cement (Fig. 5.5A). Microbial elements are composed of grey micrite and darkens towards the edges, sometimes with sparry cement in interior chambers. Isolated or chained micropeloids and rounded quartz grains are found sparingly within the background matrix. Overlaying this background matrix are macropeloids with wavy, irregular laminations, but are not horizontally contiguous for more than a few millimeters. Occasionally, a clotted texture is found encrusting hard surfaces, but there is no characteristic iterative growth of more layers overgrowing old layers. Overall, this facies is very similar to microbial wackestone facies in terms of grain composition. However, this layer has a denser background matrix that encloses small amounts of cavity space (Fig. 5.5A). This facies is only found in the West Valley section and occupies about 8% of the measured section.

Oncoid grainstone. — Roughly spherical, type R oncoids are larger (5 - 6 mm) than macropeloids (1.5 - 2 mm). They contain only very faint asymmetrical laminations, and none have obvious nuclei (Fig. 5.5B). Outer laminations are thicker than inner laminations and have a crudely clotted texture with occasional pockets of sparry cement and darkened outer crusts. Internal laminations appeared to be more densely filled with micrite compared to outer laminations. They are found alongside macro- and micropeloids, suspended in sparry cement with very little to no mud matrix. The exception are oncoids in East Hill which are in a mud-supported matrix of micrite and trilobite bioclasts. Oncoid grainstones in East Hill 2 also contain several large rectangular intraformational intraclasts (Fig. 5.5C). These intraclasts have a laminated internal structure of micrite and truncated ends. In addition to crudely laminated oncoids, aggregated oncoids with numerous grains enclosed in thin cortex are also found (Fig. 5.5D). They are smaller than laminated oncoids and possibly represent an early stage of oncoid growth (Han *et al.*, 2015). Oncoid grainstone facies cover only ~6% of section.

Laminated bindstone. — Contains vertically stacked coupled beige (dark grey in thin section) and grey submillimeter-to-millimeter scale micrite laminations (Fig. 5.5E - F). Contact between laminations is sometimes wavy and separated by irregularly-shaped fenestra. Within grey layers are occasional, but faint, laminations. SEM-EDS images suggest higher concentrations of silica in beige layers associated with large clusters, suggesting secondary silicification or chert (Fig. 5.5G - H). Angular to subrounded quartz grains and sparse micropeloids occur throughout. This layer is relatively rare and occurs only in East Hill 2, ~4% of section.

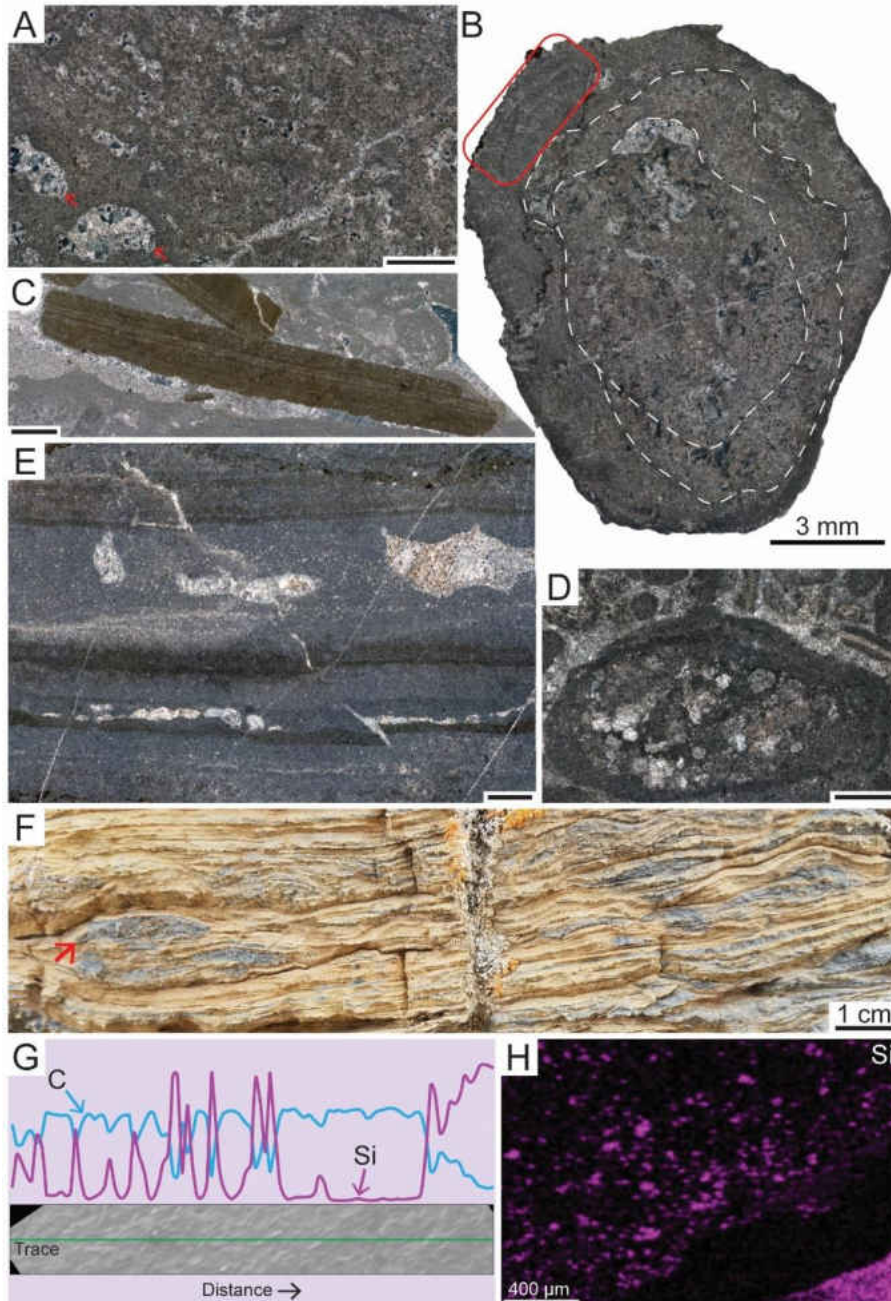


Figure 5.5: Mule Spring Limestone infrequent facies microanalysis images. Leiolite (A), oncoid grainstone (B-D), laminated bindstone (E - H). A, Leiolite matrix with previously vacant cavity space filled with sparry cement (arrows). B, Large oncoid from oncoid grainstone. Note thick laminations and radiating microbial growth highlighted in boxed area. C, Intraclast from oncoid grainstone with squared truncated ends. Matrix in intraclasts is similar to laminated bindstone. D, Aggregated oncoid with micropeloids inside, some replaced with sparry calcite. E, Laminated bindstone layering with intermixed micropeloids and fenestra filled with sparry calcite. F, Close-up of laminated bindstone in outcrop. Arrow shows minor relief. G, SEM-EDS line scan with carbon (C) and silicon (Si) alternating banding. H, SEM-EDS map of silicon concentration. Images A-E in polarized light. Scale bars equal 1 mm unless otherwise noted.

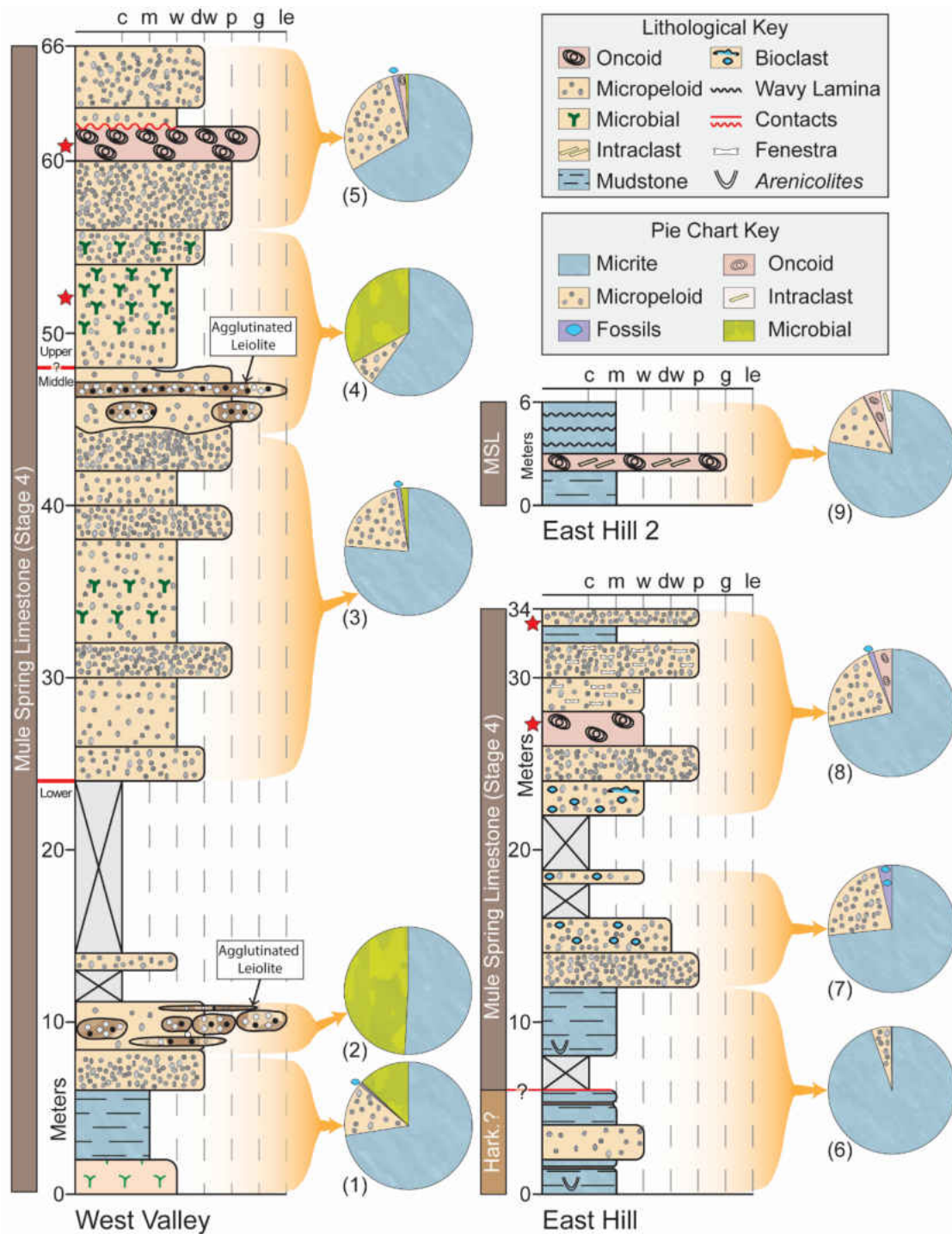


Figure 5.6: Mule Spring Limestone stratigraphy and carbonate contributions. Stratigraphic thicknesses measured from field observations. Dunham textures and composition determined from thin section analysis. Pie chart percentages calculated from point count analysis (see Table 5.1 for details). Boundaries between formations and members tentative. Stars denote samples for peloid size distribution, see Fig. 5.4. c - covered, m - mudstone, w - wackestone, dw - dense wackestone, p - packstone, g - grainstone, le - leiolite

Potential framework builders

Metazoans?. — As mentioned above, anthaspidellid sponges have been found within the late Cambrian Bonanza King Formation in the Great Basin (Shapiro and Rigby, 2004). The Bonanza King sponges are slightly obconical, thin-walled specimens of the genus *Gallatinospongia* and have a maximum diameter of 12.5 mm. Additional conical anthaspidellid sponges from the Mila Formation in Iran are known from the Furongian, specifically specimens of *Rankenella*, but are larger at 31 mm in diameter (Kruse and Zhuravlev, 2008). Both genera have a diagnostic skeletal net formed by radiating trabs. Trabs are formed from the union of ray tips and create a characteristic “ladder-and-rung” spicule pattern (Rigby and Bayer, 1971). Within the Mule Spring Limestone are several dark, globule features preserved in outcrop (Fig. 5.7A). These globule features contain several irregularly-spaced circular openings filled with background matrix. The overall size of these features are larger than surrounding oncoids (~5 mm) and contain no laminations. Thin sections near the features contain poorly-preserved elongated structures with cement-filled centers (Fig. 5.7B - C). The “walls” of these structures are composed of micrite and have a clean edge separating the central cavity. The outer edges grade into micropeloids. The structure shown in figure 5.7B measures 7.1 x 3.1 mm in size with the internal cavity measuring 3.8 x 1.2 mm. No internal spicule networks are preserved.

Additionally, several circular-to-oval shaped objects are found in East Hill. These grains have been replaced with secondary calcite and filled with micrite inside the internal hollow area (Fig. 5.7D). One appears to have dark microbes encrusting around it and measures 3.7 x 2.4 mm in diameter with an internal cavity 3.0 x 1.7 mm. Large calcitic shells, potentially of brachiopods, are also found encased within microbial crust (Fig. 5.8A).

While some potential metazoans *may* be present, identifying these organisms is not possible because of poor preservation. While, the globule feature and elongated structures have a passing gross morphological and size similarity to metazoans from the other late Cambrian localities, it is not reasonable to propose an affinity with any certainty. Additionally, there are certainly remains of sparse reef-dwelling organisms (trilobites, echinoderms, calcitic shells), however, these organisms were most likely either isolated examples or washed in after death. The general lack of these fossils suggests that if there were framework-building metazoans present, they did not create significant framework from which to seed suitable reef habitats during this interval.

Microbes?.— Several growth forms of calcifying microbial organisms are present in the Mule Spring Limestone (see Riding, 1991 for classification). However, they are a small component of the overall fabric and only occur in small clusters. *Hedstroemia*-group fans are the best preserved, but only occur in two samples. One example of these shrub-like microbes shows hemispherical growth and a secondary budding of new hemispherical growth (Fig. 5.7E). Shrubs contain parallel radiating filaments 0.03 mm in width and 0.1 mm between filaments. Note that the filaments are darker than the surrounding matrix, suggesting that they are not dissolved skeletal material that was reprecipitated with sparry cement. More robust *Renalcis*-group microbes are the most common microbial growth form in the Mule Spring Limestone (Fig. 5.7F). These were most frequent within leiolite. Finally, *Subtifloria* (*Girvanella*-group) microbes were found in two samples. Parallel, cable-like filaments stacked together form large grains and were presumably flat-lying and flexible (Fig. 5.7G - H). Unidentified low-lying encrusting microbes are also present as seen on the outside of brachiopod shells as well as

oncoids present throughout the formation (Fig. 5.8A). The *Girvanella*-group is often credited with formation of oncoids in the Cambrian, however, in the Mule Spring Limestone internal structure is rarely preserved (Han *et al.*, 2015; Wilmeth *et al.*, 2015).

The construction of primarily calcifying microbial reefs after the extinction of archaeocyaths, some with reef-dwelling sponges, has been documented previously in other global localities (see Adachi *et al.*, 2014; Kruse and Reitner, 2014; Lee *et al.*, 2014). But while calcifying microbes are present in the Mule Spring Limestone, their concentration appears considerably more sparse than other localities despite two leiolites found in the West Valley section. Outcrop in which these thin sections were collected did not appear to show substantial topographic relief. Therefore, while there are potentially some minor lenses of leiolite with very low relief, there does not appear to be a strong domal buildup from any of these components. Rather the presence of numerous oncoids, microbial mats, microbial wackestones, and sparse encrusting microbes in general suggest a very early stage of ecological restructuring. Mass oncid occurrences are known from other localities during the early-middle Cambrian transition and could suggest the beginning of microbialite resurgence during this period (Zhang *et al.*, 2014). Initially, it appears that microbes were only encrusting slightly raised surfaces (for example minor amounts of relief in mud flats or on hard shells), but were not yet strong or thick enough to create iterative layers of calcified hardground material required for reef development (Schuhmacher, 1977; Chisholm and Kelley, 2001, Perry and Smithers, 2006).

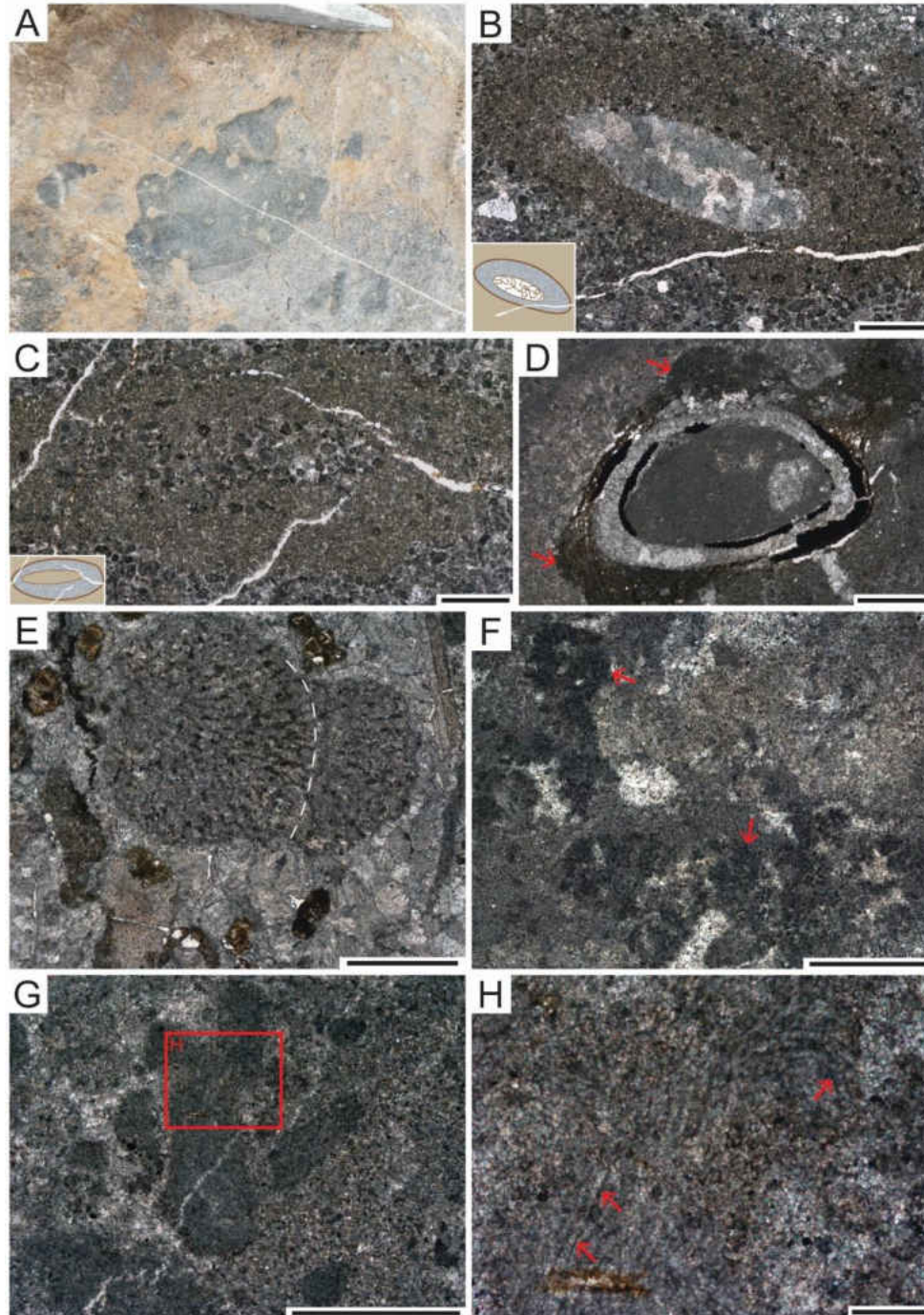


Figure 5.7: Framework building candidates of the Mule Spring Limestone. A, Outcrop photo of globular feature with circular openings inside. B and C, Micritized features with hollow centers filled with sparry calcite (B) and micropeloids matrix (C). Drawings of photos in inset images. D, Replaced grain with hollow center and potential encrusting microbial material on outer wall (arrows). E, *Hedstroemia*-group microbes with two budding bodies (separated by dashed line). F, *Renalcis*-group microbial organisms. G, *Subtifloria* microbial organisms. H, Close-up of boxed area in G. All images in polarized light. Scale bars equal to 1 mm in B-G, 0.1 mm for H. Hammer for scale in A.

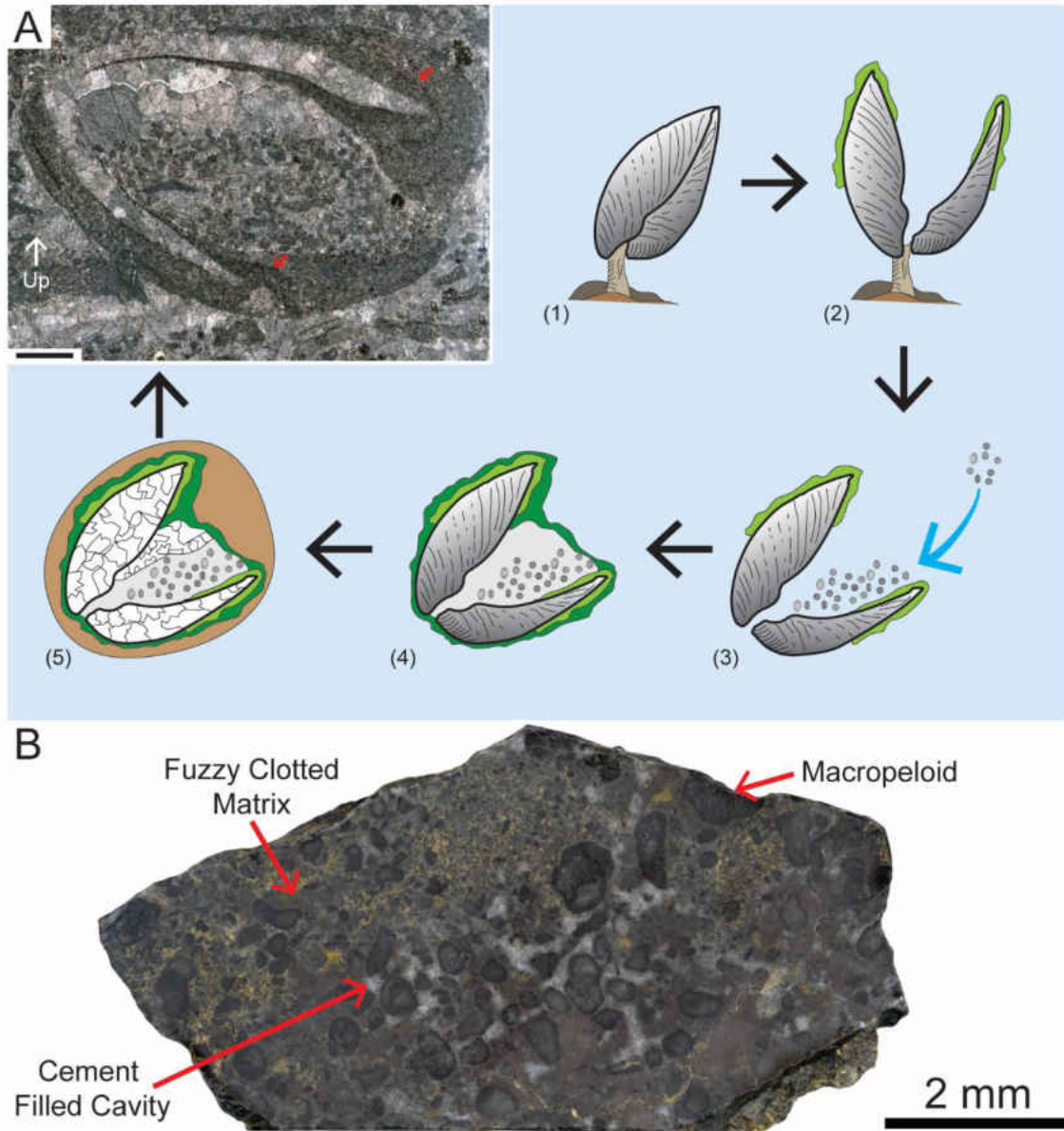


Figure 5.8: Encrusting microbial activity and leiolite hand sample. A, Thin section image of a reprecipitated shell (potentially of a brachiopod) with several generations of microbes encrusting on the exterior and micropeloids in interstitial cavity. Red arrows showing contact between generations of microbes. Scale bar equals 1 mm. (1) - Brachiopod *in vivo*. (2) Brachiopod with microbes encrusting on just apical portion of valves. (3) Brachiopod filled with micropeloids. (4) New layer of microbes encrusting on grain. (5) Dissolution of valves and filling of remaining cavity space with sparry cement. B, Macropeloids and fuzzy clotted texture as background matrix in leiolite.

Database analysis

The number of reefs rose in the first three stages of the Cambrian, concurrent with the origination and diversification of archaeocyathan sponges (Fig. 5.9). This trend quickly reverses during Stage 4 with both archaeocyaths and microbial reefs suffering heavy losses due to the Botomian extinction and Toyonian regression. The Wuliuan through Guzhangian then clearly represents a period of reduced reef building activity with only 21 documented reefs in the PaleoReefs Database compared to 144 in the early Cambrian. Reefs somewhat recover in the Paibian through Stage 10 with 58 reef localities known, but far fewer than the early Cambrian (Fig. 5.9). Notably, this recovery only occurs in microbial reefs, with very few examples of metazoan reefs occurring in the late Cambrian (Appendix Table E8). This transition is statistically supported with a significant difference in number of reefs between the three-partition separation of the Cambrian (χ^2 p -value $\ll 0.001$). This is most likely due to a resurgence of microbial-supported reefs in the late Cambrian (Lee *et al.*, 2015). Therefore, it is not unusual for the Mule Spring Limestone sections studied here to have minimal to no reef-building activity given the paucity of reefs worldwide during Stage 4 and the middle Cambrian.

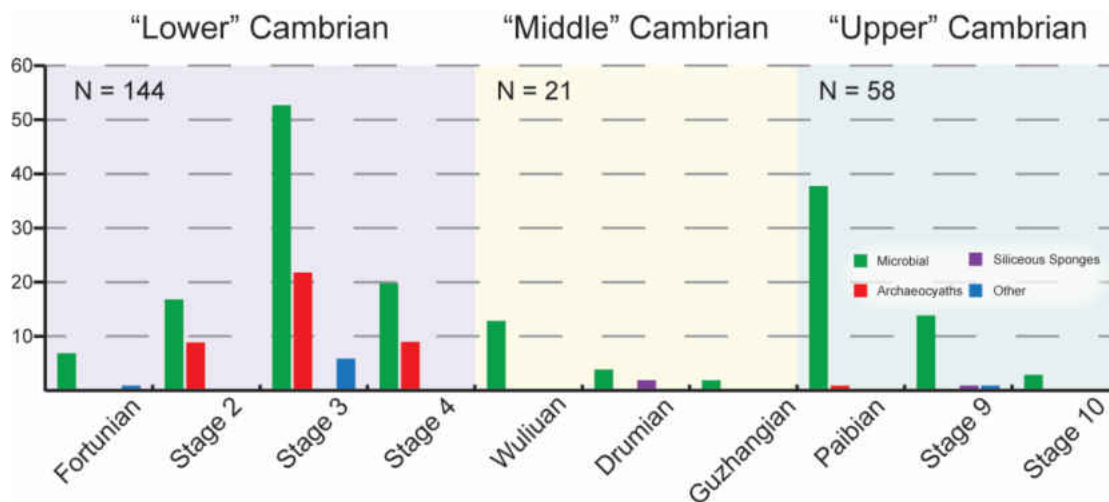


Figure 5.9: Cambrian reef occurrences from PARED. All 223 entries with system labelled as 'Cambrian' used. Other category contains reefs without designation and (2) occurrences of serpulid worm reefs from the "Lower" Cambrian.

Geochemical conditions

Stable carbon isotopic composition was generally uniform throughout the three sections measured, generally remaining around 0 ‰ VPDB. A minor negative drift of about 1 ‰ occurs around 30 m of West Valley and 12 m of East Hill (Fig. 5.10). Given the similarity of direction and magnitude of the drift, a tentative correlation between these two points can be inferred. This confirms that both sections are recording approximately the same interval of time. East Hill 2 has several data points above 0 ‰ VPDB, which is not seen in other parts of the Mule Spring Limestone studied here, suggesting it is recording a different interval from either of the other two localities. However, there are no persistently negative or dramatic changes in isotopic composition during this interval. This may suggest a relatively stable period in carbon cycling at this locality, however, further data from ICP-MS trace element samples is needed to infer redox conditions.

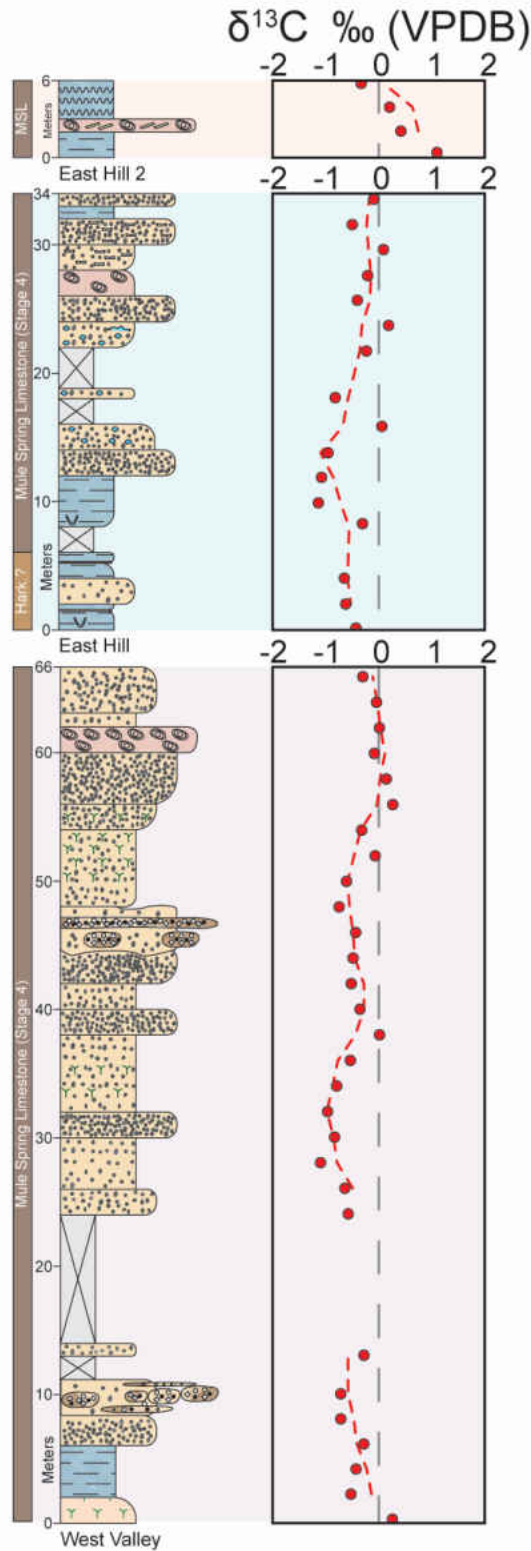


Figure 5.10: Stable carbon isotopic composition of the Mule Spring Limestone. Error bars show standard deviation between two duplicate samples. Dashed line represents three-point moving averages. Note that the three sections studied here do not represent a composite stratigraphic column. Trace element data forthcoming in a further study.

Interpretations

The Mule Spring Limestone is interpreted here to represent a shallow intertidal zone with a shallow drop off transitioning to a deeper marine environment (Fig. 5.11). The wavy laminations from East Hill 2 are interpreted as microbial/algal mud flats with frequent inundations. Sparse mud cracks and silt grains suggest that this section was occasionally subaerial. Higher energy pulses could have produced chaotic overturned layers and fractured intraclasts, though conditions were probably low energy in general to produce mudstones. Laminated oncoids also could have been produced by encrusting microbes on grains that later dropped out or were micritized.

Non-laminated peloid packstones from East Hill represent a slightly deeper transitional zone in which peloid aggregates collected. While peloids are typically polygenetic in origin, microbial sources represent one method of their formation (Chafetz, 1986; Sun and Wright, 1989) and peloids of this type do occur in post-extinction intervals (Adachi *et al.*, 2004). Specifically, the micropeloids in our study are of the same size, shape, and also occur in interstitial cavities just as others proposed to be microbial in origin (Adachi *et al.*, 2004). The fuzzy texture and hollow centers of some macropeloids is also consistent with enrolled/partially micritized microbial derived peloids (Chafetz, 1986). Furthermore, the presence of calcifying microbes in associated intervals confirms the presence of microbes in this section. Thus, the high concentration of micropeloids in this section is interpreted as a signature of cryptic microbial origin, as is common in shallow marine settings after extinctions (Pickard, 1996; Sano and Nakashima, 1997). It should be noted that undoubtedly the macro- and micropeloids observed here have multiple origins, but their appearance and distribution are consistent with

a microbial origin, potentially from microbial mat-like environments. Packstone and wackestone facies in East Hill also contain the highest concentration of trilobite segments and other bioclastic material. Oncoid grainstone also supports a shallow environment, perhaps around fair-weather wave base. This in conjunction with occasional mudstone deposits with penetrative trace fossils supports the interpretation of a shallow, restricted marine setting (Fig. 5.11).

The West Valley section contains the microbial wackestone, flat lying leiolites, and is closer to slope deposits down section. This suggests that the West Valley was a relatively deeper, though still shallow, marine setting. Clotted microbial material and leiolites suggest a sticky mat of minimally raised surface (~2 cm) into which bioclastic material and micropeloids would be captured. The higher concentration of wackestones also suggests larger amounts of mud production in this section, or less energy to wash away mud. Very few shelly fossils and only moderate to low levels of bioturbation suggest a low diversity benthic environment. The occurrence of bushy microbes also points to low predator density as well. This near slope, low diversity setting with small cryptic microbial facies in a shallow subtidal setting is known from other localities in the US; for example, the Conococheague Limestone in Maryland (Demicco, 1985).

The setting described above includes physical environments that could be colonized by calcareous benthic organisms to initiate the process of reef building. However, very little evidence that large-scale buildups by either metazoans or microbes was found. Speculative metazoans fossils alongside more definitive calcifying microbial organisms are present, however, neither substantially initiated any major reef building at this locality. This appears to

have resulted in a fossil record that is far less diverse and produces less skeletal material than the preceding reef building intervals of the Cambrian. For example, the underlying Poleta and Harkless Formations contain 2.4% and 9.9% framework building metazoans (see above) and 1.3% other fossil material. By comparison, the Mule Spring Limestone contains no substantial metazoan framework builders and only 0.8% fossil material (a 38% reduction; Table 5.1). Furthermore, there is a larger proportion of arthropod and (potentially) rhynchonellid brachiopods in the Mule Spring Limestone as compared to echinoderm and lingulid brachiopod assemblages in the preceding formations and other archaeocyath reefs (see above; Pruss *et al.*, 2012; Hicks and Rowland, 2009). It should be noted that the quality of preservation at this locality is poor. Thick-shelled brachiopods, which are normally robust to reprecipitation, were found replaced with sparry calcite. However, macroscopic observations of topographic relief still would have been present if reef building was occurring. Instead, only small amounts of encrustation on hard surfaces (such as brachiopods) and oncoids were forming as opposed to larger microbial reefs, representing an initial stage of reestablishment of a post-extinction benthic ecosystem (Whalen *et al.*, 2001). The sudden occurrence of oncoids in post-reef environments could be due to the loss of protective wave barriers from framework builders. Oncoids can only form in environments that are energetic enough to flip grains to allow growth on multiple sides of a grain. When wave barriers are lost, higher amounts of wave energy are allowed to agitate encrusting microbes and rotate grains. This locality may have been general soft sediment, (as seen by the presence of mud/wackestone, burrows) forcing microbial organisms to encrust on the minimal amount of hard surface that was available. Solidification of the substrate had not yet occurred, reducing the likelihood of renewed reef formation.

While claiming that *no* reefs were being formed during the immediate aftermath of the regional extinction of archaeocyaths is impossible, there is no evidence of reef development within the Mule Spring Limestone at this locality. Rather, this setting provides insight into the diversity and delayed nature of post-extinction ecosystem reinitiation. A destabilization of the chemical conditions of the ocean could play a role in this delayed onset of diversity, however, no evidence of this is found in our carbon isotopic composition data.

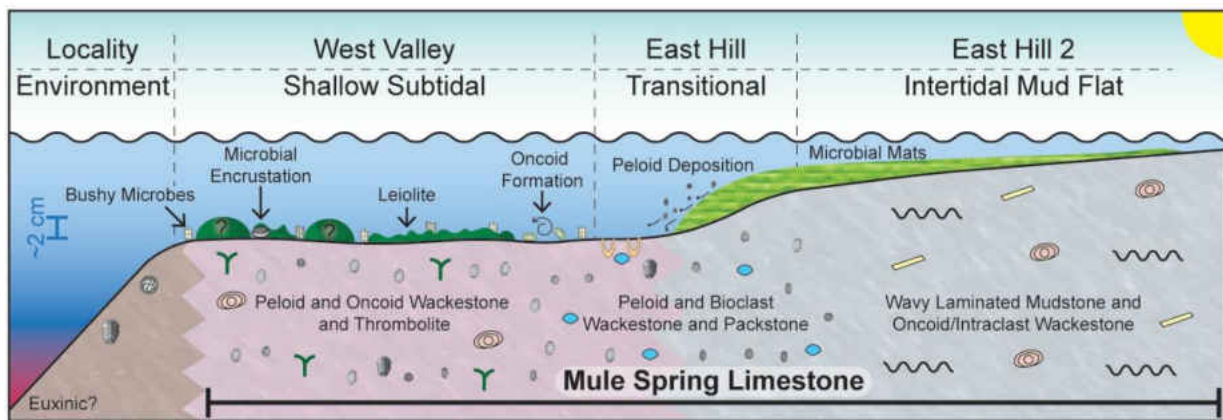


Figure 5.11: Mule Spring Limestone paleoenvironmental reconstruction. Dunham textures and composition determined from thin sections. Symbols same as lithological symbols in figure 5.6. Domal cryptic microbialites may be sporadically present based on microbial reefs from other localities but were not observed in Clayton Ridge. Figure is vertically exaggerated.

Conclusions

The Mule Spring Limestone at Clayton Ridge contains evidence of shallow marine intertidal to shallow subtidal restricted marine environments. Wavy laminated microbial mats are found preserved at the shallowest portions of this formation and grade into relatively deeper waters down slope. The formation is mostly composed of micrite and peloids of various sizes. While the origins of peloids are tentative, it is inferred that here they are primarily microbial in origin. Therefore, the Mule Spring Limestone represents a microbial mud flat community of low topographic relief. There is no evidence of either metazoan or microbial

framework reefs in this formation. Rather, evidence of encrusting activity on hard surfaces, in an otherwise soft substrate environment, is found. Field observations and database analysis both suggest that the late early Cambrian into the middle Cambrian represents the first reef eclipse of the Phanerozoic. This is accompanied by low diversity ecosystems distinct from the previous early Cambrian reefs. Future geochemical work will attempt to identify changes in the geochemical properties of global seawater to identify a cause for this delayed onset of biodiversity. What makes this locality unique is that there was not an immediate turnover of reef building activities to novel organisms as is the case in other localities around the world, particularly in China. The specific conditions that prevented rapid reestablishment of a reef community requires further research to illuminate.

References

- Adachi, N., Ezaki, Y., and Liu, J. 2004. The fabrics and origins of peloids immediately after the end-Permian extinction, Guizhou Province, South China. *Sedimentary Geology* **164**: 161-178.
- Adachi, N., Ezaki, Y., and Liu, J. 2014. The late early Cambrian microbial reefs immediately after the demise of archaeocyathan reefs, Hunan Province, South China. *Palaeogeography, Palaeoclimatology, Palaeoecology* **407**: 45-55.
- Allwood, A. C., Walter, M. R., Kamber, B. S., Marshall, C. P., and Bruch, I. W. 2006. Stromatolite reef from the early Archaean era of Australia. *Nature* **441**: 714-718.

- Álvaro, J. J., and Debrenne, F. 2010. The Great Atlasian Reef Complex: an early Cambrian subtropical fringing belt that boarded West Gondwana. *Palaeogeography, Palaeoclimatology, Palaeoecology* **294**: 120-132.
- Buhl-Mortensen, L., Vanreusel, A., Gooday, A. J., Levin, L. A., Priede, I. G., Buhl-Mortensen, P., Gheerardyn, H., King, N. J., and Raes, M. 2010. Biological structures as a source of habitat heterogeneity and biodiversity on the deep ocean margins. *Marine Ecology* **32**: 21-50.
- Cocito, S. 2004. Bioconstruction and biodiversity: their mutual influence. *Scientia Marina* **68**: 137-144.
- Cooper, P., and Jin, J. 2012. Early Silurian (Aeronian) East Point coral patch reefs of Anticosti Island, Eastern Canada: first reef recovery from the Ordovician/Silurian mass extinction in eastern Laurentia. *Geoscience* **2**: 64-89.
- Chafetz, H. S. 1986. Marine peloids; a product of bacterially induced precipitation of calcite. *Journal of Sedimentary Research* **56**: 812-817.
- Chisholm, J. R. M., and Kelley, R. 2001. Marine ecology: worms start the reef building process. *Nature* **409**: 152.
- Dahl, T. W., Boyle, R. A., Canfield, D. E., Connelly, J. N., Gill, B. C., Lenton, T. M., and Bizzarro, M. 2014. Uranium isotopes distinguish two geochemically distinct stages during the later Cambrian SPICE event. *Earth and Planetary Science Letters* **401**: 313-326.

- Demicco, R. V. 1985. Platform and off-platform carbonates of the upper Cambrian of western Maryland, U. S. A. *Sedimentology* **32**: 1-22.
- Droser, M. L., and Bottjer, D. J. 1988. Trends in depth and extent of bioturbation in Cambrian carbonate marine environments, western United States. *Geology* **16**: 233-236.
- Dupraz, C. Reid, P. R., and Visscher, P. T. 2011. Microbialites, modern. In: *Encyclopedia of Earth Sciences Series*. Springer Netherlands.
- Erwin, D. H. 2001. Lessons from the past: biotic recoveries from mass extinctions. *Proceedings of the National Academy of Sciences* **8**: 5399-5403.
- Fagerstrom, J. A., and West, R. R. 2011. Roles of clone-clone interactions in building reef frameworks: principles and examples. *Facies* **57**: 375-394.
- Flügel, E. 2004. Microfacies of carbonate rocks: analysis, interpretation and application. Springer, New York. 976 p.
- Gill, B. C., Lyons, T. W., Young, S. A., Kump, L. R., Knoll, A. H., and Saltzman, M. R. 2011. Sulphur isotope evidence for widespread euxinia in the later Cambrian ocean. *Nature* **469**: 80-83.
- Glass, L. M., and Phillips, D. 2006. The Kalkarindji continental flood basalt province: a new Cambrian large igneous province in Australia with possible links to faunal extinctions. *Geology* **34**: 461-464.
- Graham, N. A. J., and Nash, K. L. 2013. The importance of structural complexity in coral reef ecosystems. *Coral Reefs* **32**: 315-326.

- Grotzinger, J., Adams, E. W., and Schröder, S. 2005. Microbial-metazoan reefs of the terminal Proterozoic Nama Group (c. 550-543 Ma), Namibia. *Geological Magazine* **142**: 499-517.
- Guilbaud, R., Slater, B. J., Poulton, S. W., Harvey, T. H. P., Brocks, J. J., Nettersheim, B. J., and Butterfield, N. J. 2018. Oxygen minimum zones in the early Cambrian ocean. *Geochemical Perspectives Letters* **6**: 33-38.
- Hallam, A. 1996. Recovery of the marine fauna in Europe after the end-Triassic and early Toarcian mass extinctions. *Geological Society, London, Special Publications* **102**: 231-236.
- Han, Z., Zhang, X., Chi, N., Han, M., Woo, J., Lee, H. S., and Chen, J. 2015. Cambrian oncoids and other microbial-related grains on the North China Platform. *Carbonate Evaporites* **30**: 373-386.
- Hicks, M., and Rowland, S. M. 2009. Early Cambrian microbial reefs, archaeocyathan inter-reef communities, and associated facies of the Yangtze Platform. *Palaeogeography, Palaeoclimatology, Palaeoecology* **281**: 137-153.
- Hong, J., Cho, S-H., Choh, S-J., Woo, J., and Lee, D-J. 2012. Middle Cambrian siliceous sponge-calcimicrobe buildups (Daegi Formation, Korea): metazoan buildup constituents in the aftermath of the early Cambrian extinction event. *Sedimentary Geology* **523-254**: 47-57.
- Hong, J., Lee, J-H., Choh, S-J., and Lee, D-J. 2016. Cambrian Series 3 carbonate platform of Korea dominated by microbial-sponge reefs. *Sedimentary Geology* **341**: 58-69.

- Johns, R. A., Dattilo, B. F., and Spincer, B. 2007. Neotype and redescription of the upper Cambrian anthaspidellid sponge, *Wilberncyathus donegani* Wilson, 1950. *Journal of Paleontology* **81**: 435-444.
- Jourdan, F., Hodges, K., Sell, B., Schaltegger, U., Wingate, M. T. D., Evins, L. Z., Söderlund, U., Haines, P. W., Phillips, D., and Blenkinsop T. 2014. High-precision dating of the Kalkarindji large igneous province, Australia, and synchrony with early-middle Cambrian (Stage 4-5) extinction. *Geology* **42**: 543-546.
- Kah, L. C., Bartley, J. K., and Stagner, A. F. 2009. Reinterpreting a Proterozoic enigma: *Conophyton-Jacutophyton* stromatolites of the Mesoproterozoic Atar Group, Mauritania. *International Association of Sedimentologists Special Publication* **41**: 277-295.
- Kiessling, W., and Flügel, E. 2002. Paleoreefs - a database on Phanerozoic reefs. Pp. 77 - 94. *In*: Kiessling, W., Flügel, E., and Golonka, J. eds. *Phanerozoic Reef Patterns. SEPM Special Publication* **72**. SEPM, Tulsa, Oklahoma.
- Kiessling, W. 2005. Long-term relationships between ecological stability and biodiversity in Phanerozoic reefs. *Nature* **433**: 410-413.
- Kiessling, W. 2009. Geologic and biologic controls on the evolution of reefs. *Annual Reviews of Ecology, Evolution, and Systematics* **40**: 173-192.
- Kouchinsky, A., Bengtson, S., Runnegar, B., Skovsted, C., Steiner, M., and Vendrasco, M. 2012. Chronology of early Cambrian biomineralization. *Geology Magazine* **149**: 221-251.

- Kruse, P. D., and Zhuravlev, A. Y. 2008. Middle-late Cambrian *Rankenella-Girvanella* reefs of the Mila formation, northern Iran. *Canadian Journal of Earth Science* **45**: 619-639.
- Kruse, P. D., and Reitner, J. R. 2014. Northern Australian microbial-metazoan reefs after the mid-Cambrian mass extinction. *Memoirs of the Association of Australian Palaeontologists* **45**: 31-53.
- Kuznetsov, V. G. 2018. Late Ordovician reefs and the biological crisis at the Ordovician-Silurian boundary. *Stratigraphy and Geological Correlation* **26**: 261-266.
- Lee, J-H., Lee, H. S., Chen, J., Woo, J., and Chough, S. K. 2014. Calcified microbial reefs in Cambrian Series 2, North China Platform: implications for the evolution of Cambrian calcified microbes. *Palaeogeography, Palaeoclimatology, Palaeoecology* **403**: 30-42.
- Lee, J-H., Chen, J., and Chough, S. K. 2015. The middle-late Cambrian reef transition and related geological events: a review and new view. *Earth-Science Reviews* **145**: 66-84.
- Lee, J-H., Hong, J., Choh, S-J., Lee, D-J., Woo, J., and Riding, R. 2016. Early recovery of sponge framework reefs after Cambrian archaeocyath extinction: Zhangxia Formation (early Cambrian Series 3), Shandong, North China. *Palaeogeography, Palaeoclimatology, Palaeoecology* **457**: 269-276.
- Martindale, R. C., Foster, W. J., and Velledits, F. 2017. The survival, recovery, and diversification of metazoan reef ecosystems following the end-Permian mass extinction event. *Palaeogeography, Palaeoclimatology, Palaeoecology*: 10.1016/j.palaeo.2017.08.014.

- Marenco, P. J., Martin, K. R., Marenco, K. N., and Barber, D. C. 2016. Increasing global ocean oxygenation and the Ordovician Radiation: insights from Th/U carbonates from the Ordovician of western Utah. *Palaeogeography, Palaeoclimatology, Palaeoecology* **458**: 77-84.
- Mata, S. A., and Bottjer, D. J. 2012. Microbes and mass extinctions: paleoenvironmental distribution of microbialites during times of biotic crisis. *Geobiology* **10**: 3-24.
- Miller, A. J., Strauss, J. V., Halverson, G. P., Macdonald, F. A., Johnston, D. T., and Sperling, E. A. 2017. Tracing the onset of Phanerozoic-style redox-sensitive trace metal enrichments: new results from basal Ediacaran post-glacial strata in NW Canada. *Chemical Geology* **457**: 24-37.
- Montañes, I. P., Banner, J. L., Osleger, D. A., Borg, L. E., and Bosserman, P. J. 1996. Integrated Sr isotope variations and sea-level history of middle to upper Cambrian platform carbonates: implications for the evolution of Cambrian seawater $^{87}\text{Sr}/^{86}\text{Sr}$. *Geology* **24**: 917-920.
- Munday, P. L. 2004. Habitat loss, resource specialization, and extinction on coral reefs. *Global Change Biology* **10**: 1642-1647.
- Nelson, C. A. 1962. Lower Cambrian-Precambrian succession, White-Inyo Mountains, California. *Geological Society of America Bulletin* **73**: 139-144.
- Palmer, A. R., and Halley, R. B. 1979. Physical stratigraphy and trilobite biostratigraphy of the Carrara Formation (lower and middle Cambrian) in the southern Great Basin. *Geological*

- Survey Professional Paper 1047*. United States Government Printing Office, Washington DC. 121 p.
- Peng, S., Babcock, L. E., and Cooper, R. A. 2012. The Cambrian Period. Pp. 437 - 488. *In*: Gradstein, F., Ogg, J., Schmitz, M., and Ogg, G. eds. *The Geologic Timescale 2012*. Elsevier BV, Oxford.
- Perry, C. T., and Smithers, S. G. 2006. Taphonomic signatures of turbid-zone reef development: examples from Paluma Shoals and Lugger Shoal, inshore central Great Barrier Reef, Australia. *Palaeogeography, Palaeoclimatology, Palaeoecology* **242**: 1-20.
- Pickard, N. A. H. 1996. Evidence for microbial influence on the development of Lower Carboniferous buildups. *Geological Society, London, Special Publications* **107**: 65-82.
- Pruss, S. B., and Bottjer, D. J. 2005. The reorganization of reef communities following the end-Permian mass extinction. *Comptes Rendus Palevol* **4**: 553-568.
- Pruss, S. B., Clemente, H., and LaFlamme, M. 2012. Early (Series 2) Cambrian archaeocyathan reefs of southern Labrador as a locus for skeletal carbonate production. *Lethaia* **45**: 401-410.
- Qi, C., Li, C., Gabbott, S. E., Ma, X., Xie, L., Deng, W., Jin, C., and Hou, X-G. 2018. Influence of redox conditions on animal distribution and soft bodied fossil preservation of the lower Cambrian Chengjiang Biota. *Palaeogeography, Palaeoclimatology, Palaeoecology* **507**: 180-187.

- Riding, R. 1991. Calcified cyanobacteria. Pp. 55 - 87. *In: Riding, R., ed. Calcareous algae and stromatolites.* Springer-Verlag, Berlin.
- Rigby, J. K., and Bayer, T. N. 1971. Sponges of the Ordovician Maquoketa Formation in Minnesota and Iowa. *Journal of Paleontology* **45**: 608-627.
- Rowland, S. M., and Shapiro, R. S. 2002. Reef patterns and environmental influences in the Cambrian and earliest Ordovician. *In: Kiessling, W., Flügel, E., and Golonka, J. eds. Phanerozoic Reef Patterns. SEPM Special Publication 72.* SEPM, Tulsa, Oklahoma.
- Saltzman, M. R., Young, S. A., Kump, L. R., Gill, B. J., Lyons, T. W., and Runnegar, B. 2011. Pulses of atmospheric oxygen during the late Cambrian. *Proceedings of the National Academy of Sciences* **108**: 3876-3881.
- Sano, H., and Nakashima, K. 1997. Lowermost Triassic (Griesbachian) microbial bindstone-cementstone facies, Southwest Japan. *Facies* **36**: 1-24.
- Savarese, M., and Signor, P. W. 1989. New archaeocyathan occurrences in the upper Harkless Formation (lower Cambrian of western Nevada). *Journal of Paleontology* **63**: 539-549.
- Schuhmacher, H. 1977. Initial phases in reef development, studied at artificial reef types off Eilat, (Red Sea). *Helgoländer wiss. Meeresunters* **30**: 400-411.
- Scotese, C. R. 2001. Atlas of earth history. *Paleogeography* **vol. 1.** PALEOMAP, Arlington, Texas. 58 p.

- Shapiro, R. S., and Rigby, J. K. 2004. First occurrence of an *in situ* anthaspidellid sponge in a dendrolite mound (upper Cambrian; Great Basin, USA). *Journal of Paleontology* **78**: 645-650.
- Shapiro, R. S., and Awramik, S. M. 2006. *Favosamaceria cooperi* new group and form: a widely dispersed, time-restricted thrombolite. *Journal of Paleontology* **80**: 411-422.
- Skovsted, C. B. 2006. Small shelly fossils from the basal Emigrant Formation (Cambrian, uppermost Dyeran Stage) of Split Mountain, Nevada. *Canadian Journal of Earth Sciences* **43**: 487-496.
- Sun, S. Q., and Wright, V. P. 1989. Peloidal fabrics in Upper Jurassic reefal limestones, Weald Basin, southern England. *Sedimentary Geology* **65**: 165-181.
- Sundberg, F. A., and McCollum, L. B. 2003. Early and mid-Cambrian trilobites from the outer-shelf deposits of Nevada and California. *Palaeontology* **46**: 945-986.
- Tribovillard, N., Algeo, T. J., Lyons, T., Riboulleau, A. 2006. Trace metals as paleoredox and paleoproductivity proxies: an update. *Chemical Geology* **232**: 12-32.
- Vermeij, G. J. 1989. The origins of skeletons. *Palaios* **4**: 585-589.
- Waggoner, B. 2003. Non-trilobite arthropods from the Silver Peak Range, Nevada. *Journal of Paleontology* **77**: 706-720.
- Wang, D., Ling, H-F., Struck, U., Zhu, X-K., Zhu, M., He, T., Yang, B., Gamper, A., and Shields, G. A. 2018. Coupling of ocean redox and animal evolution during the Ediacaran-Cambrian transition. *Nature Communications* **9**: 2575.

- Webster, M. 2011. Stops 7A, 7B, and 7C - Upper Dyeran litho- and biostratigraphy of the Split Mountain Area, Nevada. *In*: Hollingsworth, J. S., Sundberg, F. A., and Foster, J. R. eds. Cambrian Stratigraphy and Paleontology of Northern Arizona and Southern Nevada: *Museum of Northern Arizona Bulletin* **67**: 236-246.
- Wei, G-Y., Planavsky, N. J., Tarhan, L. G., Xi, C., Wei, W., Li, D., and Ling, H-F. 2018. Marine redox fluctuation as a potential trigger for the Cambrian explosion. *Geology* **46**: 587-590.
- Weiss, A., and Martindale, R. C. 2017. Crustose coralline algae increased framework and diversity on ancient coral reefs. *PLoS ONE* **12**: e0181637.
- Whalen, M. T., Day, J., Eberli, G. P., and Homewood, P. W. 2001. Microbial carbonates as indicators of environmental change and biotic crisis in carbonate systems: examples from the Late Devonian, Alberta basin, Canada. *Palaeogeography, Palaeoclimatology, Palaeoecology* **181**: 127-151.
- Wilmeth, D. T., Corsetti, F. A., Bisenic, N., Dornbos, S. Q., Oji, T., and Gonchigdorff, S. 2015. Punctuated growth of microbial cones within early Cambrian oncoids, Bayan Gol Formation, western Mongolia. *Palaaios* **30**: 836-845.
- Woo, J., Chough, S. K., and Han, Z. 2008. Chambers of *Epiphyton* thalli microbial buildups, Zhangxia Formation (middle Cambrian), Shandong Province, China. *Palaaios* **23**: 55-64.
- Wood, R. A. 1998. The ecological evolution of reefs. *Annual Review of Ecology and Systematics* **29**: 179-206.

- Wood, R. A. 2000. Palaeoecology of a Late Devonian back reef: Canning Basin, Western Australia. *Palaeontology* **43**: 671-703.
- Wotte, T., and Sundberg, F. A. 2017. Small shelly fossils from the Montezuman-Delamaran of the Great Basin in Nevada and California. *Journal of Paleontology* **91**: 883-901.
- Zhang, W., Shi, X., Jiang, G., Tang, D., and Wang, X. 2014. Mass-occurrence of oncoids at the Cambrian Series 2-Series 3 transition: implications for microbial resurgence following an early Cambrian extinction. *Gondwana Research* **28**: 432-450.
- Zhang, M., Hong, J., Choh, S-J., and Lee, D-J. 2017. Thrombolite reefs with archaeocyaths from the Xiannüdong Formation (Cambrian Series 2), Sichuan, China: implications for early Paleozoic bioconstruction. *Geosciences Journal* **21**: 655-666.
- Zhuravlev, A. Y., and Wood, R. A. 1996. Anoxia as the cause of the mid-early Cambrian (Botomian) extinction event. *Geology* **24**: 311-314.
- Zhuravlev, A. Y., Naimark, E. B., and Wood, R. A. 2015. Controls on the diversity and structure of earliest metazoan communities: early Cambrian reefs from Siberia. *Earth-Science Reviews* **147**: 18-29.

Chapter VI. Conclusions

Outcome of Stated Goals

1. Quantify the proportion of framework-building organisms during early Cambrian archaeocyathan reefs and assess the biodiversity and geochemical conditions associated with these changes.

- Metazoans did not significantly contribute to the earliest reefs of the Cambrian.
- Micrite is by far the most common component of early Cambrian reefs.
- Carbonate from archaeocyaths, and eventually coralomorphs, increases over the course of reef establishment.
- Microbial organisms represent a larger proportion of carbonate contribution compared to metazoans.
- Biodiversity is low overall, but increases slightly when additional framework builders are incorporated.
- Positive carbon isotopic excursions occur within these reefs, but do not consistently co-occur with appearance of archaeocyaths.
- Low, but non-zero, values of redox-sensitive elements occur within these reefs.

2. Associate these changes in framework-building organisms with changes in the reef-dwelling organisms that inhabited these ecosystems. Furthermore, investigate the morphological diversity in archaeocyathan sponges and how it might relate to their ability to perform a niche creating role in reefs.

- Framework-building organisms did not necessarily correspond to abundant reef-dwelling organisms.

- Skeletal reef dwellers did not become more common in reefs until the Ordovician.
- Archaeocyaths are significantly smaller in body size than modern demosponges or lithistids.
- Archaeocyaths occupy significantly fewer gross morphological categories compared to modern demosponges sponges or lithistids.
- Lack of morphological disparity and relatively few heavily skeletonized reef-dwelling organisms contribute to depauperate reef ecosystems of the Cambrian.

3. Investigate potential occurrences of microbial reefs during the post-archaeocyath interval of the Cambrian and the diversity they may harbor.

- No evidence of metazoan reefs is found in the immediate aftermath of archaeocyath extinction in the Mule Spring Limestone.
- No evidence of large-scale microbial reefs is found, but small amounts of calcifying microbial organisms and oncoids are present.
- A smaller amount of fossil material is found in the post-extinction interval.
- No dramatic or persistent changes in carbon isotopic composition are observed.

In addition to answering the three stated goals of this project, several additional observations were made over the course of this project.

Shift Towards Metazoan Reefs

Based on data collected as part of **Chapter II**, the Cambrian appears to represent an end member of the total range of reef carbonate contribution possibilities. Cambrian reefs contain a much larger micrite component (around 90%) than reefs from later in the Phanerozoic and did not start to gain significant skeletal material until the Tommotian or Atdabanian (Stage 2/Stage

3). Both the reefs in the White-Inyo Mountains and in Mongolia show little to no skeletal material in initial reef environments. This shifts over the course of reef deposition to contain archaeocyaths, coralomorphs, and sparse reef-dwelling organisms (trilobites, brachiopods, hyoliths, etc.) in fairly low, but detectable, quantities. This indicates that reef ecosystems were for the first time - excluding rare occurrences of biomineralized metazoans in the Neoproterozoic - built primarily by enzymatic and biochemical processes rather than physical binding and trapping processes (Webb, 1996). However, these reefs still had low levels of metazoans overall, especially when compared to later reefs. This is consistent with other studies that have found the Cambrian to be a transitional period between microbial Proterozoic ecosystems and metazoan Phanerozoic environments (Dornbos *et al.*, 2005; Riding, 2006; Bottjer, 2010; Álvaro *et al.*, 2013).

This trend extends further when looking at reefs throughout the lower Paleozoic, as Ordovician reefs contained a much larger proportion of metazoan material in comparison to Cambrian examples. Within this study, there appear to be three main components of well-preserved reefs: micrite, metazoan bioclasts, and microbial bioclasts. There are additional components, such as cement and vacant cavity space, but the three listed above are most common. To briefly summarize, Cambrian reefs are largely micrite, but quickly shift towards more metazoan-based reefs by the Ordovician. This trend reverses back toward more micritic-based reefs after the end-Ordovician extinction. The upper Paleozoic, Mesozoic, and Cenozoic are by comparison more balanced (Fig. 6.1). Interestingly, the effects of several of the Big Five mass extinctions are visible in this type of diagram as a sudden swing towards more micrite-based reefs. Post-extinction restructuring does appear to be prolonged in the Cambrian

compared to later intervals of the Phanerozoic. This trend appears to be less severe (i.e., smaller increases in micrite component) after the middle Paleozoic, potentially because of more standing biodiversity during those intervals. As discussed in **Chapter V**, global reef gaps are probably local and short-term. But they do appear to revert reefs towards the micrite-based environments that were more common before the origination of archaeocyaths. Again, this brief survey suggests that the Cambrian is transitional in nature and distinct from both later and earlier time periods.

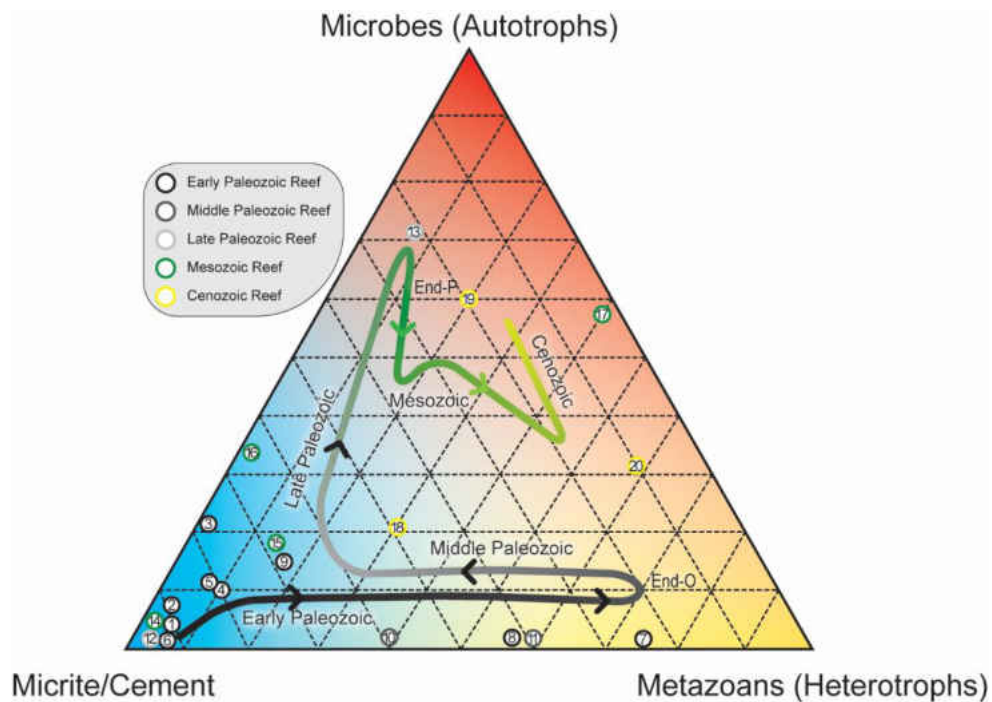


Figure 6.1: Ternary diagram of Phanerozoic reef ecosystems. Data points show percent contribution of the “3 M’s” of reef constituency measured from thin section point counts in selected literature. Microbes include algae and any photosynthetic organisms, micrite includes any non-bioclastic material, and metazoans include any heterotrophic organisms. Line with arrows represents generalized trend of reef development through the Phanerozoic as estimated by the author. 1-3 - this study; 4 - Pruss *et al.*, 2012; 5 - Creveling *et al.*, 2013; 6 - Hicks and Rowland, 2009; 7 - Li *et al.*, 2015; 8 - Kano, 1989; 9 - Adachi *et al.*, 2012; 10 - Pellegrini *et al.*, 2012; 11 - Schneider and Ausich, 2002; 12 - Webb, 1999; 13 - Webb, 2005; 14 - Wu *et al.*, 2017; 15 - Martindale *et al.*, 2010; 16 - Bonuso *et al.*, 2018; 17 - Oliver *et al.*, 2003; 18 - Nebelsick *et al.*, 2000; 19 - Pandolfi *et al.*, 1999; 20 - Gherardi and Bosence, 2001

Delayed Biodiversity of Cambrian Reefs

The addition of more skeletal material from framework builders did not necessarily mean abundance of reef dwellers increased simultaneously as well. While archaeocyaths have been shown to provide additional hard surfaces for encrusting microbial organisms to attach, this study did not observe a strong correlation between an increase in archaeocyaths and reef-dwelling organisms as expected (**Chapter II**). Data collected in **Chapter III** show that reefs took longer to diversify with reef dwellers than with framework builders. This lag between framework builders and reef dwellers suggests that archaeocyaths did not perform niche creation as efficiently as one might expect based on data from benthic metazoans in modern ecosystems (Messmer *et al.*, 2011). Alternatively, the ecology of the Cambrian may be more complex than initially realized and additional criteria may be preventing a stronger framework builder-reef dweller correlation from occurring. Thus, while the addition of archaeocyaths into Cambrian reef ecosystems did shift the biomineralizing properties, it took longer for reef dwellers to inhabit these ecosystems.

Cambrian Reefs Are Different

The Cambrian does show a variety of similarities that make them comparable to reefs today. For example, they do contain the sedimentological processes of growth, destruction, and sedimentation (Tucker and Wright, 1990). They also have cementation, though at comparably lower levels than later ecosystems. These reefs also have modular, carbonate producing benthic organisms that provide surface area for encrusting organisms (Adachi *et al.*, 2014). Finally, it appears that the basic food webs of reefs were established early in the Phanerozoic (Dunne *et al.*, 2008). However, in addition to those mentioned above, far more properties make

reefs from the early Cambrian distinct. First, they appear to occupy regions of high sedimentation and high nutrient levels, whereas modern reef ecosystems typically do not thrive in these environments (Wood, 1993). The Cambrian also has far lower diversity compared to modern ecosystems ($H' > 10$ in some modern sites), for example reef fish, which play a large role in the destruction and sedimentation of reefs today, are not found in the fossil record until the Eocene (Bellwood, 1996; Díaz-Pérez *et al.*, 2016). Cambrian reefs are also far less morphological diverse. In **Chapter IV**, the morphospace occupancy of archaeocyaths was explored and found to be substantially restricted compared to other sponges. This means that comparing the Cambrian to modern reef ecosystems remains challenging, though Cambrian reefs are useful for understanding the initial conditions of reef formation in the Phanerozoic. Lessons learned from this period may be more specific to features of the Cambrian, rather than easily applicable to younger ecosystems.

Future Directions

First, given the differences between Cambrian and later Phanerozoic reef ecosystems in terms of carbonate contribution, additional information on even earlier reefs could help illuminate when these conditions first began. Metazoan reefs from the Nama Group in the Ediacaran have not been extensively explored using the point count techniques used in this study. This could help determine carbonate abundance from metazoans occurring in these even earlier reefs. Acid digestions and CT scanning of core samples could also be used in conjunction with thin sections to further study the carbonate contribution of carbonate rocks. Second, we still do not fully understand the global timing of skeletal incorporation in the Cambrian. Studies such as this can help illustrate local conditions, but correlating them across different

depositional basins, especially in the early Cambrian when biostratigraphic material is sparse, remains an enormous hurdle in this field of study. Additional studies that incorporate chemostratigraphy alongside paleontological data can help alleviate this problem. Finally, a major understudied feature of reefs involves quantifying the amount of habitat heterogeneity present in the environment. This can be challenging even in modern reef ecosystems but can be done by quantifying the proportion of different morphologies (branching, hemispherical, etc.) present in a reef. More diverse morphologies suggest more diverse organisms are able to inhabit the wider range of microniches provided. Using an approach similar to that performed in this study, it would be interesting to extend this to more time periods in the Phanerozoic to try to assess timing of habitat heterogeneity changes and their effects on diversity.

The Cambrian is a fascinating time period that saw the evolution of major animal phyla, transition from Proterozoic to Phanerozoic substrates, and development of new reef ecosystems. The last is important to study as reefs harbor phenomenal amounts of diversity and support marine ecosystem stability. Thus, studying early Cambrian reef ecosystems can provide valuable insight into both a critical time period and essential ecosystems.

References

- Adachi, N., Ezaki, Y., and Liu, J. 2012. The oldest bryozoan reefs: a unique Early Ordovician skeletal framework construction. *Lethaia* **45**: 14-23.
- Adachi, N., Nakai, T., Ezaki, Y., and Liu, J. 2014. Late early Cambrian archaeocyath reefs in Hubei Province, South China: modes of construction during their period of demise. *Facies* **60**: 703-717.

- Álvaro, J. J., Zamora, S., Clausen, S., Vizcaíno, D., and Smith, A. B. 2013. The role of abiotic factors in the Cambrian Substrate Revolution: a review from the benthic community replacements of West Gondwana. *Earth-Science Reviews* **118**: 69-82.
- Bellwood, D. R. 1996. The Eocene fishes of Monte Bolca: the earliest coral reef fish assemblage. *Coral Reefs* **15**: 11-19.
- Bonuso, N., Loyd, S., and Lorentz, N. J. 2018. Pioneer reef communities within a Middle Triassic (Anisian) to Upper Triassic (Carnian) mixed carbonate-siliciclastic ramp system from the Star Peak Group, South Canyon, central Nevada. *Palaeogeography, Palaeoclimatology, Palaeoecology* **503**: 1-12.
- Bottjer, D. J. 2010. The Cambrian Substrate Revolution and early evolution of the phyla. *Journal of Earth Science* **21**: 21-24.
- Creveling, J. R., Fernández-Remolar, D., Rodríguez-Martínez, M., Menéndez, S., Bergmann, K. D., Gill, B. C., Abelson, J., Amils, R., Ehlmann, B. L., García-Bellido, D. C., Grotzinger, J. P., Hallmann, C., Stack, K. M., and Knoll, A. H. 2013. Geobiology of a lower Cambrian carbonate platform, Pedroche Formation, Ossa Morena Zone, Spain. *Palaeogeography, Palaeoclimatology, Palaeoecology* **386**: 459-478.
- Díaz-Pérez, L., Rodríguez-Zaragoza, F. A., Ortiz, M., Cupul-Magaña, A. L., Carriquiry, J. D., Ríos-Jara, E., Rodríguez-Troncoso, A. P., and García-Rivas, M. del C. 2016. Coral reef health indices versus the biological, ecological and functional diversity of fish and coral assemblages in the Caribbean Sea. *PLoS ONE* **11**: e0161812

- Dornbos, S. Q., Bottjer, D. J., and Chen, J-Y. 2005. Paleoeecology of benthic metazoans in the early Cambrian Maotianshan Shale biota and the Middle Cambrian Burgess Shale biota: evidence for the Cambrian Substrate revolution. *Palaeogeography, Palaeoclimatology, Palaeoecology* **220**: 47-67.
- Dunne, J. A., Williams, R. J., Martinez, N. D., Wood, R. A., and Erwin, D. H. 2008. Compilation and network analysis of Cambrian food webs. *PLoS Biology* **6**: e102.
- Gherardi, D. F. M., and Bosence, D. W. J. 2001. Composition and community structure of the coralline algal reefs from Atol das Rocas, South Atlantic, Brazil. *Coral Reefs* **19**: 205-219.
- Hicks, M., and Rowland, S. M. 2009. Early Cambrian microbial reefs, archaeocyathan inter-reef communities, and associated facies of the Yangtze Platform. *Palaeogeography, Palaeoclimatology, Palaeoecology* **281**: 137-153.
- Kano, A. 1989. Depositional and palaeoecology of an upper Silurian stromatoporoid reef on southernmost Gotland, Sweden. *Geological Journal* **24**: 295-315.
- Li, Q., Li, Y., Wang, J., and Kiessling, W. 2015. Early Ordovician lithistid sponge-*Calathium* reefs on the Yangtze Platform and their paleoceanographic implications. *Palaeogeography, Palaeoclimatology, Palaeoecology* **425**: 84-96.
- Martindale, R. C., Zonneveld, J-P., and Bottjer, D. J. 2010. Microbial framework in Upper Triassic (Carnian) patch reefs from Williston Lake, British Columbia, Canada. *Palaeogeography, Palaeoclimatology, Palaeoecology* **297**: 609-620.

- Messmer, V., Jones, G. P., Munday, P. L., Holbrook, S. J., Schmitt, R. J., and Brooks, A. J. 2011. Habitat biodiversity as a determinant of fish community structure on coral reefs. *Ecology* **92**: 2285-2298.
- Nebelsick, J. H., Bassi, D., and Drobne, K. 2000. Microfacies analysis and palaeoenvironmental interpretation of Lower Oligocene, shallow-water carbonates (Gornji Grad Beds, Slovenia). *Facies* **43**: 157-176.
- Oliver, N., Hantzpergue, P., Gaillard, C., Pittet, B., Leinfelder, R. R., Schmid, D. U., and Werner, W. 2003. Microbialite morphology, structure and growth: a model of the Upper Jurassic reefs of the Chay Peninsula (Western France). *Palaeogeography, Palaeoclimatology, Palaeoecology* **193**: 383-404.
- Pandolfi, J. M., Llewellyn, G., and Jackson, J. B. C. 1999. Pleistocene reef environments, constituent grains, and coral community structure: Curaçao, Netherlands Antilles. *Coral Reefs* **18**: 107-122.
- Pellegrini, A. F. A., Soja, C. M., and Minjin, C. 2012. Post-tectonic limitations on Early Devonian (Emsian) reef development in the Gobi-Altai region, Mongolia. *Lethaia* **45**: 46-61.
- Pruss, S. B., Clemente, H., and LaFlamme, M. 2012. Early (Series 2) Cambrian archaeocyathan reefs of southern Labrador as a locus for skeletal carbonate production. *Lethaia* **45**: 401-410.
- Riding, R. 2006. Microbial carbonate abundance compared with fluctuations in metazoan diversity over geological time. *Sedimentary Geology* **185**: 229-238.

- Schneider, K. A., and Ausich, W. I. 2002. Paleocology of framebuilders in early Silurian reefs (Brassfield Formation, southwestern Ohio). *Palaios* **17**: 237-248.
- Tucker, M. E., and Wright, V. P. 1990. *Carbonate Sedimentology*. Wiley-Blackwell Publishing. Oxford. 496 p.
- Webb, G. E. 1996. Was Phanerozoic reef history controlled by the distribution of non-enzymatically secreted reef carbonates (microbial carbonate and biologically induced cement)? *Sedimentology* **43**: 947-971.
- Webb, G. E. 1999. Youngest early Carboniferous (late Visean) shallow-water patch reefs in eastern Australia (Rockhampton Group, Queensland): combining quantitative micro- and macro-scale data. *Facies* **41**: 111-139.
- Webb, G. E. 2005. Quantitative analysis and paleoecology of earliest Mississippian microbial reefs, Gudman Formation, Queensland, Australia: not just post-disaster phenomena. *Journal of Sedimentary Research* **75**: 877-896.
- Wood, R. A. 1993. Nutrients, predation and history of reef-building. *Palaios* **8**: 526-543.
- Wu, S., Chen, Z-Q., Fang, Y., Pei, Y., Yang, H., and Ogg, J. 2017. A Permian-Triassic boundary microbialite deposit from the eastern Yangtze Platform (Jiangxi Province, South China): geobiologic features, ecosystems composition and redox conditions. *Palaeogeography, Palaeoclimatology, Palaeoecology* **486**: 58-73.

Appendices

Appendix A: Point count data

Table A1: Raw point count numbers for White-Inyo Mountains thin sections, out of 200 points. Locality (m) - locality collected and meterage; Mi - micrite; Sp - sparry calcite; Cl - clastic material; An - anhydrite gypsum; Arch - Di - archaeocyath with discrete septa; Arch - St - archaeocyath with bubbly septa; Cn - coralomporhs; Gi - *Girvanella*; Re - *Renalcis*; Ec - echinoderms; Ar - trilobite; Li - lingulid

White-Inyo Mountains Thin Sections												
Locality (m)	Mi	Sp	Cl	An	Arch - Di	Arch - St	Cn	Gi	Re	Ec	Ar	Li
GPH 1.81	115	13	14	1	3	0	30	0	23	0	1	0
GPH 1.77B	63	11	5	0	91	0	3	0	27	0	0	0
GPH 1.77A	111	15	8	0	0	0	60	0	6	0	0	0
GPH 1.72B	117	14	21	0	29	0	4	0	13	0	2	0
GPH 1.72A	92	15	12	1	29	36	12	0	1	1	1	0
GPH 1.35	98	26	33	0	0	1	0	0	2	29	10	1
GPH 1.01	13	0	164	2	0	0	0	0	21	0	0	0
GPH 0.84	22	4	160	1	0	0	0	0	13	0	0	0
GPH 0.05	1	0	190	5	0	0	0	0	4	0	0	0
CoralFloat	26	55	3	3	0	0	106	0	3	4	0	0
WGP64.49	195	3	0	0	0	0	0	0	0	2	0	0
WGP50.93	130	0	0	0	0	0	0	0	66	4	0	0
WGP49.36	198	1	0	0	0	0	0	0	0	1	0	0
WGP46.84	168	31	0	0	0	0	0	0	1	0	0	0
WGP 45.89	185	3	0	0	0	0	0	0	9	2	1	0
WGP43.46	199	0	0	0	0	0	0	0	0	1	0	0
WGP40.20	172	0	0	0	0	0	0	0	27	1	0	0
WGP34.41	179	7	0	0	0	10	0	0	0	4	0	0
WGP28.23	195	0	0	0	0	0	0	0	0	5	0	0
WGP26.97	193	3	0	0	0	0	0	0	0	4	0	0
WGP24.00	191	4	0	0	0	0	0	0	5	0	0	0
WGP18.71	196	2	0	0	0	0	0	0	0	2	0	0
WGP17.76	196	4	0	0	0	0	0	0	0	0	0	0
WGP13.73	198	2	0	0	0	0	0	0	0	0	0	0
WGP6.33	195	0	0	1	0	0	0	0	0	4	0	0
WGP4.78	191	0	0	0	0	0	0	0	7	2	0	0
WGP2.36	96	0	0	0	0	0	0	0	104	0	0	0
WGP1.32	196	3	0	0	0	0	0	0	1	0	0	0
WGP0.01	177	3	0	0	0	8	0	0	3	9	0	0
SMN56.03	187	0	0	0	2	0	0	0	10	1	0	0
SMN50.51	171	1	0	0	7	0	0	0	18	2	1	0
SMN44.60	53	24	0	0	60	0	0	0	62	0	1	0
SMN43.22	133	19	0	0	28	0	0	0	0	18	2	0
SMN34.80	120	20	0	0	26	0	0	0	25	7	1	1
SMN16.80	182	4	0	0	0	0	0	0	11	2	1	0
SMN15.92	191	0	0	0	0	0	0	0	9	0	0	0
SMN14.56	193	0	0	0	0	0	0	0	5	2	0	0
SMN13.54	138	0	0	0	0	0	0	0	50	2	0	0
SMN12.92	189	1	4	0	0	0	0	0	5	1	0	0
SMN1.06	192	1	2	0	0	0	0	0	5	0	0	0
SMNE89.82	182	8	0	0	0	0	0	0	9	1	0	0
SMNE72.51	99	5	0	0	0	0	0	0	86	9	1	0
SMNE52.79	101	20	0	0	14	0	0	0	63	0	1	1
SMNE50.62	186	10	0	0	2	0	0	0	2	0	0	0
SMNE46.70	132	27	0	0	37	0	0	0	4	0	0	0

SMNE44.14	167	12	0	0	19	1	0	0	1	0	0	0
SMNE39.30	181	13	0	0	3	0	0	0	1	2	0	0
SMNE36.97	183	4	0	0	0	0	0	0	12	1	0	0
SMNE35.12	174	20	0	0	0	0	0	0	1	5	0	0
SMNE30.70	196	2	0	0	0	0	0	0	2	0	0	0
SMNE29.44	193	6	0	0	0	0	0	0	0	1	0	0
SMNE25.79	187	2	0	0	0	2	0	0	4	5	0	0
SMNE16.60	186	0	0	0	0	0	0	0	14	0	0	0
SMNE15.30	86	18	0	0	14	0	0	1	81	0	0	0
SMNE12.78	144	0	0	0	0	0	0	0	45	11	0	0
SMNE8.90	182	0	0	0	0	0	0	0	14	4	0	0
SMNE4.46	169	10	0	0	0	0	0	0	20	1	0	0
SMNE2.45	155	34	0	0	0	0	0	0	8	3	0	0
SMNE0.86	182	3	0	0	0	0	0	0	15	0	0	0
SMS 44.24	198	2	0	0	0	0	0	0	0	0	0	0
SMS 36.53	135	3	0	0	0	0	0	0	52	10	0	0
SMS 33.67	162	4	0	0	8	2	0	0	24	0	0	0
SMS 31.16	154	7	0	0	18	0	0	0	19	2	0	0
SMS 29.08	194	1	0	0	0	1	0	0	4	0	0	0
SMS 28.65	188	4	0	0	7	0	0	0	0	1	0	0
SMS 27.72	181	8	0	0	0	0	0	0	10	1	0	0
SMS 24.12	169	0	0	0	9	21	0	0	0	1	0	0
SMS 21.52	170	12	0	0	16	0	0	0	0	2	0	0
SMS 21.17	181	17	0	0	0	0	0	0	2	0	0	0
SMS 17.90	179	21	0	0	0	0	0	0	0	0	0	0
SMS 15.91	192	7	0	0	0	0	0	0	1	0	0	0
SMS 15.01	105	93	0	0	0	2	0	0	0	0	0	0
SMS 12.81	178	21	0	0	1	0	0	0	0	0	0	0
SMS 9.27	152	32	0	0	0	2	0	0	14	0	0	0
SMS 6.77	193	7	0	0	0	0	0	0	0	0	0	0
SMS 2.73	160	40	0	0	0	0	0	0	0	0	0	0
SMS 0.45	160	35	0	0	0	0	0	0	3	2	0	0
SMSE2.45	185	4	0	0	5	4	0	0	2	0	0	0
SMSE45.27	180	3	0	0	10	0	0	0	3	4	0	0
SMSE43.97	187	0	0	0	0	0	0	0	13	0	0	0
SMSE41.54	150	14	0	0	0	5	0	0	29	2	0	0
SMSE41.24	123	3	0	0	2	24	0	0	46	2	0	0
SMSE39.61	190	10	0	0	0	0	0	0	0	0	0	0
SMSE34.68	184	5	0	0	7	0	0	0	4	0	0	0
SMSE33.27	135	46	0	0	0	0	0	0	18	1	0	0
SMSE26.79	141	18	0	0	34	4	0	0	3	0	0	0
SMSE26.72	176	18	0	0	0	0	0	0	6	0	0	0
SMSE22.00	154	38	0	0	0	0	0	0	7	1	0	0
SMSE20.34	143	5	0	0	0	7	0	0	44	1	0	0
SMSE18.23	194	0	0	0	2	0	0	0	4	0	0	0
SMSE13.02	163	28	0	0	0	0	1	0	2	5	1	0
SMSE7.63	194	2	1	0	0	0	0	0	3	0	0	0
SMSE4.33	198	1	0	0	0	0	0	0	1	0	0	0
SMSE3.11	197	0	3	0	0	0	0	0	0	0	0	0
SMSE1.92	191	8	0	0	0	0	0	0	1	0	0	0
SMSE0.92	190	0	0	0	0	0	0	0	4	0	0	6
BCT 78.78	192	2	0	0	3	0	0	0	0	3	0	0
BCT 78.54	122	4	0	0	44	11	0	0	7	12	0	0
BCT 78.15	92	0	1	0	0	0	0	0	90	16	1	0
BCT 46.20	193	1	0	0	0	0	0	0	0	6	0	0
BCT 45.94	191	3	0	0	0	0	0	0	0	6	0	0
BCT 45.80	189	0	0	2	0	0	0	0	9	0	0	0
BCT 5.56	186	9	5	0	0	0	0	0	0	0	0	0
BCT 1.16	143	0	2	0	0	0	0	0	40	15	0	0
BCT 1.13	191	0	4	0	0	0	0	0	3	2	0	0

Table A2: Raw point count numbers for Mongolia thin sections, out of 300 points. Locality (m) - locality collected and meterage; Mi - micrite; Sp - sparry calcite; Cl - clastic material; Mic - microbial material; Ec - echinoderms; Arch - archaeocyath; ReG - replaced grains; Un - unknown

Mongolia Thins Sections								
Locality (m)	Mi	Sp	Cl	Mic	Ec	Arch	ReG	Un
SGL 0	260	16	3	17	0	0	4	0
SGL 5	248	46	2	4	0	0	0	0
SGL 10	200	22	0	78	0	0	0	0
SGL 15	220	42	0	38	0	0	0	0
SGL 20	211	27	0	62	0	0	0	0
SGL 25	220	44	0	36	0	0	0	0
SGL 29.2	193	57	0	50	0	0	0	0
SGU 0	213	15	0	67	0	5	0	0
SGU 5	264	25	0	0	0	11	0	0
SGU 10	215	40	0	17	0	28	0	0
SGU 15	241	2	0	0	0	57	0	0
SGU 20	233	44	0	0	0	23	0	0
SGU 25	290	8	0	0	0	2	0	0
SGU 30	152	148	0	0	0	0	0	0
SGU 35	258	41	0	0	0	0	0	1
SGU 40	256	38	0	0	0	6	0	0
SGU 45	254	10	0	0	0	36	0	0
SGU 50A	255	17	0	0	0	28	0	0
SGU 55	227	73	0	0	0	0	0	0
SGU 60	291	4	0	0	0	3	0	2
SGU 65	262	15	0	13	0	10	0	0
SGU 70	254	8	0	13	0	25	0	0
SGU 75	257	15	0	3	0	25	0	0
SGU 80	275	25	0	0	0	0	0	0
SGU 85	258	16	0	11	0	14	0	1
SGU 90	218	3	0	66	0	13	0	0
SGU 95	279	11	0	0	0	10	0	0
SGU 100	270	12	0	0	0	18	0	0
SGU 105	253	47	0	0	0	0	0	0
SGU 110	232	16	0	0	0	52	0	0
SGU 115	283	16	0	0	0	1	0	0
SGU 120	292	4	0	0	0	4	0	0
SGU 125	278	20	0	0	0	2	0	0
SGU 130	271	5	0	0	0	24	0	0
ZAC 0	292	8	0	0	0	0	0	0
ZAC 5	277	17	0	2	0	2	0	2
ZAC 10	289	11	0	0	0	0	0	0
ZAC 15	238	1	2	58	0	1	0	0
ZAC 20	281	8	11	0	0	0	0	0
ZAC 30	272	28	0	0	0	0	0	0
ZAC 35	229	17	5	9	0	40	0	0
ZAC 40	229	4	9	47	0	11	0	0
ZAC 45	290	10	0	0	0	0	0	0
ZAC 50	266	14	0	0	0	20	0	0
ZAC 55	252	15	0	3	0	30	0	0
ZAC 60	241	37	0	20	0	2	0	0
ZAC 65	254	42	0	0	0	4	0	0
ZAC 70	205	7	0	75	0	11	2	0
ZAC 72.5	270	2	0	0	0	28	0	0
ZAC 75	287	12	0	1	0	0	0	0
ZAC 80	257	1	0	36	0	6	0	0
ZAC 85	263	30	0	0	0	7	0	0
ZAC 90	299	1	0	0	0	0	0	0
ZAC 95	248	11	0	34	0	7	0	0

ZAC 100	209	5	3	77	0	0	6	0
ZAC 105	278	19	0	0	0	3	0	0
ZAC 110	265	13	0	3	0	19	0	0
ZAC 115	227	16	0	0	0	57	0	0
ZAC 120	211	7	0	74	0	7	0	1
ZAC 125	194	33	0	7	0	57	9	0
ZAC 130	207	52	0	0	0	38	3	0
ZAC 135	259	1	0	30	0	8	2	0
ZAC 140	215	20	0	61	0	4	0	0
ZAC 145	238	21	0	0	0	40	1	0
ZAC 150	191	45	0	0	0	55	9	0
ZAC 155	224	3	1	11	0	57	4	0
ZAC 160	168	67	0	2	0	61	1	1
ZAC 165	225	8	0	6	0	55	6	0
ZAC 170	178	24	0	86	0	9	2	1

Table A3: Raw point count numbers for Clayton Ridge thin sections, out of 300 points. Locality (m) - locality collected and meterage; Mi - micrite; Sp - sparry calcite; Do - dolomite; Ar - arthropod; Cal - caliche; ReG - replaced grains; On - oncoïd; Intra - intraclast; Qu - quartz; Mic - microbial material; Un - unknown

Mule Spring Limestone Thin Sections												
Locality (m)	Mi	Sp	Do	Pel	Ar	Cal	ReG	On	Intra	Qu	Mic	Un
EH 0	266	34	0	0	0	0	0	0	0	0	0	0
EH 2	208	17	0	54	1	20	0	0	0	0	0	0
EH 4	270	5	0	25	0	0	0	0	0	0	0	0
EH 8	293	4	0	0	1	0	2	0	0	0	0	0
EH 10	265	10	17	6	2	0	0	0	0	0	0	0
EH 12	300	0	0	0	0	0	0	0	0	0	0	0
EH 14	157	18	10	112	3	0	0	0	0	0	0	0
EH 16	238	11	0	31	5	0	15	0	0	0	0	0
EH 18	210	36	0	49	5	0	0	0	0	0	0	0
EH 22	252	7	0	33	2	0	6	0	0	0	0	0
EH 24	170	7	0	120	0	0	3	0	0	0	0	0
EH 26	191	2	0	19	5	0	0	83	0	0	0	0
EH 28	252	3	0	32	0	0	1	12	0	0	0	0
EH 30	201	10	20	60	4	0	4	0	0	0	0	1
EH 32	275	8	0	17	0	0	0	0	0	0	0	0
EH 34	112	20	2	164	1	0	1	0	0	0	0	0
EH-2 0	280	6	0	13	0	0	1	0	0	0	0	0
EH-2 2	51	37	0	131	1	0	0	48	32	0	0	0
EH-2 4	280	5	0	15	0	0	0	0	0	0	0	0
EH-2 6	272	24	0	4	0	0	0	0	0	0	0	0
WH 0	112	38	87	4	2	0	0	0	0	0	57	0
WH 2	212	18	38	28	1	0	1	0	0	0	2	0
WH 4	88	201	6	5	0	0	0	0	0	0	0	0
WH 6	113	60	28	62	1	0	0	2	0	0	34	0
WH 8	148	28	1	0	0	0	0	0	0	0	123	0
WH 10	113	47	11	0	0	0	0	0	0	0	129	0
WH 13	192	20	5	80	1	0	0	0	0	0	2	0
WH 24	217	30	0	53	0	0	0	0	0	0	0	0
WH 26	260	11	0	23	2	0	2	0	0	0	2	0
WH 28	230	4	0	39	4	0	3	2	0	0	18	0
WH 30	208	6	0	85	0	0	1	0	0	0	0	0
WH 32	209	24	12	50	1	0	4	0	0	0	0	0
WH 34	215	8	20	36	1	0	0	0	0	0	20	0
WH 36	176	22	38	54	6	0	0	0	0	0	2	2
WH 38	205	13	6	74	2	0	0	0	0	0	0	0
WH 40	166	8	72	51	0	0	0	0	0	0	3	0
WH 42	183	10	17	88	1	0	0	0	0	0	0	1

WH 44	143	28	0	0	0	0	0	0	0	0	129	0
WH 46	132	9	0	1	0	0	0	0	0	0	158	0
WH 48	192	22	10	52	2	0	0	0	0	0	22	0
WH 50	150	49	0	6	0	0	0	0	0	0	95	0
WH 52	190	30	12	32	0	0	0	0	0	0	36	0
WH 54	242	17	0	24	4	0	0	0	0	0	12	1
WH 56	161	46	0	89	4	0	0	0	0	0	0	0
WH 58	110	27	3	153	1	0	0	0	0	0	1	5
WH 60	60	108	40	53	0	0	3	33	0	2	1	0
WH 62	185	12	42	61	0	0	0	0	0	0	0	0
WH 64	208	25	9	57	1	0	0	0	0	0	0	0
WH 66	174	8	55	60	1	0	2	0	0	0	0	0

Appendix B: Geochemical data

Table B1: Geochemical data for White-Inyo Mountain samples. Orange shaded boxes excluded. See methods for unit notation. Carbon isotopes in VPDB.

White-Inyo Mountain Samples											
Locality (m)	$\delta^{13}\text{C}$ ‰	X _{Sr} %	X _{Mn} %	X _{Na+Al} %	X _{Mg} %	X _{Fe} %	X _{Th} ppm	X _U ppm	X _{Mo} ppm	X _V ppm	Ca+Mg %
GPH 1.81	-0.75	0.06	0.23	0.79	0.49	0.79	6.24	0.89	2.45	-	3.01
GPH 1.77A	-	0.08	0.42	1.04	0.87	1.04	5.50	0.53	0.00	-	2.28
GPH 1.72A	-1.92	0.08	0.12	0.00	1.06	0.66	0.31	0.63	0.17	-	4.47
GPH 1.35A	-1.67	0.08	0.46	0.22	0.64	1.14	1.87	3.96	0.00	-	4.36
GPH 1.01	-	0.09	0.99	2.49	0.00	1.25	74.30	4.89	9.15	-	0.71
GPH 1.00	-	0.67	3.90	26.96	2.07	14.44	363.86	19.34	10.70	-	0.11
GPH 0.05	-	0.21	0.59	47.82	7.17	25.29	275.66	14.18	0.00	-	0.10
Coral Float	-3.17	0.10	0.41	0.32	0.76	1.25	1.00	2.46	0.02	-	3.72
WGP 64.49	-	0.13	0.03	0.09	4.50	1.02	3.20	0.22	4.10	-	4.25
WGP 58.29	-	0.15	0.11	0.01	2.66	1.08	1.44	0.28	1.69	-	3.85
WGP 50.93	-0.08	0.11	0.05	0.46	0.94	1.34	6.07	0.38	2.29	-	3.80
WGP 49.36	-	0.09	0.05	0.40	4.18	2.08	2.67	0.37	0.53	-	4.04
WGP 46.84	-	0.08	0.04	0.24	0.99	0.81	1.61	0.87	0.17	-	4.13
WGP 45.84	-	0.11	0.07	0.33	0.96	1.29	4.35	0.48	1.60	-	4.33
WGP 43.46	-	0.10	0.06	0.42	6.59	2.67	1.96	0.30	1.60	-	4.41
WGP 40.20	-0.19	0.11	0.04	0.39	1.69	1.50	1.70	0.84	0.00	-	4.05
WGP 34.41	-	0.12	0.04	0.96	7.11	2.65	15.55	1.29	0.25	-	3.28
WGP 28.23	0.01	0.11	0.05	0.42	3.07	1.75	2.08	0.40	0.00	-	3.75
WGP 26.97	-	0.12	0.04	0.09	0.69	1.10	2.76	0.09	1.27	-	4.94
WGP 24.00	0.09	0.12	0.05	0.06	1.27	1.17	0.34	0.15	0.00	-	4.59
WGP 18.71	-	0.11	0.05	0.40	7.06	2.89	3.40	0.40	0.00	-	4.06
WGP 17.76	-0.04	0.07	0.03	0.08	0.55	0.97	2.47	0.42	1.37	-	4.66
WGP 13.73	-	0.07	0.04	0.15	0.39	0.93	1.71	0.16	0.00	-	4.69
WGP 6.33	0.86	0.09	0.03	0.59	8.55	3.27	1.31	0.20	0.00	-	4.03
WGP 4.78	-	0.10	0.04	0.31	0.95	1.18	2.34	0.10	0.06	-	4.49
WGP 2.36	0.01	0.13	0.08	0.41	8.34	2.55	2.56	0.21	0.00	-	3.68
WGP 1.32	-	0.13	0.11	0.59	6.38	2.24	6.21	0.24	1.52	-	3.98
WGP 0.01	-2.85	0.05	0.21	0.03	0.16	0.00	1.19	0.20	0.01	-	4.67
SMNE 97.32	-1.02	0.11	0.07	0.07	0.73	0.71	2.35	0.97	1.55	-	4.55
SMNE 89.82	-0.70	0.06	0.06	0.91	19.85	2.62	2.51	0.45	0.00	-	3.31
SMNE 85.21	-1.24	0.12	0.07	0.09	4.59	0.85	0.89	1.23	0.00	-	4.89
SMNE 77.91	-0.65	0.10	0.09	0.07	1.64	0.00	0.68	1.12	0.41	-	4.18
SMNE 74.52	-0.40	0.09	0.03	0.11	0.93	0.66	1.10	0.54	0.00	-	4.91
SMNE 72.51	-1.30	0.11	0.07	0.37	1.50	1.01	5.38	1.01	1.71	-	3.73
SMNE 70.93	-0.88	0.09	0.04	0.06	1.14	0.68	0.49	0.41	0.00	-	4.14
SMNE 55.43	-0.64	0.10	0.05	0.10	1.23	0.69	0.09	0.75	0.00	-	5.02
SMNE 52.49	-0.60	0.13	0.05	0.56	8.35	1.67	4.84	0.66	1.56	-	4.21
SMNE 50.62	-0.06	0.10	0.06	0.15	0.81	0.91	1.74	0.37	0.00	-	4.98
SMNE 46.70	-0.40	0.09	0.09	0.79	0.85	0.87	5.05	0.33	0.00	-	3.62
SMNE 44.14	-0.80	0.14	0.08	0.33	2.01	0.95	3.43	0.78	0.15	-	4.24
SMNE 39.30	-0.50	0.14	0.05	0.15	1.01	0.93	1.06	0.17	0.00	-	4.69
SMNE 36.97	-0.70	0.17	0.06	0.23	1.34	0.86	0.80	0.40	0.00	-	4.53
SMNE 35.12	-0.40	0.20	0.04	0.18	1.80	1.15	3.14	0.48	1.64	-	4.08
SMNE 30.20	-0.50	0.16	0.07	0.30	0.95	1.01	3.46	0.53	0.21	-	4.51
SMNE 25.79	-0.10	0.17	0.04	0.25	1.33	0.83	1.31	0.36	0.00	-	4.31
SMNE 24.44	0.10	0.19	0.07	0.11	0.93	0.92	0.60	0.45	0.00	-	4.34
SMNE 16.60	0.30	0.22	0.01	0.18	1.25	0.92	3.22	0.53	1.55	-	4.34
SMNE 15.30	1.20	0.16	0.03	1.24	5.68	2.02	3.77	0.43	0.00	-	3.56
SMNE 12.78	0.80	0.21	0.01	0.29	2.67	1.00	2.06	0.24	0.13	-	4.06
SMNE 8.90	1.65	0.15	0.03	0.36	1.55	0.82	0.97	0.46	0.00	-	4.40
SMNE 4.46	1.72	0.16	0.04	0.60	2.87	0.98	4.43	0.75	1.94	-	3.90
SMNE 2.45	0.40	0.16	0.08	0.56	6.30	2.15	2.72	0.63	0.38	-	3.77
SMNE 0.86	0.70	0.16	0.01	0.44	3.86	1.34	0.52	0.34	0.00	-	3.67

Diagenetic control	0.44	0.11	0.01	0.00	0.27	0.93	0.00	0.03	0.00	-	6.35
BCT 78.78	0.23	0.16	0.06	0.17	3.89	1.50	0.57	0.17	0.00	-	3.50
BCT 78.54	-0.40	0.13	0.05	0.43	14.98	2.94	4.71	1.08	1.65	-	3.96
BCT 78.15	-1.05	0.13	0.07	0.21	4.77	1.37	0.33	0.58	0.00	-	4.47
BCT 76.76	0.11	0.13	0.06	0.34	13.04	3.14	2.07	0.23	0.20	-	4.31
BCT 75.33	-0.49	0.15	0.03	0.48	1.63	0.82	4.74	0.78	0.00	-	4.04
BCT 71.76	-0.37	0.15	0.04	0.12	4.22	1.17	3.85	0.64	1.55	-	4.11
BCT 67.65	-0.43	0.13	0.05	0.11	2.07	1.03	2.62	0.34	0.29	-	4.89
BCT 64.65	-0.66	-	-	-	-	-	-	-	-	-	-
BCT 63.95	-0.61	0.16	0.04	0.17	5.20	1.61	1.70	0.30	0.00	-	4.12
BCT 46.20	-0.46	0.14	0.07	0.10	0.89	0.86	0.60	0.18	0.20	-	4.50
BCT 45.94	-0.32	0.13	0.11	0.20	1.52	1.11	3.34	0.43	1.88	-	3.87
BCT 45.80	-	0.16	0.08	0.08	1.45	0.90	1.06	0.24	0.23	-	4.12
BCT 5.80	-0.65	-	-	-	-	-	-	-	-	-	-
BCT 5.56	-0.56	0.17	0.24	0.24	0.68	1.78	5.33	0.37	0.63	-	5.30
BCT 1.16	-1.34	0.08	0.15	0.02	0.26	0.83	1.10	0.81	1.15	-	4.26
BCT 1.13	-1.33	0.15	0.24	0.06	0.59	1.34	6.57	0.48	8.36	-	4.64
Average	-0.37	0.02	0.02	0.03	0.05	0.13	1.02	0.05	1.28	-	0.24
SD	0.07	0.12	0.08	0.31	3.11	1.31	2.69	0.51	0.66	-	3.95

Table B2: Geochemical data for Mongolia samples. Orange shaded boxes excluded. See methods for unit notation. Carbon isotopes in VPDB.

Mongolia Samples											
Locality (m)	$\delta^{13}\text{C}$ ‰	X _{Sr} %	X _{Mn} %	X _{Na+Al} %	X _{Mg} %	X _{Fe} %	X _{Th} ppm	X _U ppm	X _{Mo} ppm	X _V ppm	Ca+Mg %
SGL 0	2.91	0.003	0.001	0.4	2.46	0.72	0.487	0.59	-	0.29	15.4
SGL 5	3.89	0.001	0.000	0.4	0.87	0.34	0.729	0.09	-	0.06	14.6
SGL 10	4.18	0.001	0.000	0.1	1.39	0.25	0.241	0.20	-	0.05	16.6
SGL 15	3.95	0.002	0.000	0.1	1.33	0.30	0.000	0.21	-	0.04	16.0
SGL 20	5.30	0.001	0.000	0.1	3.21	0.27	0.000	0.35	-	0.07	16.3
SGL 25	4.88	0.001	0.000	0.3	0.92	0.29	0.224	0.15	-	0.16	16.4
SGL 29.2	3.41	0.002	0.000	0.2	0.45	0.31	0.000	0.46	-	0.14	13.6
SGU 0	-0.86	0.002	0.000	0.3	1.00	0.69	0.480	0.72	-	2.78	14.7
SGU 5	-1.52	0.002	0.001	0.2	1.98	0.30	0.630	0.83	-	2.58	21.1
SGU 10	-1.57	0.002	0.001	0.8	1.19	0.54	2.689	0.95	-	8.07	16.5
SGU 15	-1.10	0.002	0.002	0.3	5.10	0.35	0.140	0.63	-	2.82	18.1
SGU 20	-1.36	0.002	0.001	0.0	0.24	0.45	0.000	0.68	-	0.08	14.7
SGU 25	-0.60	0.007	0.001	0.1	1.17	0.51	0.000	3.91	-	2.17	16.8
SGU 30	-0.60	0.002	0.001	1.6	0.46	1.56	10.10	0.94	-	17.58	11.3
SGU 35	-1.78	0.006	0.002	0.1	1.07	0.30	0.000	2.50	-	0.19	16.2
SGU 40	-1.33	0.005	0.002	0.3	11.51	0.47	0.102	2.57	-	2.47	18.6
SGU 45	-1.69	0.005	0.002	0.2	2.17	0.31	0.000	2.11	-	2.99	17.1
SGU 50	-1.24	0.002	0.010	0.1	0.52	0.29	0.000	0.68	-	0.09	15.3
SGU 55	-0.06	0.003	0.006	0.2	0.44	0.79	0.000	0.67	-	3.18	15.9
SGU 60	-1.71	0.003	0.002	0.1	0.81	0.29	0.000	1.83	-	3.10	17.5
SGU 65	-0.47	0.002	0.003	0.4	0.61	0.42	0.275	0.46	-	5.72	18.1
SGU 70	-0.74	0.002	0.017	0.6	0.60	0.51	1.459	12.64	-	11.17	17.6
SGU 75	-0.48	0.003	0.003	0.1	1.22	0.63	0.000	1.20	-	3.25	16.5
SGU 80	0.01	0.002	0.005	0.1	0.55	0.45	0.000	0.19	-	0.25	18.4
SGU 85	-0.39	0.002	0.003	0.3	0.49	0.64	0.192	0.35	-	4.34	18.2
SGU 90	-0.64	0.001	0.003	0.1	0.43	0.27	0.000	0.97	-	0.29	17.3
SGU 95	-0.45	0.003	0.004	0.2	5.41	0.47	0.000	0.69	-	0.33	16.2
SGU 100	0.13	0.002	0.006	0.2	0.52	0.58	0.245	0.30	-	1.84	17.2
SGU 105	0.12	0.004	0.003	0.1	1.70	0.69	0.000	0.81	-	0.03	13.7
SGU 110	0.25	0.002	0.002	0.6	1.67	0.70	1.638	0.55	-	7.54	15.5
SGU 115	0.13	0.002	0.002	0.1	0.28	0.44	0.000	0.57	-	0.29	15.2
SGU 120	0.73	0.003	0.003	0.2	2.26	0.58	0.000	0.96	-	3.49	15.6
SGU 125	0.38	0.004	0.003	0.1	4.74	0.63	0.000	1.12	-	4.83	11.9
SGU 130	0.82	-	-	-	-	-	-	-	-	-	-
ZAC 0	-0.85	-	-	-	-	-	-	-	-	-	-

ZAC 5	-0.73	-	-	-	-	-	-	-	-	-	-
ZAC 10	-0.97	-	-	-	-	-	-	-	-	-	-
ZAC 15	-1.85	0.003	0.001	0.7	3.89	0.78	2.580	1.30	-	13.84	20.7
ZAC 20	-1.27	0.001	0.000	0.8	3.24	0.58	2.370	0.38	-	8.06	17.6
ZAC 30	-0.81	0.005	0.000	0.4	2.50	0.46	0.204	5.94	-	4.90	24.6
ZAC 35	-1.39	0.002	0.004	1.3	1.92	0.94	1.399	0.78	-	13.33	14.0
ZAC 40	-1.40	0.003	0.002	1.6	1.88	1.24	10.28	3.26	-	24.61	14.7
ZAC 45	-0.60	0.020	0.000	0.1	4.52	0.48	0.008	4.10	-	2.52	19.6
ZAC 50	-0.95	0.003	0.003	0.8	1.28	0.71	0.573	1.06	-	7.77	14.8
ZAC 55	-1.20	0.003	0.004	0.5	2.22	0.36	0.589	0.49	-	4.51	16.3
ZAC 60	-1.05	0.003	0.001	0.2	1.12	0.24	0.000	0.45	-	3.89	14.8
ZAC 65	-0.95	0.002	0.001	0.2	1.04	0.23	0.000	0.30	-	1.95	16.0
ZAC 70	-1.20	0.002	0.001	0.8	1.55	0.46	2.453	0.97	-	10.03	13.1
ZAC 72.5	-	0.003	0.001	0.7	1.59	0.65	1.411	2.10	-	14.73	15.1
ZAC 75	-1.15	0.002	0.001	0.8	1.37	0.43	2.433	0.59	-	5.95	16.8
ZAC 80	-0.75	0.002	0.001	0.3	1.40	0.28	0.056	2.77	-	5.99	17.7
ZAC 85	-1.35	0.002	0.001	0.4	1.08	0.31	0.487	0.32	-	3.28	15.7
ZAC 90	-1.05	0.002	0.001	1.4	0.89	0.67	4.990	1.36	-	17.00	10.5
ZAC 95	-1.25	0.002	0.001	0.9	4.79	0.71	3.203	0.85	-	7.40	14.6
ZAC 100	-1.20	0.002	0.001	1.1	1.37	0.52	2.911	1.06	-	10.88	11.7
ZAC 105	-1.15	0.001	0.000	0.5	1.11	0.39	1.895	0.40	-	4.36	18.3
ZAC 110	-1.20	0.003	0.003	0.8	2.19	0.43	2.026	3.76	-	14.61	14.4
ZAC 115	-1.25	0.002	0.002	0.3	1.28	0.23	0.676	0.83	-	5.23	18.3
ZAC 120	-1.25	0.003	0.002	1.1	2.13	0.47	3.122	1.52	-	11.27	13.9
ZAC 125	-1.15	0.002	0.003	1.2	1.19	0.47	5.188	0.70	-	10.91	13.1
ZAC 130	-0.65	0.001	0.002	0.4	1.31	0.19	0.073	1.97	-	7.60	15.9
ZAC 135	-1.15	0.002	0.002	0.7	1.22	0.47	0.896	1.19	-	6.88	13.7
ZAC 140	-1.45	0.002	0.001	1.9	2.47	0.89	5.190	1.37	-	25.31	11.5
ZAC 145	-1.15	0.001	0.002	0.6	1.10	0.34	1.331	0.38	-	6.01	17.9
ZAC 150	-1.20	0.002	0.002	0.5	1.45	0.25	1.055	0.98	-	5.26	15.6
ZAC 155	-1.05	0.002	0.004	1.7	2.10	0.59	8.043	1.45	-	16.80	12.5
ZAC 160	-1.30	0.001	0.001	0.3	1.75	0.35	0.726	0.46	-	2.84	16.3
ZAC 165	-0.90	0.002	0.001	1.3	2.08	0.53	5.201	1.12	-	11.32	16.0
ZAC 170	-1.45	0.002	0.001	1.0	1.75	0.58	1.236	1.36	-	10.32	16.4
Average	-0.38	0.003	0.002	0.49	2.07	0.48	1.34	1.34	-	5.63	18.28
SD	1.63	0.002	0.002	0.45	2.10	0.24	2.23	1.89	-	5.66	9.95

Table B3: Geochemical data for Clayton Ridge samples. See methods for unit notation. Carbon isotopes in VPDB. ICP-MS trace element data coming in a future study.

Clayton Ridge Samples	
Locality (m)	$\delta^{13}\text{C}$ ‰
EH 0	-0.45
EH 2	-0.65
EH 4	-0.67
EH 8	-0.32
EH 10	-1.15
EH 12	-1.10
EH 14	-0.97
EH 16	0.05
EH 18	-0.84
EH 22	-0.26
EH 24	0.17
EH 26	-0.41
EH 28	-0.23
EH 30	0.07
EH 32	-0.51
EH 34	-0.12
EH-2 0	1.29
EH-2 2	0.43
EH-2 4	0.21

EH-2 6	-0.33
WH 0	0.26
WH 2	-0.53
WH 4	-0.41
WH 6	-0.27
WH 8	-0.71
WH 10	-0.73
WH 13	-0.28
WH 24	-0.58
WH 26	-0.63
WH 28	-1.10
WH 30	-0.84
WH 32	-0.97
WH 34	-0.79
WH 36	-0.53
WH 38	0.02
WH 40	-0.35
WH 42	-0.51
WH 44	-0.47
WH 46	-0.43
WH 48	-0.74
WH 50	-0.60
WH 52	-0.07
WH 54	-0.31
WH 56	0.27
WH 58	0.15
WH 60	-0.06
WH 62	0.02
WH 64	-0.02
WH 66	-0.30
Average	-0.35
SD	0.46

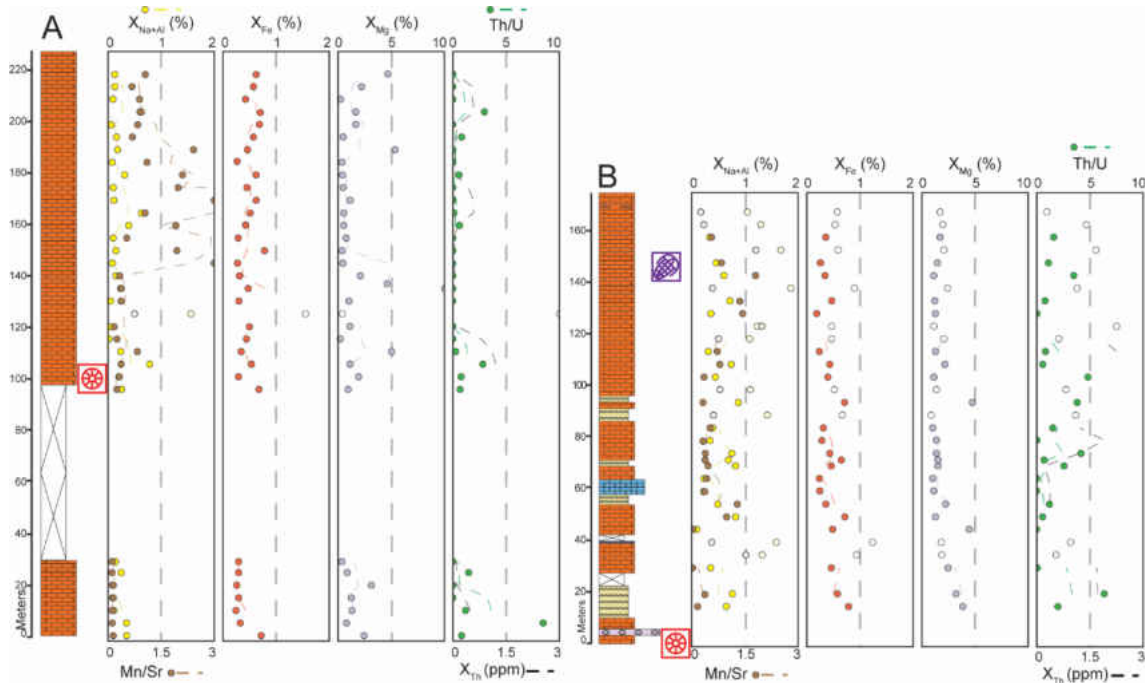


Figure B1: Additional trace element data from Salaa Gorge and Zuun-Arts Ridge. From left to right lithology, Na+Al and Mn/Sr, Fe, Mg, Th and Th/U with three point moving averages trend lines. White circles denote samples with $> 1\%$ Na+Al. Zuun-Arts Ridges had on average more terrestrial input. Fe concentrations were stable and samples were below dolomite concentrations (which is 50%) of Mg suggesting minimal diagenetic alteration. Red and purple symbols denote first occurrences of archaeocyaths and reef-dwelling fauna respectively.

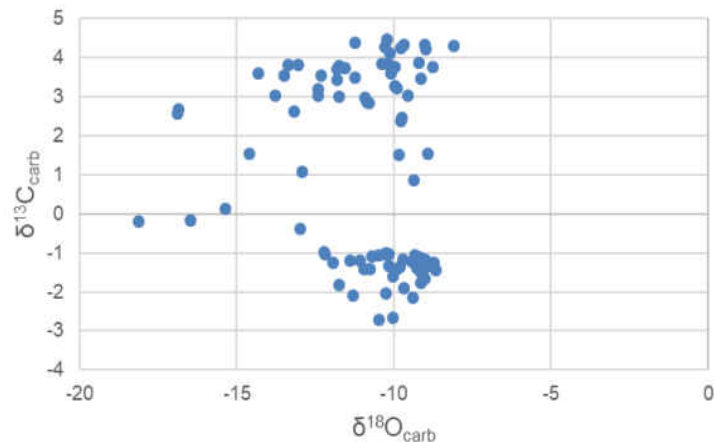


Figure B2: Carbon and oxygen isotope cross plot for Salaa Gorge. Data from Smith *et al.*, 2016. No strong covariation (Pearson's $r = -0.18$).

Appendix C: Functional characters and literature survey data

Functional Characters

The White-Inyo data used 12 characters to define the ecological roles of organisms in ancient reef environments. The characters are listed in bold with a brief description of why each is included. Character states are in italics with an explanation for how to code for each character. In some instances, an organism may fall into more than one state and was coded as the state in which the organism spends the majority of its time. Colonial organisms were coded based on colony characteristics. Based on Novack-Gottshall (2007) and Dineen *et al.* (2014).

1. Substrate Composition - Describes what type of surfaces an organism can live on and whether it can build (encrust) on other organisms. *Biotic* describes organisms that can attach to any living or dead material produced by other organisms. *Lithic* describes organisms that predominantly attach to inorganic surfaces. *Either* describes organisms that show no or equal preferences. (0) Biotic; (1) Lithic; (2) Either

2. Substrate Attachment - Organisms can have a solid connection to their substrate or move around their environment freely. *Attached* organism will have holdfasts or other attachment apparatus to keep them stationary in their environments. *Free-living* organism do not attach to substrate at any time in their adult forms. (0) Attached; (1) Free-living

3. Substrate Microhabitat - Organisms can stratify themselves to utilize a greater proportion of their environment. As a result, they either disturb the sediment or retard water flow in their immediate environment. *Erect* means that the organism extends their body or appendages into the water column a significant distance. *Epifaunal* means the organism remains within the benthic environment and does not extend into the water column. *Infaunal* describes organisms that burrow into their substrate. *Pelagic* organisms live within the water column. (0) Erect; (1) Epifaunal; (2) Infaunal; (3) Pelagic

4. Sediment Consolidation Ability - Organisms that cause sediment to collect or form around them will be more likely to produce the large topographic relief necessary for reef formation. This can occur by the organism producing sticky material that glues together sediment, buildup of material from dead skeletons, or by baffling moving seawater to cause sediment to deposit in the area. *High* consolidating organisms produce large amounts of topographic relief. *Low* consolidating organisms do not produce large relief. (0) High; (1) Low

5. Mobility - Organisms that move around their habitats will affect a greater area within their ecosystem compared to those that cannot move. *Sessile* organisms cannot move in their adult stage. *Vagile* organism can move throughout their lifecycle. (0) Sessile; (1) Vagile

6. Condition of Food - This character refers to the form of an organism's food, regardless of how this food is collected and processed. Organisms that collect the same type of food may be in competition with one another. *Incorporeal* organisms are able to produce food within their own bodies by combining the needed chemical molecules. *Particle* refers to organisms that eat indiscriminate organic material. *Bulk* refers to organisms that eat all or part of macroscopic organisms. (0) Incorporeal; (1) Particle; (2) Bulk

7. Feeding Habit - Describes how an organism collects and manipulates food. *Ambient* feeders collect raw inorganic material needed to produce their own food sources internally. *Filter* feeders select and pick out organic material from the water column. *Deposit* feeders sift through loose sediment to select out organic or decaying material. *Mass* feeders gather resources by either consuming portions of, or attaching to, other organisms. (0) Ambient; (1) Filter; (2) Deposit; (3) Mass

8. Diet - Organisms can breakdown food via different metabolic pathways and consume food of different nutritional value. *Autotrophs* produce their resources by photosynthesis. *Microbivores* consume microscopic organisms. *Carnivores* consume food as predators. (0) Autotroph; (1) Microbivore; (2) Carnivore

9. Feeding Energetics - Organisms expend large amounts of energy while collecting food. Organisms that expend less energy can therefore devote more energy reserves to reproduction and defensive traits. *Passive absorption* organisms absorb their resources without any external macroscopic appendages moving. Often this is done through cellular membranes. *Passive entrainment* describes organisms that allow water to flow through their bodies and internally separate fluid from their desired resource. *Active entrainment* describes organisms that extend appendages (lophophores, mucus, tentacles) into the water column to collect their food. *Active searching* denotes organisms that expend large amounts of time searching for and hunting prey. (0) Passive absorption; (1) Passive entrainment; (2) Active entrainment; (3) Active searching

10. Rigidity - Some organisms are more effective as attachment sites for encrusting organisms and provide more structure to a reef framework. *Rigid, non-permeable* organisms are completely incapable of bending or flexing. *Rigid, permeable* organisms do not flex or bend, but do allow water to pass through their bodies. *Flexible* organisms can bend in response to increases in energy level. (0) Rigid and non-permeable; (1) Rigid and permeable; (2) Flexible

11. Wave Resistance - Reefs experience constant disturbance from wave energy and certain organisms may provide shelter for other organisms. *High stress* organisms can attach to substrate securely or have large hypercalcifying skeletons that resist breakage. *Intermediate stress* organisms have hard skeletons, however, they tend to break in shallow

water high energy environments. These organisms are often found in between normal and storm wave base. *Low stress* organisms can easily break or be destroyed by waves and live below storm wave base, in burrows or in secluded cavities. (0) High stress; (1) Intermediate stress; (2) Low stress

12. Size - Organisms with a greater biovolume can often be of greater functional importance to and define the processes occurring within an ecosystem. *Large* organisms are greater than 10 cm³. *Small* organisms are between 1 and 10 cm³. *Microscopic* organisms are smaller than 1 cm³. (0) Large; (1) Small; (2) Microscopic

Table C1: Coding for ecological characters for functional analysis of White-Inyo data. Ch. 1 - character 1

Taxa	Ch.1	Ch.2	Ch.3	Ch.4	Ch.5	Ch.6	Ch.7	Ch.8	Ch.9	Ch.10	Ch.11	Ch.12
<i>Harklessia</i>	2	0	1	0	0	2	3	2	2	0	0	0
Echinoderms	1	0	0	0	0	1	1	1	2	2	2	1
Trilobites	1	1	1	1	1	1	2	1	3	0	2	1
<i>Renalcis</i>	2	0	1	0	0	0	0	0	0	2	0	2
Lingulid	1	1	2	1	1	1	1	1	2	0	2	1
Archaeo. gen. 1	2	0	1	0	0	1	1	1	1	1	1	1
Archaeo. gen. 2	2	0	1	0	0	1	1	1	1	1	1	1
Archaeo. gen. 3	2	0	1	0	0	1	1	1	1	1	1	1
Archaeo. gen. 4	2	0	1	0	0	1	1	1	1	1	1	1

Table C2: Functional groups for literature survey. Functional groups labelled as F1-F14 with representative taxa listed in first row. A (?) used to denote dubious or unknown classification.

		Namacalathus, Corumbella	Sinotubulites, Cloudina	Hyoilithelminthida (polychaeta)	Chancelloriids	Hyoiliths, Bivalves, Mollusc?	Trilobite	Plumetazoans	Brachiopods, Stenothecoids	Ostracodes	Gastropods	Bryozoa	Cephalopods	Namapoikia	Rugosa
		F1	F2	F3	F4	F5	F6	F7	F8	F9	F10	F11	F12	F13	F14
Substrate Composition	Biotic	X	X	X			X	X	X					X	X
	Lithic					X									
Substrate Relationship	Attached	X			X			X						X	X
	Free-living		X	X		X	X		X						
Substrate Microhabitat	Erect	X			X			X							
	Epifaunal		X			X	X				X			X	
Sediment Consolidator	Infaunal			X					X						
	Pelagic									X			X		
Mobility	High							X						X	X
	Low	X	X	X	X	X	X		X						
Condition of Food	Sessile	X	X		X	X		X						X	X
	Vagile			X			X		X						
Feeding Habit	Incoporeal									X					
	Particle	X	X	X	X	X	X	X	X	X	X	X	X	X	X
Diet	Bulk														
	Ambient Feeder														
Feeding Energetics	Filter Feeder	X	?		?	X		X	X					X	X
	Deposit Feeder			X			X								
Rigidity	Mass Feeder														
	Autotroph	X			X	X		X		X	X	X	X	X	X
Wave Resistance	Microbivore	X	?	X	X	X	X	X	X	X	X	X	X	X	X
	Carnivore													?	?
Size	Passive Absorption														
	Passive Entrainment		?		?										
Wave Resistance	Active Entrainment	X				X		X	X					X	X
	Active Searching			X			X		X		X		X	X	X
Size	Rigid, nonpermeable			X		X	X		X		X		X	X	X
	Rigid, permeable				X										
Size	Flexible	X	?					X							
	High Stress													X	X
Size	Intermediate Stress														
	Low Stress	X	X	X	X	X	X	X	X	X	X	X	X	X	X
Size	Large, > 10cm													X	X
	Small, 1-10 cm	X		X	X	X	X	X	X		X				
	Micro, <1cm		X							X					

References for functional group classification

- Bengtson, S., and D. Collins. 2015. Chancelloriids of the Cambrian Burgess Shale. *Palaeontologia Electronica* **18**: 1-67.
- Chen, Z., S. Bengtson, C. M. Zhou, H. Hua, and Z. Yue. 2008. Tube structure and original composition of *Sinotubulites*: shelly fossils from the late Neoproterozoic in southern Shaanxi, China. *Lethaia* **41**: 37-45.
- Elicki, O., and G. L. Pillola. 2004. Cambrian microfauna and palaeoecology of the Campo Pisano Formation at Gutturu Pala (Iglesiente, SW Sardinia, Italy). *Bolletino della Società Paleontologica Italiana* **43**: 383-401.
- Forancelli Pacheco, M. L. A., D. Galante, F. Rodrigues, J. D. M. Leme, P. Bidola, W. Hagadorn, M. Stockmar, J. Herzen, I. D. Rudnitzki, F. Pfeiffer, and A. C. Marques. 2015. Insights into the skeletonization, lifestyles, and affinity of the unusual Ediacaran fossil *Corumbella*. *PloS One* **10**: e0114219.
- Mehra, A., and Maloof, A. 2018. Multiscale approach reveals that *Cloudina* aggregates are detritus and not in situ reef constructions. *Proceedings of the National Academy of Science* **115**: E2519-E2527.
- Moysiuk, J., M. R. Smith, and J-B. Caron. 2017. Hyololiths are Palaeozoic lophophorates. *Nature* **541**: 394-397.
- Smith, E. F., Macdonald, F. A., Petach, T. A., Bold, U., and Schrag, D. P. 2016 Integrated stratigraphic, geochemical, and paleontological late Ediacaran to early Cambrian records from southwestern Mongolia. *GSA Bulletin* **128**: 442-468.
- Wood, R. A. 2011. Paleoecology of the earliest skeletal metazoan communities: implications for early biomineralization. *Earth-Science Reviews* **106**: 184-190.
- Wood, R. A., J. P. Grotzinger, and J. A. D. Dickson. 2002. Proterozoic modular biomineralized metazoan from the Nama Group, Namibia. *Science* **296**: 2383-2386.

Table C3: Dataset for literature survey. Justification column includes brief reasoning for classification of reef-dwelling organisms as rare, frequent, or abundant. TS - thin section; PC - point count

Ediacaran					<5 % (rare, sparse)	6 - 50% (occasional, common, frequent)	>50 % (abundant, dominant, dense)					
Author	Year	Region	Formation	Regional Stage	Rare Orgs	Frequent	Abundant	SSF or Macroalgae	Framework Builders	Trace Fossils	Method	Justification
Hong <i>et al</i>	2007	China	Dengying Fm	Nama	Sinotubulites, Cloudina				Thrombolite	horizontal traces	outcrop	dense, but very small
Penny <i>et al</i>	2014	Namibia	Nama Group	Nama	Namacalathus, Namapoikia, Cloudina				Thrombolite	horizontal traces	outcrop	"entrapped skeletons"
Amthor <i>et al</i>	2003	Oman	Ara Group	Nama	Namacalathus, Cloudina				Thrombolite	none reported	outcrop, core	percent data
Warren <i>et al</i>	2017	Paraguay	Itapucumi Group	Nama	Namacalathus, Corumbella, Cloudina				Thrombolite	Archaeonassa	outcrop	"fragmentary carapaces"
Hofmann and Mountjoy	2001	Canada	Miette Group	Nama	Namacalathus	Cloudina			Thrombolite	horizontal traces	outcrop	contained coquina
Early Cambrian					<5 % (rare, sparse)	6 - 50% (occasional, common, frequent)	>50 % (abundant, dominant, dense)					
Author	Year	Region	Formation	Regional Stage	Rare Orgs	Frequent	Abundant		Framework Builders	Trace Fossils	Method	Justification
Kruse <i>et al</i>	1995	Russia	Pestrotsvet Fm	Tommotian	Hyalolithelminths, Chancelloriids, Molluscs	Hyaloliths		Sachitids, Halkieriids, Tommotiids, Coleolids, Anabaritiids	Thrombolite, Archaeocyaths, Coralomorphs	burrows	outcrop	"volumetrically minor"
Creveling <i>et al</i>	2013	Spain	Pedroche Fm	Atdabanian	Brachiopod, Trilobite, Chancelloriids (?)			SSF	Thrombolite, Archaeocyaths	none reported	outcrop and PC	low PC
Kruse <i>et al</i>	1996	Mongolia	Salaangol Fm	Atdabanian	Molluscs, Stenothecoids	Hyaloliths, Chancelloriids		Coleolids	Thrombolite, Archaeocyaths, Coralomorphs, Radiocyaths	micro-burrows	outcrop and TS	abundance table
This study	2018	Mongolia	Salaagol Fm	Atdabanian	Trilobite, Hyaloliths			SSF	Thrombolite, Archaeocyaths, Coralomorphs, Radiocyaths	none reported		
Álvaro <i>et al</i>	2006	Morocco	Amouslek Fm	Atdabanian	Trilobites, Chancelloriids, Hyalolithelminths, Hyaloliths			Torelleniids, Tannuolitiids	Thrombolite, Archaeocyaths	lack of bioturbation	outcrop and TS	not discussed
James and Gravestock	1990	Australia	Upper Wilkawillina Fm	Atdabanian	Brachiopod, Trilobites, Chancelloriids, Echinoderms			Tannuolitiids	Thrombolite, Archaeocyaths, Spongimorphs	none reported	outcrop and TS	uncertain identity, some coquina
Hicks and Rowland	2009	China	Xiannudong Fm	Atdabanian	Brachiopods, Trilobites, Hyaloliths, Echinoderms	Chancelloriids			Thrombolite, Archaeocyaths	burrows	outcrop and PC	low PC, one thin layer of abundant chanc
Debrene <i>et al</i>	1989	Mexico	Puerto Blanco Fm	Botomian	Echinoderms, Hyaloliths, Brachiopods, Chancelloriids	Trilobites			Thrombolite, Archaeocyaths	Skolithos, horizontal traces	outcrop and TS	described trilobites as common
Cordie <i>et al</i>	in prep	California/Nevada	Poleta Fm	Botomian	Brachiopod, Trilobites, Echinoderms				Thrombolite, Archaeocyaths, Coralomorphs	Skolithos	outcrop and PC	low PC
Read	1980	Canada	correlated to Sekwi Fm	Botomian	Trilobites, Echinoderms, Brachiopods	Hyaloliths			Thrombolite, Archaeocyaths	horizontal burrows	outcrop and TS	"fragments", "sporadic" hyaloliths

											abundant in some lenses
Rees <i>et al</i>	1989	Antarctica	Shackleton Limestone	Botomian	Echinoderms	Trilobite		Thrombolite, Archaeocyaths	bioturbated mottled limestone	outcrop and TS	"fragments" in reef, more elsewhere
McMena <i>min et al</i>	2000	Virginia	Shady Dolomite Fm	Botomian	Trilobites, Echinoderms			Salterella, Thrombolite, Archaeocyaths	Autophycus	outcrop and TS	Sporadic lenses for Salterella, scattered echinoderm ossicles
Pillola <i>et al</i>	1998	Sardinia	Santa Barbara Fm	Botomian	Trilobites, Brachiopods	Hyaloliths, Echinoderms		Thrombolite, Archaeocyaths	"other trace fossils"	outcrop	"well-represented" hyaloliths, "abundant echinoderms"
Debre <i>nn et al</i>	2002	France	Pardailhan Fm	Botomian	Chancellorriids, Trilobites, Echinoderms, Hyaloliths, Bivalves, Brachiopods			Thrombolite, Archaeocyaths	none reported	outcrop and TS	"small fragments"
Pruss <i>et al</i>	2012	Newfoundland	Forteau Fm	Botomian	Trilobite, Brachiopod, Hyaloliths	Echinoderm		Salterella, Thrombolite, Archaeocyaths	none reported	outcrop and PC	low PC
Perejón <i>et al</i>	2012	N. Spain	Láncara Fm	Toyonian	Echinoderms, Brachiopods, Trilobites, Hyaloliths			Thrombolite, Archaeocyaths	burrows	Outcrop and TS	Listed as >5%
Kruse <i>et al</i>	1991	Australia	Wirrealpa Fm	Toyonian	Brachiopods, Chancellorriids, Trilobites, Hyaloliths, Molluscs, Echinoderms			Thrombolite, Archaeocyaths, Radiocyaths	burrows	outcrop and TS	fragments
Adachi <i>et al</i>	2013	South China	Tianheban Fm	Toyonian	Hyaloliths, Chancellorriids	Trilobite, Brachiopods, Echinoderms		Thrombolite, Archaeocyaths	none reported	outcrop and TS	"...are common"
Late Cambrian					<5% (rare, sparse)	6 - 50% (occasionally, common, frequent)	>50% (abundant, dominant, dense)				
Author	Year	Region	Formation	Regional Stage	Rare Orgs	Frequent	Abundant	Framework Builders	Trace Fossils	Method	Justification
Kruse and Reitner	2014	Australia	Tindall Lm	Stage 4-Stage 5	Trilobites, Hyaloliths, Brachiopods, Bivalves	No indication of abundance		Spiculate Sponges, Thrombolite	burrows	outcrop and TS	no indication, but "diverse fauna"
Lee <i>et al</i>	2016	Inner Mongolia	Kushanian Fm	Stage 5	Trilobites			Thrombolite	burrows	outcrop and TS	fragments
Hong <i>et al</i>	2012	Korea	Daegi Fm	Drumian	Trilobite, Echinoderms			Non-Rigid Siliceous Sponges	burrows	outcrop and TS	fragments
Kruse and Zhuravlev	2008	Iran	Mila Fm	Guzhangian-Paibian	Trilobites, Hyaloliths	Echinoderms, Brachiopods		Lithistids, Thrombolite	ichnofossils	outcrop and TS	"rich in..."
Shapiro and Rigby	2004	USA	Bonanza King Fm	Paibian	Trilobites, Brachiopods, Echinoderms			Lithistids, Stromatolite	burrows	outcrop	fragmented, "moderately diverse"
Chen <i>et al</i>	2014	North China	Chaomidian Fm	Jiangshanian	Cephalopods, Gastropods, Trilobites, Brachiopods			Thrombolite	burrows	outcrop and TS	fragments
Ordovician					<5% (rare, sparse)	6 - 50% (occasionally, common, frequent)	>50% (abundant, dominant, dense)				
Author	Year	Region	Formation	Regional Stage	Rare Orgs	Frequent	Abundant	Framework Builders	Trace Fossils	Method	Justification

Carrera <i>et al</i>	2017	Argentina	La Silla Fm	Tremadocian	Trilobites, Cephalopods	Gastropods		macroalgae	Coralomorph, Thrombolite	Thalassinoides	TS	mostly "scattered fragments", but some "abundant in situ gastropods"
Li <i>et al</i>	2004	South China	Xiazhen and Sanjushan Fms	Tremadocian-Floian	Cephalopods, Echinoderms, Trilobites	Brachiopods, Bryozoa, Rugosa		macroalgae	Tabulates, Bryozoa and Lithistid sponges	none reported	outcrop	numerous species of frequent types
Adachi <i>et al</i>	2013	South China	Fenhsiang and Hunghuayuan Fms	Tremadocian-Floian	Gastropods	Brachiopods, Cephalopods, Trilobite	Echinoderms, Bryozoa		Anthaspidellids, Calathium, Stromatoporoids	none reported	outcrop and TS	Pelmetazoans fragments "commonly found throughout"; non-encrusting bryozoans "dominate d"
Pruss <i>et al</i>	2010	Utah	Pogonip Group	Tremadocian-Floian	Gastropods, Bivalves, Ostracods	Brachiopod, Echinoderms, Trilobites		macroalgae	Lithistid sponges?	none reported	TS and PC	PC data
Choh <i>et al</i>	2013	Korea	Dumugol Fm	Floian	Trilobites, Echinoderms, Brachiopods, Cephalopods, Gastropods, Ostracods				Lithistids, Stromatolites	burrows	outcrop and TS	all described as minor
Pratt	1989	Canada	Laval Fm	Darriwilian ?	Ostracods, Trilobites, Gastropods, Bivalves	Brachiopods, Bryozoans	Echinoderms		Bryozoa, Tabulates, and Lithistids	none reported	outcrop and TS	dominated, but as bioclastics
Alberstadt	1974	Tennessee	Carters Limestone	Darriwilian ?	Cephalopods, Gastropods, Ostracods, Trilobites, Brachiopods	Bryozoa, Echinoderms			Stromatoporoids and Tabulates	none reported	outcrop and TS	large amount of bioclastics
Zhang <i>et al</i>	2014	North China	Lianglitaog Fm	Katian	Bryozoa, Brachiopods, Trilobites, Bivalves, Ostracods	Gastropods, Echinoderms			Calathium and Stromatolites	none reported	outcrop and TS	table 2, abundance chart
Kroger <i>et al</i>	2017	Estonia	Vasalemma Fm	Katian	Brachiopods, Ostracods, Trilobite, Rugose		Echinoderms, Bryozoa		Tabulates, Bryozoa, Receptaculites	heavy bioturbated	core and TS	low diversity mud mounds, but echinoderms and bryozoan framestone (bryozoan both encrusting and dwelling)
Harland	1981	Norway	Bunes Member	Katian	Trilobites, Bryozoans, Ostracods, Brachiopods, Gastropods	Echinoderms, Cephalopods, Rugose			Corals, Stromatoporoids	none reported	outcrop	table of abundances
Antoshkina	1999	Russia	Malaya Fm	Hirnantian	Bryozoa, Gastropods, Echinoderms, Rugosa				Tabulates	none reported	outcrop	"low diversity buildup"

Appendix D: Morphological data

Table D1: Archaeocyath continuous morphology measurements. All from field samples in Lida Valley, Nevada. All measurements in millimeters. OBR - osculum: body ratio; Aj - Ajacicyathida; Ar - Archaeocyathida

Taxonomy	Geologic Formation	Body Size	Osculum Size	OBR
Aj	Harkless	30.0	14.5	0.5
Aj	Harkless	15.0	4.5	0.3
Aj	Harkless	58.0	52.5	0.9
Aj	Harkless	15.0	3.5	0.2
Aj	Harkless	25.0	12.0	0.5
Aj	Harkless	8.5	4.0	0.5
Aj	Harkless	18.5	8.0	0.4
Aj	Harkless	7.5	3.5	0.5
Aj	Harkless	74.0	59.5	0.8
Aj	Harkless	14.0	7.0	0.5
Aj	Harkless	12.5	5.0	0.4
Aj	Harkless	28.0	13.0	0.5
Aj	Harkless	11.5	5.0	0.4
Aj	Harkless	12.0	7.5	0.6
Aj	Harkless	13.5	7.0	0.5
Aj	Harkless	17.5	7.5	0.4
Aj	Harkless	22.0	12.5	0.6
Aj	Harkless	27.0	16.5	0.6
Aj	Harkless	39.0	23.5	0.6
Aj	Harkless	23.0	15.5	0.7
Aj	Harkless	11.0	7.5	0.7
Aj	Harkless	5.0	4.0	0.8
Aj	Harkless	10.5	5.5	0.5
Aj	Harkless	18.5	10.0	0.5
Aj	Harkless	4.0	2.0	0.5
Aj	Harkless	8.5	5.0	0.6
Aj	Harkless	50.5	44.5	0.9
Aj	Harkless	10.0	7.0	0.7
Aj	Harkless	24.0	19.0	0.8
Aj	Harkless	10.0	5.5	0.6
Aj	Harkless	19.0	9.5	0.5
Aj	Harkless	10.5	4.0	0.4
Aj	Harkless	30.5	21.0	0.7
Aj	Harkless	14.0	7.5	0.5
Aj	Harkless	15.0	7.0	0.5
Aj	Harkless	12.5	7.0	0.6
Aj	Harkless	25.0	17.0	0.7
Aj	Harkless	26.0	16.5	0.6
Aj	Harkless	28.5	17.5	0.6
Aj	Harkless	8.0	5.0	0.6
Aj	Harkless	16.0	7.5	0.5
Aj	Harkless	17.5	6.5	0.4
Aj	Harkless	22.5	11.0	0.5
Aj	Harkless	17.0	8.0	0.5
Aj	Harkless	3.0	2.0	0.7
Aj	Harkless	14.0	9.0	0.6
Aj	Harkless	5.5	3.5	0.6
Aj	Harkless	16.0	9.0	0.6
Aj	Harkless	20.0	16.5	0.8
Aj	Harkless	37.5	29.5	0.8

Aj	Harkless	20.5	16.0	0.8
Aj	Harkless	11.0	5.0	0.5
Aj	Harkless	27.0	17.0	0.6
Aj	Harkless	28.0	23.0	0.8
Aj	Harkless	7.0	4.0	0.6
Aj	Harkless	32.5	16.0	0.5
Aj	Harkless	19.0	9.5	0.5
Aj	Harkless	13.0	8.0	0.6
Aj	Harkless	40.0	32.0	0.8
Aj	Harkless	40.0	22.0	0.6
Aj	Harkless	44.0	38.5	0.9
Aj	Harkless	15.0	7.5	0.5
Aj	Harkless	7.0	4.0	0.6
Aj	Harkless	34.0	22.5	0.7
Aj	Harkless	15.0	8.5	0.6
Aj	Harkless	15.5	8.0	0.5
Aj	Harkless	19.0	9.0	0.5
Aj	Harkless	24.5	19.5	0.8
Aj	Harkless	20.0	7.5	0.4
Aj	Harkless	24.5	11.0	0.4
Aj	Harkless	13.5	5.0	0.4
Aj	Harkless	20.5	11.5	0.6
Aj	Harkless	8.0	4.5	0.6
Aj	Harkless	17.0	12.0	0.7
Aj	Harkless	13.0	4.5	0.3
Aj	Harkless	15.0	12.0	0.8
Aj	Harkless	19.0	12.0	0.6
Aj	Harkless	22.5	12.5	0.6
Aj	Harkless	17.5	14.5	0.8
Aj	Harkless	11.0	10.0	0.9
Aj	Harkless	14.0	8.0	0.6
Aj	Harkless	9.5	4.5	0.5
Aj	Harkless	10.0	6.0	0.6
Aj	Harkless	5.5	4.0	0.7
Aj	Harkless	28.0	23.0	0.8
Aj	Harkless	14.0	8.0	0.6
Aj	Harkless	15.5	9.0	0.6
Aj	Harkless	13.0	7.5	0.6
Aj	Harkless	25.5	13.5	0.5
Aj	Harkless	12.0	3.5	0.3
Aj	Harkless	5.0	4.0	0.8
Aj	Harkless	21.5	9.5	0.4
Aj	Harkless	14.0	6.0	0.4
Aj	Harkless	12.0	5.5	0.5
Aj	Harkless	7.5	2.0	0.3
Aj	Harkless	7.5	3.0	0.4
Aj	Harkless	12.0	5.5	0.5
Aj	Harkless	6.0	4.0	0.7
Aj	Harkless	10.5	4.0	0.4
Aj	Harkless	10.0	5.0	0.5
Aj	Harkless	18.0	12.0	0.7
Aj	Harkless	12.5	6.0	0.5
Aj	Harkless	31.0	19.0	0.6
Aj	Harkless	22.0	13.5	0.6
Aj	Harkless	7.5	4.5	0.6
Aj	Harkless	11.0	7.0	0.6
Aj	Harkless	7.0	3.0	0.4
Aj	Harkless	21.5	9.5	0.4
Aj	Harkless	20.0	11.0	0.6
Aj	Harkless	15.0	10.0	0.7
Aj	Harkless	5.5	2.0	0.4
Aj	Poleta	10.5	2.5	0.2
Aj	Poleta	5.0	3.0	0.6

Aj	Poleta	11.5	4.0	0.3
Aj	Poleta	11.0	6.0	0.5
Aj	Poleta	7.0	4.0	0.6
Aj	Poleta	9.0	1.0	0.1
Aj	Poleta	9.0	1.5	0.2
Aj	Poleta	11.0	4.5	0.4
Aj	Poleta	6.0	2.5	0.4
Aj	Poleta	7.5	3.5	0.5
Aj	Poleta	5.5	2.5	0.5
Aj	Poleta	7.0	1.0	0.1
Aj	Poleta	6.0	2.5	0.4
Aj	Poleta	5.5	2.5	0.5
Aj	Poleta	3.5	2.5	0.7
Aj	Poleta	5.0	1.5	0.3
Aj	Poleta	7.0	2.5	0.4
Aj	Poleta	14.0	8.0	0.6
Aj	Poleta	7.5	2.0	0.3
Aj	Poleta	28.5	16.5	0.6
Aj	Poleta	6.0	3.0	0.5
Aj	Poleta	2.5	1.5	0.6
Aj	Poleta	8.0	3.5	0.4
Aj	Poleta	11.0	7.0	0.6
Aj	Poleta	4.0	1.5	0.4
Aj	Poleta	7.5	1.5	0.2
Aj	Poleta	4.0	2.0	0.5
Aj	Poleta	3.5	2.5	0.7
Aj	Poleta	4.5	2.5	0.6
Aj	Poleta	2.5	2.0	0.8
Aj	Poleta	8.5	4.0	0.5
Aj	Poleta	2.5	1.0	0.4
Aj	Poleta	7.0	2.5	0.4
Aj	Poleta	4.0	2.0	0.5
Aj	Poleta	5.0	3.5	0.7
Aj	Poleta	20.5	12.5	0.6
Aj	Poleta	6.5	3.5	0.5
Aj	Poleta	5.0	1.5	0.3
Aj	Poleta	3.0	1.0	0.3
Aj	Poleta	7.0	2.0	0.3
Aj	Poleta	4.0	1.0	0.3
Aj	Poleta	7.5	3.0	0.4
Aj	Poleta	4.0	2.0	0.5
Aj	Poleta	5.0	2.0	0.4
Aj	Poleta	12.0	4.5	0.4
Aj	Poleta	4.5	2.0	0.4
Aj	Poleta	4.5	3.5	0.8
Aj	Poleta	7.0	2.0	0.3
Aj	Poleta	10.5	3.0	0.3
Aj	Poleta	2.5	1.0	0.4
Aj	Poleta	4.0	2.5	0.6
Aj	Poleta	3.5	1.5	0.4
Aj	Poleta	7.0	3.5	0.5
Aj	Poleta	6.0	3.0	0.5
Aj	Poleta	6.0	2.0	0.3
Aj	Poleta	4.0	1.0	0.3
Aj	Poleta	5.0	4.0	0.8
Aj	Poleta	4.0	1.0	0.3
Aj	Poleta	3.5	1.0	0.3
Aj	Poleta	8.5	4.0	0.5
Aj	Poleta	6.0	2.0	0.3
Aj	Poleta	4.0	1.0	0.3
Aj	Poleta	10.5	5.0	0.5
Aj	Poleta	3.0	1.5	0.5
Aj	Poleta	8.0	4.5	0.6

Aj	Poleta	8.5	2.5	0.3
Aj	Poleta	4.5	2.0	0.4
Aj	Poleta	10.0	4.5	0.5
Aj	Poleta	13.0	7.0	0.5
Aj	Poleta	8.0	3.0	0.4
Aj	Poleta	12.0	5.0	0.4
Aj	Poleta	4.0	2.0	0.5
Aj	Poleta	8.5	2.5	0.3
Aj	Poleta	2.5	1.0	0.4
Ar	Harkless	13.0	4.5	0.3
Ar	Harkless	11.0		
Ar	Harkless	7.0	3.0	0.4
Ar	Harkless	13.5	4.0	0.3
Ar	Harkless	33.5	13.0	0.4
Ar	Harkless	20.0	8.0	0.4
Ar	Harkless	7.0	2.0	0.3
Ar	Harkless	32.0	20.5	0.6
Ar	Harkless	15.0	8.5	0.6
Ar	Harkless	12.0	4.0	0.3
Ar	Harkless	19.5	8.0	0.4
Ar	Harkless	15.0	6.0	0.4
Ar	Harkless	12.0	3.5	0.3
Ar	Harkless	12.0	6.0	0.5
Ar	Harkless	19.5	8.5	0.4
Ar	Harkless	19.5	9.0	0.5
Ar	Harkless	9.0	4.5	0.5
Ar	Harkless	7.0	3.5	0.5
Ar	Harkless	5.0	2.0	0.4
Ar	Harkless	11.0	3.0	0.3
Ar	Harkless	7.0	2.0	0.3
Ar	Harkless	10.5	4.5	0.4
Ar	Harkless	10.0	4.5	0.5
Ar	Harkless	12.0		
Ar	Harkless	11.5	3.5	0.3
Ar	Harkless	20.5	8.5	0.4
Ar	Harkless	10.5	6.0	0.6
Ar	Harkless	9.5	4.5	0.5
Ar	Harkless	14.5	10.0	0.7
Ar	Harkless	18.5	9.0	0.5
Ar	Harkless	9.0	3.5	0.4
Ar	Harkless	7.5	3.5	0.5
Ar	Harkless	13.0	5.0	0.4
Ar	Harkless	11.5	7.0	0.6
Ar	Harkless	8.5	5.0	0.6
Ar	Harkless	15.0	6.5	0.4
Ar	Harkless	3.0	1.0	0.3
Ar	Harkless	12.5	6.5	0.5
Ar	Harkless	6.0	4.0	0.7
Ar	Harkless	8.0	2.0	0.3
Ar	Harkless	17.0	8.5	0.5
Ar	Harkless	10.0	3.0	0.3
Ar	Harkless	28.5	13.5	0.5
Ar	Harkless	10.0	6.0	0.6
Ar	Harkless	13.5	5.0	0.4
Ar	Harkless	10.0	4.0	0.4
Ar	Harkless	10.0		
Ar	Harkless	17.5	5.0	0.3
Ar	Harkless	21.0	7.5	0.4
Ar	Harkless	19.0	3.0	0.2
Ar	Harkless	7.5	3.5	0.5
Ar	Harkless	13.5	4.0	0.3
Ar	Harkless	7.5	3.5	0.5
Ar	Harkless	35.0	18.5	0.5

Ar	Harkless	12.0	4.0	0.3
Ar	Harkless	5.0	2.0	0.4
Ar	Harkless	31.0	10.0	0.3
Ar	Harkless	20.0	10.5	0.5
Ar	Harkless	29.0	7.5	0.3
Ar	Harkless	10.0	4.0	0.4
Ar	Harkless	7.5	3.5	0.5
Ar	Harkless	37.0	19.5	0.5
Ar	Harkless	42.0	17.0	0.4
Ar	Harkless	10.0	2.0	0.2
Ar	Harkless	18.0	9.0	0.5
Ar	Harkless	16.0	5.0	0.3
Ar	Harkless	17.0	3.5	0.2
Ar	Harkless	13.0	5.5	0.4
Ar	Harkless	22.5	7.0	0.3
Ar	Harkless	13.0	4.5	0.3
Ar	Harkless	10.0	4.0	0.4
Ar	Harkless	8.0	4.0	0.5
Ar	Harkless	14.0	4.0	0.3
Ar	Harkless	5.0	1.0	0.2
Ar	Harkless	17.5	10.0	0.6
Ar	Harkless	21.0	10.5	0.5
Ar	Harkless	16.0	9.0	0.6
Ar	Harkless	16.5	5.0	0.3
Ar	Harkless	15.0	4.0	0.3
Ar	Harkless	9.0	3.5	0.4
Ar	Harkless	15.0	6.0	0.4
Ar	Harkless	12.0	5.0	0.4
Ar	Harkless	5.0	2.0	0.4
Ar	Harkless	22.5	9.5	0.4
Ar	Harkless	13.0	7.0	0.5
Ar	Harkless	12.0	4.0	0.3
Ar	Harkless	23.0	10.5	0.5
Ar	Harkless	10.5	4.5	0.4
Ar	Harkless	6.0	3.5	0.6
Ar	Harkless	12.0	2.0	0.2
Ar	Harkless	6.0	2.0	0.3
Ar	Harkless	23.5	9.5	0.4
Ar	Harkless	8.0	2.0	0.3
Ar	Harkless	19.5	7.5	0.4
Ar	Harkless	7.0	3.5	0.5
Ar	Harkless	8.0	4.5	0.6
Ar	Harkless	9.5	4.5	0.5
Ar	Harkless	7.5	3.5	0.5
Ar	Harkless	9.5	4.5	0.5
Ar	Harkless	9.0	4.0	0.4
Ar	Harkless	15.0	6.0	0.4
Ar	Harkless	9.5	4.5	0.5
Ar	Harkless	13.5	5.0	0.4
Ar	Harkless	16.5	8.0	0.5
Ar	Harkless	27.0	12.0	0.4
Ar	Harkless	15.0	5.0	0.3
Ar	Harkless	10.0	5.0	0.5
Ar	Harkless	17.0	7.5	0.4
Ar	Harkless	10.5	4.0	0.4
Ar	Harkless	6.5	2.0	0.3
Ar	Harkless	13.0	5.0	0.4
Ar	Harkless	23.5	10.0	0.4
Ar	Harkless	17.0	5.5	0.3
Ar	Harkless	9.0	4.0	0.4
Ar	Harkless	10.0	3.0	0.3
Ar	Harkless	9.5	3.0	0.3
Ar	Harkless	15.0	5.0	0.3

Ar	Harkless	18.0	5.5	0.3
Ar	Harkless	14.0	5.0	0.4
Ar	Harkless	19.5	4.5	0.2
Ar	Harkless	8.0	3.0	0.4
Ar	Harkless	15.0	5.0	0.3
Ar	Harkless	7.5	1.5	0.2
Ar	Harkless	19.5	10.0	0.5
Ar	Harkless	33.0	10.5	0.3
Ar	Harkless	9.0	4.5	0.5
Ar	Harkless	8.0	3.5	0.4
Ar	Harkless	20.5	9.0	0.4
Ar	Harkless	20.0	7.0	0.4
Ar	Harkless	10.0	2.0	0.2
Ar	Harkless	5.5	3.0	0.5
Ar	Harkless	7.5	4.0	0.5
Ar	Harkless	20.5	5.0	0.2
Ar	Harkless	19.0	10.0	0.5
Ar	Harkless	6.5	3.5	0.5
Ar	Harkless	17.5	11.5	0.7
Ar	Harkless	13.0	4.5	0.3
Ar	Harkless	6.0	2.0	0.3
Ar	Harkless	6.0	1.0	0.2
Ar	Harkless	11.0	4.0	0.4
Ar	Harkless	20.5	10.0	0.5
Ar	Harkless	7.0	3.0	0.4
Ar	Harkless	6.0	2.0	0.3
Ar	Harkless	10.0	3.0	0.3
Ar	Poleta	8.5		
Ar	Poleta	14.5	5.5	0.4
Ar	Poleta	7.0		
Ar	Poleta	12.0	5.0	0.4
Ar	Poleta	8.5		
Ar	Poleta	12.5	4.5	0.4
Ar	Poleta	14.0	4.0	0.3
Ar	Poleta	10.0	3.5	0.4
Ar	Poleta	11.5	5.5	0.5
Ar	Poleta	7.0	2.0	0.3
Ar	Poleta	12.5		
Ar	Poleta	9.5	2.5	0.3
Ar	Poleta	10.5		
Ar	Poleta	11.5		
Ar	Poleta	10.5	3.0	0.3
Ar	Poleta	8.0	1.0	0.1
Ar	Poleta	12.0	5.0	0.4
Ar	Poleta	9.5		
Ar	Poleta	14.5	4.5	0.3
Ar	Poleta	8.0	3.0	0.4
Ar	Poleta	6.0	4.0	0.7
Ar	Poleta	11.5	3.0	0.3
Ar	Poleta	14.0	5.5	0.4
Ar	Poleta	10.0	1.0	0.1
Ar	Poleta	10.5		
Ar	Poleta	9.5		
Ar	Poleta	7.5	1.5	0.2
Ar	Poleta	12.5	4.0	0.3
Ar	Poleta	12.5	2.5	0.2
Ar	Poleta	4.0	2.0	0.5
Ar	Poleta	12.5		
Ar	Poleta	9.0	3.0	0.3
Ar	Poleta	9.0	3.0	0.3
Ar	Poleta	7.0	1.5	0.2
Ar	Poleta	5.0	1.5	0.3
Ar	Poleta	11.0	3.0	0.3

Ar	Poleta	10.0	5.0	0.5
Ar	Poleta	17.0	6.0	0.4
Ar	Poleta	16.0	11.0	0.7
Ar	Poleta	17.0	7.5	0.4
Ar	Poleta	15.5	3.5	0.2
Ar	Poleta	14.0	5.5	0.4
Ar	Poleta	12.5	7.0	0.6
Ar	Poleta	7.5	2.5	0.3
Ar	Poleta	7.0	4.0	0.6
Ar	Poleta	7.0	2.0	0.3
Ar	Poleta	17.0	5.5	0.3
Ar	Poleta	13.0	4.5	0.3
Ar	Poleta	12.5	5.5	0.4
Ar	Poleta	8.5	1.5	0.2
Ar	Poleta	12.0	6.0	0.5
Ar	Poleta	15.5		
Ar	Poleta	5.0	2.0	0.4
Ar	Poleta	14.5	4.5	0.3
Ar	Poleta	5.5	1.5	0.3
Ar	Poleta	12.0	4.0	0.3
Ar	Poleta	10.0	2.5	0.3
Ar	Poleta	10.5	2.5	0.2
Ar	Poleta	12.5	5.5	0.4
Ar	Poleta	5.5	3.5	0.6
Ar	Poleta	12.0	3.5	0.3
Ar	Poleta	8.0	2.0	0.3
Ar	Poleta	9.0	3.5	0.4
Ar	Poleta	8.0	2.5	0.3
Ar	Poleta	15.5	6.0	0.4
Ar	Poleta	10.0	2.5	0.3
Ar	Poleta	10.5	4.5	0.4
Ar	Poleta	6.5		
Ar	Poleta	10.0	2.5	0.3
Ar	Poleta	13.0	3.5	0.3
Ar	Poleta	10.0	2.0	0.2
Ar	Poleta	12.0	2.5	0.2
Ar	Poleta	14.0	4.0	0.3
Ar	Poleta	10.5	4.0	0.4
Ar	Poleta	10.5	3.0	0.3
Ar	Poleta	13.0	4.5	0.3
Ar	Poleta	18.5	7.0	0.4
Ar	Poleta	8.0	3.5	0.4
Ar	Poleta	15.0	7.0	0.5
Ar	Poleta	14.0	2.5	0.2
Ar	Poleta	11.5	4.0	0.3
Ar	Poleta	5.5	2.0	0.4
Ar	Poleta	12.5	6.5	0.5
Ar	Poleta	9.5	2.0	0.2
Ar	Poleta	4.0	1.5	0.4
Ar	Poleta	8.5	3.0	0.4
Ar	Poleta	9.0		
Ar	Poleta	10.0	3.0	0.3
Ar	Poleta	6.0	1.5	0.3
Ar	Poleta	6.0		
Ar	Poleta	7.0	1.0	0.1
Ar	Poleta	7.0	3.0	0.4
Ar	Poleta	9.0	1.5	0.2
Ar	Poleta	7.5	2.0	0.3
Ar	Poleta	17.5	5.0	0.3
Ar	Poleta	8.0	3.0	0.4
Ar	Poleta	6.0	2.0	0.3
Ar	Poleta	13.0	5.0	0.4
Ar	Poleta	6.5	2.0	0.3

Ar	Poleta	12.5	4.5	0.4
Ar	Poleta	16.5	5.0	0.3
Ar	Poleta	8.0	2.0	0.3
Ar	Poleta	7.5	2.5	0.3
Ar	Poleta	10.5	3.5	0.3
Ar	Poleta	9.0	2.0	0.2
Ar	Poleta	10.5	3.5	0.3
Ar	Poleta	4.5	1.0	0.2
Ar	Poleta	9.5		
Ar	Poleta	10.0	2.0	0.2
Ar	Poleta	11.0	4.5	0.4
Ar	Poleta	12.5	3.5	0.3
Ar	Poleta	10.0	4.0	0.4
Ar	Poleta	11.0	4.5	0.4
Ar	Poleta	7.5	4.0	0.5
Ar	Poleta	12.0	4.0	0.3
Ar	Poleta	8.0	4.0	0.5
Ar	Poleta	4.5	1.0	0.2
Ar	Poleta	7.5	2.5	0.3
Ar	Poleta	6.0	3.5	0.6
Ar	Poleta	4.5	3.0	0.7
Ar	Poleta	14.5	4.5	0.3
Ar	Poleta	7.0	3.5	0.5
Ar	Poleta	11.5	3.0	0.3
Ar	Poleta	3.5	2.5	0.7
Ar	Poleta	7.0	1.5	0.2
Ar	Poleta	9.5	4.5	0.5
Ar	Poleta	6.5	2.0	0.3
Ar	Poleta	7.0	4.5	0.6
Ar	Poleta	9.5	4.5	0.5
Ar	Poleta	9.0	3.5	0.4
Ar	Poleta	5.0	2.0	0.4
Ar	Poleta	7.0	3.0	0.4
Ar	Poleta	5.5	2.0	0.4
Ar	Poleta	6.5	2.5	0.4
Ar	Poleta	4.5	2.0	0.4
Ar	Poleta	12.0	3.0	0.3
Ar	Poleta	5.0	3.0	0.6
Ar	Poleta	7.5	3.0	0.4
Ar	Poleta	4.0	2.5	0.6
Ar	Poleta	5.0	2.0	0.4
Ar	Poleta	9.0	3.0	0.3
Ar	Poleta	5.0	1.5	0.3
Ar	Poleta	9.0	3.0	0.3
Ar	Poleta	5.0	2.0	0.4
Ar	Poleta	4.5	1.0	0.2
Ar	Poleta	9.5	3.5	0.4
Ar	Poleta	9.5	4.0	0.4
Ar	Poleta	9.5	5.5	0.6
Ar	Poleta	6.0	3.0	0.5

Table D2: Archaeocyath continuous morphology measurements. All from University of Alaska, Fairbanks Museum of the North (UAMES). All measurements in millimeters. OBR - osculum: body ratio; Aj - Ajacicyathida; Ar - Archaeocyathida; Al - Alaska; W. US - western USA; JR - Jones Ridge; AA - Adams Argillite; HL - Hillard Limestone

Specimen #	Taxonomy	Regional Locality	Geologic Formation	Body Size	Osculum Size	OBR	Loculi Width	Intervallum Area %	Sepal Thickness
A-1678	~	Al	~	4.38	2.85	0.65	0.41	0.42	0.18
A-1680	~	Al	JR	13.90	4.61	0.33		0.11	

A-1680	~	Al	JR	2.32	1.14	0.49	0.40	0.24	0.13
A-1680	~	Al	JR	2.90	1.55	0.54		0.29	
A-1680	~	Al	JR	12.23	4.17	0.34	0.57	0.12	0.23
A-1680	~	Al	JR	5.85	2.13	0.36	0.50	0.13	0.25
A-1680	~	Al	JR	16.97	8.89	0.52	0.63	0.27	0.31
A-1680	~	Al	JR	3.03	0.57	0.19	0.32	0.03	0.09
A-21-W-1-e	~	Al	AA	5.75	2.98	0.52	0.56	0.27	0.20
A-289-A-3-C	~	Al	~	3.20	1.10	0.34	0.41	0.12	0.12
A-289-A-3-C	~	Al	~	19.58	9.79	0.50	0.35	0.25	0.21
A-289-A-3-C	~	Al	~	18.05	2.57	0.14	0.61	0.02	0.31
12692	~	Al	AA	9.13	2.66	0.29	0.44	0.08	0.21
12692	~	Al	AA	14.93	4.00	0.27	0.48	0.07	0.12
12692	~	Al	AA	31.00	15.47	0.50	1.18	0.25	0.44
12692	~	Al	AA	3.80	1.83	0.48	0.60	0.23	0.21
12692	~	Al	AA	27.66	20.37	0.74	1.00	0.54	0.53
12692	~	Al	AA	6.06	3.47	0.57	0.81	0.33	0.41
12692	~	Al	AA	17.46	8.01	0.46	0.95	0.21	0.26
12291	~	Al	JR	1.90	0.64	0.34	0.44	0.11	0.40
12291	~	Al	JR	8.42	1.84	0.22	0.61	0.05	0.15
12294	~	Al	JR	1.17	0.57	0.49	0.67	0.24	0.17
12294	~	Al	JR	11.26	2.90	0.26	0.46	0.07	0.27
12294	~	Al	JR	1.86	0.47	0.25	0.54	0.06	0.27
12295	~	Al	JR	14.06	6.46	0.46		0.21	
12295	~	Al	JR	12.07	4.03	0.33	0.50	0.11	0.10
12295	~	Al	JR	11.45	4.58	0.40		0.16	
12296	~	Al	JR	6.13	3.67	0.60	0.37	0.36	0.14
12296	~	Al	JR	3.89	2.39	0.61	0.20	0.38	0.09
12296	~	Al	JR	1.66	0.74	0.45	0.39	0.20	0.20
12302	~	Al	JR	5.36	2.22	0.41	0.64	0.17	0.15
12431	~	Al	JR	7.03	2.51	0.36	0.40	0.13	0.16
12432	~	Al	JR	6.15	1.91	0.31	0.45	0.10	0.13
12433	~	Al	JR	6.89	1.86	0.27	0.40	0.07	0.10
12434	~	Al	JR	3.90	2.16	0.55	0.45	0.31	0.24
12434	~	Al	JR	2.25	0.96	0.43	0.55	0.18	0.29
12434	~	Al	JR	2.99	1.27	0.42	0.52	0.18	0.17
12434	~	Al	JR	2.32	0.95	0.41	0.60	0.17	0.30
12436	~	Al	JR	6.46	2.17	0.34	0.36	0.11	0.11
12436	~	Al	JR	5.75	1.89	0.33	0.45	0.11	0.16
12436	~	Al	JR	7.89	2.49	0.32	0.29	0.10	0.12
12436	~	Al	JR	9.11	1.69	0.19	0.39	0.03	0.15
12438	~	Al	JR	5.82	2.35	0.40	0.54	0.16	0.25
12439	~	Al	JR	8.64	4.22	0.49	0.48	0.24	0.32
12441	~	Al	JR	4.26	2.74	0.64	0.47	0.41	0.19
12443	~	Al	JR	6.38	1.78	0.28	0.39	0.08	0.15
12443	~	Al	JR	5.10	1.23	0.24	0.21	0.06	0.09
12443	~	Al	JR	4.03	1.06	0.26	0.38	0.07	0.13
12443	~	Al	JR	2.13	0.90	0.42	0.41	0.18	0.10
12443	~	Al	JR	3.63	1.11	0.30	0.44	0.09	0.31
12445	~	Al	JR	6.55	1.33	0.20	0.46	0.04	0.20
12446	~	Al	JR	6.83	2.57	0.38	0.48	0.14	0.31
12446	~	Al	JR	5.47	1.44	0.26	0.37	0.07	0.20
12446	~	Al	JR	4.13	1.47	0.35	0.41	0.13	0.19
12446	~	Al	JR	3.52	1.08	0.31	0.39	0.09	0.11
12447	~	Al	JR	12.85	6.80	0.53	0.31	0.28	0.08
12447	~	Al	JR	3.87	1.84	0.47	0.29	0.23	0.18
12447	~	Al	JR	3.80	1.40	0.37	0.32	0.13	0.11
12448	~	Al	JR	15.76	7.27	0.46	0.54	0.21	0.29
12464	~	Al	AA	5.96	3.04	0.51	0.45	0.26	0.15
12469	~	Al	AA	8.01	3.29	0.41		0.17	
12470	~	Al	AA	6.24	2.95	0.47	0.30	0.22	0.19
12470	~	Al	AA	4.76	1.83	0.38	0.19	0.15	0.11
12471	~	Al	AA	25.12	12.07	0.48	1.08	0.23	0.45
12472	~	Al	AA	7.08	1.95	0.28	0.56	0.08	0.28

12480	~	Al	AA	9.50	1.54	0.16	0.56	0.03	0.22
12480	~	Al	AA	8.11	2.31	0.28	0.53	0.08	0.14
12480	~	Al	AA	6.07	2.30	0.38	0.32	0.14	
12480	~	Al	AA	5.54	1.29	0.23		0.05	
12480	~	Al	AA	5.59	1.61	0.29		0.08	0.21
12481	~	Al	AA	10.28	1.97	0.19	0.30	0.04	0.20
12485	~	Al	AA	9.18	2.77	0.30	0.41	0.09	0.10
12487	~	Al	AA	21.19	7.98	0.38	0.70	0.14	0.36
12549	~	Al	AA	11.83	6.06	0.51		0.26	
12556	~	Al	AA	14.59	6.92	0.47		0.22	
12557	~	Al	AA	9.78	2.99	0.31	0.79	0.09	0.21
12566	~	Al	AA	27.44	16.69	0.61	1.51	0.37	0.40
12665	~	Al	AA	9.63	4.09	0.42	0.42	0.18	0.11
12665	~	Al	AA	9.46	5.00	0.53	0.41	0.28	0.26
12665	~	Al	AA	9.05	4.75	0.52	0.62	0.28	0.26
12665	~	Al	AA	8.47	4.36	0.51	0.44	0.26	0.22
12670	~	Al	AA	15.69	5.31	0.34	0.79	0.11	0.32
12673	~	Al	AA	17.90	5.05	0.28	0.97	0.08	0.48
12674	~	Al	AA	23.56	5.18	0.22	0.83	0.05	0.22
12677	~	Al	AA	9.35	3.17	0.34	0.60	0.12	0.21
12678	~	Al	AA	24.16	8.56	0.35	0.67	0.13	0.37
12678	~	Al	AA	21.46	10.05	0.47	0.82	0.22	0.37
12681	~	Al	AA	13.32	6.68	0.50	0.63	0.25	0.37
12682	~	Al	AA	8.85	3.95	0.45	0.53	0.20	0.27
12683	~	Al	AA	15.90	4.58	0.29	0.60	0.08	0.29
12685	~	Al	AA	3.66	1.70	0.46	0.40	0.22	0.17
12687	~	Al	AA	13.96	7.98	0.57		0.33	
12689	~	Al	AA	29.01	13.29	0.46	0.79	0.21	0.34
12690	~	Al	AA	10.52	2.34	0.22	0.43	0.05	0.22
12695	~	Al	AA	12.15	4.89	0.40	0.73	0.16	0.23
12787	~	Al	AA	9.00	3.41	0.38		0.14	
12792	~	Al	AA	8.68	2.41	0.28	0.66	0.08	0.26
12792	~	Al	AA	8.44	3.61	0.43	0.67	0.18	0.20
12794	~	Al	AA	15.31	4.76	0.31	0.49	0.10	0.26
12814	~	Al	AA	20.69	10.03	0.48		0.24	
12816	~	Al	AA	28.69	15.64	0.54	0.63	0.30	0.32
12823	~	Al	AA	8.45	2.17	0.26	0.85	0.07	0.32
12824	~	Al	AA	51.40	39.91	0.78	0.85	0.60	0.50
12880	~	Al	AA	15.77	8.08	0.51	0.75	0.26	0.49
12887	~	Al	AA	9.13	4.35	0.48	0.68	0.23	0.28
12891	~	Al	AA	20.55	10.86	0.53	0.42	0.28	0.30
13044	~	Al	AA	8.77	4.31	0.49	0.75	0.24	0.39
13044	~	Al	AA	6.02	2.13	0.35	0.75	0.13	0.24
13142	~	Al	AA	6.19	1.68	0.27	0.95	0.07	0.40
13232	~	Al	AA	11.87	3.38	0.28	0.65	0.08	0.17
13232	~	Al	AA	16.40	4.96	0.30	0.63	0.09	0.43
13232	~	Al	AA	6.08	2.63	0.43	0.33	0.19	0.28
13237	~	Al	AA	10.36	5.57	0.54	0.81	0.29	0.34
25648	~	Al	AA	8.23	1.65	0.20	0.48	0.04	0.17
25648	~	Al	AA	7.69	4.04	0.53		0.28	
25651	~	Al	AA	12.15	6.51	0.54	0.96	0.29	0.34
25651	~	Al	AA	12.47	6.02	0.48	0.86	0.23	0.12
25651	~	Al	AA	19.39	11.61	0.60	1.11	0.36	0.24
25651	~	Al	AA	13.14	6.12	0.47	0.95	0.22	0.33
25651	~	Al	AA	17.21	8.01	0.47	0.72	0.22	0.31
25652	~	Al	AA	6.94	1.37	0.20	1.01	0.04	0.26
25655	~	Al	HL	5.74	2.05	0.36	0.42	0.13	0.16
25657	~	Al	HL	3.67	1.65	0.45	0.43	0.20	0.11
2992g	~	Al	AA	10.17	3.48	0.34	0.76	0.12	0.14
2995a	~	Al	AA	7.08	3.61	0.51	0.32	0.26	0.21
2996	~	Al	AA	11.77	4.68	0.40	0.57	0.16	0.17
2997g	~	Al	AA	16.98	13.76	0.81	0.82	0.66	0.43
2999a	~	Al	AA	8.32	4.33	0.52	0.62	0.27	0.29

3000b	~	Al	AA	32.08	17.76	0.55	0.46	0.31	0.23
3000g	~	Al	AA	9.39	5.48	0.58		0.34	
3002b	~	Al	AA	4.85	1.74	0.36	0.55	0.13	0.26
3003c	~	Al	AA	5.68	2.86	0.50	0.29	0.25	0.17
3004a	~	Al	HL	2.63	1.04	0.39	0.39	0.16	0.17
3005d	~	Al	HL	9.48	3.50	0.37	1.15	0.14	0.29
3011e	~	Al	JR	11.03	4.51	0.41		0.17	
3012b	~	Al	AA	1.86	0.49	0.26	0.42	0.07	0.16
3013a	~	Al	HL	1.89	0.47	0.25	0.28	0.06	0.15
3014e	~	Al	HL	30.70	22.62	0.74	0.78	0.54	0.31
3135	~	Al	HL	9.16	4.09	0.45	0.55	0.20	0.23
3138	~	Al	HL	6.88	4.66	0.68	0.41	0.46	0.07
3138	~	Al	HL	10.50	4.80	0.46	0.54	0.21	0.24
3140	~	Al	HL	11.36	8.02	0.71	0.48	0.50	0.26
3140	~	Al	HL	12.41	6.19	0.50	0.58	0.25	0.32
3148	~	Al	HL	14.45	13.14	0.91	0.45	0.83	0.27
3151	~	Al	HL	19.90	11.18	0.56	0.64	0.32	0.21
3155	~	Al	HL	24.51	18.52	0.76	0.80	0.57	0.41
3156	~	Al	HL	9.56	6.92	0.72	0.38	0.52	0.22
5971	~	Al	HL	10.68	5.69	0.53	0.69	0.28	0.29
5977	~	Al	HL	12.32	7.75	0.63	1.12	0.40	0.28
5980	~	Al	HL	5.99	2.70	0.45	0.48	0.20	0.21
5981	~	Al	HL	0.89	0.28	0.31		0.10	
5981	~	Al	HL	2.69	0.70	0.26	0.48	0.07	0.11
5982	~	Al	HL	14.14	2.59	0.18	0.71	0.03	0.36
5983	~	Al	HL	10.62	3.59	0.34	0.51	0.11	0.21
5983	~	Al	HL	6.00	1.25	0.21		0.04	
5996	~	Al	AA	4.47	0.83	0.19	0.30	0.03	0.18
6000	~	Al	AA	11.48	2.92	0.25	1.44	0.06	0.34
6072	~	Al	AA	33.34	22.61	0.68	1.54	0.46	0.73
6075	~	Al	AA	14.43	8.08	0.56	1.09	0.31	0.44
6079	~	Al	AA	11.20	3.95	0.35	1.21	0.12	0.38
6079	~	Al	AA	12.31	5.65	0.46	1.12	0.21	0.32
6080	~	Al	AA	18.66	7.36	0.39	1.21	0.16	0.51
6080	~	Al	AA	11.82	3.24	0.27	0.82	0.08	0.36
6080	~	Al	AA	14.31	5.12	0.36	0.94	0.13	0.37
6085	~	Al	AA	5.38	2.33	0.43		0.19	
6092	~	Al	AA	13.39	6.82	0.51	0.76	0.26	0.17
6092	~	Al	AA	8.31	2.15	0.26	0.50	0.07	0.21
6094	~	Al	AA	23.95	10.11	0.42		0.18	
6095	~	Al	AA	6.34	1.31	0.21	0.52	0.04	0.19
6098	~	Al	AA	27.09	11.79	0.44	0.96	0.19	0.45
6099	~	Al	AA	18.21	5.04	0.28	0.51	0.08	0.18
6099	~	Al	AA	17.67	8.08	0.46	0.99	0.21	0.38
6099	~	Al	AA	21.27	6.64	0.31	0.48	0.10	0.19
6100	~	Al	AA	6.30	2.84	0.45		0.20	
6105	~	Al	AA	3.05	1.56	0.51	0.29	0.26	0.18
42652	Ar	Australia	~	7.29	2.63	0.36	0.65	0.13	0.21
42652	Ar	Australia	~	7.44	3.70	0.50	0.93	0.25	0.20
42652	Ar	Australia	~	6.27	4.00	0.64	0.36	0.41	0.05
42652	Ar	Australia	~	3.15	1.15	0.36	0.44	0.13	0.17
42652	Ar	Australia	~	6.15	2.60	0.42	0.48	0.18	0.14
42652	Ar	Australia	~	6.46	2.63	0.41	0.53	0.17	0.15
42652	Ar	Australia	~	7.25	2.78	0.38	0.46	0.15	0.16
42652	Ar	Australia	~	9.96	4.74	0.48	0.48	0.23	0.25
42652	Ar	Australia	~	6.91	3.19	0.46	0.90	0.21	0.30
42652	Ar	Australia	~	13.64	7.68	0.56	0.54	0.32	0.21
42652	Ar	Australia	~	8.94	4.21	0.47	0.38	0.22	0.24
42652	Ar	Australia	~	20.09	17.00	0.85	0.87	0.72	0.38
42652	Ar	Australia	~	3.73	1.49	0.40	0.85	0.16	0.35
42652	Ar	Australia	~	2.91	1.37	0.47	0.60	0.22	0.17
42652	Ar	Australia	~	6.75	2.61	0.39	0.47	0.15	0.30
42652	Ar	Australia	~	6.58	3.93	0.60	0.91	0.36	0.32

42652	Ar	Australia	~	2.42	0.89	0.37	0.63	0.13	0.32
42652	Ar	Australia	~	13.51	9.14	0.68	0.77	0.46	0.55
42652	Ar	Australia	~	6.54	3.37	0.52	0.84	0.27	0.20
42652	Ar	Australia	~	7.73	4.84	0.63	0.78	0.39	0.44
42652	Ar	Australia	~	3.19	1.55	0.49	0.49	0.24	0.25
42652	Ar	Australia	~	16.40	12.46	0.76	0.93	0.58	0.31
42652	Ar	Australia	~	9.62	6.72	0.70	1.07	0.49	0.33
42653	~	Australia	~	11.84	7.98	0.67	0.66	0.45	0.18
42653	~	Australia	~	6.10	3.02	0.49	0.43	0.24	0.19
42653	~	Australia	~	4.41	2.13	0.48	0.67	0.23	0.37
42653	~	Australia	~	6.57	4.18	0.64	0.66	0.41	0.19
42653	Ar	Australia	~	6.16	3.01	0.49	0.95	0.24	0.28
42654	Ar	Australia	~	5.35	2.88	0.54	0.61	0.29	0.30
42654	Ar	Australia	~	4.09	1.64	0.40	0.87	0.16	0.42
42654	Ar	Australia	~	7.33	3.97	0.54	0.79	0.29	0.40
42654	Ar	Australia	~	4.57	2.32	0.51	0.52	0.26	0.29
42654	Ar	Australia	~	3.36	1.31	0.39	0.44	0.15	0.21
42654	Ar	Australia	~	17.93	10.83	0.60	1.08	0.36	0.37
42654	Ar	Australia	~	13.58	8.08	0.59	0.85	0.35	0.20
42654	Ar	Australia	~	10.94	6.99	0.64	0.78	0.41	0.31
42654	Ar	Australia	~	6.25	2.86	0.46	0.55	0.21	0.19
42654	Ar	Australia	~	5.92	2.05	0.35	0.40	0.12	0.12
42654	Ar	Australia	~	4.54	2.04	0.45	0.45	0.20	0.14
42654	Ar	Australia	~	7.30	1.99	0.27	0.48	0.07	0.16
42655	Ar	Australia	~	3.02	0.99	0.33	0.54	0.11	0.17
42655	Ar	Australia	~	16.20	7.55	0.47	0.89	0.22	0.17
42655	Ar	Australia	~	3.99	1.37	0.34	0.77	0.12	0.17
42655	Ar	Australia	~	4.26	1.79	0.42	0.26	0.18	0.09
C-1015651	Aj	Canada	~	18.28	9.32	0.51	1.74	0.26	0.30
C-1015654	~	Canada?	~	20.24	4.14	0.20	0.54	0.04	0.08
C-1015654	~	Canada?	~	4.50	2.36	0.53	0.35	0.28	0.13
AK-2335-P-1	~	Washington	Chewelah	7.18	3.24	0.45	0.43	0.20	0.19
AK-2335-P-1	~	Washington	Chewelah	5.73	2.32	0.40	0.44	0.16	0.18
AK-2335-P-1	~	Washington	Chewelah	7.63	1.73	0.23	0.42	0.05	0.25
AK-2655-P-1	Aj	W. US	Poleta	7.03	3.41	0.49	0.84	0.24	0.30

Table D3: Archaeocyath continuous morphology measurements. All from University of California Museum of Paleontology (UCMP). All measurements in millimeters. OBR - osculum: body ratio; Aj - Ajacicyathida; Ar - Archaeocyathida; Ca - Capsulocyathida; W. US - western USA

Specimen #	Taxonomy	Regional Locality	Geologic Formation	Body Size	Osculum Size	OBR	Loculi Width	Intervallum Area %	Septal Thickness
220777A	~	~	~	10.06	2.71	0.27	0.46	0.07	0.13
220777B	~	~	~	3.55	0.86	0.24	0.23	0.06	0.05
220777C	~	~	~	2.56	0.72	0.28	0.26	0.08	0.15
220835	~	Australia	~	17.18	7.72	0.45	1.36	0.20	0.23
220836A	~	Australia	~	12.84	6.79	0.53	0.56	0.28	0.08
220836B	~	Australia	~	10.33	5.08	0.49	0.61	0.24	0.18
220836C	~	Australia	~	23.99	20.80	0.87	0.47	0.75	0.26
220836D	~	Australia	~	3.19	1.23	0.39	0.75	0.15	0.20
220836E	~	Australia	~	20.97	8.54	0.41	0.78	0.17	0.20
220836F	~	Australia	~	6.20	3.63	0.59	0.68	0.34	0.24
220836G	~	Australia	~	3.99	1.59	0.40	1.00	0.16	0.26
220837A	~	Australia	~	11.80	7.41	0.63	0.65	0.39	0.25
220837B	~	Australia	~	5.23	1.90	0.36	0.75	0.13	0.16

220837C	~	Australia	~	19.69	12.57	0.64	1.19	0.41	0.46
220837D	~	Australia	~	10.31	3.34	0.32	0.78	0.10	0.14
220838A	~	Australia	Ajax	17.05	6.95	0.41	0.44	0.17	0.12
220838B	~	Australia	Ajax	3.98	2.27	0.57	0.57	0.33	0.37
220838C	~	Australia	Ajax	4.63	2.20	0.47	0.52	0.22	0.18
220838D	~	Australia	Ajax	11.30	3.16	0.28	1.74	0.08	0.43
220841A	~	Canada	Mural	10.47	5.44	0.52	0.64	0.27	0.13
220841B	~	Canada	Mural	11.63	3.53	0.30	0.82	0.09	0.26
220841C	~	Canada	Mural	7.65	2.94	0.38	0.60	0.15	0.18
220841D	~	Canada	Mural	12.81	7.94	0.62	0.86	0.38	0.19
220841E	~	Canada	Mural	12.38	6.48	0.52	0.62	0.27	0.23
220841F	~	Canada	Mural	9.59	2.95	0.31	0.47	0.09	0.20
220841G	~	Canada	Mural	13.46	4.58	0.34	0.49	0.12	0.23
220710	Aj	W. US	Harkless	34.33	19.97	0.58	0.56	0.34	0.53
220711	~	W. US	Harkless	13.77	7.36	0.53	0.59	0.29	0.37
220712	~	W. US	Harkless	12.55	4.53	0.36	1.00	0.13	0.48
220713	~	W. US	Harkless	19.55	12.04	0.62	0.74	0.38	0.47
220714	Aj	W. US	Harkless	31.11	15.60	0.50	1.39	0.25	0.64
220715	Aj	W. US	Poleta	11.36	7.20	0.63	0.51	0.40	0.24
220716	~	W. US	Harkless	12.35	6.91	0.56	0.36	0.31	0.33
220717	Ar	W. US	Harkless	45.09	19.25	0.43	1.31	0.18	0.56
220718	Aj	W. US	Harkless	15.86	9.76	0.62	0.73	0.38	0.31
220720	~	W. US	Poleta	16.03	4.67	0.29	0.40	0.08	0.10
220721	~	W. US	Poleta	10.16	2.43	0.24	0.37	0.06	0.28
220722	~	W. US	Poleta	4.97	1.65	0.33	0.22	0.11	0.10
220723	Aj	W. US	Poleta	10.25	7.08	0.69	0.35	0.48	0.10
220724	~	W. US	Poleta	9.17	3.80	0.41	0.36	0.17	0.18
220725	~	W. US	Poleta	3.78	1.14	0.30	0.82	0.09	0.11
220726	~	W. US	Poleta	7.56	3.43	0.45	0.82	0.21	0.19
220727	~	W. US	Poleta	5.81	2.12	0.36		0.13	
220728	Aj	W. US	Poleta	6.54	2.57	0.39	0.71	0.15	0.21
220729	~	W. US	Poleta	8.19	4.12	0.50	0.33	0.25	0.10
220730	~	W. US	Poleta	23.96	8.76	0.37	1.14	0.13	0.25
220731	Ar	W. US	Poleta	13.56	2.64	0.19	0.69	0.04	0.21
220732	~	W. US	Poleta	11.92	5.05	0.42		0.18	
220733	Ar	W. US	Poleta	6.96	1.82	0.26	0.57	0.07	0.14
220734	~	W. US	Poleta	2.78	1.26	0.45		0.21	
220735	~	W. US	Poleta	9.58	3.70	0.39	0.61	0.15	0.05
220736	Ar	W. US	Poleta	5.19	1.18	0.23	0.20	0.05	0.10
220737	~	W. US	Poleta	3.72	1.04	0.28		0.08	
220738	Aj	W. US	Poleta	5.79	3.06	0.53		0.28	
220739	Aj	W. US	Poleta	3.74	2.28	0.61	0.38	0.37	0.09
220740	~	W. US	Poleta	14.92	4.30	0.29	0.93	0.08	0.48
220741	~	W. US	Poleta	4.71	1.64	0.35	0.63	0.12	0.18
220742	~	W. US	Poleta	8.85	4.52	0.51	0.79	0.26	0.23
220743	Ar	W. US	Poleta	11.79	4.47	0.38	0.15	0.14	0.24
220744	Ar	W. US	Poleta	15.11	5.73	0.38	1.37	0.14	0.50
220745	~	W. US	Harkless	15.72	8.44	0.54	0.92	0.29	0.29
220746	~	W. US	Poleta	5.12	2.06	0.40	0.91	0.16	0.39
220747	~	W. US	Poleta	5.90	3.07	0.52	0.56	0.27	0.43
220748	~	W. US	Poleta	12.68	8.76	0.69	0.95	0.48	0.12
220749	~	W. US	Harkless	9.87	2.42	0.24	0.72	0.06	0.21
220750	Ar	W. US	Harkless	26.57	19.01	0.72	0.92	0.51	0.30
220751	~	W. US	Poleta	8.98	4.15	0.46	0.84	0.21	0.61
220752	~	W. US	Poleta	10.02	3.75	0.37	0.72	0.14	0.22
220754	Aj	W. US	Poleta	6.48	4.16	0.64	0.33	0.41	0.15
220755	Aj	W. US	Poleta	10.79	6.18	0.57	0.77	0.33	0.47
220756	~	W. US	Poleta	5.76	2.78	0.48	0.52	0.23	0.23
220757	~	W. US	Poleta	8.72	4.17	0.48	0.55	0.23	0.30
220758	~	W. US	Poleta	8.23	2.44	0.30	0.55	0.09	0.22
220759	Aj	W. US	Poleta	10.16	7.22	0.71	0.55	0.50	0.15
220760	Ar	W. US	Poleta	4.87	1.93	0.40	0.52	0.16	0.10
220761	Aj	W. US	Poleta	5.92	2.18	0.37	0.39	0.14	0.16

220762	~	W. US	Poleta	7.42	2.45	0.33	0.89	0.11	0.48
220763	Ar	W. US	Poleta	5.15	1.23	0.24	0.57	0.06	0.25
220764	~	W. US	Poleta	5.62	4.13	0.73	0.60	0.54	0.14
220765	Ar	W. US	Poleta	20.95	17.02	0.81	0.79	0.66	0.30
220766	~	W. US	Poleta	4.15	2.28	0.55	0.76	0.30	0.38
220767	~	W. US	Poleta	8.95	3.41	0.38	1.31	0.15	0.41
220768	~	W. US	Poleta	9.98	5.87	0.59	0.56	0.35	0.13
220769	~	W. US	Poleta	10.93	1.80	0.16	0.75	0.03	0.23
220771	Ar	W. US	Poleta	10.82	5.49	0.51	1.15	0.26	0.43
220772	Ar	W. US	Poleta	9.24	3.99	0.43	0.58	0.19	0.21
220773	Aj	W. US	Poleta	10.64	5.95	0.56	0.74	0.31	0.15
220775	Ar	W. US	Poleta	12.76	3.69	0.29	0.72	0.08	0.30
220776	Aj	W. US	Poleta	15.60	6.38	0.41	0.70	0.17	0.22
220778	Aj	W. US	Poleta	5.32	2.09	0.39	0.38	0.15	0.12
220782	Aj	W. US	Poleta	9.74	6.39	0.66	0.83	0.43	0.31
220783	Aj	W. US	Poleta	6.90	2.99	0.43	0.71	0.19	0.12
220784	Aj	W. US	Poleta	14.03	10.17	0.73	0.76	0.53	0.07
220785	Aj	W. US	Poleta	7.09	3.47	0.49	0.58	0.24	0.07
220786	Aj	W. US	Poleta	5.53	2.08	0.38	0.52	0.14	0.14
220789	~	W. US	~	7.00	2.52	0.36	0.67	0.13	0.23
220790	~	W. US	Poleta	6.97	2.29	0.33	1.03	0.11	0.30
220791	~	W. US	Poleta	8.47	2.39	0.28	0.56	0.08	0.33
220792	Ar	W. US	Poleta	12.49	4.15	0.33	0.72	0.11	0.26
220793	Ar	W. US	Poleta	11.87	4.73	0.40	0.44	0.16	0.35
220794	Ar	W. US	Poleta	7.15	2.63	0.37	0.87	0.13	0.33
220795	~	W. US	Poleta	7.44	2.18	0.29	0.47	0.09	0.14
220796	Aj	W. US	Poleta	6.60	2.77	0.42	0.53	0.18	0.24
220799	Ar	W. US	Poleta	11.79	3.08	0.26	0.62	0.07	0.25
220800	Ar	W. US	Poleta	4.22	0.58	0.14		0.02	
220801	Ar	W. US	Poleta	12.24	5.63	0.46	0.93	0.21	0.29
220802	~	W. US	Poleta	4.95	1.97	0.40		0.16	
220803	Aj	W. US	Poleta	9.43	6.42	0.68	1.04	0.46	0.29
220804	Aj	W. US	Poleta	10.14	7.08	0.70	0.60	0.49	0.28
220805	Ar	W. US	Poleta	7.99	4.62	0.58	0.69	0.33	0.27
220806	Aj	W. US	Campito	9.96	5.28	0.53	0.46	0.28	0.12
220807	~	W. US	Campito	8.91	3.96	0.44	0.26	0.20	0.25
220808	~	W. US	Campito	12.42	9.58	0.77	0.59	0.59	0.25
220809	Aj	W. US	Poleta	8.95	4.57	0.51	0.63	0.26	0.38
220810	~	W. US	Poleta	9.79	3.06	0.31	0.65	0.10	0.29
220811	~	W. US	Poleta	13.70	5.03	0.37	0.80	0.13	0.42
220812	Ar	W. US	Poleta	6.96	2.64	0.38	0.67	0.14	0.22
220813	Aj	W. US	Poleta	8.04	3.69	0.46	0.65	0.21	0.24
220814	~	W. US	Poleta	7.02	3.39	0.48	0.66	0.23	0.33
220815	~	W. US	Poleta	18.63	8.29	0.45	0.89	0.20	0.37
220817	~	W. US	Poleta	5.57	2.83	0.51	0.70	0.26	0.24
220818	~	W. US	Poleta	5.05	2.60	0.51	0.51	0.26	0.22
220819	~	W. US	Poleta	10.08	7.35	0.73	0.87	0.53	0.27
220821	~	W. US	Poleta	4.32	1.21	0.28	0.70	0.08	0.21
220822	Aj	W. US	Campito	10.50	8.58	0.82	0.60	0.67	0.25
220823	Aj	W. US	Harkless	36.15	19.20	0.53	0.72	0.28	0.29
220824	~	W. US	Poleta	6.37	3.42	0.54	0.71	0.29	0.18
220825	~	W. US	Poleta	7.79	3.66	0.47	0.38	0.22	0.05
220826	~	W. US	Poleta	11.62	8.53	0.73	0.75	0.54	0.38
220827	~	W. US	Poleta	12.05	7.96	0.66	0.74	0.44	0.41
220828	Ar	W. US	Poleta	7.72	1.51	0.20	0.64	0.04	0.33
220829	~	W. US	Poleta	6.22	2.32	0.37	0.37	0.14	0.37
220830	Ar	W. US	Poleta	22.21	7.55	0.34	0.55	0.12	0.55
220831	~	W. US	Poleta	5.33	1.27	0.24	0.49	0.06	0.18
220834	Ar	W. US	Poleta	30.42	11.45	0.38	1.03	0.14	0.48
220842	~	W. US	~	11.94	10.12	0.85	0.62	0.72	0.22
220843	~	W. US	Scott Canyon	5.42	2.66	0.49	0.42	0.24	0.17
220845	Aj	W. US	Poleta	5.54	1.79	0.32	0.54	0.10	0.16
220846	Ca	W. US	Harkless	38.89	21.38	0.55	0.66	0.30	0.26

220848	Ca	W. US	Harkless	36.23	21.91	0.60	0.91	0.37	0.53
220850	Ar	W. US	Harkless	7.45	2.95	0.40	0.19	0.16	0.05
220851	~	W. US	Harkless	4.32	1.34	0.31	0.35	0.10	0.11
220852	Ar	W. US	Harkless	5.67	1.22	0.21	0.12	0.05	0.10
220854	Ca	W. US	Poleta	15.72	6.47	0.41	0.89	0.17	0.33
220855	Ca	W. US	Poleta	13.20	4.64	0.35	0.66	0.12	0.35
220858	Ca	W. US	Poleta	42.48	18.87	0.44	0.86	0.20	0.40
220859	Ar	W. US	Poleta	18.28	10.26	0.56	0.94	0.32	0.40
220860	Ca	W. US	Poleta	8.09	2.60	0.32	0.46	0.10	0.29
220864	Aj	W. US	Poleta	6.83	5.36	0.78	0.22	0.62	0.10
220865	Ar	W. US	Poleta	9.44	2.97	0.31	0.56	0.10	0.25
220868	Ar	W. US	Poleta	7.83	3.86	0.49	0.57	0.24	0.30
220869	Ar	W. US	Poleta	10.44	2.05	0.20	0.55	0.04	0.39
220870	Ar	W. US	Poleta	12.85	3.64	0.28	0.65	0.08	0.31
220871	Ar	W. US	Poleta	11.57	2.21	0.19	0.53	0.04	0.26
220873	Ar	W. US	Poleta	16.72	4.17	0.25	0.84	0.06	0.46
220878	Ar	W. US	Poleta	15.54	4.62	0.30	1.00	0.09	0.37
220879	Ar	W. US	Poleta	5.31	1.71	0.32	0.50	0.10	0.11
220882	Ar	W. US	Poleta	10.77	3.25	0.30	0.73	0.09	0.23
220883	Ar	W. US	Poleta	9.19	2.65	0.29	0.96	0.08	0.22
220885	Ar	W. US	Poleta	46.59	19.97	0.43	0.93	0.18	0.73
220886	Ar	W. US	Poleta	38.28	21.72	0.57	0.76	0.32	0.38
220887	~	W. US	Poleta	33.29	16.58	0.50	0.94	0.25	0.89
220888	Ar	W. US	Poleta	17.60	3.78	0.21	0.74	0.05	0.51
220890	~	W. US	Campito	15.82	9.51	0.60	0.42	0.36	0.26
220891	~	W. US	Campito	21.69	14.49	0.67	0.71	0.45	0.33
220892	~	W. US	Campito	20.47	10.40	0.51	0.80	0.26	0.28
220893	Aj	W. US	Campito	11.20	6.40	0.57	0.58	0.33	0.33
220894	Aj	W. US	Campito	22.66	16.31	0.72	0.90	0.52	0.31
220895	Ca	W. US	Harkless	47.08	33.55	0.71	1.14	0.51	0.43
220880	Ar	W. US	Poleta	14.09	3.37	0.24	0.41	0.06	0.11
220719A	Aj	W. US	Poleta	6.40	2.29	0.36	0.42	0.13	0.21
220719B	Aj	W. US	Poleta	6.24	2.08	0.33	0.47	0.11	0.22
220753A	~	W. US	Poleta	11.43	3.11	0.27	0.89	0.07	0.40
220753B	~	W. US	Poleta	7.23	3.74	0.52	0.82	0.27	0.30
220753C	~	W. US	Poleta	7.50	3.77	0.50	0.44	0.25	0.50
220770A	Aj	W. US	Poleta	15.62	5.95	0.38	0.49	0.14	0.34
220770B	~	W. US	Poleta	3.29	1.43	0.43	0.25	0.19	0.11
220774A	Aj	W. US	Poleta	4.48	1.50	0.33	0.67	0.11	0.24
220774B	~	W. US	Poleta	7.76	3.25	0.42	0.81	0.17	0.18
220774C	~	W. US	Poleta	6.99	3.41	0.49	0.28	0.24	0.10
220779A	~	W. US	Poleta	12.24	3.84	0.31	0.93	0.10	0.15
220779B	~	W. US	Poleta	6.47	2.90	0.45	0.50	0.20	0.05
220780A	Aj	W. US	Poleta	3.91	1.64	0.42	0.51	0.18	0.06
220780B	Aj	W. US	Poleta	7.99	3.94	0.49	0.60	0.24	0.07
220780C	Aj	W. US	Poleta	7.56	3.89	0.51	0.67	0.26	0.05
220781A	~	W. US	Poleta	9.55	3.17	0.33	0.61	0.11	
220781B	~	W. US	Poleta	6.22	1.18	0.19		0.04	
220781C	~	W. US	Poleta	3.26	1.06	0.32		0.10	
220787A	Aj	W. US	~	4.73	2.24	0.47	0.85	0.22	0.28
220787B	Aj	W. US	~	4.50	1.95	0.43	0.97	0.19	0.38
220787C	Aj	W. US	~	4.75	1.93	0.41	0.79	0.17	0.43
220788A	~	W. US	Poleta	5.00	2.08	0.42	0.62	0.17	0.11
220788B	~	W. US	Poleta	5.25	3.00	0.57	0.60	0.33	0.26
220788C	~	W. US	Poleta	6.33	2.88	0.46	0.56	0.21	0.14
220797A	~	W. US	Poleta	9.18	2.03	0.22	0.86	0.05	0.36
220797B	~	W. US	Poleta	5.33	2.39	0.45	0.83	0.20	0.19
220797C	~	W. US	Poleta	3.92	1.22	0.31		0.10	
220797D	~	W. US	Poleta	5.89	1.53	0.26	0.64	0.07	0.27
220798A	Ar	W. US	Poleta	5.82	1.10	0.19	0.85	0.04	0.31
220798B	Ar	W. US	Poleta	3.16	0.89	0.28	0.62	0.08	0.21
220816A	~	W. US	Poleta	7.16	4.66	0.65		0.42	
220816b	~	W. US	Poleta	7.80	1.99	0.26	0.77	0.07	0.24

220820A	~	W. US	Poleta	6.74	2.31	0.34	0.84	0.12	0.35
220820B	~	W. US	Poleta	3.14	0.78	0.25	0.58	0.06	0.21
220832A	~	W. US	Poleta	5.19	1.52	0.29		0.09	
220832B	~	W. US	Poleta	4.24	2.21	0.52		0.27	
220833A	~	W. US	Poleta	7.81	2.59	0.33	0.95	0.11	0.27
220833B	~	W. US	Poleta	7.86	1.01	0.13	0.91	0.02	0.46
220839A	~	W. US	Poleta	3.37	1.35	0.40	0.42	0.16	0.24
220839B	~	W. US	Poleta	5.55	2.16	0.39	0.47	0.15	0.11
220840A	~	W. US	Poleta	10.88	6.35	0.58	0.75	0.34	0.30
220840B	~	W. US	Poleta	17.49	5.73	0.33	0.68	0.11	0.29
220840C	~	W. US	Poleta	4.33	1.47	0.34	0.44	0.12	0.19
220840D	~	W. US	Poleta	8.83	3.90	0.44	0.44	0.20	0.19
220844A	~	W. US	Poleta	8.92	2.73	0.31	0.30	0.09	0.14
220844B	~	W. US	Poleta	8.28	4.34	0.52	0.51	0.27	0.22
220844C	~	W. US	Poleta	12.99	7.19	0.55	0.49	0.31	0.34
220844D	~	W. US	Poleta	10.77	7.56	0.70		0.49	
220847A	~	W. US	Poleta	4.07	1.86	0.46	0.69	0.21	0.13
220847B	~	W. US	Poleta	9.88	4.55	0.46	0.70	0.21	0.36
220847C	~	W. US	Poleta	11.01	5.50	0.50	0.61	0.25	0.33
220849A	~	W. US	Silver Peak	9.49	1.45	0.15	0.74	0.02	0.30
220849B	~	W. US	Silver Peak	6.17	3.48	0.56	0.88	0.32	0.25
220849C	~	W. US	Silver Peak	13.11	5.27	0.40	0.83	0.16	0.27
220853A	Aj	W. US	Harkless	7.14	4.31	0.60	0.57	0.36	0.19
220853B	Aj	W. US	Harkless	2.71	1.11	0.41	0.16	0.17	0.10
220856A	Aj	W. US	Harkless	6.70	3.97	0.59	0.43	0.35	0.13
220856B	Aj	W. US	Harkless	1.26	0.51	0.40	0.15	0.16	0.10
220857A	Aj	W. US	Poleta	10.84	6.89	0.64	0.59	0.40	0.21
220857B	Aj	W. US	Poleta	7.13	3.94	0.55	0.59	0.31	0.15
220857C	Aj	W. US	Poleta	5.83	3.16	0.54	0.36	0.29	0.37
220861A	Aj	W. US	Poleta	7.01	2.79	0.40	0.91	0.16	0.32
220861B	Aj	W. US	Poleta	8.24	3.88	0.47	0.92	0.22	0.21
220861C	Aj	W. US	Poleta	7.93	3.52	0.44	1.02	0.20	0.30
220861D	Aj	W. US	Poleta	7.35	2.97	0.40	0.86	0.16	0.28
220862A	~	W. US	Bonanza King	5.70	2.49	0.44		0.19	
220862B	~	W. US	Bonanza King	2.59	0.72	0.28		0.08	
220863A	~	W. US	Poleta	7.61	2.81	0.37	0.38	0.14	0.12
220863B	~	W. US	Poleta	6.50	2.77	0.43	0.48	0.18	0.33
220863C	~	W. US	Poleta	3.94	1.62	0.41	0.43	0.17	0.21
220866A	~	W. US	Poleta	7.76	3.70	0.48	0.59	0.23	0.25
220866B	~	W. US	Poleta	7.29	3.84	0.53	0.43	0.28	0.26
220867A	~	W. US	Poleta	5.97	3.25	0.54	0.53	0.30	0.33
220867B	~	W. US	Poleta	7.05	2.90	0.41	0.90	0.17	0.26
220867C	~	W. US	Poleta	5.89	3.35	0.57	0.56	0.32	0.27
220872A	~	W. US	Poleta	8.87	4.46	0.50	0.38	0.25	0.15
220872B	~	W. US	Poleta	5.81	2.46	0.42	0.44	0.18	0.14
220872C	~	W. US	Poleta	9.05	2.50	0.28		0.08	
220872D	~	W. US	Poleta	5.62	3.01	0.54	0.37	0.29	0.20
220874A	Ar	W. US	Poleta	16.55	3.35	0.20	0.93	0.04	0.42
220874B	Ar	W. US	Poleta	8.68	2.12	0.24	0.77	0.06	0.22
220875A	Ar	W. US	Poleta	5.54	2.02	0.36	0.49	0.13	0.24
220875B	Ar	W. US	Poleta	4.67	1.41	0.30	0.40	0.09	0.18
220875C	Ar	W. US	Poleta	3.94	1.65	0.42	0.51	0.17	0.24
220876A	Ar	W. US	Poleta	8.67	2.70	0.31	0.46	0.10	0.29
220876B	Ar	W. US	Poleta	7.89	3.98	0.50	0.63	0.25	0.34
220877A	~	W. US	Poleta	8.73	4.34	0.50	0.49	0.25	0.13
220877B	~	W. US	Poleta	7.65	3.54	0.46	1.00	0.21	0.22
220881A	~	W. US	Poleta	7.21	3.63	0.50	0.74	0.25	0.28
220881B	~	W. US	Poleta	4.78	1.92	0.40	0.34	0.16	0.20
220881C	~	W. US	Poleta	5.26	1.82	0.35	0.24	0.12	0.05
220884A	~	W. US	Poleta	15.87	4.16	0.26	0.80	0.07	0.31
220884B	~	W. US	Poleta	11.49	4.11	0.36	0.74	0.13	0.30
220884C	~	W. US	Poleta	3.93	1.98	0.50	0.62	0.25	0.32
220884D	~	W. US	Poleta	7.07	4.28	0.60	0.35	0.37	0.28

220884E	~	W. US	Poleta	7.65	4.12	0.54	0.48	0.29	0.06
220889A	~	W. US	Poleta	3.14	1.43	0.45	0.47	0.21	0.17
220889B	~	W. US	Poleta	4.08	1.58	0.39	0.37	0.15	0.22
220889C	~	W. US	Poleta	6.36	4.08	0.64	0.63	0.41	0.35
220889D	~	W. US	Poleta	3.01	1.55	0.51	0.44	0.27	0.07
220889E	~	W. US	Poleta	6.86	2.12	0.31	0.47	0.10	0.16

Table D4: Archaeocyath continuous morphology measurements. All from University of Wisconsin-Milwaukee and Mongolia University of Science and Technology (UWM/MUST). All measurements in millimeters. All samples from Mongolia, Salaagol Formation.

Specimen #	Body Size	Osculum Size	OBR	Loculi Width	Intervallum Area %	Septal Thickness
IESAG0001	1.72	1.01	0.59	0.22	0.35	
IESAG000J	2.53	1.04	0.41		0.17	
IESAG0002	3.32	1.35	0.41	0.51	0.17	0.11
IESAG0002	2.57	1.12	0.44	0.52	0.19	0.22
IESAG0002	4.87	2.28	0.47	0.46	0.22	0.18
IESAG0002	5.00	2.51	0.50	0.43	0.25	0.10
IESAG0002	2.96	1.32	0.45	0.32	0.20	0.21
IESAG0002	5.75	2.94	0.51	0.40	0.26	0.14
IESAG0006	4.88	1.96	0.40	0.30	0.16	0.10
IESAG0006	9.09	6.03	0.66	0.37	0.44	0.19
IESAG0007	11.23	7.70	0.69	0.70	0.47	0.24
IESAG0008	13.38	11.02	0.82	0.47	0.68	0.20
IESAG0008	13.27	8.54	0.64	0.60	0.41	0.28
IESAG0003	4.15	1.07	0.26	0.47	0.07	0.19
IESAG0003	5.93	3.21	0.54	0.66	0.29	0.28
IESAG0003	7.15	3.95	0.55	0.44	0.31	0.24
IESAG0003	1.78	0.80	0.45	0.40	0.20	0.16
IESAG0003	1.58	0.97	0.61		0.37	
IESAG0003	1.32	0.65	0.49	0.13	0.24	0.10
IESAG0003	1.63	0.99	0.61		0.37	
IESAG0005	6.00	3.65	0.61	0.53	0.37	0.20
IESAG0005	5.91	3.98	0.67	0.31	0.45	0.15
IESAG0005	7.40	4.36	0.59	0.52	0.35	0.17
IESAG0005	9.18	6.31	0.69	0.58	0.47	0.22
IESAG0005	7.71	5.55	0.72	0.46	0.52	0.29
IESAG0004	5.81	2.90	0.50	0.90	0.25	0.25
IESAG000A	5.73	2.46	0.43	0.47	0.18	0.15
IESAG000A	4.60	2.79	0.61	0.35	0.37	0.05
IESAG000A	3.33	1.83	0.55	0.31	0.30	0.15
IESAG000K	2.19	0.60	0.27	0.29	0.07	0.14
IESAG000K	8.42	6.66	0.79	0.26	0.63	0.12
IESAG000L	2.75	0.86	0.31		0.10	
IESAG000L	3.65	1.71	0.47	0.48	0.22	0.16
IESAG000L	3.26	1.71	0.52	0.37	0.28	0.16
IESAG000L	2.99	1.59	0.53	0.45	0.28	0.25
IESAG000L	2.73	1.08	0.40		0.16	
IESAG000L	3.69	1.72	0.47	0.44	0.22	0.17
IESAG000L	2.04	0.81	0.39	0.18	0.16	
IESAG000M	2.46	1.05	0.43		0.18	
IESAG000N	8.55	6.23	0.73		0.53	
IESAG000N	4.60	2.45	0.53	0.17	0.28	0.10
IESAG000N	6.26	2.84	0.45	0.44	0.21	0.17
IESAG000N	2.93	0.65	0.22	0.48	0.05	0.13
IESAG000N	2.89	0.72	0.25		0.06	
IESAG000N	1.41	0.57	0.40		0.16	
IESAG000O	5.17	1.77	0.34	0.39	0.12	0.17
IESAG000P	6.54	2.05	0.31	0.28	0.10	0.14

IESAG000Q	24.38	16.72	0.69	0.70	0.47	0.10
IESAG000Q	7.19	2.69	0.37	0.32	0.14	0.14
IESAG000Q	2.97	1.00	0.34	0.37	0.11	0.15
IESAG000Q	4.98	1.94	0.39	0.37	0.15	0.12
IESAG000R	13.20	9.96	0.75	0.50	0.57	0.14
IESAG000R	21.10	17.66	0.84	0.53	0.70	0.24
IESAG000R	4.60	1.93	0.42	0.44	0.18	0.19
IESAG000R	1.74	0.54	0.31		0.10	
IESAG000R	1.44	0.77	0.54		0.29	
IESAG000R	3.18	1.27	0.40		0.16	
IESAG000R	2.63	1.01	0.38	0.47	0.15	0.24
IESAG000R	4.31	2.38	0.55	0.36	0.30	0.12
IESAG000R	4.47	2.08	0.46	0.50	0.22	0.11
IESAG000R	2.61	1.15	0.44	0.17	0.19	0.16
IESAG000R	4.70	1.69	0.36	0.34	0.13	0.20
IESAG000R	1.88	0.78	0.42		0.17	
IESAG000R	1.93	0.76	0.39		0.16	
IESAG000R	1.89	0.63	0.33		0.11	
IESAG000R	7.33	2.98	0.41	0.55	0.16	0.36
IESAG000R	1.94	0.63	0.32		0.10	
IESAG000R	2.74	1.02	0.37		0.14	
IESAG000R	3.76	1.93	0.51		0.26	
IESAG000R	5.28	3.30	0.62	0.23	0.39	0.16
IESAG000R	2.39	1.14	0.48	0.23	0.23	0.06
IESAG000S	6.76	4.42	0.65	0.36	0.43	0.11
IESAG000S	3.84	1.57	0.41	0.31	0.17	0.12
IESAG000S	2.92	0.87	0.30		0.09	
IESAG000T	8.90	4.74	0.53	0.31	0.28	0.12
IESAG000T	4.99	1.71	0.34		0.12	
IESAG000T	4.16	0.91	0.22		0.05	
IESAG000T	3.06	1.35	0.44		0.19	
IESAG0009	3.62	1.69	0.47		0.22	
IESAG0009	3.93	2.10	0.53		0.29	
IESAG0009	5.68	3.12	0.55	0.45	0.30	0.28
IESAG0009	5.46	2.40	0.44	0.32	0.19	0.18
IESAG0009	4.04	2.18	0.54	0.31	0.29	0.10
IESAG0009	4.02	2.55	0.63		0.40	
IESAG0009	2.76	1.74	0.63		0.40	
IESAG0009	3.60	2.18	0.60		0.37	
IESAG0009	2.51	1.27	0.51	0.25	0.26	0.10
IESAG0009	2.67	1.13	0.42	0.21	0.18	0.12
IESAG0009	2.16	0.83	0.38		0.15	
IESAG0009	2.41	0.49	0.20		0.04	
IESAG000B	2.96	1.49	0.50		0.25	
IESAG000B	2.09	0.47	0.23		0.05	
IESAG000B	1.89	0.86	0.45		0.21	
IESAG000C	6.20	4.34	0.70		0.49	
IESAG000C	5.85	2.62	0.45	0.63	0.20	0.15
IESAG000C	3.59	1.22	0.34	0.56	0.11	0.18
IESAG000C	7.61	4.69	0.62	0.31	0.38	0.07
IESAG000C	1.87	0.90	0.48	0.79	0.23	0.12
IESAG000C	1.65	0.78	0.47		0.22	
IESAG000C	1.41	0.53	0.38		0.14	
IESAG000D	4.16	2.28	0.55	0.19	0.30	0.12
IESAG000D	3.08	1.49	0.48		0.23	
IESAG000D	5.97	2.89	0.48	0.25	0.23	0.17
IESAG000D	8.63	4.80	0.56	0.43	0.31	0.18
IESAG000D	6.94	5.14	0.74	0.50	0.55	0.25
IESAG000D	8.53	5.09	0.60	0.46	0.36	0.17
IESAG000E	5.24	1.89	0.36	0.33	0.13	0.14
IESAG000F	2.80	1.39	0.50		0.25	
IESAG000F	5.29	3.06	0.58	0.28	0.33	0.13
IESAG000G	6.31	3.12	0.49	0.70	0.24	0.29

IESAG000G	2.15	0.80	0.37		0.14	
IESAG000H	2.56	1.26	0.49		0.24	
IESAG000H	4.49	1.52	0.34		0.11	
IESAG000I	4.97	2.84	0.57	0.45	0.33	0.15
IESAG000U	2.36	0.91	0.38	0.27	0.15	0.08
IESAG000U	2.59	0.92	0.36		0.13	
IESAG000U	2.03	0.85	0.42	0.28	0.17	0.15
IESAG0011	2.25	1.12	0.50		0.25	
IESAG0013	10.22	4.86	0.48	0.55	0.23	0.23
IESAG0013	7.25	3.95	0.54	0.52	0.30	0.17
IESAG0012	5.80	1.69	0.29	0.43	0.08	0.23
IESAG000V	27.16	24.62	0.91	0.43	0.82	0.11
IESAG000V	2.13	0.69	0.32		0.11	
IESAG000W	1.75	0.76	0.43		0.19	
IESAG000W	2.19	0.53	0.24		0.06	
IESAG000X	3.72	1.50	0.40	0.37	0.16	0.08
IESAG000Y	12.68	8.87	0.70		0.49	
IESAG000Y	1.32	0.49	0.37		0.14	
IESAG000Z	2.28	1.13	0.49	0.21	0.24	0.10
IESAG0010	0.78	0.33	0.43		0.18	
IESAG0010	0.95	0.43	0.46		0.21	
IESAG0010	0.85	0.45	0.52	0.12	0.27	0.05
IESAG0010	1.09	0.50	0.46	0.12	0.21	0.06

Table D5: Lithistid sponge continuous morphological measurements from literature survey. Bolded line denotes break between fossil and modern specimens.

Age	Locality	Taxa	Diameter (mm)	Height (mm)	Reference
Stage 5	North China	<i>Rankenella zhangxianensis</i>	21	61	Lee <i>et al.</i> (2016)
Middle Cambrian	Utah, USA	<i>Sentinelia cf Sentinelia? draco</i>	30	75	Rigby <i>et al.</i> (2010)
Guzhangian	Montana, USA	<i>Cambrophyllum</i> (Chaetetid?)	30	15	Fritz and Howell (1955)
Paibian	Nevada, USA	<i>Gallatinospongia conica</i>	33	30	Shapiro and Rigby (2004)
Paibian	Iran	<i>Rankenella hamdii</i>	31	70	Kruse and Zhuravlev (2008)
Jiangshanian	Nevada, USA	<i>Wilberniyathus donegani</i>	41	62	Johns <i>et al.</i> (2007)
Stage 10	Nevada, USA	<i>Anthaspidellid</i>	140	100	Mrozek <i>et al.</i> (2003)
Lower Ordovician	China	<i>Anthaspidella lamellata</i>	70	40	Bingli <i>et al.</i> (1997)
Lower Ordovician	China	<i>Archaeoscyphia minganensis</i>	95	60	Bingli <i>et al.</i> (1997)
Lower Ordovician	China	<i>Archaeoscyphia nana</i>	23		Bingli <i>et al.</i> (1997)
Lower Ordovician	China	<i>Jianghanian yichangensis</i>	35	40	Bingli <i>et al.</i> (1997)
Lower Ordovician	China	<i>Archaeoscyphia pulchria</i>	43	300	Bingli <i>et al.</i> (1997)
Lower Ordovician	China	<i>Rhopalocoelia sanxiaensis</i>	31	50	Bingli <i>et al.</i> (1997)
Lower Ordovician	China	<i>Vellicospongia adnata</i>	8	15	Bingli <i>et al.</i> (1997)
Tremadocian	South China	<i>Anthaspidellid</i>	30	50	Adachi <i>et al.</i> (2011, 2012)
Tremadocian-Floian	Argentina	<i>Archaeoscyphia</i>	70	150	Canas and Carrera (1993)
Tremadocian-Floian	South China	<i>Anthaspidellid</i>	30	50	Adachi <i>et al.</i> (2009)
Floian	Utah, USA	<i>Archaeoscyphia</i>	40	110	Church (1974)
Floian	Korea	<i>Archaeoscyphia</i>	50	100	Hong <i>et al.</i> (2015)
Floian	Canada	<i>Archaeoscyphiid</i>	140	500	Pratt and James (1982)
Middle Ordovician	China	<i>Zittelella xinjiangensis</i>	65	143	Bingli <i>et al.</i> (2003)
Middle Ordovician	China	<i>Hudsonospongia cyclostoma</i>	48	58	Bingli <i>et al.</i> (2003)
Middle Ordovician	China	<i>Calycocoelia profunda sichuanensis</i>	25	40	Bingli <i>et al.</i> (2003)
Middle Ordovician	China	<i>Calycocoelia sp.</i>	60	32	Bingli <i>et al.</i> (2003)
Middle Ordovician	China	<i>Rhopalocoelia kalpinensis</i>	49	90	Bingli <i>et al.</i> (2003)
Middle Ordovician	China	<i>Rhopalocoelia bachuensis</i>	67	75	Bingli <i>et al.</i> (2003)
Middle Ordovician	China	<i>Annulospongia tarimensis</i>	140	30	Bingli <i>et al.</i> (2003)
Middle Ordovician	China	<i>Pseudopalmatohindia sp.</i>	35	11	Bingli <i>et al.</i> (2003)
Middle Ordovician	China	<i>Archaeoscyphia minganensis</i>	74	39	Bingli <i>et al.</i> (2003)

Middle Ordovician	China	<i>Aulocopium? sp.</i>	70	50	Bingli <i>et al.</i> (2003)
Floian	Oklahoma, USA	<i>Archaeoscyphia</i>	40	170	Toomey and Nitechi (1979)
Dapingian or Darriwilian	China	<i>Craterospongiella sinensis</i>	76	47	Rigby <i>et al.</i> (2006)
Darriwilian	Canada	<i>Archaeoscyphia</i>	45	200	Klappa and James (1980)
Darriwilian	Argentina	<i>Multispongia aspera</i>	70	48	Carrera (2006)
Darriwilian	Canada	<i>Anthaspidellid</i>	50	150	Desrochers and James (1989)
Late Ordovician	Utah, USA	<i>Hindia sphaeroidalis</i>	15		Rigby and Jamison (1994)
Late Ordovician	Utah, USA	<i>Hudsonospongia? sp.</i>	13	10	Rigby and Jamison (1994)
Late Ordovician	Sweden	<i>Brevaspidella dispersa</i>	66	66	Rhebergen (2014)
Middle Silurian	Quebec	<i>Calycocoelia annulata</i>	38	80	Rigby (1973)
Early Devonian	New South Wales	<i>Devonospongia garrae</i>	60		Pickett and Rigby (1983)
Early Devonian	New South Wales	<i>Brianispongia quadratipora</i>	10		Pickett and Rigby (1983)
Early Devonian	New South Wales	<i>Isispongia (?) monilifera</i>	130	110	Pickett and Rigby (1983)
Middle Jurassic	India	<i>Rhizotetraclis plana</i>	80		Mehl and Fursich (1997)
Middle Jurassic	India	<i>Cnemidiastrum stellatum</i>	50		Mehl and Fursich (1997)
Middle Jurassic	India	<i>Hyalotragos patella</i>	120		Mehl and Fursich (1997)
Middle Jurassic	India	<i>Hyalotragos radiatum</i>	102		Mehl and Fursich (1997)
Middle Jurassic	India	<i>Platychnonia schlotheimi</i>	40		Mehl and Fursich (1997)
Middle Jurassic	India	<i>Melonella radiata</i>	25		Mehl and Fursich (1997)
Middle Jurassic	India	<i>Mastosia rhytidodes</i>	68		Mehl and Fursich (1997)
Middle Jurassic	India	<i>Jumarella astrorhiza</i>	45		Mehl and Fursich (1997)
Oligocene	Ukraine	<i>Theonella ukrainica</i>	70	50	Pisera (2000)
Oligocene	Ukraine	<i>Lerouxia digitata</i>	40	150	Pisera (2000)
Oligocene	Ukraine	<i>Chenendopora piaskovskii</i>	80		Pisera (2000)
Oligocene	Ukraine	<i>Plinthosella magna</i>	40	75	Pisera (2000)
Eocene	New Zealand	<i>Pleroma aotea</i>	25	22	Kelly <i>et al.</i> (2003)
Holocene	New Zealand	<i>Discodermia proliferans</i>	20	53	Kelly (2007)
Holocene	New Zealand	<i>Neoaulaxinia clavata</i>	80	160	Kelly (2007)
Holocene	New Zealand	<i>Neoaulaxinia zingiberadix</i>	30	50	Kelly (2007)
Holocene	New Zealand	<i>Neoaulaxinia persicum</i>	50	50	Kelly (2007)
Holocene	New Zealand	<i>Neosiphonia superstes</i>	35	35	Kelly (2007)
Holocene	New Zealand	<i>Neosiphonia motukawanui</i>	50	35	Kelly (2007)
Holocene	New Zealand	<i>Reidispongia coerulea</i>	95	70	Kelly (2007)
Holocene	New Zealand	<i>Reidispongia coerulea</i>	300	150	Kelly (2007)
Holocene	New Zealand	<i>Neoschrammeniella fulvodesmus</i>	65	38	Kelly (2007)
Holocene	New Zealand	<i>Neoschrammeniella antarctica</i>	55	65	Kelly (2007)
Holocene	New Zealand	<i>Herengeria auriculata</i>	14	20	Kelly (2007)
Holocene	New Zealand	<i>Herengeria vasiformis</i>	83	42	Kelly (2007)
Holocene	New Zealand	<i>Awhiowhio osheai</i>	51	38	Kelly (2007)
Holocene	New Zealand	<i>Awhiowhio sepulchrum</i>	300	210	Kelly (2007)
Holocene	New Zealand	<i>Homophymia stipitata</i>	45	185	Kelly (2007)
Holocene	New Zealand	<i>Callipelta punctata</i>	5	8	Kelly (2007)
Holocene	New Zealand	<i>Callipelta punctata</i>	17	10	Kelly (2007)
Holocene	New Zealand	<i>Neopelta pulvinus</i>	7	10	Kelly (2007)
Holocene	New Zealand	<i>Lepidothenea incrustans</i>	10	10	Kelly (2007)
Holocene	New Zealand	<i>Macandrewia spinifoliata</i>	13	4	Kelly (2007)
Holocene	New Zealand	<i>Pleroma turbinatum</i>	240	240	Kelly (2007)
Holocene	New Zealand	<i>Pleroma menoui</i>	140	110	Kelly (2007)
Holocene	New Zealand	<i>Pleroma aotea</i>	40	30	Kelly (2007)
Holocene	New Zealand	<i>Costifer wilsoni</i>	400	160	Kelly (2007)
Holocene	New Zealand	<i>Microscleroderma novaezelandiae</i>	60	45	Kelly (2007)
Holocene	New Zealand	<i>Scleritoderma flabelliformis</i>	60	20	Kelly (2007)
Holocene	New Zealand	<i>Aciculites pulchra</i>	125	30	Kelly (2007)
Holocene	New Zealand	<i>Aciculites manawatawhi</i>	100	70	Kelly (2007)
Holocene	New Zealand	<i>Aciculites manawatawhi</i>	85	110	Kelly (2007)

Holocene	New Zealand	<i>Aciculites sulcus</i>	23	35	Kelly (2007)
Holocene	New Zealand	<i>Leiodermatium intermedia</i>	100	70	Kelly (2007)
Holocene	New Zealand	<i>Leiodermatium intermedia</i>	110	77	Kelly (2007)
Holocene	New Zealand	<i>Leiodermatium colini</i>	125	0	Kelly (2007)
Holocene	New Zealand	<i>Leiodermatium dampieri</i>	20	13	Kelly (2007)
Holocene	New Zealand	<i>Leiodermatium linea</i>	55	22	Kelly (2007)
Holocene	Lebanon	<i>Gastrophanella phoeniciensis</i>	35	50	Perez <i>et al.</i> (2004)
Holocene	Lebanon	<i>Microscleroderma lamina</i>	100	80	Perez <i>et al.</i> (2004)
Holocene	Sardinia	<i>Aciculites mediterranea</i>	44	28	Manconi <i>et al.</i> (2006)

Table D6: Modern demosponge continuous morphology measurements. All from Milwaukee Public Museum (MPM). All measurements in millimeters unless otherwise noted.

Specimen #	Taxonomy	Taxonomy (accepted)	Body Size	Osculum Size	Max Height (cm)
1871	???		11.38		38.50
1908	???		106.50		17.10
20	Acanthella		82.50		10.50
2109	Aplysina		30.17	21.67	8.50
620	Axinella		17.50		41.50
51	Chalinopsilla	Dactylia	9.89	3.08	34.50
39	Chalinopsilla	"	9.21	3.07	23.50
50	Chalinopsilla	"	24.50		39.50
772	Chondrilla		19.50	4.41	45.50
613	Cliona		49.50		13.00
740	Coscinoderus	Coscinoderma	110.00		14.00
608	Dactylochalina	Callyspongia sp. A	10.50	1.16	35.50
2623	Demosponia		151.50	7.50	7.50
588	Euspongia	Spongia	90.94		11.00
587	Euspongia	"	255.00	16.00	21.00
1894	Finger Sponge		21.33	15.17	22.00
776	Geodia		75.00		3.50
2236	Hippospongia		130.09		14.25
2000	Hippospongia		75.00		12.00
1796	Hippospongia		80.70		8.50
44	Hircinia	Ircinia	207.50		29.00
29	Hircinia	"	113.13		24.50
2116	Hircinia	"	136.50		21.00
2115	Hircinia	"	166.00		15.00
1994	Hircinia	"	114.38		20.00
2001	Hircinia	"	60.00		16.00
2010	Hircinia	"	9.07		13.80
709	Hymeniacidon		27.50	7.50	2.50
606	Janthella	lanthella	311.50		2.00
605	Janthella	"	310.00		12.00
736	Microciona		93.45		8.00
???"Parade of Life"	Cliona		320.50		77.00
53	Cliona		400.00		68.50
???	Cliona		490.00		77.00
714	Pandoras	Pandaros	49.25		7.50
742	Petrosia		110.50	12.20	10.80
738	Phyllospongia		161.25		14.50
1334	Phyllospongia		335.00		5.25
756A	Phyllospongia		43.50		11.50
756B	Phyllospongia		70.00		15.00
42	Phyllospongia		45.00		13.00
1333	Phyllospongia		117.50		18.00
2111	Porifera		21.60	13.20	12.00
1858	Porifera				62.00
730	Sigmatella	Chondropsis	75.03	1.83	10.50
604	Sigmatella	"	107.50		16.50

1992A	Spinosella	Callyspongia sp. B	24.50	14.88	16.40
1992B	Spinosella	"	20.00	17.50	13.40
1992C	Spinosella	"	18.25	14.75	15.50
1992D	Spinosella	"	35.00	19.00	16.50
1651	Spinosella	"	145.00	16.64	13.90
1993	Spinosella	"	50.00	40.50	14.40
17	Spinosella	"	62.50	43.00	11.90
743	Spinosella	"	20.40	9.90	13.00
745	Spinosella	"	17.33	10.50	13.80
2376A	Spinosella	"	67.50	45.00	12.30
2376B	Spinosella	"	54.00	53.50	16.50
2376C	Spinosella	"	66.50	49.50	20.20
1480	Spinosella	"	48.00	27.50	8.00
764	Spongelia		87.50	11.33	12.50
760	Spongia		72.50		12.50
746	Spongia		24.88	12.88	10.80
2013	Spongilla		47.50	6.33	11.20
2014	Stellospongia	Fasciospongia	42.50		12.00
726	Stellospongia	"	45.70		18.00
731	Stellospongia	"	44.00		16.80
1623	Stellospongia	"	35.50	25.75	16.00
1161	Tethya		72.50	9.00	7.60
707	Thecophora	Tentorium	25.50		1.80
755	Thorecta		121.00		11.50
739	Thorecta		84.00		17.00

Table D7:

Archaeocyath discrete morphological characters. A (1) marks that trait as present. G - Gondwana; S - Siberia; L - Laurentia; To - Tommotian; Bo - Botomian; At - Atdabanian; Ty - Toyonian; Cy - Cylindrical-conical Cup shape; Ss - Subspherical; D/D - Discoid/Domal cup shape; El - Elaboration; Ca - Catenulate gross morphology; Br - Branching gross morphology; Ma - Massive gross morphology; Co - Conical gross morphology

Genus	Locality	Age	Cy	Ss	D/D	El	Ca	Br	Ma	Co
Archaeolyntus	G/S	To	1				1	1		
Kyarocyathus	G/S	Bo	1				1	1		
Palaeoconularia	S	Bo	1				1	1		
Butakovicyathus	S	At	1				1	1		
Tumuliolyntus	G/S	To	1				1	1		
Sajanolyntus	S	Bo	1				1	1		
Propriolyntus	S	At	1				1	1		
Melkanicyathus	S	Bo	1				1	1		
Favilyntus	G/S	At	1				1	1		
Robertiolyntus	L/S	Bo	1				1	1		
Dokidocyathus	G/S	To	1				1	1		
Dokidocyathella	S	At	1				1	1		
Incurvocyathus	S	At	1			1	1	1		
Cordobicyathus	G	At	1				1	1		
Kidrjasocyathus	S	At	1				1	1		
Kaltatocyathus	G/S	At	1				1	1		
Papillocyathus	S	At	1				1	1		
Subtilocyathus	S	At	1				1	1		
Batschykyathus	S	At	1			1	1	1		
Zhuravlevaocyathus	S	Bo	1				1	1		
Kymbecyathus	G	At	1				1	1		
Ajacicyathus	G/L/S	At	1				1	1		
Davidicyathus	G	At	1				1	1		
Dentatocyathus	S	Bo	1			1	1	1		
Iljinicyathus	S	At	1			1	1	1		
Kisasacyathus	G/S	At	1				1	1		
Nochoroicyathus	G/S	To	1				1	1		
Orbiasterocyathus	S	At	1			1	1	1		

Orbicyathellus	S	At	1			1	1	1		
Orbicyathus	G/S	To	1			1	1	1		
Robustocyathellus	L/S	At	1				1	1		
Rotundocyathus	G/S	To	1				1	1		
Sibirecyathus	G/S	To	1				1	1		
Stapicyathus	G/S	At	1				1	1		
Urcyathus	G/S	At	1			1	1	1		
Densocyathus	S	Bo	1				1	1		
Cadniacyathus	G	Bo	1				1	1		
Dailyathus	G/S	At	1				1	1		
Deceptioncyathus	G	At	1				1	1		
Khargisocyathus	S	At	1				1	1		
Leptosocyathellus	G/S	At	1				1	1		
Leptosocyathus	G/S	At	1				1	1		
Natalijaecyathus	S	At	1				1	1		
Rectannulus	G	At	1				1	1		
Tennericyathus	S	At	1				1	1		
Thalamocyathus	G/S	At	1				1	1		
Compositocyathus	S	At	1				1	1		
Conannulofungia	Other	At	1				1	1		
Cyathocricus	G/S	At	1				1	1		
Cyclocyathella	S	At	1				1	1		
Denaecyathus	S	Bo	1				1	1		
Gordonicyathus	G/S	At	1				1	1		
Gordonifungia	G/S	At	1				1	1		
Morenicyathus	G/S	At	1				1	1		
Pseudotennericyathellus	S	At	1				1	1		
Sagacyathus	G/S	At	1				1	1		
Stillicidocyathus	G/S	Bo	1				1	1		
Svetlanocyathus	S	Bo	1				1	1		
Taylorcyathus	G/S	At	1				1	1		
Taylorfungia	G/S	At	1				1	1		
Trininaecyathus	S	Bo	1				1	1		
Ethmocyathus	G	Bo	1				1	1		
Afiacyathus	G/S	At	1				1	1		
Baikalocyathus	G/S	At	1				1	1		
Carpicyathus	G/S	At	1				1	1		
Degeletticyathus	G/S	At	1				1	1		
Diplocyathellus	G	Bo	1				1	1		
Frinalicyathus	S	At	1				1	1		
Gnaltacyathus	G/S	Bo	1				1	1		
Hyptocyathus	G	Bo	1				1	1		
Inessocyathellus	S	Bo	1				1	1		
Inessocyathus	G/S	At	1				1	1		
Mackenziocyathus	L/S	Bo	1				1	1		
Rasetticyathus	G	At	1				1	1		
Terraecyathus	G/S	At	1				1	1		
Ussuricyathellus	G/S	Bo	1				1	1		
Zonacyathellus	S	Bo	1				1	1		
Sajanocyathus	G/L/S	Bo	1				1	1		
Chakassicyathus	S	Bo	1				1	1		
Formosocyathus	S	At	1				1	1		
Irinaecyathus	S	Bo	1				1	1		
Kiwicyathus	G	Bo	1				1	1		
Palmericyathus	L	Bo	1				1	1		
Siderocyathus	L	Bo	1				1	1		
Zonacyathus	G/S	Bo	1				1	1		
Emucyathus	G	Bo	1				1	1		
Bipallicyathus	S	At	1				1	1		
Heckericyathus	S	At	1				1	1		
Robertocyathus	G/S	At	1				1	1		
Mattajacyathus	S	Bo	1			1	1	1		
Urcyathella	S	At	1			1	1	1		

Pretiosocyathus	S	At	1				1	1		
Jangudacyathus	S	Bo	1				1	1		
Loculicyathopsis	S	At	1				1	1		
Pluralicyathus	S	Bo	1				1	1		
Ladaecyathus	G/S	At	1				1	1		
Milaecyathus	S	At	1				1	1		
Peregrinicyathus	S	Bo	1				1	1		
Vologdinocyathus	G/S	Bo	1				1	1		
Gumbycyathus	G/S	Bo	1				1	1		
Inacyathella	G	Bo	1				1	1		
Kordecyathus	S	Bo	1				1	1		
Sanarkophyllum	G	Bo	1				1	1		
Syringocyathus	S	Bo	1				1	1		
Tegerocyathus	G/L/S	Bo	1				1	1		
Krasnopeevaecyathus	L/S	Bo	1			1	1	1		
Tumulocyathus	G/S	To	1				1	1		
Isiticyathus	S	At	1				1	1		
Kotuyicyathellus	S	At	1				1	1		
Plicocyathus	G/L/S	At	1			1	1	1		
Sanarkocyathus	S	Bo	1				1	1		
Neokolbicyathus	L/S	At	1				1	1		
Ringifungia	S	At	1				1	1		
Geocyathus	G/S	At	1				1	1		
Konjuschkovicyathus	S	Bo	1				1	1		
Torosocyathus	S	At	1				1	1		
Torosocyathella	S	At	1				1	1		
Japhanicyathus	S	At	1				1	1		
Lenocyathus	G/S	At	1				1	1		
Tumulifungia	G/S	At	1				1	1		
Sclerocyathus	G/S	To	1				1	1		
Subtumulocyathellus	S	At	1				1	1		
Tologoicyathus	S	To	1				1	1		
Annulocyathus	S	Bo	1				1	1		
Annulocyathella	S	At	1				1	1		
Annulofungia	S	At	1				1	1		
Hemithalamocyathus	S	At	1				1	1		
Jakutocarinus	S	At	1				1	1		
Kosticyathus	S	Bo	1				1	1		
Kruseicyathus	S	Bo	1				1	1		
Rossocyathella	S	Bo	1				1	1		
Russocyathus	S	At	1				1	1		
Gagarinicyathus	S	At	1				1	1		
Fallocyathus	S	Bo	1				1	1		
Sekwicyathus	G/L/S	Bo	1				1	1		
Yukonocyathus	L	Bo	1				1	1		
Gloriosocyathus	G/S	Bo	1				1	1		
Gandinocyathus	G	Bo	1				1	1		
Nalivkinicyathus	G/S	At	1				1	1		
Kijacyathus	S	At	1				1	1		
Aporosocyathus	G/L/S	Bo	1				1	1		
Fansycyathus	S	At	1				1	1		
Flexanulus	G	Bo	1				1	1		
Protocyathus	L	Bo	1				1	1		
Yudjaicyathus	S	At	1				1	1		
Qinlingocyathus	Other	At	1				1	1		
Carinacyathus	S	At	1				1	1		
Hupecyathellus	S	Bo	1				1	1		
Porocyathellus	G	Bo	1				1	1		
Vologdinocyathellus	S	Bo	1				1	1		
Ethmophyllum	L	At	1				1	1		
Angaricyathus	S	Ty	1				1	1		
Aulocricus	L	Bo	1				1	1		
Cordilleracyathus	L/S	At	1				1	1		

Dupliporocyathus	S	At	1			1	1		
Kolbicyathus	S	Bo	1			1	1		
Parethmophyllum	L	Bo	1			1	1		
Squamosocyathus	S	At	1			1	1		
Stephencyathus	L	Bo	1			1	1		
Piamaecyathellus	S	Bo	1			1	1		
Botomocyathus	S	At	1			1	1		
Clathrithalamus	G	Bo	1			1	1		
Olgaecyathus	S	Bo	1			1	1		
Tercyathus	S	Bo	1			1	1		
Clathricyathellus	S	Bo	1			1	1		
Clathricyathus	S	Bo	1			1	1		
Tercyathellus	S	Bo	1			1	1		
Sigmocyathus	G	Bo	1			1	1		
Didymocyathus	G	Bo	1			1	1		
Wrighticyathus	G	Bo	1			1	1		
Asterocyathus	S	At	1		1	1	1		
Antoniocoscinus	G/S	At	1			1	1		
Erismacoscinus	G/S	To	1			1	1		
Ichnusocyathus	G	Bo	1			1	1		
Retecoscinus	G/S	To	1			1	1		
Rozanovicoscinus	G	At	1		1	1	1		
Rudanulus	G	At	1		1	1	1		
Pilidicoscinus	Other	At	1		1	1	1		
Yhecyathus	Other	Bo	1		1				1
Salairocyathus	S	At	1			1	1		
Kotuyicoscinus	S	At	1			1	1		
Polystillicidocyathus	G/S	Bo	1			1	1		
Crassicoscinus	S	At	1			1	1		
Crucicyathus	G	At	1		1	1	1		
Dentatocoscinus	S	Bo	1		1	1	1		
Agyrekocyathus	G/S	At	1			1	1		
Xestecyathus	G	Bo	1			1	1		
Kasyricyathus	S	Bo	1			1	1		
Membranacyathus	S	At	1			1	1		
Anaptyctocyathus	G	At	1			1	1		
Polycoscinus	G	At	1			1	1		
Lunulacyathus	G	Bo	1			1	1		
Veronicacyathus	G	At	1			1	1		
Bractocyathus	G	At	1			1	1		
Zonacoscinus	G	Bo	1			1	1		
Orienticyathus	S	Bo	1			1	1		
Tumulocoscinus	S	At	1			1	1		
Asterotumulus	S	At	1		1	1	1		
Orbicoscinus	G	Bo	1		1	1	1		
Retetumulus	G	Bo	1			1	1		
Ethmocoscinus	G	Bo	1			1	1		
Geyericoscinus	G	At	1			1	1		
Coscinoptycta	G	Bo	1		1	1	1		
Jebileticoscinus	G	Bo	1			1	1		
Irhoudicoscinus	G	Bo	1			1	1		
Sylviacoscinus	G	Bo	1			1	1		
Sigmocoscinus	G	Bo	1			1	1		
Statanulocyathus	G	Bo	1			1	1		
Rozanovicyathus	S	Bo	1			1	1		
Muchattocyathus	S	Bo	1			1	1		
Schumnyicyathus	S	Bo	1			1	1		
Porocoscinus	G	Bo	1			1	1		
Genulicyathus	G	At	1			1	1		
Tubicoscinus	G	Bo	1			1	1		
Mootwingecyathus	G	Bo	1			1	1		
Alphacyathus	G	Bo	1						1
Aptocyathus	G/S	Bo	1						1

Putapacyathus	G	Bo	1							1
Hupecyathus	G	At	1							1
Chabakovicyathus	S	Bo	1							1
Cryptoporocyathus	S	To		1						1
Capsulocyathus	G/S	To		1						1
Complicatocyathus	S	At		1		1				1
Gerbicanicyathus	S	Bo		1						1
Mirandocyathus	S	Bo		1						1
Polythalamia	L/S	Bo		1						1
Rhabdolyntus	S	Bo		1						1
Tylocyathus	S	Bo		1						1
Korshunovicyathus	S	To		1						1
Fransuasaecyathus	S	At		1						1
Yukonensis	L	Bo		1		1				1
Tubericyathus	S	Bo		1						1
Coscincyathus	G/S	At		1						1
Mawsonicoscinus	G	Bo	1							1
Coscincyathellus	S	Bo	1							1
Calyptocoscinus	G	Bo	1							1
Coscincyathella	S	At	1							1
Alatacyathus	S	At	1							1
Clathricoscinus	S	At	1							1
Lanicyathus	S	Bo	1							1
Loculicyathus	G/L/S	At	1					1		
Antarcticocyathus	G	Ty	1					1		
Ardrossacyathus	G/S	Bo	1					1		
Cambrocyathellus	G/S	To	1					1		
Mikhnocyathus	G/S	At	1					1		
Neoloculicyathus	G/S	At	1					1		
Okulitchicyathus	G/S	To			1			1		
Paranacyathus	G/L/S	Bo	1					1		
Eremitacyathus	G	At	1					1		
Sakhacyathus	S	To	1					1		
Chankacyathus	G/S	Bo	1					1		
Tchojacyathus	S	At	1					1		
Anthomorpha	G/S	Bo	1					1		
Tollicyathus	S	Bo	1					1		
Shiveligocyathus	S	Bo	1					1		
Dictyocyathus	G/L/S	To	1					1		
Cellicyathus	S	Bo	1					1		
Chouberticyathus	G	Bo	1					1		
Graphoscyphia	G/L/S	At	1					1		
Paracoscinus	G/S	Bo	1					1		
Retilamina	L	Bo			1			1		
Claruscoscinus	L/S	Bo	1					1		
Fenestrocyathus	L/S	Bo	1					1		
Landercyathus	L	Bo	1					1		
Stevocyathus	L	Bo	1					1		
Pycnoidocoscinus	G/L	Bo	1					1		
Archaeopharetra	G/S	At	1					1		
Dictyosyon	G/S	At	1					1		
Markocyathus	L	Bo	1					1		
Protopharetra	L/S	At	1					1		
Spirocyathella	G/L/S	At	1					1		
Archaeocyathus	G/L/S	At	1					1		
Arrythmocricus	L	Bo	1					1		
Pycnoidocyathus	G/L/S	Bo	1					1		
Sigmofungia	G/L	Bo	1					1		
Archaeosyon	L	Bo	1					1		
Copleicyathus	G	At	1					1		
Agastrocyathus	G	At	1					1		
Gabrielsoyathus	L	Bo	1					1		
Metacyathellus	G/L	At	1					1		

Spinosocyathus	G/S	To	1							1		
Spirillicyathus	G	At	1							1		
Tabulacyathellus	S	At	1							1		
Jugaliccyathus	G	At	1							1		
Alaskacoscinus	L	Bo	1							1		
Metaldetes	G/L/S	At	1							1		
Changicyathus	Other	At	1							1		
Naimarkcyathus	G	Bo	1							1		
Warriootacyathus	G	At	1							1		
Maiandrocyathus	G	Bo	1							1		
Ataxiocyathus	G	Bo	1							1		
Beltanacyathus	G	At	1							1		
Taeniaecyathellus	S	Bo	1							1		
Usloncyathus	G/S	At	1							1	1	
Kechikacyathus	L	Bo	1							1	1	
Zunyicyathus	L	Bo	1							1	1	
Keriocyathus	L/S	Bo	1							1	1	
Gatagacyathus	L	Bo	1							1	1	
Auliscocyathus	G/S	At	1							1		
Tuvacnema	S	Bo	1							1		
Syringocnema	G	Bo	1							1		
Pseudosyringocnema	G/L/S	Bo	1							1		
Syringothalamus	L	Bo	1							1		
Williamicyathus	L	Bo	1							1		
Kruseicnema	G	Bo	1							1		
Fragilicyathus	S	Bo	1							1		
Korovinella	S	Bo	1								1	
Bicoscinus	G	Bo	1								1	
Altaicyathus	G/L/S	Bo	1								1	

Table D8: Lithistid sponge

discrete morphological characters. A (1) marks that trait as present. En - encrusting; Ma - massive; Gl - globular; Pe - pedunculate; Co - conical; Fl - flabellate; Re - repent; Ar - arborescent; Pa - papillate; Ot - other

Taxa	En	Ma	Gl	Pe	Co	Fl	Re	Ar	Pa	Ot
<i>Rankenella zhangxianensis</i>	1									
<i>Sentinella cf Sentinella? draco</i>					1					
<i>Cambrophyllum</i> (Chaetetid?)	1									
<i>Gallatinospongia conica</i>					1					
<i>Rankenella hamdii</i>	1									
<i>Wilbernicyathus donegani</i>					1					
<i>Anthaspidellid</i>					1					
<i>Anthaspidella lamellata</i>		1			1					
<i>Archaeoscyphia minganensis</i>					1					
<i>Archaeoscyphia nana</i>					1					
<i>Jianghania yichangensis</i>					1					
<i>Archaeoscyphia pulchria</i>					1					
<i>Rhopalocoelia sanxiaensis</i>					1					
<i>Vellelospongia adnata</i>	1									1
<i>Anthaspidellid</i>					1					
<i>Archaeoscyphia</i>			1							
<i>Anthaspidellid</i>					1					
<i>Archaeoscyphia</i>					1					
<i>Archaeoscyphia</i>	1				1					
<i>Archaeoscyphiid</i>		1			1					
<i>Zittlella xinjiangensis</i>					1					
<i>Hudsonospongia cyclostoma</i>					1					
<i>Calycocoelia profunda sichuanensis</i>					1					
<i>Calycocoelia sp.</i>										
<i>Rhopalocoelia kalpinensis</i>				1	1					
<i>Rhopalocoelia bachuensis</i>					1					
<i>Annulospongia tarimensis</i>			1			1				

<i>Pseudopalmatohindia</i> sp.					1				
<i>Archaeoscyphia manganensis</i>				1					
<i>Aulocopium?</i> sp.				1					
<i>Archaeoscyphia</i>									
<i>Craterospongiella sinensis</i>				1					
<i>Archaeoscyphia</i>			1						
<i>Multispongia aspera</i>								1	
<i>Anthaspidellid</i>									
<i>Hindia sphaeroidalis</i>			1						
<i>Hudsonospongia?</i> sp.					1				
<i>Brevaspidella dispersa</i>			1						
<i>Calycocoelia annulata</i>					1				
<i>Devonospongia garrae</i>					1				
<i>Brianispongia quadratipora</i>								1	
<i>Isispongia (?) monilifera</i>	1								
<i>Rhizotetraclis plana</i>						1			
<i>Cnemidiastrum stellatum</i>								1	
<i>Hyalotragos patella</i>					1				
<i>Hyalotragos radiatum</i>			1						
<i>Platychnonia schlotheimi</i>					1	1			
<i>Melonella radiata</i>			1						
<i>Mastosia rhytidodes</i>			1						
<i>Jumarella astrorhiza</i>			1						
<i>Theonella ukrainica</i>								1	
<i>Lerouxia digitata</i>									1
<i>Chenendopora piaskovskii</i>					1				
<i>Plinthosella magna</i>			1						
<i>Pleroma aotea</i>			1						
<i>Discodermia proliferans</i>								1	
<i>Neoaulaxinia clavata</i>			1						
<i>Neoaulaxinia zingiberadix</i>									1
<i>Neoaulaxinia persicum</i>			1						
<i>Neosiphonia superstes</i>			1						
<i>Neosiphonia motukawanui</i>	1								
<i>Reidispongia coerulea</i>	1				1				
<i>Reidispongia coerulea</i>	1				1				
<i>Neoschrammeniella fulvodesmus</i>					1				
<i>Neoschrammeniella antarctica</i>					1				
<i>Hereengeria auriculata</i>			1						
<i>Hereengeria vasiformis</i>			1						
<i>Awhiowhio osheai</i>					1				
<i>Awhiowhio sepulchrum</i>						1			
<i>Homophymia stipitata</i>			1						
<i>Callipelta punctata</i>			1						
<i>Callipelta punctata</i>			1						
<i>Neopelta pulvinus</i>			1						
<i>Lepidothenea incrustans</i>	1								
<i>Macandrewia spinifoliata</i>			1						
<i>Pleroma turbinatum</i>								1	
<i>Pleroma menoui</i>									1
<i>Pleroma aotea</i>			1						
<i>Costifer wilsoni</i>								1	
<i>Microscleroderma novaezelandiae</i>					1				
<i>Scleritoderma flabelliformis</i>						1			
<i>Aciculites pulchra</i>					1	1			
<i>Aciculites manawatawhi</i>								1	
<i>Aciculites manawatawhi</i>								1	
<i>Aciculites sulcus</i>	1								
<i>Leiodermatium intermedia</i>						1			
<i>Leiodermatium intermedia</i>						1			
<i>Leiodermatium colini</i>					1				
<i>Leiodermatium dampieri</i>				1					
<i>Leiodermatium linea</i>					1				

<i>Gastrophanella phoeniciensis</i>		1							
<i>Microscleroderma lamina</i>	1			1					
<i>Aciculites mediterranea</i>	1								

Table D9: Modern demosponge discrete morphological body shape characters. Notation same as table D8.

Taxa	E	M	G	P	C	F	R	A	P	O
<i>Acanthella costata</i> Kieschnick, 1900						1		1	1	
<i>Acarnus primigenius</i> Hiemstra & Hooper, 1991	1	1								
<i>Acarnus souriei</i> (Lévi, 1952)	1	1								
<i>Acarnus tortilis</i> Topsent, 1892	1	1								
<i>Adreus fascicularis</i> (Bowerbank, 1866)								1		
<i>Agelas dilatata</i> Duchassaing & Michelotti, 1864	1				1	1		1	1	
<i>Agelas gracilis</i> Whitelegge, 1897	1				1	1		1	1	
<i>Agelas incrustans</i> Sim & Kim, 2014	1				1	1		1	1	
<i>Agelas marmarica</i> Lévi, 1958	1				1	1		1	1	
<i>Agelas mauritiana</i> (Carter, 1883)	1				1	1		1	1	
<i>Amorphinopsis atlantica</i> Carvalho, Hajdu, Mothes & van Soest, 2004	1	1						1		
<i>Amphilectus dactylus</i> Goodwin, Jones, Neely & Brickle, 2011	1		1					1	1	
<i>Amphilectus fimbriatus</i> Goodwin, Jones, Neely & Brickle, 2016	1		1					1	1	
<i>Amphilectus fleecei</i> Goodwin, Jones, Neely & Brickle, 2011	1		1					1	1	
<i>Amphilectus strepsichelifer</i> van Soest, Beglinger & De Voogd, 2012	1		1					1	1	
<i>Amphimedon calyx</i> Goodwin, Jones, Neely & Brickle, 2011		1				1		1		
<i>Amphimedon maresi</i> (Sarà, 1978)		1				1		1		
<i>Antho</i> (<i>Antho</i>) <i>atlantidae</i> Van Soest, Beglinger & De Voogd, 2013	1	1	1			1			1	
<i>Antho</i> (<i>Isopenectya</i>) <i>chartacea</i> (Whitelegge, 1907)	1	1	1			1			1	
<i>Antho</i> (<i>Isopenectya</i>) <i>punicea</i> Hooper, 1996	1	1	1			1			1	
<i>Antho</i> (<i>Jia</i>) <i>lithistica</i> Van Soest, Rützler & Sim, 2016	1	1	1			1			1	
<i>Aplysilla glacialis</i> (Merejkowski, 1878)	1									
<i>Aplysilla sulfurea</i> Schulze, 1878	1									
<i>Aplysina procumbens</i> Lendenfeld, 1889										1
<i>Aplysinopsis elegans</i> Lendenfeld, 1888					1					1
<i>Asbestopluma</i> (<i>Asbestopluma</i>) <i>flabellum</i> Koltun, 1970				1				1		
<i>Asbestopluma</i> (<i>Asbestopluma</i>) <i>ramosa</i> Koltun, 1958				1				1		
<i>Asteropus haeckeli</i> Dendy, 1905		1								
<i>Atergia corona</i> Dickinson, 1945			1							
<i>Axinella amorpha</i> Tanita & Hoshino, 1989						1		1		
<i>Axinella digitiformis</i> Lehnert & van Soest, 1996						1		1		
<i>Axinella halichondrioides</i> Dendy, 1905						1		1		
<i>Axinella natalensis</i> (Kirkpatrick, 1903)						1		1		
<i>Axinella symbiotica</i> Whitelegge, 1907						1		1		
<i>Biemna chujaensis</i> Sim & Shim, 2006		1			1					
<i>Biemna cribaria</i> (Alcolado & Gotera, 1986)		1			1					
<i>Biemna gellioides</i> Lévi & Lévi, 1989		1			1					
<i>Biemna microstyla</i> de Laubenfels, 1950		1			1					
<i>Biemna rhabderemioides</i> Bergquist, 1961		1			1					
<i>Callyspongia</i> (<i>Callyspongia</i>) <i>scutica</i> Van Soest, 2017					1	1	1	1	1	
<i>Callyspongia</i> (<i>Toxochalina</i>) <i>dendyi</i> (Burton, 1931)					1	1	1	1	1	
<i>Callyspongia</i> (<i>Toxochalina</i>) <i>folioides</i> (Bowerbank, 1875)					1	1	1	1	1	
<i>Callyspongia arcesiosa</i> Laubenfels, 1936					1	1	1	1	1	
<i>Callyspongia californica</i> Dickinson, 1945					1	1	1	1	1	
<i>Callyspongia clathrata</i> (Dendy, 1905)					1	1	1	1	1	
<i>Callyspongia ecklonia</i> Hoshino, 1981					1	1	1	1	1	
<i>Callyspongia globosa</i> Pulitzer-Finali, 1982					1	1	1	1	1	
<i>Callyspongia sphaericuslobata</i> (Hoshino, 1981)					1	1	1	1	1	
<i>Callyspongia truncata</i> (Lendenfeld, 1887)					1	1	1	1	1	
<i>Calyx imperialis</i> (Dendy, 1924)		1		1	1	1				
<i>Caminella velata</i> Lebwahl, 1914			1							

Caminus albus Pulitzer-Finali, 1996			1					1	
Candidaspongia flabellata Bergquist, Sorokin & Karuso, 1999						1			
Chalinula spiculifera (Lendenfeld, 1887)	1		1						1
Characella agassizi Sollas, 1888			1		1				
Characella aspera Sollas, 1886			1		1				
Chondrilla oxyastera Tanita & Hoshino, 1989	1	1							
Chondrocladia (Chondrocladia) saffronae Goodwin, Berman, Downey & Hendry, 2017								1	
Chondrocladia (Chondrocladia) verticillata Topsent, 1920								1	
Chondrocladia (Meliiderma) latrunculioides Lopes, Bravo & Hajdu, 2011								1	
Chondrocladia (Meliiderma) latrunculioides Lopes, Bravo & Hajdu, 2011								1	
Chondrocladia (Meliiderma) occulta (Lehnert, Stone & Heimler, 2006)								1	
Cladocroce guyanensis Van Soest, 2017					1	1			
Cladocroce infundibulum Lehnert & Stone, 2013					1	1			
Cladorhiza corallophila Göcke, Hestetun, Uhlir, Freiwald, Beuck & Janussen, 2016								1	
Cladorhiza grimaldii Topsent, 1909								1	
Clathria (Axosuberites) flabellata (Topsent, 1916)	1	1			1		1	1	1
Clathria (Clathria) inanchorata Ridley & Dendy, 1886	1	1			1		1	1	1
Clathria (Clathria) pauper Brøndsted, 1927	1	1			1		1	1	1
Clathria (Microciona) levii (Sarà & Siribelli, 1960)	1	1			1		1	1	1
Clathria (Microciona) mytilifila Hajdu, Desqueyroux-Faúndez, Carvalho, Lôbo-Hajdu & Willenz, 2013	1	1			1		1	1	1
Clathria (Microciona) primitiva (Koltun, 1955)	1	1			1		1	1	1
Clathria (Thalysias) araiosa Hooper & Lévi, 1993	1	1			1		1	1	1
Clathria (Thalysias) micropunctata (Burton & Rao, 1932)	1	1			1		1	1	1
Clathria (Thalysias) vulpina (Lamarck, 1814)	1	1			1		1	1	1
Clathria (Wilsonella) lindgreni Hooper, 1996	1	1			1		1	1	1
Cliona adriatica Calcinai, Bavestrello, Cuttone & Cerrano, 2011	1								
Cliona celata Grant, 1826	1								
Cliona euryphylle Topsent, 1888	1								
Cliona flavifodina Rützler, 1974	1								
Cliothisa aurivillii (Lindgren, 1897)	1								
Collosporgia auris Bergquist, Cambie & Kernan, 1990						1			
Columnitis anomala Sarà & Bavestrello, 1996									1
Cornulella santamartae van Soest, Zea & Kielman, 1994	1								
Craniella azorica (Topsent, 1913)			1						
Craniella oxeata (Burton, 1959)			1						
Crella (Pytheas) plana Picton & Goodwin, 2007	1								
Cyamon hamatum van Soest, Carballo & Hooper, 2012	1	1							
Darwinella duplex Topsent, 1905	1								
Darwinella oxeata Bergquist, 1961	1								
Delectona alborans Rosell, 1996	1								
Desmacella tylostrongyla Li, 1986	1	1							
Diacarnus bellae Kelly-Borges & Vacelet, 1995		1			1				1
Diacarnus tubifera Kelly-Borges & Vacelet, 1995		1			1				1
Discodermia proliferans Lévi & Lévi, 1983	1				1			1	
Dotona pulchella Carter, 1880	1								
Dysidea cinerea Keller, 1889	1	1						1	
Dysidea clathrata (Hentschel, 1912)	1	1						1	
Dysidea tupha (Pallas, 1766)	1	1						1	
Ectyonopsis ramosa Carter, 1883						1			
Endectyon (Endectyon) hornelli (Dendy, 1905)								1	
Erylus cornutus Wilson, 1925	1	1							
Esperiopsis bathyalis Lopes & Hajdu, 2004	1			1		1			
Esperiopsis incognita Stephens, 1916	1			1		1			
Eurypon cactoides (Burton & Rao, 1932)	1	1							1
Fasciospongia cavernosa (Schmidt, 1862)			1		1	1			
Fasciospongia turgida (Lamarck, 1814)			1		1	1			
Gelliodes truncata (Kieschnick, 1896)	1	1			1			1	
Gelliodes tubulosa Lendenfeld, 1887	1	1			1			1	
Geodia crustosa Börsraug, 1913	1	1	1						
Geodia dysoni Bowerbank, 1873	1	1	1						
Geodia erinacea (Lendenfeld, 1888)	1	1	1						

Geodia ovis Lendenfeld, 1910	1	1	1						
Geodia philippinensis Wilson, 1925	1	1	1						
Halichondria (Eumastia) sitiens (Schmidt, 1870)	1	1					1	1	
Halichondria (Halichondria) fallax (Marshall, 1892)	1	1					1	1	
Halichondria (Halichondria) poa (de Laubenfels, 1947)	1	1					1	1	
Halichondria (Halichondria) velamentosa (Hansen, 1885)	1	1					1	1	
Haliclona (Gellius) foraminosa (Topsent, 1904)	1		1	1	1	1	1	1	1
Haliclona (Gellius) marismedi (Pulitzer-Finali, 1978)	1		1	1	1	1	1	1	1
Haliclona (Gellius) rudis (Topsent, 1901)	1		1	1	1	1	1	1	1
Haliclona (Gellius) toxophora (Hentschel, 1912)	1		1	1	1	1	1	1	1
Haliclona (Halichoelona) magna (Vacelet, 1969)	1		1	1	1	1	1	1	1
Haliclona (Halichoelona) perlucida (Griessinger, 1971)	1		1	1	1	1	1	1	1
Haliclona (Haliclona) simulans (Johnston, 1842)	1		1	1	1	1	1	1	1
Haliclona (Haliclona) stilensis Burton, 1933	1		1	1	1	1	1	1	1
Haliclona (Haliclona) sumenyoensis Kim, Lee & Kang, 2017	1		1	1	1	1	1	1	1
Haliclona (Reniera) altera (Topsent, 1901)	1		1	1	1	1	1	1	1
Haliclona digitata Tanita & Hoshino, 1989	1		1	1	1	1	1	1	1
Haliclona elegans (Lendenfeld, 1887)	1		1	1	1	1	1	1	1
Haliclona firma (Swartschewsky, 1906)	1		1	1	1	1	1	1	1
Haliclona flava (Nardo, 1847)	1		1	1	1	1	1	1	1
Haliclona flavescens (Topsent, 1893)	1		1	1	1	1	1	1	1
Haliclona lentus Hoshino, 1981	1		1	1	1	1	1	1	1
Haliclona papillifera (Swartschewsky, 1906)	1		1	1	1	1	1	1	1
Haliclona polychotoma (Carter, 1885)	1		1	1	1	1	1	1	1
Haliclona pons (Schmidt, 1870)	1		1	1	1	1	1	1	1
Haliclona ramosa (Lendenfeld, 1887)	1		1	1	1	1	1	1	1
Haliclona similis (Topsent, 1897)	1		1	1	1	1	1	1	1
Haliclona swartschewskiji (Hentschel, 1929)	1		1	1	1	1	1	1	1
Haliclona texta Sarà, 1978	1		1	1	1	1	1	1	1
Haliclona ulreungia Sim & Byeon, 1989	1		1	1	1	1	1	1	1
Haliclona utriculus (Topsent, 1904)	1		1	1	1	1	1	1	1
Halisarca tessellata Carter, 1886	1								
Hamacantha (Hamacantha) simplex Burton, 1959	1		1						
Hamigera tarangaensis Bergquist & Fromont, 1988	1	1							
Hexadella kirkpatricki Burton, 1926	1								
Hexadella topsenti Reveillaud, Allewaert, Pérez, Vacelet, Banaigs & Vanreusel, 2012	1								
Higginsia coralloides Higgin, 1877		1		1	1			1	
Holopsamma macropora (Lendenfeld, 1888)									1
Holopsamma simplex (Lendenfeld, 1886)									1
Holoxea violacea Boury-Esnault, 1973	1	1							
Homaxinella subdola (Bowerbank, 1866)							1		
Hymedesmia (Hymedesmia) canadensis Ginn, Logan, Thomas & van Soest, 1998	1								
Hymedesmia (Hymedesmia) murrayi Burton, 1959	1								
Hymedesmia (Stylopus) dermatata Lundbeck, 1910	1								
Hymeniacion adreissiformis Dickinson, 1945	1							1	
Hyrtios caracasensis (Carter, 1882)				1				1	
Ianthella quadrangulata Bergquist & Kelly-Borges, 1995					1				
Iophon aceratum Hentschel, 1914	1	1					1		
Iophon flabellodigitatum Kirkpatrick, 1907	1	1					1		
Iophon nigricans (Bowerbank, 1858)	1	1					1		
Iophon proximum var. reticulare Hentschel, 1914	1	1					1		
Iotroata magna (Lambe, 1895)	1	1						1	
Ircinia flagelliformis (Carter, 1886)		1					1		
Isodictya deichmannae (de Laubenfels, 1949)					1			1	
Isodictya staurophora (Hentschel, 1911)					1			1	
Janulum spinispiculum (Carter, 1876)	1				1				
Jaspis biangulata (Lindgren, 1897)	1	1							
Jaspis wondoensis Sim & Kim, 1995	1	1							
Kaliopsis incrustans (Vacelet & Vasseur, 1971)	1								
Laminospongia subtilis Pulitzer-Finali, 1983					1				
Latrunculia (Biannulata) microacanthoxea Samaai, Gibbons, Kelly & Davies-Coleman, 2003	1			1					
Leiodermatium pfeifferae (Carter, 1873)					1		1		

Lissodendoryx (Anomodoryx) sigmata (de Laubenfels, 1949)			1				1			1
Lissodendoryx (Ectyodoryx) plumosa (Hentschel, 1914)			1				1			1
Lissodendoryx (Lissodendoryx) ivanovi Koltun, 1958			1				1			1
Lycopodina cupressiformis (Carter, 1874)						1				1
Lycopodina infundibulum (Levinsen, 1887)						1				1
Manihinea lynbeazleyae Fromont & Pisera, 2011				1	1					
Monanchora clathrata Carter, 1883			1						1	1
Mycale (Aegogropila) cavernosa Bergquist, 1965			1				1		1	1
Mycale (Aegogropila) rotalis (Bowerbank, 1874)			1				1		1	1
Mycale (Aegogropila) tapetum Samaai & Gibbons, 2005			1				1		1	1
Mycale (Arenochalina) tenuityla (Pulitzer-Finali, 1982)			1				1		1	1
Mycale (Carmia) carlilei Lehnert, Stone & Heimler, 2006			1				1		1	1
Mycale (Carmia) nullarosette Hoshino, 1981			1				1		1	1
Mycale (Carmia) raphidiophora Hentschel, 1911			1				1		1	1
Mycale (Carmia) tasmani (Bergquist & Fromont, 1988)			1				1		1	1
Mycale (Mycale) longistyla Koltun, 1958			1				1		1	1
Mycale (Mycale) macrochela Burton, 1932			1				1		1	1
Mycale (Mycale) madraspatana Annandale, 1914			1				1		1	1
Mycale (Oxymycale) acerata Kirkpatrick, 1907			1				1		1	1
Mycale (Zygomycale) sierraleonensis Van Soest, Beglinger & De Voogd, 2014			1				1		1	1
Myxilla (Burtonanchora) araucana Hajdu, Desqueyroux-Faúndez, Carvalho, Lôbo-Hajdu & Willenz, 2013		1	1						1	1
Myxilla (Burtonanchora) asigmata (Topsent, 1901)		1	1						1	1
Myxilla (Myxilla) inequitornota Burton, 1931		1	1						1	1
Myxilla (Myxilla) iophonoides Swartschewsky, 1906		1	1						1	1
Myxilla (Myxilla) mollis Ridley & Dendy, 1886		1	1						1	1
Neofibularia mordens Hartman, 1967			1				1			
Neopelta perfecta Schmidt, 1880						1	1			
Neopetrosia chaliniformis (Thiele, 1899)									1	
Neophrissospongia radjae Pisera & Vacelet, 2011							1		1	
Neosiphonia schmidtii Sollas, 1888				1						
Oceanapia aberrans (Dendy, 1924)			1	1			1			
Oceanapia sessilis (Kirkpatrick, 1900)			1	1			1			
Pachastrella monilifera Schmidt, 1868		1	1				1			
Petromica (Chaladesma) ciocalyptoides (van Soest & Zea, 1986)			1							
Petromica (Chaladesma) citrina Muricy, Hajdu, Minervino, Madeira & Peixinho, 2001			1							
Petromica (Petromica) digitata (Burton, 1929)			1							
Petrosia (Petrosia) solida Hoshino, 1981			1							
Petrosia (Strongylophora) septata (Thomas, 1991)			1							
Petrosia armata (Lendenfeld, 1887)			1							
Phakellia carduus (Lamarck, 1814)								1		
Phakellia ventilabrum (Linnaeus, 1767)								1		
Phorbis purpureus (Carter, 1886)		1	1						1	
Phorbis tenuispiculatus (Dendy, 1896)		1	1						1	
Phoriospongia papillosa (Lamarck, 1815)					1					
Placospongia mixta Thiele, 1900		1							1	1
Plocamione hystrix (Ridley & Duncan, 1881)		1								1
Plocamionida microcionides (Carter, 1876)		1								
Pocillastra compressa (Bowerbank, 1866)							1		1	
Pocillastra incrustans Sollas, 1888							1		1	
Polymastia boletiformis (Lamarck, 1815)		1		1						
Polymastia janeirensis (Boury-Esnault, 1973)		1		1						
Polymastia polytylota Vacelet, 1969		1		1						
Polymastia tissieri (Vacelet, 1961)		1		1						
Protosuberites longispiculus (Burton, 1959)		1								
Protosuberites modestus (Pulitzer-Finali, 1978)		1								
Psammastra conulosa Kieschnick, 1896					1					
Psammocinia jejuensis Sim, 1998						1		1		1
Psammoclema inordinatum (Kirkpatrick, 1903)			1						1	
Pseudohalichondria fibrosa Whitelegge, 1901			1					1		
Pseudosuberites mollis Topsent, 1925		1	1							
Ptilocaulis walpersii (Duchassaing & Michelotti, 1864)						1		1		1
Radiella sol Schmidt, 1870					1					

<i>Raspailia (Parasyringella) agnata</i> (Topsent, 1896)									1	1
<i>Raspailia (Raspaxilla) bouryesnaultae</i> Lerner, Carraro & van Soest, 2006									1	1
<i>Raspailia longispicula</i> Breiffuss, 1912									1	1
<i>Raspailia microacanthoxea</i> Hoshino, 1976									1	1
<i>Raspailia uncinata</i> Pick, 1905									1	1
<i>Reniochalina condylia</i> Hooper & Lévi, 1993							1		1	1
<i>Rhabderemia indica</i> Dendy, 1905	1									
<i>Rhabderemia minutula</i> (Carter, 1876)	1									
<i>Rhizaxinella clavata</i> Thiele, 1898			1	1	1					
<i>Rhizaxinella elevata</i> Thiele, 1898			1	1	1					
<i>Scleritoderma cyaneum</i> van Soest & Stentoft, 1988	1	1					1	1		
<i>Siphonidium dendyi</i> (Burton, 1928)	1	1	1	1	1					
<i>Smenospongia aurea</i> (Hyatt, 1875)		1								1
<i>Spheciospongia robusta</i> (Carter, 1886)										1
<i>Spheciospongia spiculifera</i> (Kieschnick, 1898)										1
<i>Spirastrella cunctatrix</i> Schmidt, 1868	1									
<i>Spirastrella pachyspira</i> Lévi, 1958	1									
<i>Spongilla shikaribensis</i> Sasaki, 1934	1	1							1	
<i>Spongionella ramodigitata</i> (Topsent, 1901)			1				1			
<i>Stelletta addita</i> (Topsent, 1938)			1							
<i>Stelletta atrophia</i> Hoshino, 1981			1							
<i>Stelletta capensis</i> Lévi, 1967			1							
<i>Stelletta crusta</i> Shim & Sim, 2009			1							
<i>Stelletta defensa</i> Pulitzer-Finali, 1983			1							
<i>Stelletta digitata</i> (Pulitzer-Finali, 1993)			1							
<i>Stelletta fibrosa</i> (Schmidt, 1870)			1							
<i>Stelletta mediterranea</i> (Topsent, 1893)			1							
<i>Stelletta megaspina</i> Lendenfeld, 1907			1							
<i>Stelletta plagioreducta</i> Lévi, 1961			1							
<i>Stelletta pudica</i> (Wiedenmayer, 1977)			1							
<i>Stelletta solidissima</i> (Wilson, 1902)			1							
<i>Stelletta trichotriaena</i> Dendy & Burton, 1926			1							
<i>Stelodoryx toporoki</i> Koltun, 1958	1	1		1						1
<i>Strongylacidon stelligerum</i> (Whitelegge, 1906)	1	1								
<i>Stryphnus unguiculus</i> Sollas, 1886		1								1
<i>Stylissa caribica</i> Lehnert & van Soest, 1998							1			1
<i>Stylocordyla borealis</i> var. <i>globosa</i> Ridley & Dendy, 1886					1					
<i>Stylocordyla chupachups</i> Uriz, Gili, Orejas & Pérez-Porro, 2011					1					
<i>Suberites affinis</i> Brøndsted, 1924		1	1							
<i>Suberites excellens</i> (Thiele, 1898)		1	1							
<i>Sulcastrella clausa</i> Schmidt, 1879	1									
<i>Tedania (Tedania) anhelans</i> (Vio in Olivi, 1792)		1								1
<i>Tedania armata</i> Sarà, 1978		1								1
<i>Tentorina sigmatophora</i> Burton, 1959							1			
<i>Tethya magna</i> Kirkpatrick, 1903			1							
<i>Tethya novaecaledoniae</i> Sarà, 1988			1							
<i>Tethya peracuta</i> (Topsent, 1918)			1							
<i>Tethya pulitzeri</i> Sarà & Sarà, 2004			1							
<i>Tethyopsis plurima</i> (Pulitzer-Finali, 1993)			1							
<i>Tetilla globosa</i> (Carter, 1886)			1							
<i>Tetilla praecipua</i> Wiedenmayer, 1989			1							
<i>Tetrapocillon kurushimensis</i> Tanita, 1961	1									
<i>Thenea grayi</i> var. <i>lateralis</i> Thiele, 1898			1						1	
<i>Thenea schmidti</i> Sollas, 1886			1						1	
<i>Thorecta donar</i> Lendenfeld, 1889			1	1	1	1				
<i>Thorecta murrayella</i> Lendenfeld, 1889			1	1	1	1				
<i>Thorecta pumilus</i> Lendenfeld, 1889			1	1	1	1				
<i>Timea stellifasciata</i> Sarà & Siribelli, 1960	1									
<i>Topsentia garciae</i> Bibiloni, 1993		1								1
<i>Trachostylea semota</i> Topsent, 1928			1			1	1			1
<i>Triakentron flabelliforme</i> Hentschel, 1912							1		1	1
<i>Vulcanella acanthoxea</i> (Tanita & Hoshino, 1989)	1						1			
<i>Vulcanella osculanigera</i> (Dickinson, 1945)	1						1			

Reference list for lithistid sponge data

- Adachi, N., Ezaki, Y., and Liu, J. 2011. Early Ordovician shift in reef construction from microbial to metazoan reefs. *Palaios* **26**: 106-114.
- Adachi, N., Ezaki, Y., and Liu, J. 2012. The oldest bryozoan reefs: a unique Early Ordovician skeletal framework construction. *Lethaia* **45**: 14-23.
- Adachi, N., Ezaki, Y., Liu, J., and Cao, J. 2009. Early Ordovician reef construction in Anhui Province, South China: A geobiological transition from microbial- to metazoan-dominant reefs. *Sedimentary Geology* **220**: 1-11.
- Bingli, L., Rigby, J. K., Yanwen, J., and Zhongde, Z. 1997. Lower Ordovician lithistid sponges from the eastern Yangtze Gorge Area, Hubei, China. *Journal of Paleontology* **71**: 194-207.
- Cañas, F., and Carrera, M. 1993. Early Ordovician Microbial-Sponge-Receptaculitid Bioherms of the Precordillera, Western Argentina. *Facies* **29**: 169-178.
- Carrera, M. G. 2006. The new genus *Multispongia* (Porifera) from the Lower Ordovician limestones of the Argentine Precordillera. *Ameghiniana* **43**: 493-498.
- Church, S.B., 1974. Lower Ordovician patch reefs in western Utah. *Brigham Young University Geology Studies* **21**: 41-62.
- Desrochers, A., and James, N.P. 1989. Middle Ordovician (Chazyan) bioherms and biostromes of the Mingan Islands, Quebec. In: H.H.J. Geldsetzer, N.P. James, G.E. Tebbutt (eds.), *Reefs: Canada and adjacent areas. Canadian Society of Petroleum Geologists Memoir 13*, Canadian Society of Petroleum Geologists, pp. 183-191.
- Fritz, M.A., and Howell, B.F. 1955. An Upper Cambrian coral from Montana. *Journal of Paleontology* **29**: 181-183.
- Hong, J., Choh, S.-J., and Lee, D.-J. 2015. Untangling intricate microbial–sponge frameworks: The contributions of sponges to Early Ordovician reefs. *Sedimentary Geology* **318**: 75-84.
- Johns, R.A., Dattilo, B.F., and Spincer, B. 2007. Neotype and redescription of the Upper Cambrian anthaspidellid sponge, *Wilberncyathus donegani* Wilson, 1950. *Journal of Paleontology* **81**: 435-444.
- Kelly, M. 2007. Porifera: Lithistid Demospongiae (Rock Sponges). In: Gordon, D. P. ed. *The Marine Fauna of New Zealand. NIWA Biodiversity Memoir 121*.
- Kelly, M., Lee, D., Kelly, S., and Buckeridge, J. S. 2003. A recent sponge, *Pleroma aotea* Kelly ("Order" Lithistidia: Family Pleromidae), in the late Eocene Ototara Limestone of Otago, New Zealand. *New Zealand Journal of Marine and Freshwater Research* **37**: 129-148.
- Klappa, C.F., and James, N.P. 1980. Small lithistid sponge bioherms, early Middle Ordovician Table Head Group, western Newfoundland. *Bulletin of Canadian Petroleum Geology* **28**: 425-451.
- Kruse, P.D., and Zhuravlev, A.Y. 2008. Middle-Late Cambrian *Rankenella-Girvanella* reefs of the Mila Formation, northern Iran. *Canadian Journal of Earth Sciences* **45**: 619-639.
- Lee, J.-H., Woo, J., and Lee, D.-J. 2016. The earliest reef-building anthaspidellid sponge *Rankenella zhangxianensis* n. sp. from the Zhangxia Formation (Cambrian Series 3), Shandong Province, China. *Journal of Paleontology* **90**: 1-9.
- Manconi, R., Serusi, A., and Pisera, A. 2006. A new Mediterranean 'lithistid' sponge, *Aciculites mediterranea* sp. nov. (Porifera: Demospongiae) from a dark marine cave in Sardinia. *Journal of Marine Biological Association of the United Kingdom* **86**: 691-698.
- Mehl, D., and Fursich, F. T. 1997. Middle Jurassic Porifera from Kachchh, western India. *Palaontologische Zeitschrift* **71**: 19-33.
- Mrozek, S., Dattilo, B.F., Hicks, M., and Miller, J.F. 2003. Metazoan reefs from the Upper Cambrian of the Arrow Canyon Range, Clark County, Nevada. *Geological Society of America Abstracts with Programs* **35**: 500.
- Perez, T., Vacelet, J., Bitar, G., and Zibrowius, H. 2004. Two new lithistids (Porifera: Demospongiae) from a shallow eastern Mediterranean cave (Lebanon). *Journal of Marine Biological Association of the United Kingdom* **84**: 15-24.
- Pickett, J., and Rigby, J. K. 1983. Sponges from the early Devonian Garra Formation, New South Wales. *Journal of Paleontology* **57**: 720-741.
- Pisera, A. 2000. New species of lithistid sponges from the Paleogene of the Ukraine. *Zoosystema* **22**, 285-298.

- Pratt, B.R., and James, N.P. 1982. Cryptalgal-metazoan bioherms of early Ordovician age in the St George Group, western Newfoundland. *Sedimentology* **29**: 543-569.
- Rhebergen, F. 2014. A new Late Ordovician erratic anthaspidellid sponge (Porifera) originating from Baltica. *Scripta Geologica* **146**: 1-15.
- Rigby, J. K. 1973. A new anthaspidellid sponge from the Silurian of Lake Timiskaming, Quebec. *Journal of Paleontology* **47**: 801-804.
- Rigby, J. K., and Jamison, P. 1994. Lithistid sponges from the Late Ordovician Fish Haven Dolomite, Bear River Range, Cache County, Utah. *Journal of Paleontology* **68**: 722-726.
- Rigby, J. K., Church, S. B., and Anderson, N. K. 2010. Middle Cambrian sponges from the Drum Mountains and House Range in western Utah. *Journal of Paleontology* **84**: 66-78.
- Rigby, J. K., Kessel, B. J., Ritts, B. D., and Friedman, S. J. 2006. A new Ordovician Chiastoclonellid sponge from Inner Mongolia, China. *Journal of Paleontology* **80**: 775-779.
- Shapiro, R.S., and Rigby, J.K. 2004. First occurrence of an in situ anthaspidellid sponge in a dendrolite mound (Upper Cambrian; Great Basin, USA). *Journal of Paleontology* **78**: 645-650.
- Toomey, D.F., and Nitecki, M.H. 1979. Organic buildups in the Lower Ordovician (Canadian) of Texas and Oklahoma. *Fieldiana Geology* **2**, Field Museum of Natural History, 181 pp.

Appendix E: Additional statistical data

Table E1: Pairwise p -values with Bonferroni corrections for fabric analysis (associated with NMDS) below diagonal and pairwise diversity t-tests above diagonal. NS – not significant.

	BCT - M	BCT - P	GPH	SM	WGP	SAL	SALM	ZAC
BCT - M		>> 0.001	>> 0.001	>> 0.001	0.035	0.002	NS	0.034
BCT - P	NS		> 0.001	NS	>> 0.001	>> 0.001	NS	NS
GPH	0.038	NS		>> 0.001	>> 0.001	>> 0.001	0.019	NS
SM	NS	NS	NS		>> 0.001	>> 0.001	NS	NS
WGP	NS	NS	>> 0.001	NS		0.002	NS	0.043
SAL	NS	NS	0.018	NS	NS		0.003	>> 0.001
SALM	NS	NS	>> 0.001	NS	NS	NS		NS
ZAC	NS	NS	>> 0.001	NS	NS	NS	NS	

Table E2: Mann-Whitney pairwise p -values with Bonferroni corrections for average contributions from microbes and archaeocyaths compared across localities in Salaagol Formation. Statistically significant values in bold. Kruskal-Wallis p -values equal **0.0006** (microbial material) and **0.0025** (archaeocyath material).

(microbes : archaeocyaths)	Lower Salaa Gorge	Upper Salaa Gorge
Lower Salaa Gorge		
Upper Salaa Gorge	(> 0.001 : 0.003)	
Zuun-Arts Ridge	(0.045 : 0.003)	(0.068 : 0.999)

Table E3: Pairwise Mann-Whitney test p -values with Bonferroni correction for functional richness values. NS – not significant.

	Ediacaran (w/o)	Ediacaran	Early Cambrian	Late Cambrian
Ediacaran (w/o tubular fossils)				
Ediacaran	NS			
Early Cambrian	0.011	0.044		
Late Cambrian	NS	NS	NS	
Ordovician	0.018	0.013	0.002	0.021

Table E4: Pairwise comparisons with Bonferroni correction for archaeocyathan continuous morphological variables grouped by locality. See main text for PERMANOVA results. NS – not significant.

	Australia	Alaska	Western USA
Australia			
Alaska	0.0102		
Western USA	NS	0.0132	
Mongolia	0.0006	0.0006	0.0006

Table E5: Pairwise comparisons with Bonferroni correction for archaeocyathan continuous morphological variables grouped by taxonomic order. See main text for PERMANOVA results.

	Ajacycyathida	Archaeocyathida
Ajacycyathida		
Archaeocyathida	0.0003	
Capsulocyathida	0.0006	0.0003

Table E6: Pairwise comparisons with Bonferroni correction for archaeocyathan continuous morphological variables grouped by geologic formation. See main text for PERMANOVA results. NS – not significant.

	Adams Argillite	Bonanza King	Campito	Chewelah	Harkless	Hillard	Jones Ridge	Poleta	Salaagol	Scott Canyon	Silver Peak
Adams Argillite											
Bonanza King	NS										
Campito	NS	NS									
Chewelah	NS	NS	NS								
Harkless	0.0066	0.0066	NS	NS							
Hillard	NS	NS	NS	NS	NS						
Jones Ridge	NS	0.0066	0.0066	NS	0.0066	NS					
Poleta	NS	0.0066	NS	NS	0.0066	NS	NS				
Salaagol	0.0066	0.0066	0.0066	NS	0.0066	0.0066	NS	0.0066			
Scott Canyon	NS	NS	NS	NS	NS	NS	NS	NS	NS		
Silver Peak	NS	NS	NS	NS	NS	NS	NS	NS	NS	NS	

Table E7: Statistical tests using minimum diameters only. Values above the diagonal are *p*-values for variances. Values below the diagonal are *p*-values for difference in means. Values in parenthesis are osculum results, all others are body size. All tests done with log transformed data. NS – not significant.

	Archaeocyaths	Modern Demosponges	Lithistid Sponges
Archaeocyaths		<< 0.001 (0.022)	0.003
Modern Demosponges	<< 0.001 (<< 0.001)		0.004
Lithistid Sponges	<< 0.001	NS	

Table E8: PARED data used in post-extinction analysis. Number of reefs built by each primary framework building organism shown.

Reef Type	Fortunia	Stage 2	Stage 3	Stage 4	Wuliuan	Drumian	Guzhang	Paibian	Stage 9	Stage 10
Microbial	7	17	53	20	13	4	2	38	14	3
Archaeocyath	0	9	22	9	0	0	0	1	0	0
Sponge	0	0	0	0	0	2	0	0	1	0
Other	1	0	6	0	0	0	0	0	1	0

Table E9: Peloid size distribution for post-extinction analysis. All sizes in mm.

	N	Average	SD
EH 26	250	0.049	0.129
EH 34	250	0.014	0.003
WH 52	250	0.050	0.092
WH 60	250	0.079	0.120
Class 1	981	0.037	0.040
Class 2	19	0.630	0.352

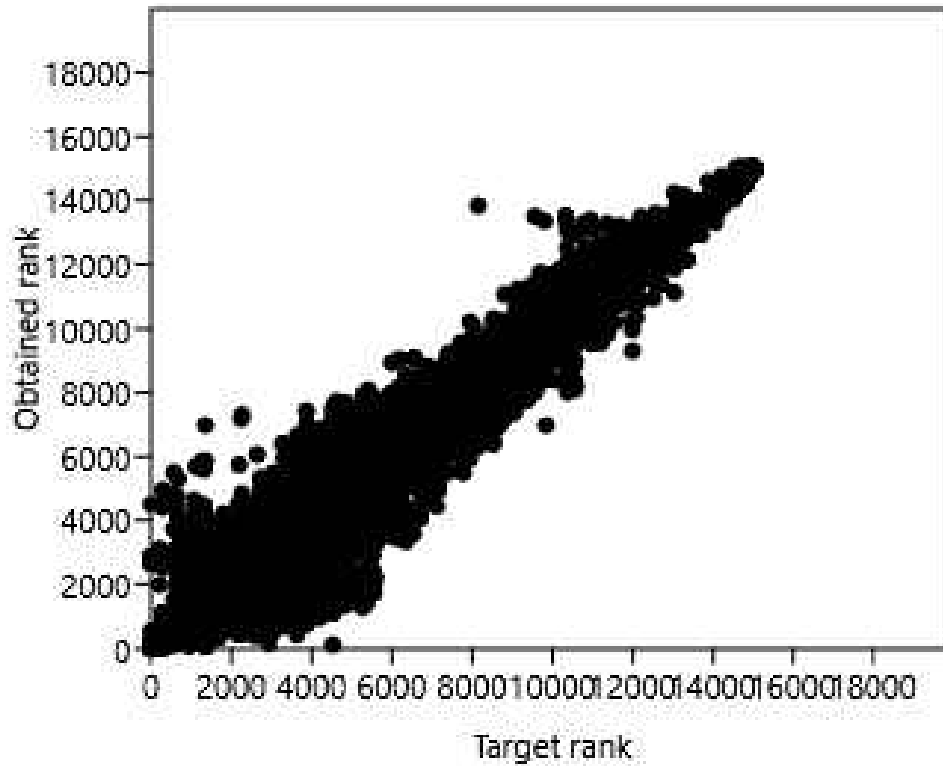


Figure E1: Shepard's plot for NMDS ordination. R^2 equals 0.8639. Stress equals 0.1068.

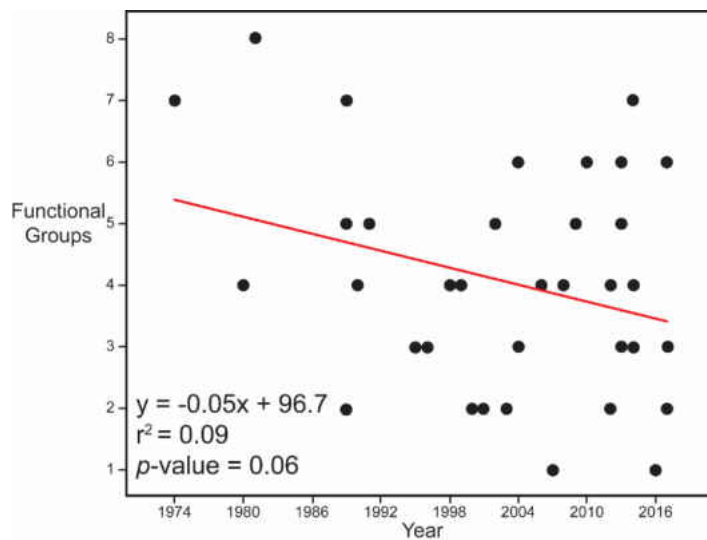


Figure E2: Regression analysis for literature survey. Trend of year of publication vs. functional richness is not significantly different from zero. More recent publications have the benefit of prior literature with which to refer and could therefore identify more organisms that past researchers. However, data from more recent publications did not contain a significantly different number of functional groups, thereby suggesting that year of publication is not an important factor in any trends presented here.

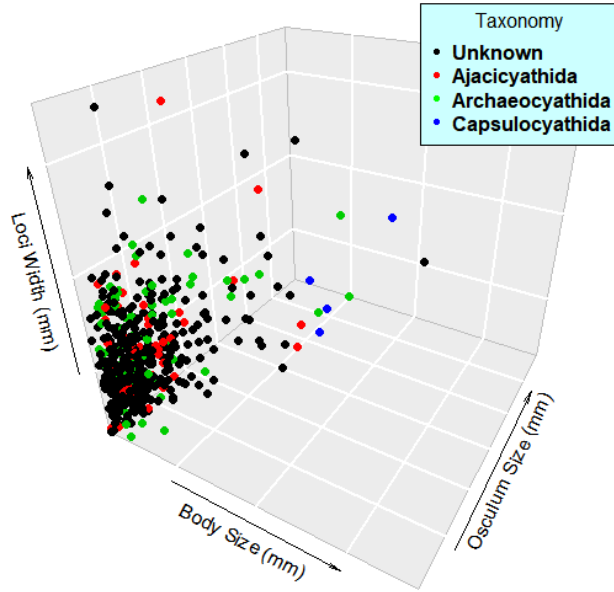


Figure E3: Continuous variables of archaeocyaths based on taxonomy. Minimal separation of taxa.

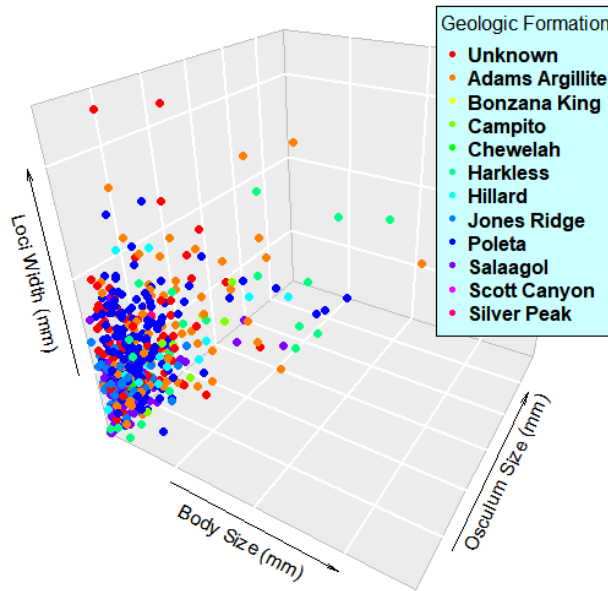


Figure E4: Continuous variables of archaeocyaths based on geological formation. Minimal separation of formations.

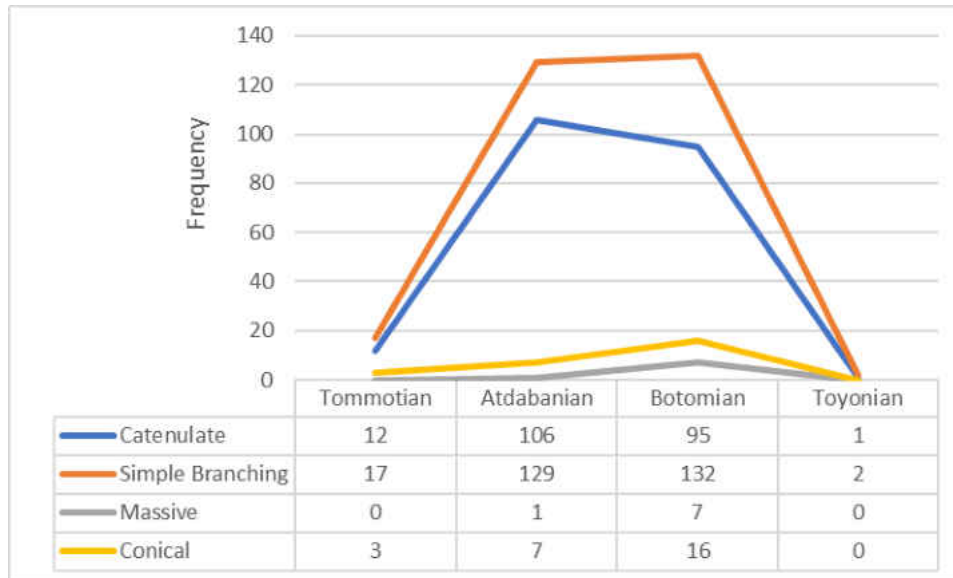


Figure E5: Archaeocyath gross morphology through time. Siberia regional stage names used. Changes in relative percentage of gross morphology are dominated by changes in most abundant (simple branching) morphological category. Excluding FAD and LAD stages there is no change in relative diversity ($\chi^2 = 8.58$, p-value = 0.35).

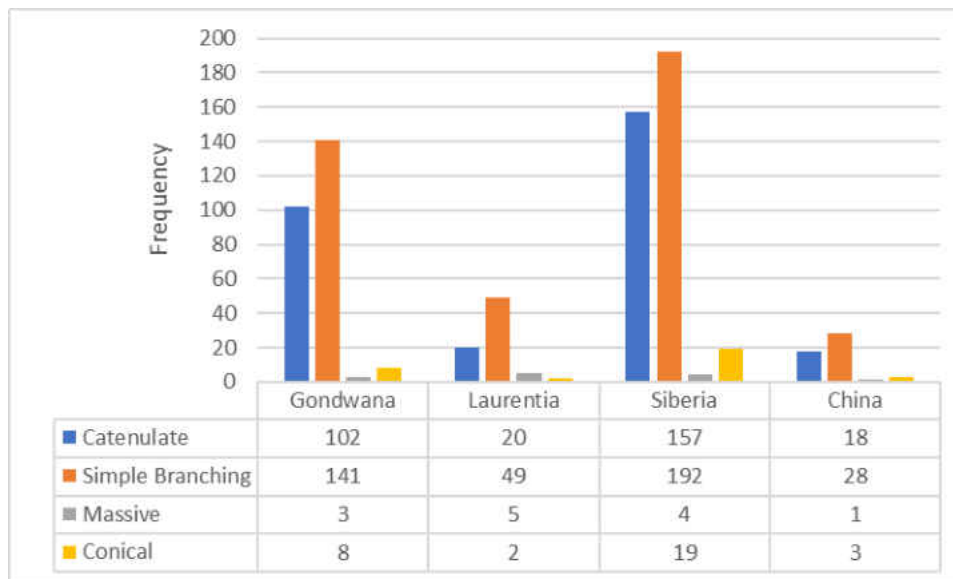


Figure E6: Archaeocyath gross morphology by locality. Only largest four localities shown. No differences in percent composition observed across regions ($\chi^2 = 16.01$, p-value = 0.067).

Curriculum Vitae

DAVID RUSSELL CORDIE

University of Wisconsin-Milwaukee
Department of Geosciences

Education

University of Wisconsin-Milwaukee; Milwaukee, Wisconsin (2019)
PhD in Geoscience, G.P.A. 3.9/4.0
Concentration in Invertebrate Paleontology

University of Iowa; Iowa City, Iowa (2015)
Masters of Science in Geoscience, G.P.A. 3.9/4.0
Concentration in Paleontology/Systematics

Lawrence University; Appleton, Wisconsin (2013)
Bachelor of Arts Degree in Biology, G.P.A. 3.7/4.0 *Magna cum laude*
Concentration in Ecology; Minor in Geology

Publications

Cordie, David R., Dornbos, S. Q., and Marenco, P. J. 2019. Increase in carbonate contribution from framework-building metazoans through early Cambrian reefs in the western basin and range, USA. *PALAIOS* **34**. DOI: <http://dx.doi.org/10.2110/palo.2018.085>

Cordie, David R., and Dornbos, S. Q. 2019. Restricted morphospace occupancy of early Cambrian reef-building archaeocyaths. *Paleobiology*. DOI: 10.1017/pab.2019.5

Cordie, David R., Dornbos, S. Q., Marenco, P. J., Oji, T., Gonchigdorj, S. 2019. Depauperate skeletonized reef-dwelling fauna of the early Cambrian: insights from archaeocyathan reef ecosystems of western Mongolia. *Palaeogeography, Palaeoclimatology, Palaeoecology* **514**: 206-221. DOI: <https://doi.org/10.1016/j.palaeo.2018.10.027>

Cordie, David R., and Witzke, B. J. 2017. A new crinoid genus from the Middle Devonian of Iowa, USA (Camerata, Melocrinitidae). *Paleontological Research* **21**: 7-13. DOI: 10.2517/2016PR014

Cordie, David R., and Budd, A. F. 2016. Histological data in a combined phylogenetic analysis of scleractinian reef corals. *Journal of Morphology* **277**: 494-511. DOI: 10.1002/jmor.20514

Scholarly Presentations

- Cordie, David R.**, Dornbos, S. Q., and Marengo, P. J. 2018. Searching for framework builders after the regional extinction of archaeocyathan reefs in the Cambrian Mule Spring Limestone near Split Mountain, Nevada, USA. *Geological Society of America Abstracts with Programs* **Vol. 50, No. 6.** (poster)
- Cordie, David R.**, Dornbos, S. Q., and Marengo, P. J. 2017. Paleoecology and geochemistry of early Cambrian calcimicrobial-archaeocyathans reefs from the western Basin and Range, USA. *Geological Society of America Abstracts with Programs* **Vol. 49, No. 6:** 186. (oral)
- Cordie, David R.**, Dornbos, S. Q., and Gulbranson, E. L. 2016. Paleoecology and geochemistry of early Cambrian microbial-archaeocyathan reefs from the western USA and Mongolia. *Geological Society of America Abstracts with Programs* **Vol. 48, No. 7:** 182. (poster)
- Cordie, David R.**, and Budd, A. F. 2015. Histological data in a combined phylogenetic analysis of scleractinian reef corals. *Geological Society of America Abstracts with Programs* **Vol. 47, No. 7:** 221. (oral)
- Cordie, David R.**, and Budd, A. F. 2015. Scleractinia soft tissue systematics: use of histological characters in coral taxonomy and phylogenetic reconstructions. *North-Central Geological Society of America Abstracts with Programs* **Vol. 47, No. 5:** 95. (poster)
- Cordie, David R.** 2015. Soft tissue systematics of Indo-Pacific corals. *Jakobsen Conference.* (oral only)
- Cordie, David R.**, Humphries, J., and DeStasio, B. 2013. Testing alternate hypotheses of parasitic communities and aquatic invasive species interactions in Green Bay, Lake Michigan. *AMCOP 65:* 7. (oral)

Completed Theses

Scleractinia soft tissue systematics: use of histological characters in coral taxonomy and phylogenetic reconstruction, <http://ir.uiowa.edu/etd/1574/>

Advisor: Ann F. Budd, August 2013 - May 2015

Fossil factory: evidence of climate change in the Carboniferous based on leaf morphology

Adviser: Judith Humphries (Joanne Kluessendorf consulting), June 2013

Academic Appointments

Associate Lecture, University of Wisconsin-Milwaukee, January 2019

Courses: Dinosaurs (online)

Adjunct Instructor, Upper Iowa University, August 2016 - present
Courses: Intro to Dinosaurs, Global Warming and Climate Change

Teaching Assistant, UW-Milwaukee, August 2015 - present
Courses: History of Life, Intro to Earth Science, Historical Geology

Teaching Assistant, University of Iowa, August 2013 - May 2015
Courses: Envir. Sci., History of Life, Marine Ecosystems, Principles of Paleo.

Collections Evaluator, Museum of Natural History at University of Iowa, Summer 2014

Student Researcher, Lawrence University, June 2012 - June 2013

Internship, Weis Earth Science Museum, June 2012 - June 2013

Honors

American Federation of Mineralogical Societies Scholarship, 2018

Distinguished Dissertator Fellowship, 2017

Levine Science Fellowship, 2016

UWM Research Award, 2016

Nelson Cherkauer Lasca Legacy Scholarship, 2016

Chancellor's Award, 2015, 2016, 2017

Jakobsen Conference Award for Best Abstract, 2015

RM Cable Award for Best Undergrad Presentation, 2013

Dean's List Lawrence University, 2010 - 2013

Beta Theta Pi Freshmen Scholarship, 2009

External Grants

Geological Society of America, 2017 (\$1550)

Paleontological Society, 2017 (\$800)

SEPM Graduate Student Award, 2017 (\$1200)

Wisconsin Geological Society Research Grant, 2016 (\$780)

Wisconsin Geological Society Scholarship, 2016 (\$550)

Lerner-Gray Fund, 2016 (\$1000)

Geological Society of America, 2016 (\$1875)

Sigma Xi Grants-in-Aid, 2016 (\$500)

White Mountain Research Center Minigrant, 2016 (\$770)

Clem Nelson Award, 2016, (\$3500)

Lerner-Gray Fund, 2014 (\$1800)

CGRER Grad Student Travel Fund, 2014 (\$920)

AMCOP Student Research Grant, 2012 (\$250)

Total: \$15,495

Certifications

Kolb's Experimental Learning, UW-Milwaukee, 2016

Certified to promote Kolb's learning techniques in college courses

Lerner-centered Course Design, UW-Milwaukee, 2016

Certified to design college courses with active learning techniques

SCUBA

Skills

Computer Software: Mesquite, TNT, WinClada, R, Adobe Illustrator, ArcGIS, PAST
SEM Microscopy

French Reading Comprehension

Additional Work History

Biology Content Tutor, Lawrence University, March 2012 - June 2013

Biological Stockroom Assistant, Lawrence University, March 2010 - June 2013

Resident Life Advisor, Lawrence University, August 2010 - June 2011

Music Teacher, Waukesha, WI, 2007 - 2009

Volunteering

Wisconsin Science Olympiad, Milwaukee, WI, 2017, 2018

Wisconsin Science Festival Speaker, Milwaukee, WI, 2016

Tour Guide for Devonian Fossil Gorge, Coralville, IA, 2015

Eastern Iowa Science and Engineering Fair Judge, Cedar Rapids, IA, 2015

Science Lab Days Activity Designer, Appleton, WI, 2012

Habitat for Humanity, Appleton, WI, 2011

Collaborators

Dr. Stephen Q. Dornbos (University of Wisconsin-Milwaukee)

Dr. Pedro J. Marenco (Bryn Mawr College)

Dr. Tatsuo Oji (Nagoya University Museum)

Dr. Sersmaa Gonchigdorj (Mongolian University of Science and Technology)

Dr. Mark Harris (University of Wisconsin-Milwaukee)

Dr. Peter Sheehan (University of Wisconsin-Milwaukee, Milwaukee Public Museum)

Involvement

American Association for the Advancement of Science

Sigma Xi

Geological Society of America

Paleontological Society
Society for Sedimentary Geology
NCAA Varsity Fencing

Lawrence University; Captain - 2012; Lettered 2009 - 2013

University of Iowa; Club Member 2013 - 2015

Milwaukee Youth Symphony Orchestra 2004 - 2009

❧ FINE ❧